INVESTIGATION OF LIQUID METAL BOILING HEAT TRANSFER

Richard E. Balzhiser
Project Director
The University of Michigan

Robert E. Barry
Bruce F. Caswell
Robert L. Gahman
Herman Merte, Jr.
Andrew Padilla, Jr.
Michael R. Samuels
Anthony J. Sartor
Lowell R. Smith

FOREWORD

This report summarizes work performed in the Liquid Metals Laboratory of the Department of Chemical Engineering at The University of Michigan on Air Force Contract AF 33(657)-11548. The work was administered under the direction of the Air Force Aero Propulsion Laboratory, Research and Technology Division, Air Force Systems Command, Wright-Patterson Air Force Base, Ohio. Mr. Charles Delaney and Lt. Ronald Bane have served as project engineers for the Air Force. This contract represents a continuation of work initiated under Contract AF 33(616)-8377 originated in June 1961. Technical reports ASD Technical Report 61-594 and RTD-TDR-63-4130, discuss results obtained under the original contract. The experimental program discussed in this report originated in May 1963 and was terminated on April 30, 1966. The preliminary draft of the report was submitted to the Aero Propulsion Laboratory in June 1966.

This technical report has been reviewed and is approved.

G. M. Kevern, Branch Chief
Energy Conversion Branch
Aerospace Power Division
Air Force Aero Propulsion Laboratory

ABSTRACT

This report covers all studies conducted for the Air Force Aero Propulsion Laboratory at The University of Michigan under AF 33(657)-11548. The contract was initiated on 1 May 1963 as a follow-up to an initial study conducted at The University of Michigan for ASD.

Analytical and experimental heat transfer and fluid flow investigations with metallic fluids were conducted during this period. Both pool boiling configurations and forced convection loops were used for these studies.

Nucleate boiling, with particular emphasis on the critical heat flux, was studied using a 3/8" diameter bayonet heater in a liquid pool. Fluids studied included sodium, rubidium, cesium and water (for comparison purposes). Results tended to confirm earlier potassium results as critical heat fluxes were lower than hydrodynamic theory had predicted and less pressure dependence was evident.

Film boiling of potassium from a horizontal plate was studied at pressures of 2 mm Hg and 50 mm Hg. Both the flux level and temperature difference (between surface and fluid), at which the change from the transition regime to the stable film boiling regime occurred, differed from earlier predictions.

Agravic studies with mercury under pool boiling conditions were conducted at accelerations up to 20 g's. Pressure levels between 20 and 300 psia and flux levels between 18,000 and 405,000 Btu/hr ft^2 were obtained. The wetting behavior of mercury was observed to have an effect in these studies. Increases in both pressure and acceleration seemed to improve the heat transfer coefficient in most instances.

Condensing studies with sodium on the outside of a vertical 2" length of 1/2" diameter tubing were conducted as part of the overall program. Results supported earlier studies with metallic fluids which fell substantially below Nusselt's theory. Coefficients of approximately 10,800 Btu/hr ft2 °F were obtained and appeared to be independent of heat flux and saturation pressure.

Two phase pressure drop and void fraction studies with flowing potassium were conducted. Pressure drops were generally lower than predicted by Lockhart - Martinelli procedures as were void fractions. "Pure" potassium void studies exhibited good agreement with the void fraction predictions of Baroczy.

Heat transfer studies were conducted with two phase potassium mixtures. Coefficients between 4000 and 9000 Btu/hr ft^2 °F were obtained. Qualities of up to 17% and heat fluxes up to 424,000 Btu/hr ft^2 were obtained. Unstable operations of the primary heat source at higher fluxes suggested the critical heat flux had been reached in some instances.

TABLE OF CONTENTS

Page

CRITICAL HEAT FLUX DETERMINATIONS
IN SATURATED POOL BOILING

Introduction..... 1
Review of Literature..... 2
Equipment and Procedure..... 6
Experimental Results..... 10
Correlation of Critical Heat Flux Data..... 18

FILM BOILING IN POTASSIUM

Introduction..... 23
Literature Review..... 24
Description of Equipment..... 33
Experimental Procedure..... 50
Experimental Results..... 54
Discussion of Results..... 63
Conclusions..... 89

LIQUID METAL BOILING IN AGRAVIC FIELDS

Introduction..... 92
Test Conditions and Procedures..... 92
Experimental Accuracy..... 97
Experimental Results..... 98
Conclusions..... 134

SODIUM CONDENSING STUDIES

Introduction..... 141
Review of Literature..... 143
Description of Equipment..... 155
Experimental Procedure..... 167
Experimental Data..... 168
Discussion of Results..... 177
Conclusions..... 183

Page

TWO PHASE FLOW INVESTIGATIONS

I. TWO PHASE PRESSURE DROP

Introduction..... 185
Literature Review..... 185
Description of Equipment..... 188
Experimental Procedures..... 191
Results..... 192
Discussion of Results..... 196

II. VOID FRACTION STUDIES.

Introduction..... 198
Description of Radiation Attenuation Apparatus..... 201
Experimental Program..... 207
Results..... 210
Discussion of Results..... 210
Conclusions..... 213

III. TWO PHASE HEAT TRANSFER

Introduction..... 213
Review of Potassium Forced Convection Boiling Literature..... 217
Description of Equipment..... 220
Experimental Procedure..... 222
Discussion of Results..... 223

APPENDICES..... 229
REFERENCES..... 291

LIST OF FIGURES

Figure No.		Page
1	Apparatus Used in Study	7
2	View of Tube Assembly	8
3	Cross Sectional Drawing of Boiling Tube Assembly	9
4	Comparison of Water Data with Correlations	11
5	Comparison of Sodium Burnout Data with Correlations	13
6	Comparison of Rubidum Burnout Data with Correlations	15
7	Heater Surface Temperatures	16
8	Comparison of Cesium Data with Author's Correlation	17
9	Summary of Alkali Metal Burnout Data	20
10	Comparison of Sodium Burnout Data with Correlation	21
11	Correlation of Burnout Data	22
12	Data of Lyon (114) for Film Boiling of Mercury and Cadmium	28
13	Data of Bonilla (26) for Pool Boiling of Mercury; parameter: pressure over the liquid in mm Hg absolute or lb/sq inch gauge	29
14	Data of Merte (125) for Saturated Pool Boiling of Mercury	30
15	Data of the General Electric Company (69) for Average Transition and Film Boiling Coefficients of Potassium in Forced Convection	32
16	Schematic Diagram of Film Boiling Apparatus	34
17	General View of Experimental Apparatus	35
18	Boiler Assembly	36
19	Boiler and Heater Assembly	38
20	Diagram of Drip Plate	39
21	Boiling Plate	40
22	Location of Boiling Plate Thermocouples	42
23	Graphite Main Heater	43
24	Instrumented Boiler Assembly	44
25	Instrumented and Insulated Boiler Assembly	45
26	Diagram of Charging System	46
27	Location of Temperature Measurements	48
28	Temperature Recorders and Potentiometer	49
29	Heat Fluxes for Potassium in Film Boiling	57
30	Heat Transfer Coefficients for Potassium in Film Boiling	58
31	Effect of Pressure on the Heat Flux in Film Boiling	59
32	Heat Fluxes for Potassium in Nucleate Boiling	61
33	Vapor Pressure of Potassium	62
34	Comparison of Film Boiling Coefficient with Correlations	64

Figure No.		Page
35	Heat Transfer Due to Radiation	67
36	Correction of Film Boiling Heat Transfer Coefficients for Radiation	68
37	Correction of Film Boiling Heat Transfer Coefficients for Vapor Dimerization Reaction	70
38	Correlation of Film Boiling Data for Horizontal Surfaces	74
39	Rapidly Increasing Film Boiling Heat Transfer Coefficients	76
40	Model for Computer Simulation of Boiling Plate	82
41	Temperature Distribution in Boiling Plate Obtained by Computer Simulation	83
42	Comparison Between Boiling Surface Flux and Flux Calculated from the Temperature Distribution Obtained by Computer Simulation	85
43	Effect of Boiling Coefficient on Edge Effect Due to Radial Gradients	86
44	Temperature Distribution in Boiling Plate for Computer Simulation to Determine Maximum Effect of Heat Drain Down Busbars	87
45	Comparison of Temperature Gradient Method and Heat Loss Method for Calculating the Heat Flux	90
46	Test Vessel for Boiling Mercury Study Under High Gravity	93
47	Mercury Boiling Test Vessel In Centrifuge	94
48	Thermocouples Locations for Reference	95
49	Time-Temperature Data for Run No. 6	99
50	Time-Temperature Data for Run No. 8	101
51	Boiling Data for Mercury	102
52	Non-Boiling Natural Convection Data for Mercury Under High Gravity	105
53	Mercury Boiling Data Under High Gravity, Run No. 22	107
54	Mercury Boiling Data Under High Gravity, Run No. 23	109
55	Mercury Boiling Data Under High Gravity, Run No. 24	110
56	Mercury Boiling Data Under High Gravity, Run No. 25	111
57	Mercury Boiling Data Under High Gravity, Run No. 26	112
58	Mercury Boiling Data Under High Gravity, Run No. 27 and 28	113
59	Mercury Boiling Data Under High Gravity, Run No. 29	115
60	Mercury Boiling Data Under High Gravity, Run No. 30	116
61	Composite of Influence of High Gravity on Subcooling for P=80 psia	117
62	Composite of Influence of High Gravity on ΔT_{sat} for P=80 psia	118

Figure No. Page

63 Heat Flux Versus ΔT_{sat} for Levels of Acceleration for P=80 psia 119
64 Influence of High Gravity on Normalized ΔT_{sat} for P=80 psia 120
65 Mercury Boiling Data Under High Gravity, Run No. 31 122
66 Mercury Boiling Data Under High Gravity, Run No. 32 123
67 Mercury Boiling Data Under High Gravity, Run No. 35 124
68 Composite of Influence of High Gravity on Subcooling for P=20 psia 125
69 Composite of Influence of High Gravity on ΔT for P=20 psia 127
70 Heat Flux Versus ΔT_{sat} for Levels of Acceleration for P=20 psia 128
71 Influence of High Gravity on Normalized ΔT_{sat} for P=20 psia 129
72 Mercury Boiling Data Under High Gravity, Run No. 37 130
73 Mercury Boiling Data Under High Gravity, Run No. 38 131
74 Mercury Boiling Data Under High Gravity, Run No. 39 132
75 Mercury Boiling Data Under High Gravity, Run No. 40 133
76 Mercury Boiling Data Under High Gravity, Run No. 41 135
77 Composite of Influence of High Gravity on Subcooling for P=300 psia 136
78 Composite of Influence of High Gravity on ΔT for P=300 psia 137
79 Heat Flux Versus ΔT_{sat} for Levels of Acceleration for P=300 psia 138
80 Influence of High Gravity on Normalized ΔT_{sat} for P=300 psia 139
81 Liquid Metal Condensing Heat Transfer Coefficients Compared with Nusselt's theory 146
82 Potassium and Sodium Data of Labuntsov and Smirnov (102) 153
83 Potassium Data of Aladyev et al (4) 154
84 Flow Schematic - Boiling Liquid Metal System 156
85 Loop, North Elevation 158
86 Loop, North Elevation 159
87 Loop, East Elevation 160
88 Heat Transfer Test Section 162
89 Liquid Metal Loop - Control Panel 165
90 Sodium Condensing Heat Transfer Coefficient Versus Film Reynolds Number 171
91 Condensing Heat Transfer Coefficient Versus $\Delta T_{vapor-wall}$ 172

Figure No.		Page
92	Sodium Condensing Heat Transfer Coefficient Versus Vapor Temperature	173
93	Sodium Condensing Heat Transfer Coefficient Versus Vapor Temperature	174
94	Accommodation Coefficient Versus Saturation Pressure	175
95	Sodium Condensing Heat Transfer Coefficient Versus Vapor Temperature	176
96	Condensing Heat Transfer Coefficient Versus Heat Flux	178
97	Resistances to Condensing Heat Transfer	179
98	Flow Schematic-Boiling Liquid Metal System	189
99	Typical Section of Taylor Transcope Recorder Chart, Showing Pressure Drop and Flow Meter Traces	193
100	Comparison of Friction Factors from 1963 and 1966 Data	194
101	Comparison of Experimental Data with Other Correlations and Predictions	195
102	Uncertainty in Calculated Qualities, Based on Average Loop Operating Characteristics	197
103	Schematic Diagram of Void Fraction Measuring System	202
104	Differential Pulse Height Spectra	204
105	Temperature Dependence of Noise	205
106	Gamma-Ray Source and Scintillation Crystal Holder	206
107	Alignment with Pipe	208
108	Effect of Quality on Gross Count Rate	209
109	Metallic Liquid Fraction Data Compared with Other Data and Correlations	211
110	Lurie's (112) Liquid Fraction for Vertical Upflow of Sodium	212
111	Flow Regimes	215
112	Correlation for Flow Regimes	216
113	Comparison of Superheated Liquid Film Models with GE Boiling Potassium Data	219
114	Heat Transfer Test Section	221
115	Boiler Loss Calibration	224
116	Preheat Loss Calibration	225
117	Two Phase Heat Transfer Characteristics	227
118	Heat Flux Versus Temperature Difference	228

APPENDICES

E-1	Thermal Conductivity of Type 316 Stainless Steel (17)	240
E-2	Heat Loss Calibration	241
G-1	Effective Thermal Conductivity of Potassium Vapor at 0.1 atm	247
K-1	Correction Factor for Thermal Entrance Region	261
M-1	End Effects on Thin-Wall Tube	269

LIST OF TABLES

Table No.		Page
I	Burnout Data for Water	10
II	Burnout Data for Sodium	12
III	Burnout Data on Rubidium	14
IV	Burnout Results on Cesium	18
V	Film Boiling Results	55
VI	Nucleate Boiling Results	60
VII	Comparison of Minimum Heat Fluxes with Theoretical Predictions	65
VIII	Film Boiling Correlations	72
IX	Comparison of Experimental Film Boiling Data	75
X	Comparison of Minimum Heat Flux Data	79
XI	Test Run No. 8 a/g = 1	103
XII	Test Run No. 17	104
XIII	Physical Properties for Saturated Liquids and Vapors at 1 atm	142

APPENDICES

A	Heat Loss Calibration for Film Boiling Apparatus	230
B	Film Boiling Data	231
C	Nucleate Boiling Data	234
D	Preliminary Film Boiling Data	236
F-1	Physical Properties of Potassium	243
H-1	Calibration of Boiling Plate Thermocouples	250
I	Data for Boiling Mercury under High Gravity	251
J-A	Experimental Data - Barry	255
J-B	Experimental Data - Gahman, Sartor and Balzhiser	257
N-A	Pressure Drop Data from 1963 Run for 92% Potassium and 8% Sodium	274
N-B	Pressure Drop Data from 1966 Run for 100% Potassium	278

NOMENCLATURE

a	Acceleration or constant defined by Equation (33)
a'	Constant defined by Equation (37)
A	Area
b	Exponent in Equation (31), constant in Dussler reation, Appendix K
c	Constant defined by Equation (18)
C_p	Heat capacity
D	Diameter
E	Correction factor for thermal entrance region assuming ψ = 1.0 in Appendix K
E'	Correction factor for thermal entrance region assuming ψ = 1.0 in Appendix K
f	Friction factor
F	Flowmeter calibration - Appendix K
g	Acceleration of gravity
g_c	Gravitational constant
G	Mass velocity
Gr	Grashof number
Gr'	Modified Grashof number
h	Heat transfer coefficient
k	Thermal conductivity
K	Constant in Equation (3)
L	Length
m	Mass flow rate
M	Molecular weight
n	Constant

N	Count rate
Nu	Nusselt number
P	Pressure
ΔP	Pressure drop
Pe	Peclet number
Pr	Prandtl number
q	Heat transferred
(q/A)	Heat flux
r_e	Electrical resistivity
R	Gas constant, radius of tube wall, radius of thermocouple well
Ra'	Modified Rayleigh number
T	Temperature
ΔT	Temperature difference
T_f	Surface temperature of the condensate film
u	Local velocity
U	Overall heat transfer coefficient
V	Flowmeter signal, velocity
V_o	Superficial velocity
x	Mass fraction vapor
X	Lockhart - Martinelli parameter
y	Distance from tube wall

Greek Symbols

α	Void fraction, ratio of coolant to condensing heat transfer area, or thermal diffusivity
β	Three phase contact angle
Γ	Mass rate of condensation per unit perimeter

Γ_1 Factor accounting for net condensation Equation (44)

ε_o Normal emissivity

λ Latent heat of vaporization

λ' Effective latent heat of vaporization

μ Viscosity

ρ Density

ϕ Factor in Equation (45); Lockhart - Martinelli two phase multiplier

ψ Ratio of eddy diffusivity for heat to eddy diffusivty for momentum

σ Surface tension, accommodation coefficient

τ Time, shear stress

Subscripts

b Bubble

B Bulk

c Condensing; critical

e Evaporation coefficient

f Film

F.S. Free surface

H.S. Heater surface

i inlet

k Potassium

l Liquid property

m Mean value

min At the minimum heat flux

o Outlet

r Reflected

s	Surface
sat	Saturated
TP	Two Phase
v	Vapor property
w	Wall

CRITICAL HEAT FLUX DETERMINATIONS IN SATURATED POOL BOILING

Bruce F. Caswell

INTRODUCTION

Heat transfer systems utilizing boiling liquid metals provide one method for efficiently exchanging large quantities of heat at relatively high temperature levels. The fact that the first three alkali metals, lithium, potassium and sodium have densities less than water and possess high latent heats of vaporization (approximately equal to water for potassium while up to ten times that of water for lithium) makes them extremely attractive as heat transfer fluids in power cycles for space applications.

In order to determine useful design information for such systems it becomes necessary to simulate actual conditions with relatively simple and yet similar experiments. Ultimately, it would be hoped to derive analytical or semi-empirical expressions, or use previously derived relationships substantiated by liquid metal boiling experiments, or provide reliable engineering design information.

Some liquid metal boiling heat transfer data have been reported, but only a limited amount of burnout data was obtained. Comparison of both the experimental heat transfer and burnout results with theoretical and semi-empirical predictions has shown at best only fair agreement and indicated that more boiling data with different liquid metals is needed.

This investigation was concerned with pool boiling sodium, rubidium and cesium at heat fluxes up to and including the burnout point. The information gathered is used to test existing correlations for nucleate boiling and for the burnout heat flux. The scope of the investigation included operating at different pressures in the range of a few inches of mercury to over atmospheric pressure. A correlation was developed which predicts the critical heat flux for metallic fluids.

REVIEW OF LITERATURE

Experimental Studies

Critical heat flux data at normal gravity for saturated pool boiling of non-metallic fluids, such as water and organic liquids have been reported by several investigators. (6, 9, 28, 29, 36-39, 43, 62, 64, 68, 80, 83, 85, 88, 91, 92, 107, 108, 121, 132, 134, 147, 174, 181.)

Pool boiling burnout data on nitrogen and other liquefied gases were reported by Clark and Merte (44, 126, 127), Lyon (113), Park (142) and Roubeau (157). Sawle (158) published burnout data for sulfur.

Noyes (135-138), who studied sodium, was the first to report liquid metal burnout results. Carbon (35) and Subbotin (167) have also obtained sodium data. Burnout data on potassium were reported by Colver (49, 50). Kutateladze (100) reported results on magnesium amalgam. Recently, Adams (2) obtained subcooled burnout data on magnesium.

The effect on the critical heat flux of heater conductance, thickness and orientation has been studied in part by Averin (6), Bernath (21), Carne (36), Carne and Charlesworth (37), Ishigai (85), Ivey and Morris (88) and Lienhard and Watanabe (108). Frea and co-workers (64) reported results obtained with a porous graphite heater having an air flow through its wall. They also determined the critical flux for water containing varying amounts of calcium sulfate. Costello and Heath (53) studied the interrelation of heater surface conditions and gravitational acceleration on the critical flux. Costello and Frea (52) measured the critical heat flux for water using heaters wrapped in capillary wicking.

Ivey (86, 87) and Costello and Adams (51) have reported data on the effect of gravitational acceleration on the critical heat flux for water. Merte and Clark (44, 126, 127) have reported similar results for liquid nitrogen.

Critical Heat Flux Predictions

As noted by Gambill (67), at least fifty equations have been proposed for predicting critical heat fluxes in various types of boiling regions. Several apply to boiling with forced convection. Many of the correlations are based on data obtained on specific reactor flow channels and cannot be considered as generalized correlations. Only those generalized correlations that apply to saturated pool boiling burnout will be discussed here.

For boiling taking place on heaters of sufficient conductance and size so as not to burn out prematurely, the primary factors influencing burnout seem to be local acceleration, fluid properties and pressure.

The correlation of Rhosenow and Griffith (153) gives a good fit of water and organic fluid pool boiling burnout data and, at the same time, contains fewer factors then most of the other commonly used equations. Their correlation is:

$$(q/A)_c = 143\,\lambda\,\rho_v \left(\frac{a}{g}\right)^{1/4} \left(\frac{\rho_l - \rho_v}{\rho_v}\right)^{0.6} \qquad (1)$$

which is dimensional and requires the units of BTU/(hr)(sq ft), BTU/lb., and lb/ft.^{3}. This correlation is typical of those containing hydrodynamic properties.

Addoms (3) proposed the dimensionless correlation:

$$(q/A)_c = 2.5 \lambda \rho_v (g \alpha)^{1/3} \left(\frac{\rho_l - \rho_v}{\rho_v}\right)^{0.5} \qquad (2)$$

which also agrees well with data on water and organic fluids. Sawle (158) reported that his sulfur data at atmospheric pressure were also in good agreement. Addoms' correlation differs from the purely hydrodynamic ones in that it contains the liquid thermal diffsuivity, α. However, it seems to overpredict slightly the effect of g which has been predicted theoretically and now confirmed experimentally to be a 1/4 rather than 1/3 order effect.

Kutateladze (97-101), from dimensional analysis, developed the following dimensionless equation for predicting pool boiling burnout:

$$(q/A)_c = K \lambda \rho_v^{1/2} \left[g \sigma (\rho_l - \rho_v)\right]^{1/4}, \qquad (3)$$

which agreed well with a large amount of water and organic fluid data. The value of K which he now recommends is 0.13. This correlation was modified by Borishanskii (27) who showed that K is weakly dependent on a dimensionless group which includes μ. Borishanskii also showed that K decreases with pressure.

Zuber (184-187) developed a burnout prediction by analyzing the hydrodynamic instability of a two dimensional model having a vapor-liquid interface. The equation he obtained is as follows:

$$(q/A)_c = 0.137 \lambda \rho_v \left[\frac{\sigma g (\rho_l - \rho_v)}{\rho_v^2}\right]^{1/4} \left[\frac{\rho_l}{\rho_l + \rho_v}\right]^{1/2} \qquad (4)$$

This is essentially the same as Kutataladze's result, however it was derived by theoretical considerations and did not require the correlation of experimental data. It is in good agreement with data on water and organic fluids.

Adams developed a burnout prediction from a three dimensional stability analysis of a cylindrical vortex sheet. He obtained the following equation:

$$(q/A)_c = \frac{6570\ \rho_v\ \lambda}{\left[1 + \left(\frac{\rho_v}{\rho_l}\right)^{1/2}\right]^2} \left(1 + 0.318\ \frac{\rho_l}{\rho_v}\right)^{1/2} \left[\frac{g\ g_c\ \sigma(\rho_l - \rho_v)}{\beta^2\ \rho_l^2}\right]^{1/4} \quad (5)$$

The constants were obtained from $(q/A)_c$, bubble diameter, and bubble contact angle data on water. This prediction is, unfortunately, somewhat limited in usefulness at this time because of the limited availability of data on the three phase contact angle, β, for various combinations of fluids and solids.

Chang and Snyder (41) developed the following burnout prediction by assuming a certain arrangement of bubble sites and analyzing the buoyant and inertial forces on a bubble:

$$(q/A)_c = 1/2 \left(\frac{\pi}{6}\right)^{5/6} (0.0119\ \beta)^{1/2}\ \lambda\ \rho_v^{1/2} \left[g\ \sigma\ (\rho_l - \rho_v)\right]^{1/4} \quad (6)$$

where β is the three phase contact angle which, according to the authors, varies only within a narrow range for water and organic fluids. They also developed a similar equation by two-dimensional interfacial stability analysis. It is as follows:

$$(q/A)_c = 0.145\ \lambda\ \rho_v^{1/2} \left[\frac{\rho_l + \rho_v}{\rho_l}\right]^{1/2} \left[g\ \sigma\ (\rho_l - \rho_v)\right]^{1/4}, \quad (7)$$

which does not differ greatly from the equations of Zuber and of Kutataladze.

Except for Addoms, each of the forementioned investigators developed their burnout correlation by assuming that the critical heat flux in pool boiling is determined by purely hydrodynamic limitations on the two phase counter-current flow of vapor and liquid.

It has been pointed out by several investigators (8, 39, 49, 138) that for liquid metals at moderate pressure nearly all of the hydrodynamic-based correlations predict values of the critical heat flux that are much lower than the measured results. These correlations also overpredict the effect of pressure on the burnout flux for liquid metals. Addoms' correlation predicts values that are higher than the measured results for liquid metals and also overpredicts the effect of pressure.

Because of these discrepancies between the available correlations and his measured results for sodium, Noyes (138) developed a correlation by in serting the factor $(\text{Prandtl number})^n$ into Zuber's correlation. He obtained the following result:

$$(q/A)_c = 0.144\,\lambda\,\rho_v \left[\frac{\rho_l - \rho_v}{\rho_v}\right]^{1/2} \left[\frac{g\,g_c\,\sigma}{\rho_l}\right]^{1/4} Pr^{-0.245}, \qquad (8)$$

which agreed well with his first sodium results and with water and organic fluid burnout data. The range of Prandtl numbers used in obtaining the correlation was from 3×10^{-3} for sodium to 11 for ethanol. Later, Noyes (135) made a similar modification to Addoms' correlation which introduced a dependence on liquid viscosity and corrected Addoms' exponent on local acceleration. It also reduced the exponent on thermal conductivity. He obtained the following:

$$(q/A)_c = 1.19\,\lambda\,\rho_v\,(g\,\alpha)^{1/3} \left(\frac{\rho_l - \rho_v}{\rho_v}\right)^{0.56} \left(\frac{Pr\,g_c}{g}\right)^{1/12}, \qquad (9)$$

which agrees within $\pm$ 30% with 90% of the data used, including results on sodium and sulfur.

In view of the foregoing, it appears that both hydrodynamic and liquid thermal transport properties must be considered in predicting the critical heat flux for all types of fluids. Balzhiser (7) in reviewing the pool temperature profiles measured by Colver suggested that the increase in critical flux observed experimentally over that predicted analytically by the hydrodynamic theory is attributable to a conduction component similar to that which Zuber has treated for subcooled boiling. The contribution in the case of liquid metals however, appeared to result from superheating in the fluid near the surface with a drop to saturation temperatures in the bulk. The effect is similar to that achieved in water for saturation near the surface and subcooled conditions in the bulk except that the higher fluid conductivities in metal systems produce larger heat flows for a given fluid temperature difference between surface and bulk.

All attempts, thus far, to incorporate liquid thermal transport properties into burnout correlations have consisted of strictly empricial modifications of existing expressions. For liquid metals, these modifications raised the predicted value of the critical flux and corrected the pressure dependency to give somewhat better agreement with the experimental results. No experimental or theoretical work has yet been carried out, to our knowledge, which could enable one to gain a more fundamental understanding of the extent to which thermal transport in the liquid influences burnout. This effect should be much more significant for liquid metals than for other types of fluids and, as described previously, it is with liquid metals that the greatest discrepancy exists between the experimental results and the hydrodynamic predictions.

EQUIPMENT AND PROCEDURE

The same equipment was used for these studies as was used by Colver for his potassium work with substantial modification of the guard heaters, vacuum system, and charging procedure. Figure 1 illustrates the apparatus used for this study. Boiling took place from a 3/8-in. O.D. by 1 1/4-in. long Haynes-25 bayonet tube inserted horizontally into a vertical 2-ft. Haynes-25 pipe 2.15-in. O.D. by 2 1/4-in. I. D. The bayonet tube was inserted 2 in. above the bottom of the boiling chamber by means of a Swagelok fitting (see Figure 2). The threaded connection permitted relatively easy replacement of tubes following a destructive burnout. Liquid metal was charged and removed through a tube attached to the base of the vessel.

Five guard heaters, each independently controlled, were installed around the base of the boiling vessel. Nine chromel-alumel thermocouples attached to a 16-point Leeds and Northrup recorder were used for control purposes. Control of the 500-w. units was accomplished manually by using variable transformers. The guard heaters were used to achieve and sustain a temperature level for test purposes and were themselves capable of providing for all heat losses from the pool at the temperatures of these studies.

Condensation occurred in the upper portion of the vessel. Although water coils were available, the system generally radiated sufficient energy to the surroundings without circulating water to maintain steady state conditions for all liquid metal studies. Cooling water was circulated only when boiling water.

The bayonet tube shown in Figure 3 was heated by passing a current through the graphite core. The electrical circuit consisted of the following series resistances: the leads, a molybdenum rod, the graphite, the Haynes cap at the end of the tube, the liquid metal, and the boiling vessel walls. The graphite comprised approximately 90% of the total electrical resistance. A boron nitride sleeve was used to insulate the tube wall from the graphite core as shown in Figure 2. Three longitudinal grooves 0.040-in. wide by 0.040-in. deep were made in the surface of the Haynes bayonet tube. Type-304 stainless steel hypodermic tubes were brazed in these grooves and served as thermocouple wells. Swaged chromel-alumel micro thermocouples 0.020-in. diameter, obtained from Pyro Electric Company, were inserted in the wells and were used to detect surface temperature excursions resulting from burnout. Each was connected to a Leeds and Northrup Speedomax H recorder which had a full scale response time of 1 sec. An alarm circuit attached to the recorders automatically cut off power to the boiling tube when a temperature excursion of several hundred degrees occurred.

Approximately 6 in. of liquid was charged for each run. The depth was determined by noting a temperature change on a moveable thermocouple which entered the chamber at the top through a Conax gland and extended

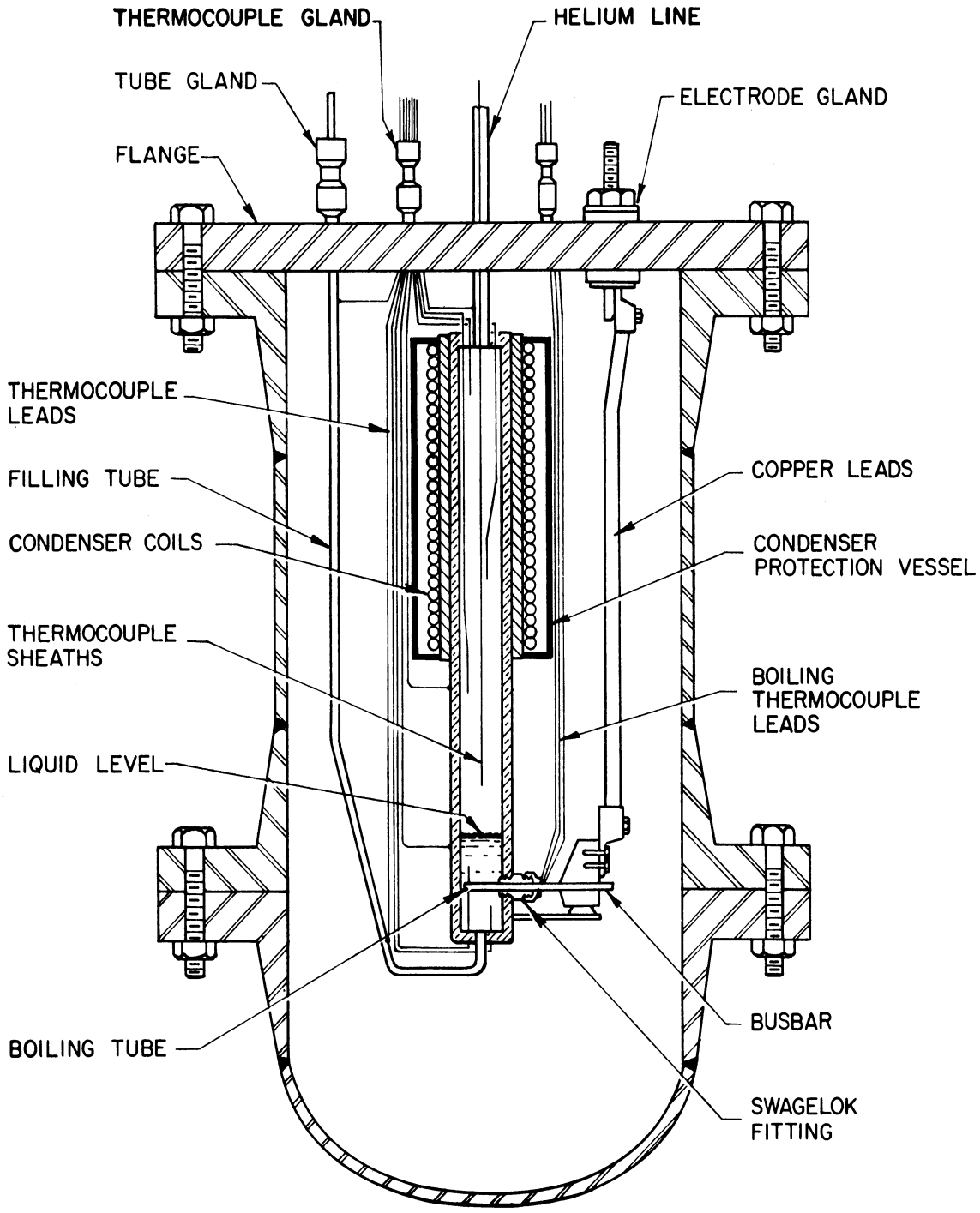

Figure 1 Apparatus Used in Study

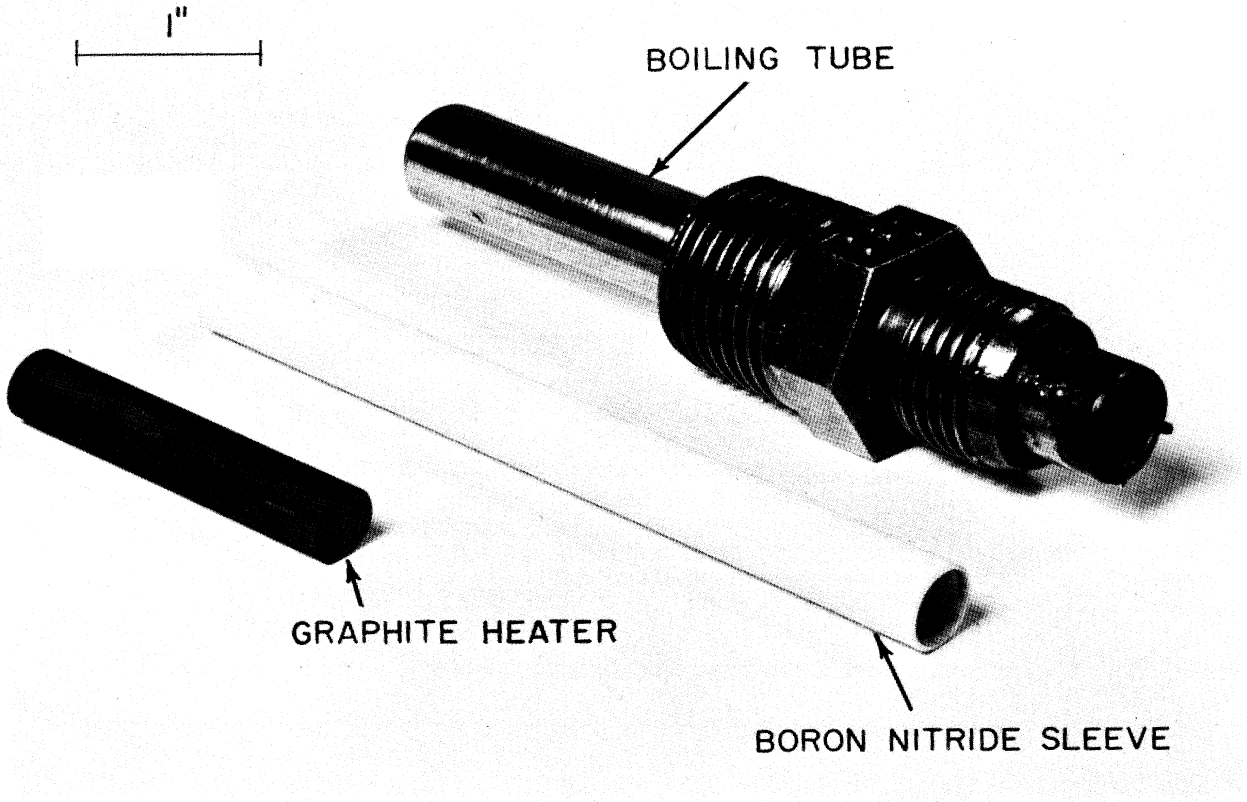

Figure 2 View of Boiling Tube Assembly

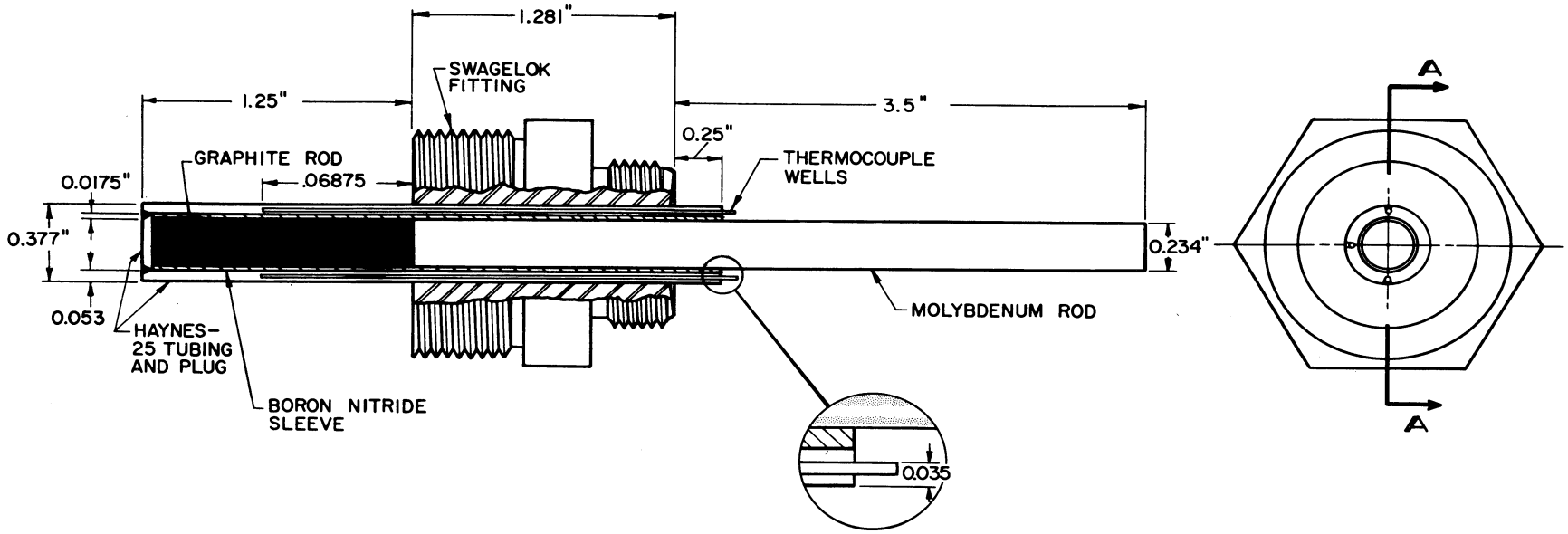

Figure 3 Cross Sectional Drawing of Boiling Tube Assembly

down the axis of the vessel to the pool. It was also used to measure pool temperatures at different positions during burnout determinations. The couple enclosed in a 3/16-in. stainless steel sheath was made of chromel-alumel and was calibrated against a platinum-plantinum rhodium (10%) standard before use. Pressures were measured with a mercury manometer.

Burnout determinations were made by two procedures; the first involved fixing the heat flux at the tube surface and lowering the system pressure until burnout occurred. The second method involved increasing the heat flux at a given pressure level until a temperature excursion took place at the surface. Reproducible and consistent results were obtained from the two methods.

Current measurements combined with the voltage drop across the boiling tube permitted a calculation of the surface heat flux. Fluid temperatures and pressures were measured directly as described elsewhere and checked for consistency with vapor pressure data in the literature.

EXPERIMENTAL RESULTS

Water

Initial studies were performed with water in the system to permit a comparison of burnout data from this apparatus with data in the literature. Such a comparison was deemed desirable to determine if system dimensions or geometries were likely to produce any abnormal effects on burnout results.

TABLE I

BURNOUT DATA FOR WATER

Pressure, lb./sq. in. abs.	$(q/A)_c$, B.t.u./(hr.)(sq. ft.)
15	490,000
15	425,000
15	485,000
35	740,000
80	705,000
118	765,000
118	800,000
135	845,000

The burnout heat flux for water was measured at pressures from 15 to 135 lb./sq. in. abs. The data are presented in Table I and are compared in

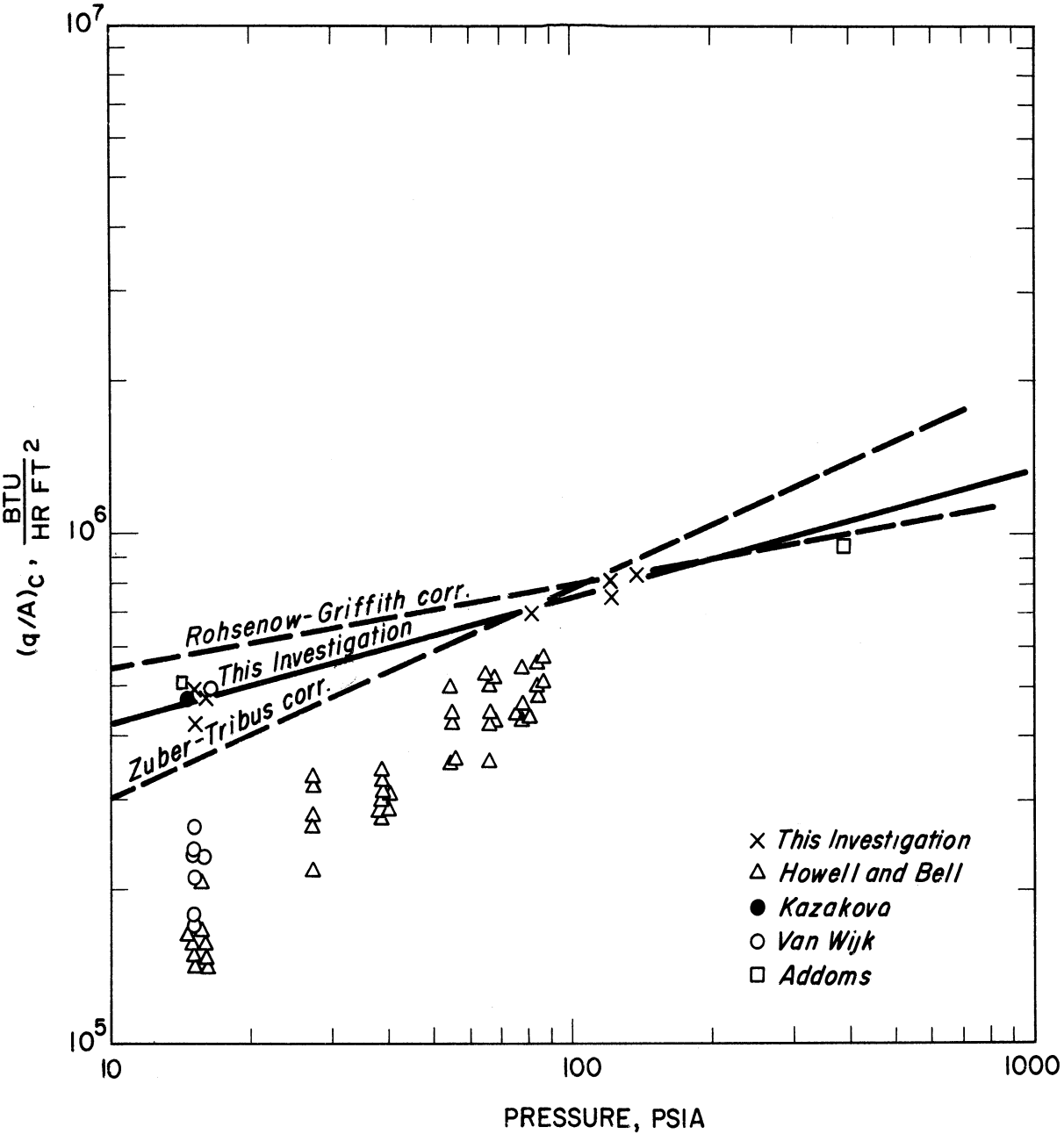

Figure 4 Comparison of Water Data with Correlations

Figure 4 with the results of Kazakova (92), from a flat plate; Addoms (3), from 0.024-in. platinum wire; Van Wijk (174), from a 0.02 x 6 cm. platinum wire; and Howell and Bell (80), from a 0.001-in. stainless steel strip. The predictions of Rohsenow-Griffith (153) and Zuber (187) are shown as dotted lines on the graph. The data from this work agree well with the data of Addoms and Kazakova but are above the results of Howell and Bell and Van Wijk. It is possible that the data of the latter two investigators, since it was taken on thin strips and wire, respectively, represents premature burnout of the heater.

The pressure dependency of the burnout heat flux measured here is 0.25 and is lower than that predicted by the Zuber correlation but slightly higher than that of the Rohsenow-Griffith correlation.

Sodium

Two burnout points for sodium were obtained. These data are tabulated in Table II and plotted in Figure 5 along with the results of other investigators.

TABLE II

BURNOUT DATA FOR SODIUM

Run	Pressure	$T_{saturated}$	$(q/A)_c$, B.t.u./(hr.)(sq. ft.)
A-2	0.80 lb./sq. in. abs.	1,150°F	530,000
A-3	2.15 lb./sq. in. abs.	1,300°F	845,000

The burnout points were obtained by maintaining a constant heat flux while slowly decreasing the pressure until burnout occurred. In run A-2 the temperature of the heating surface was fluctuating 200°F just before burnout occurred. A sudden temperature excursion during which the surface temperature exceeded its normal peak fluctuating temperature by several hundred degrees was used as an indication of burnout. The power was immediately shut off and a second point obtained the following day at a higher pressure with the same boiling tube. No apparent damage had been done to the boiling tube in the first burnout excursion.

In run A-3 a hole was formed in the boiling tube during rapid temperature fluctuations, and the run was stopped without being certain that burnout had occurred. The fluctuations were slightly less in magnitude and were

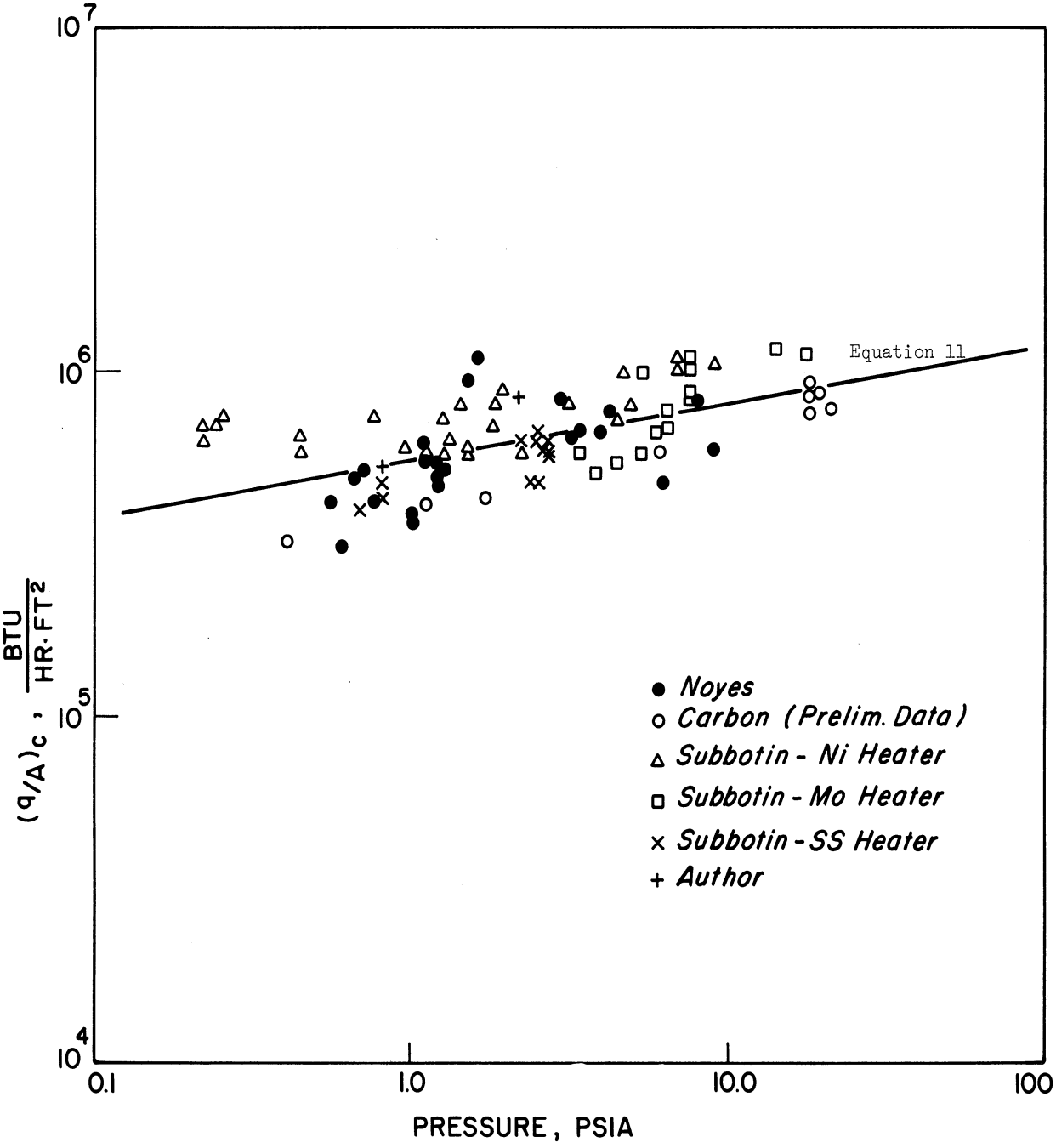

Figure 5 Comparison of Sodium Burnout Data with Correlation

accompanied by a gradually rising surface temperature. In this respect, this burnout was unlike those observed in earlier runs. The absence of a sudden large temperature excursion introduces some doubt as to the nature of the process occurring just prior to shutdown.

Similar behavior was encountered in run A-1 when a gradual temperature excursion occurred which required about a minute to cause the surface temperature to rise close to its melting point. This could be due to a gradual lowering of the sodium level below the tube. Holdup in the condenser may increase at higher pressures resulting in a drop in the liquid level. The pressure level and flux at which it occurred were about the same as in run A-3. It resembled run A-3 except that it was made by increasing the heat flux at constant pressure.

Figure 5 is a plot of all the sodium burnout data known to the authors. The correlations of Zuber-Tribus (187), Noyes (135), Rohsenow-Griffith (153) and this author (to be discussed later) are plotted for comparison.

Most of Noyes' data were taken on a 1/4-in. O.D., horizontal, stainless steel heater. Carbon's data were for a 0.443-in. O.D. stainless steel heater. The heater used in this work was a 3/8-in. O.D. by 1 1/4-in. long Haynes-25 horizontal bayonet tube.

Rubidium

Thirteen burnout points were obtained for rubidium from 0.5 to 28 lb/sq. in. abs. These are presented in Table III. The results are plotted in Figure 6.

TABLE III

BURNOUT DATA FOR RUBIDIUM

Run	Pressure	$(q/A)_c$, B.t.u./(hr.)(sq. ft.)
1	0.5 lb./sq. in. abs.	305,000
2	2.8 lb./sq. in. abs.	360,000
3	3.0 lb./sq. in. abs.	345,000
4	6.0 lb./sq. in. abs.	310,000
5	6.0 lb./sq. in. abs.	330,000
6	9.0 lb./sq. in. abs.	400,000
7	15.0 lb./sq. in. abs.	430,000
8	20.5 lb./sq. in. abs.	450,000
9	26.8 lb./sq. in. abs.	397,000
10	27.2 lb./sq. in. abs.	397,000
11	27.4 lb./sq. in. abs.	400,000
12	16.1 lb./sq. in. abs.	418,000
13	19.4 lb./sq. in. abs.	425,000

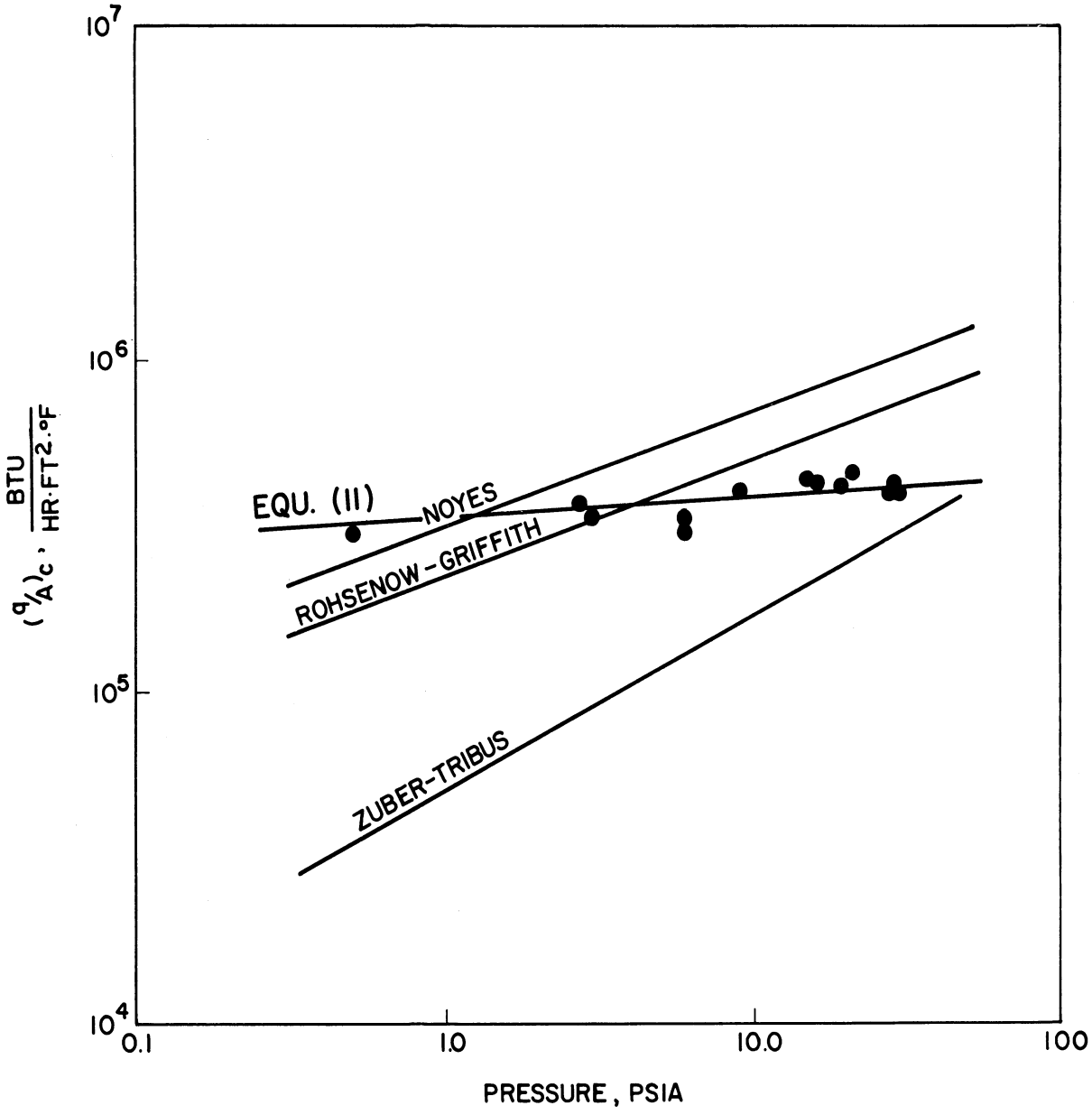

Figure 6 Comparison of Rubidium Burnout Data with Correlations

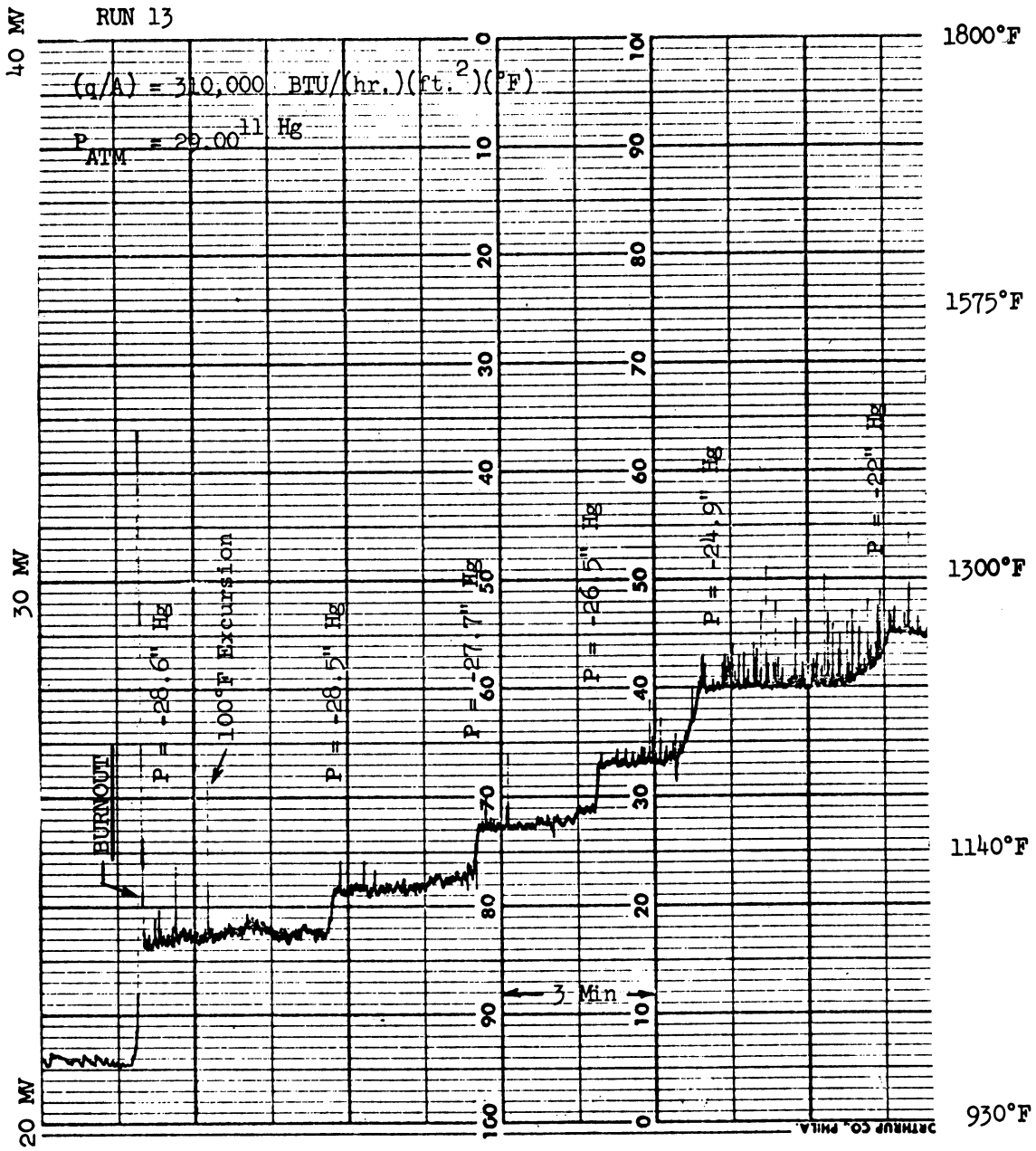

Figure 7 Heater Surface Temperature

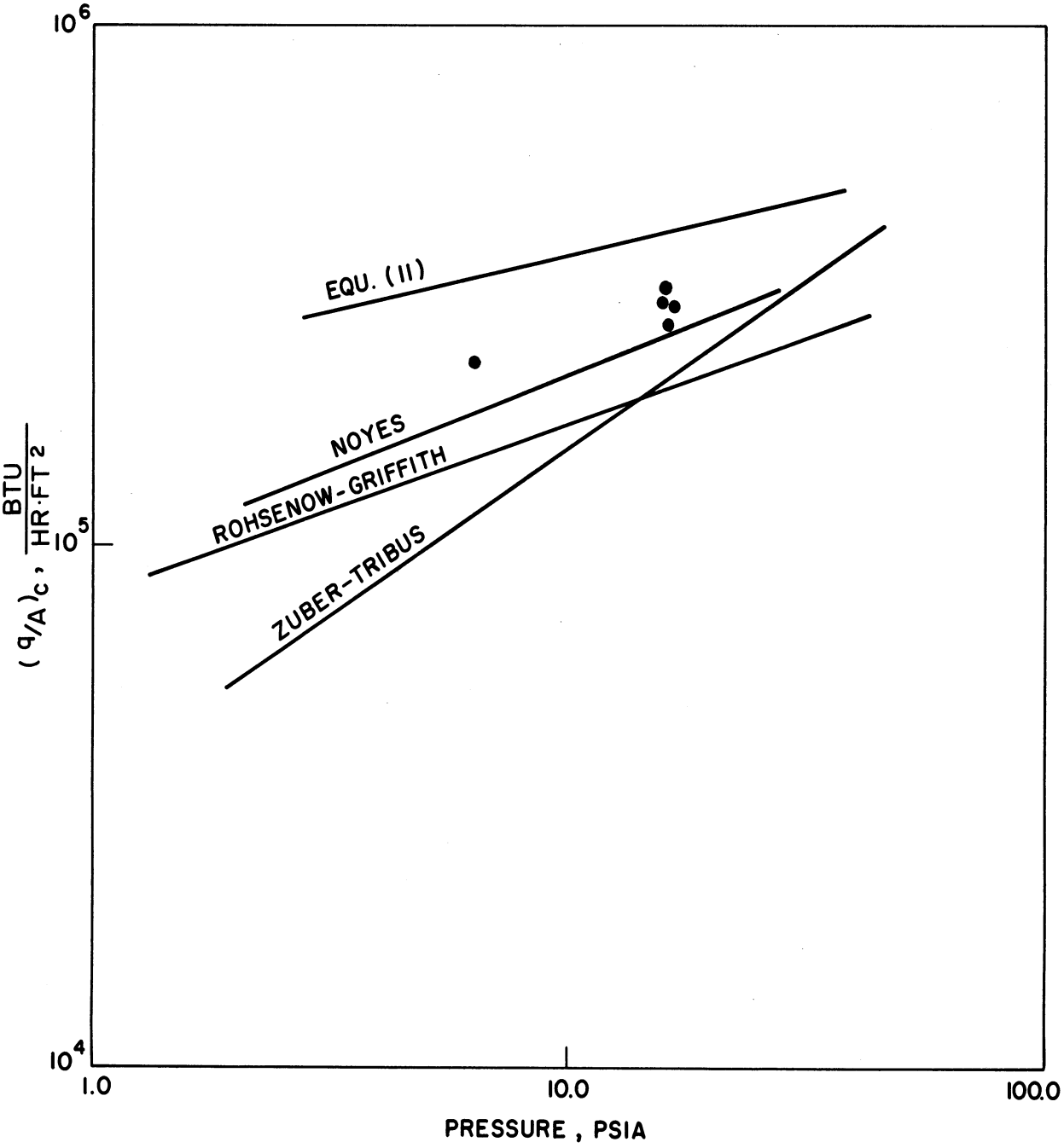

Figure 8 Comparison of Cesium Data with Author's Correlation

Depending on how one weighs the point at 0.5 lb./sq. in. abs., it is possible to obtain a pressure dependency of from 0.1 to 0.18. The low pressure point was corrected for the pressure head of the rubidium pool before plotting. These burnouts were obtained by both procedures with good agreement. Figure 7 is a heater surface temperature record made during a run in which pressure was reduced while heat flux was held constant. Temperature measurements in the liquid pool indicated superheat during the runs tending to confirm the earlier suggestion by Balzhiser (7) that conduction effects in liquid metals must not be ignored.

Cesium

One pound of cesium metal of 99.9% purity, purchased from the MSA Research Corporation, was charged to the equipment, using the same procedure as discussed previously.

A heater was fabricated by machining the cylindrical part from a solid piece of Haynes-25 rod, rather than from tubing. It was thought that this would be somewhat more resistant to failure at the closed end than those used previously, which were closed by welding a Haynes-25 disc over the end of the tubing. However, after three runs it failed at one of the thermowell grooves.

Five data points were obtained on cesium, using the same procedure as before, The results are listed in Table IV and plotted in Figure 8.

TABLE IV

BURNOUT RESULTS ON CESIUM

Run	p, psia	$(q/A)_c$, B.t.u./(hr.)(sq. ft.)
C1	6.3	225,000
C2	15.9	292,000
C3	16.0	307,000
C4	16.1	262,000
C5	16.6	285,000

CORRELATION OF CRITICAL HEAT FLUX

Flux Results

Noyes (135) proposed a slight modification of Addoms' (3) critical heat flux correlation to increase its applicability to metallic fluids and sulphur.

His expression

$$\frac{(q/A)_c}{\lambda\, \rho_v (g\, \alpha)^{1/3}\, (Pr/n)^{1/12}} = 1.19 \left[\frac{\rho_l - \rho_v}{\rho_v}\right]^{0.56} \qquad (10)$$

correlated 90% of the data (metallic and nonmetallic) on which the expression was based within $\pm$ 30%. Colver's potassium data exhibits a definite departure trend from this correlation as pressure is increased. Thus, an effort has been made to accomplish two goals: provide an expression which predicts reliably burnout levels for metallic fluids and extend, if possible, the correlation to any fluid.

All of the alkali metal burnout data presently available are represented in Figure 9. The potassium line represents the data of Colver, and the sodium line is a least-squares fit of the data from three investigators. The rubidium and cesium data were obtained in this study. These results representing sixty-five data points for sodium, potassium, rubidium and cesium were correlated as shown in Figure 10. The following nondimensional equation resulted:

$$\left[\frac{(q/A)_c\, C_p\, \sigma}{\lambda^2\, \rho_v\, k}\right] = 1.18 \times 10^{-8} \left(\frac{\rho_l - \rho_v}{\rho_v}\right)^{0.71} \qquad (11)$$

where all properties are at saturation conditions. It is noteworthy that the data used cover a significant range of values of the various properties. For instance, the value of λ^2 varied over twentyfold, k varied threefold, C_p fourfold, σ fourfold, ρ_v twentyfold, ρ_l twofold, and $(q/A)_c$ varied almost fourfold.

The above correlation was modified by introducing the Prandtl number to the 0.71 power in order to include both metallic and nonmetallic data on a single line. This is shown in Figure 11. The following dimensionless correlation was obtained:

$$\left[\frac{(q/A)_c\, C_p\, \sigma}{\lambda^2\, \rho_v\, k}\right] Pr^{-0.71} = 1.02 \times 10^{-6} \left[\frac{\rho_l - \rho_v}{\rho_v}\right]^{0.65} \qquad (12)$$

This covers a range of Prandtl numbers from 0.004 to 11, a factor of about 3,000, and is recommended for predicting the critical heat flux of materials where the physical properties are known or can be estimated. In view of the limited amount of data at accelerations other than normal gravity, no attempt was made to introduce a parameter accounting for such effects.

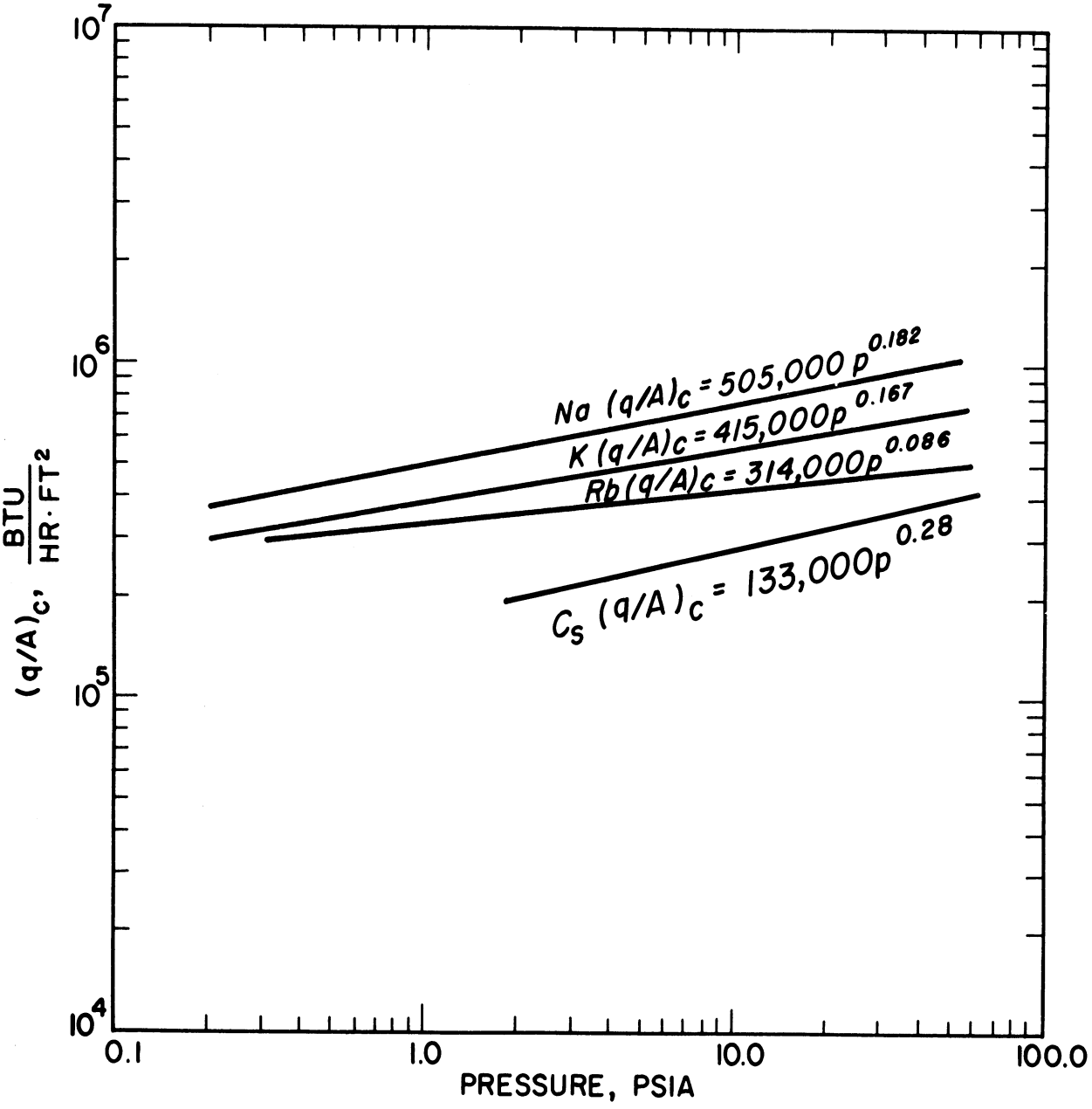

Figure 9 Summary of Alkali Metal Burnout Data

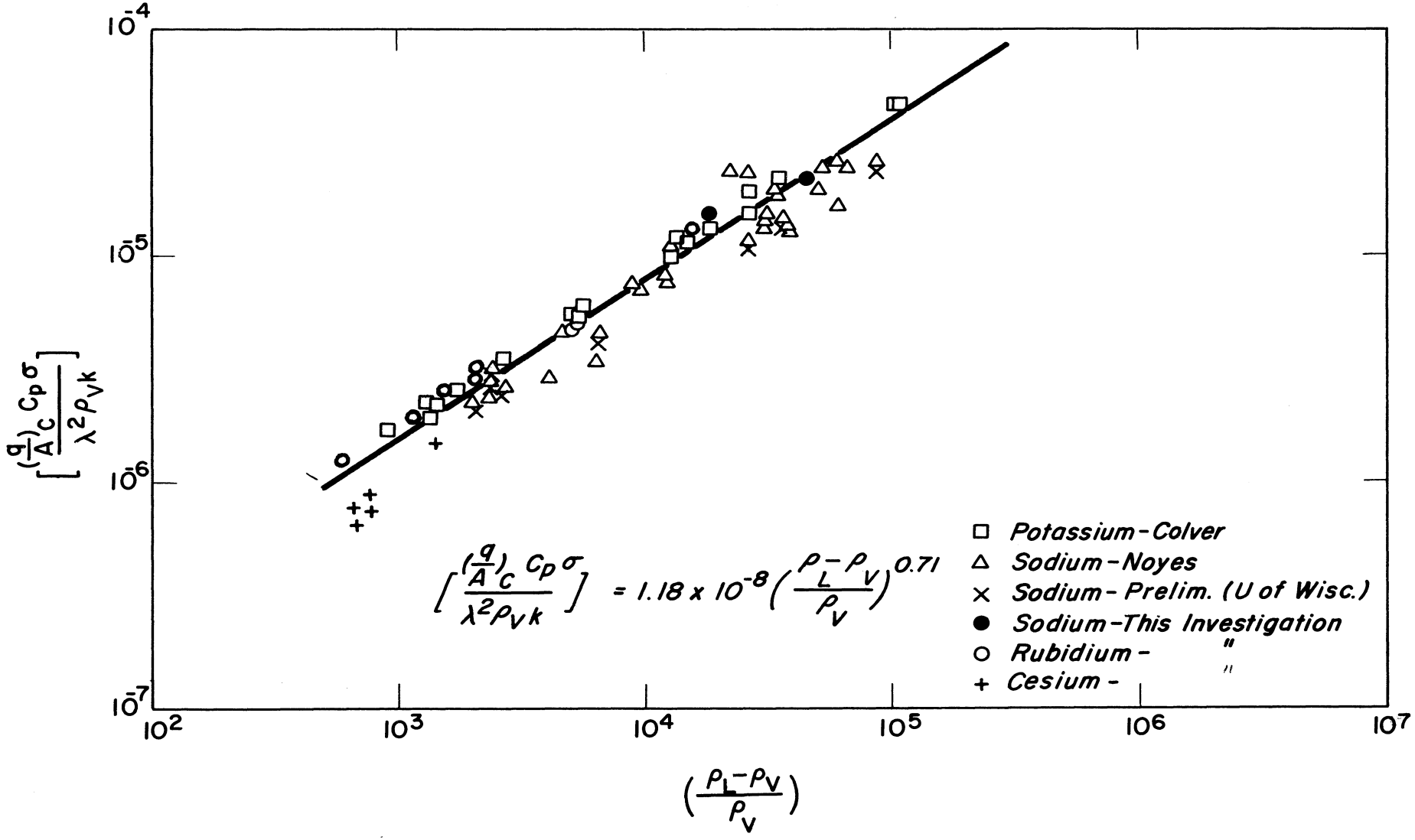

Figure 10 Correlation of Alkali Metal Burnout Data

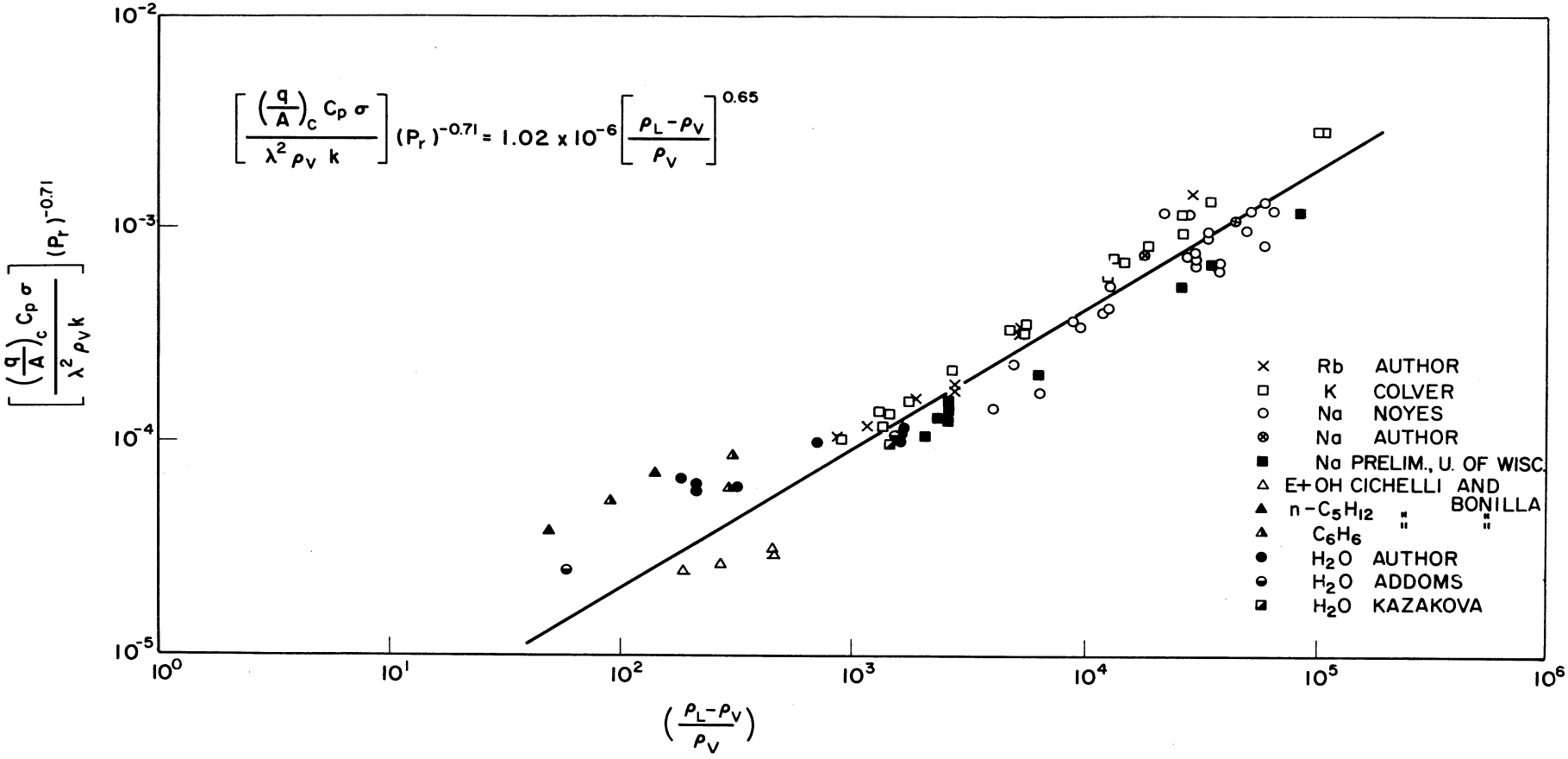

Figure 11 Correlation of Burnout Data

FILM BOILING IN POTASSIUM

Andrew Padilla, Jr.

INTRODUCTION

The design of high-temperature heat transfer systems utilizing high surface heat fluxes has led to the relatively recent interest in liquid metals. The low vapor pressure of liquid metals compared to that of water and organic fluids makes lighter designs possible. Their high thermal conductivity affords potentially higher heat transfer rates which would result in a substantial reduction in the required heat transfer area. Much of the current research being carried out on liquid metals has resulted from the feasibility of its being used as the working fluid in energy conversion cycles with nuclear reactors, especially in space applications. Even with terrestial nuclear power stations, the use of liquid metals over other fluids would greatly increase the thermodynamic efficiency of the power cycle.

Useful design information for liquid metal systems can be provided by relatively simple pool boiling experiments. They are considerably easier to set up than forced convection loops and would determine the lower heat transfer limit of the flowing system. Furthermore, the qualitative effects of additives and other similar changes in loop operation can be more easily obtained.

Unlike nucleate boiling, the film-boiling regime has been the subject of relatively few analytical and experimental investigations. Energy transfer in film boiling occurs by conduction, convection, and radiation across a layer of vapor which separates the liquid from the heating surface. Since the fluxes attainable in film boiling are usually much lower than in nucelate boiling, equipment is invariably operated to avoid passing into this regime. However, it is advantageous to operate as close as possible to the critical heat flux thus increasing the possibility of encountering film boiling. A knowledge of the entire boiling curve and the thermal capacity of a system would help the designer to determine whether transition from nucleate to film boiling would result in catastrophic failure of the heat transfer surface.

Except for mercury, which film boils at a relatively low temperature difference between the heating surface and the liquid because of its non-wetting characteristics, there has been little pool boiling data in the film regime for liquid metals. The object of this investigation was to experimentally determine the heat transfer to potassium in the stable film-boiling regime. The experiments were conducted on a pool-boiling apparatus utilizing a 3-inch diameter horizontal surface facing upwards and the heat flux-temperature difference relationship at various pressures were obtained. The experimental results have been used to test existing correlations for film boiling.

LITERATURE REVIEW

1. Film Boiling Correlations

Although the first definite observation of film boiling occurred in 1934 by Nukiyama (140), the first analytical treatment did not appear until 1950 when Bromley (31) presented his theory of stable laminar film boiling from a horizontal cylinder based on Nusselt's derivation for laminar film condensation. His results can be expressed as

$$h = 0.62\left[\frac{k_v^3 \rho_v (\rho_l - \rho_v) g \lambda'}{D\, \Delta T\, \mu_v}\right]^{1/4} \tag{13}$$

Equation (13) can be rearranged into the following form:

$$\frac{hD}{k_v} = 0.62\left[\frac{D^3 \rho_v (\rho_l - \rho_v) g}{\mu_v^2} \frac{\lambda'}{C_{pv} \Delta T} \left(\frac{C_p \mu}{k}\right)_v\right]^{1/4} \tag{14}$$

or

$$Nu = 0.62\ (Ra')^{1/4} \tag{15}$$

where Ra' denotes a modified Rayleigh number.

Bromley corrected his heat-transfer coefficient for radiation by assuming infinite parallel-plate radiation.

In 1959, Chang (40) introduced his wave theory for film boiling from a horizontal surface based on hydrodynamic considerations alone. He assumed that the phenomenon would exhibit waves whose lengths would be equal or less than the critical value for the existence of a standing wave over a horizontal surface. He then utilized the concept of an equivalent thermal diffusivity of the vapor-liquid interface due to phase change and derived an expression for the heat transfer coefficient for a saturated liquid:

$$h = \left[\frac{k_v^2 \rho_v (\rho_l - \rho_v) g \lambda}{4 \pi^2\, \Delta T\, \mu_v}\right]^{1/3} \tag{16}$$

Zuber (186, 187) later followed the approach suggested by Chang and assumed that a more significant wavelength might be the most dangerous wavelength; that is, the one for which the amplitude of the vapor-liquid interface grows most rapidly. By assuming that the process is governed by a two-phase Taylor instability, he derived an equation for predicting the minimum heat flux:

$$(q/A)_{min} = c\lambda'\rho_v\left[\frac{\sigma g_c g(\rho_l-\rho_v)}{(\rho_l+\rho_v)^2}\right]^{1/4} \tag{17}$$

where the constant c can have the range

$$\frac{\pi}{24}\frac{1}{(3)^{1/4}} \leqslant c < \frac{\pi}{24}\frac{0.4\,\pi\sqrt{2}}{(3)^{1/4}} \tag{18}$$

The uncertainty in the constant c arises because of the uncertainty of various assumptions in the derivation. Zuber's analysis predicts the minimum heat flux from the bubble spacing, bubble size, and bubble frequency from hydrodynamic considerations alone and does not take into account any thermal transport process.

Berenson (18, 19) modified and extended Zuber's approach and obtained relations for the heat-transfer coefficient, the minimum heat flux, and the temperature difference at the minimum:

$$h = 0.425\left[\frac{k_v^3\rho_v(\rho_l-\rho_v)g\lambda'}{\mu_v\Delta T\sqrt{\frac{g_c\sigma}{g(\rho_l-\rho_v)}}}\right]^{1/4} \tag{19}$$

$$(q/A)_{min} = 0.09\,\rho_v\lambda'\left[\frac{g(\rho_l-\rho_v)}{\rho_l+\rho_v}\right]^{1/2}\left[\frac{g_c\sigma}{g(\rho_l-\rho_v)}\right]^{1/4} \tag{20}$$

$$\Delta T_{min} = 0.127\,\frac{\rho_v\lambda'}{k_v}\left[\frac{g(\rho_l-\rho_v)}{\rho_l+\rho_v}\right]^{2/3}\left[\frac{g_c\sigma}{g(\rho_l-\rho_v)}\right]^{1/2}\left[\frac{\mu_v}{g_c(\rho_l-\rho_v)}\right]^{1/3} \tag{21}$$

Equation (19) can be rearranged into the following form:

$$\frac{h}{k_v}\,4.7\sqrt{\frac{g_c\sigma}{g(\rho_l-\rho_v)}} = 0.63\left[\left(4.7\sqrt{\frac{g_c\sigma}{g(\rho_l-\rho_v)}}\right)^3\,\frac{\rho_v(\rho_l-\rho_v)g}{\mu_v^2}\,\frac{\lambda'}{C_{pv}\Delta T}\left(\frac{C_p\mu}{k}\right)_v\right]^{1/4} \tag{22}$$

Since Berenson predicts that the diameter of bubbles produced during film boiling from a horizontal surface is given by

$$D_b = 4.7\sqrt{\frac{g_c\sigma}{g(\rho_l-\rho_v)}} \tag{23}$$

Equation (13) can be written as

$$\frac{hD_b}{k_v} = 0.63\left[\frac{D_b^3\rho_v(\rho_l-\rho_v)g}{\mu_v^2}\frac{\lambda'}{C_{pv}\Delta T}\left(\frac{C_p\mu}{k}\right)_v\right]^{1/4} \tag{24}$$

or,

$$Nu = 0.63\ (Ra')^{1/4} \tag{25}$$

Hence, Berenson's correlation for film boiling from a horizontal surface is practically identical with Bromley's correlation for a horizontal tube if the proper characteristic length is used.

Frederking, et al (65) analyzed film boiling about a sphere assuming a turbulent, free convection process and obtained:

$$h = 0.14\left[\frac{k_v^2\rho_v(\rho_l-\rho_v)g\lambda'}{\mu_v\Delta T}\right]^{1/3} \tag{26}$$

Note that no effect of size is predicted. This is because the correlation was derived in the form:

$$Nu = 0.14\ (Ra')^{1/3} \tag{27}$$

or,

$$\frac{hD}{K_v} = 0.14\left[\frac{D^3\rho_v(\rho_l-\rho_v)g}{\mu_v^2}\frac{\lambda'}{C_{pv}\Delta T}\left(\frac{C_p\mu}{k}\right)_v\right]^{1/3} \tag{28}$$

Equation (27) is similar in form to Bromley's correlation for a horizontal tube [Equation (15)] Bromley's coefficient is 0.62 instead of 0.14 and his exponent is 1/4 instead of 1/3.

The correlations above have been presented because they involve film boiling from a horizontal surface or can be compared to correlations for horizontal surfaces. Other film-boiling correlations are discussed in

several literature surveys: Drew and Mueller (158), Westwater (180), McFadden and Grosh (123, 124), Balzhiser, et al (10), and Kepple and Tung (93).

2. Liquid Metal Film Boiling Experiments

Lyon (114) was the first investigator to make an extensive study of boiling heat transfer to liquid metals. The metals considered were mercury, mercury containing 0.10% sodium, mercury containing 0.02% magnesium and 0.0001% titanium, sodium, sodium-potassium alloy (56-59 wt % K), and cadmium. The test section consisted of a 3/4-inch OD horizontal cylinder 5 inches long made from type 316 stainless steel. Lyon experienced only film boiling for pure mercury and cadmium and attributed this effect to their non-wetting characteristics. Figure 12 shows Lyon's film-boiling data along with Bromley's correlation for comparison.

Bonilla (26) also studied the pool boiling of mercury with and without wetting agents. The apparatus consisted of a horizontal surface made of low carbon steel fitted with a 3-inch OD stainless steel tube which served as a container and condenser. Figure 13 shows the results for mercury boiled in a 2-cm-deep pool at various pressures. Bonilla concluded that all of the 50 to 200 mm curves represented film boiling. In the initial runs, film boiling was invariably obtained regardless of how low the heat flux was. After the boiling surface had been in frequent operation for a few weeks, film boiling was never obtained. This was attributed to the mechanical removal of oxygen or oxide which yielded better wetting of the surface by the mercury.

Lin, et al (109) performed experiments with pure mercury at atmospheric pressure. No mention was made in the article about the experimental apparatus and procedure. The system was observed to enter the film-boiling regime at very low temperature differences.

It was found that the heat-transfer coefficient could be expressed by

$$h = 4850\ (q/A)^{-0.26}\ \text{Kcal/hr-in}^2\text{-°C} \qquad (29)$$

The experimental values correlated by Equation (29) fell about 50% above the theoretical line corresponding to Bromley's prediction.

Merte (125) traversed the entire boiling curve in studies with mercury using a 2-inch diameter horizontal surface made of type 347 stainless steel. The data is shown in Figure 14 along with Berenson's correlation for comparison. To determine the approximate region of the minimum heat flux, the power was reduced in small increments until the system reverted to nucleate boiling. The minimum heat flux occurred within the range 23,000-27,000 BTU/hr-sq ft at a ΔT of approximately 140°F.

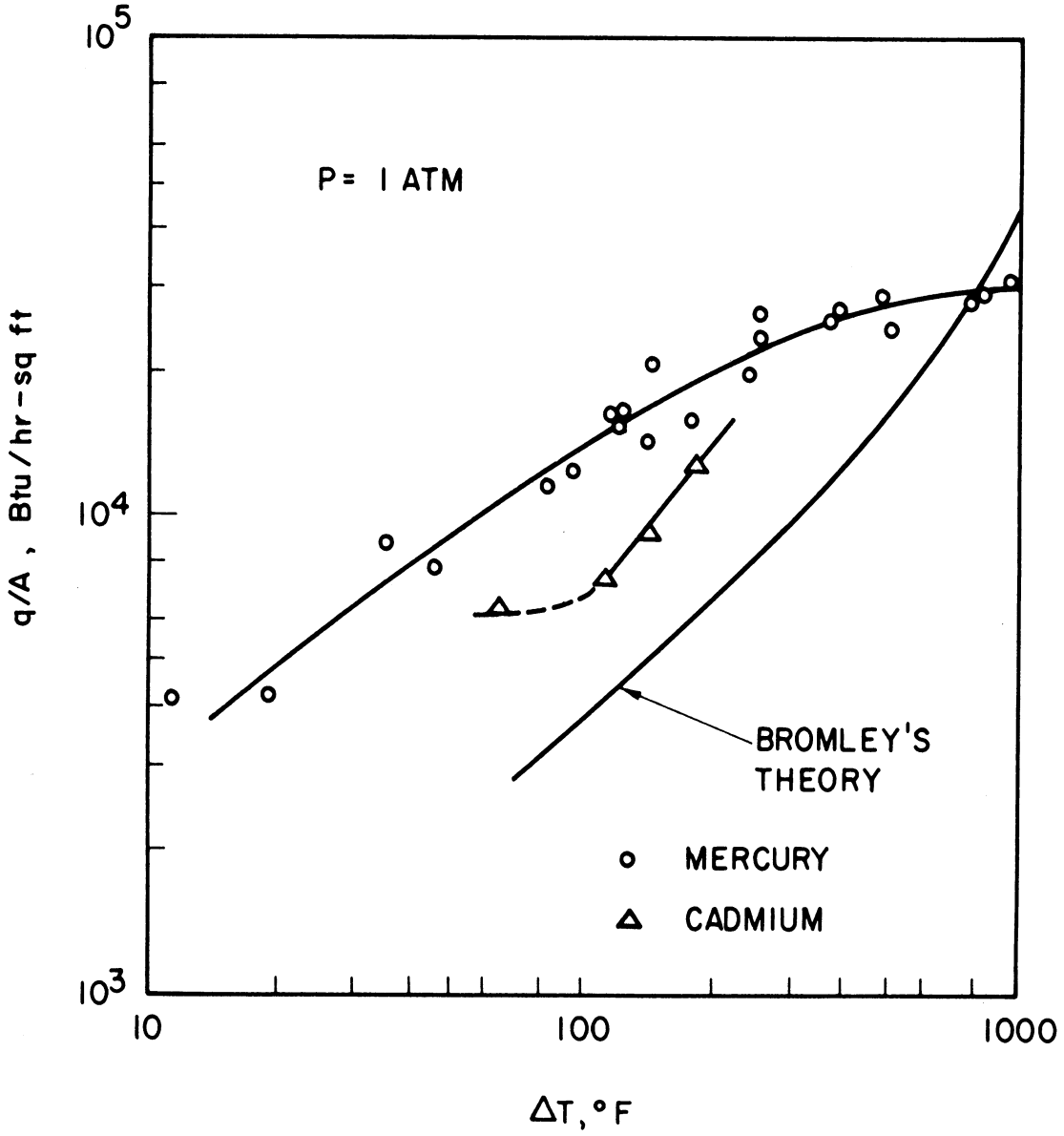

Figure 12. Date of Lyon (114) for Film Boiling of Mercury and Cadmium

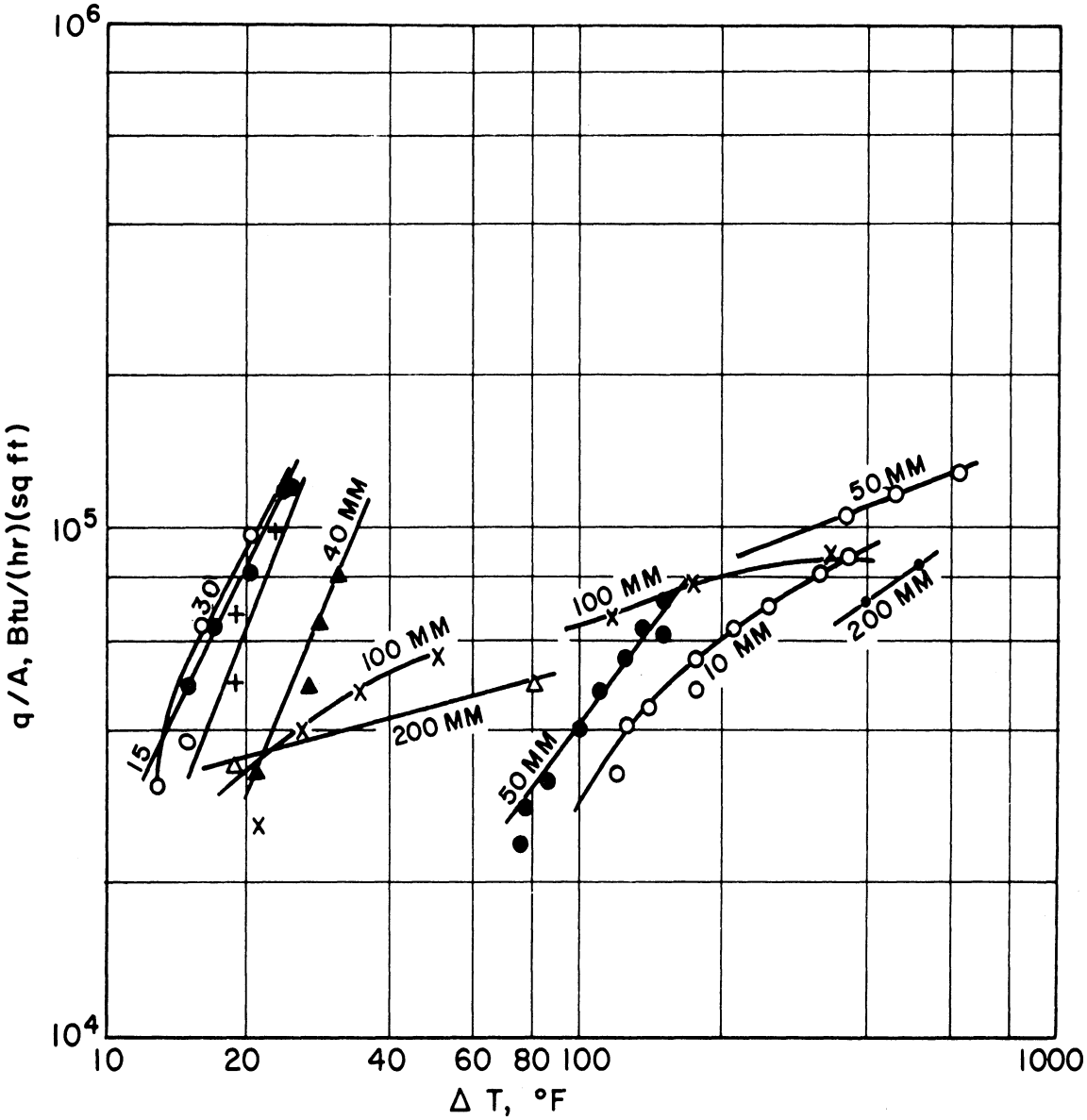

Figure 13. Data of Bonilla (26) for Pool Boiling of Mercury; parameter: pressure over the liquid in mm Hg absolute or lb/sq in. gauge

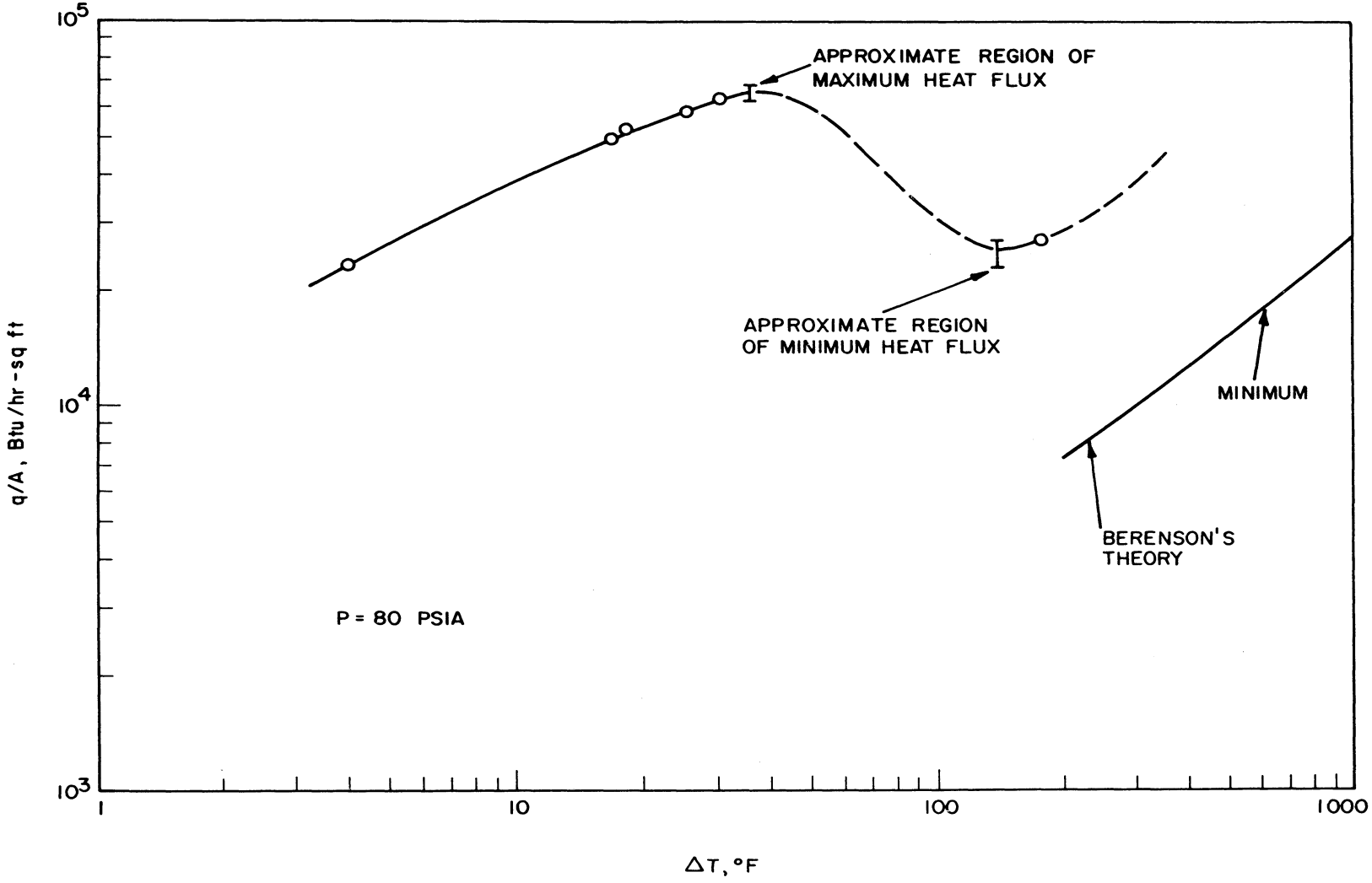

Figure 14 Data of Merte (125) for Saturated Pool Boiling of Mercury

Although there have not been any pool boiling studies of potassium in film boiling, data is available for droplet vaporization and forced convection. Poppendiek, et al (143, 144, 145) have carried out analytical and experimental studies on the vaporization of droplets suspended above a hot surface by a vapor film. They experimentally measured the lifetimes of droplets of water, mercury, potassium, benzene, Freon 11 and Freon 114 and compared them with their predictions. For the vaporization of mercury droplets on a nickel-plated copper plate, 87% of the data fell within 20% of the predicted lifetimes. The potassium droplet experiments were carried out in an argon atmosphere on nickel, stainless steel, Haynes 25, iron, and tantalum surfaces. In most of the runs, a definite surface conditioning process was observed such that the observed lifetimes increased with the number of droplets vaporized on the surface. However, the stainless steel surfaces did not appear to be subject to conditioning. With the exception of the tantalum surface, the lifetimes observed for quiet, stable film boiling droplets of potassium fell about the same amount (30-50%) above the predicted curve as did the other liquids. A marked increase in droplet lifetimes occurred at a surface-to-drop temperature difference of approximately 350°F, indicating the onset of complete film boiling. The lifetimes of two steady potassium droplets on a heated tantalum surface were almost a factor of two higher than the predictions.

Boiling coefficients for potassium in forced convection have been obtained by the General Electric Co. (69) using a 0.938 inch ID Mo-0.5% Ti boiler tube. The transition and film-boiling coefficients for qualities between 30% and 90% are shown in Figure 15. Extrapolation of the curve to 100% quality gives an estimated film-boiling coefficient range of 30-70 BTU/hr-sq ft-°F.

3. Discussion

Film-boiling data for non-metallic fluids have been used to test the correlations discussed in Section 1. Berenson (19) found that his results for n-pentane and Cl_4 on a 3-inch diameter horizontal surface agreed within $\pm$ 10% with his predictions. Hosler and Westwater (79) obtained data for water and Freon 11 on an 8-inch-square horizontal surface and concluded that Berenson's method for predicting the film-boiling curve is good, but his prediction for the ΔT at the minimum flux is not reliable. They also found that a good estimate of the minimum flux was given by the higher estimate of Zuber and that the method of Chang for predicting the film-boiling curve was not reliable. The nitrogen data of Lewis, Merte and Clark (106) using 1-inch, 1/2-inch and 1/4-inch spheres agreed well with the correlation of Frederking, et al.

The available pool-boiling data for mercury of Lyon (114), Bonilla (26), Lin (109), and Merte (125) are characterized by relatively high fluxes at moderate temperature differences and are considerably above

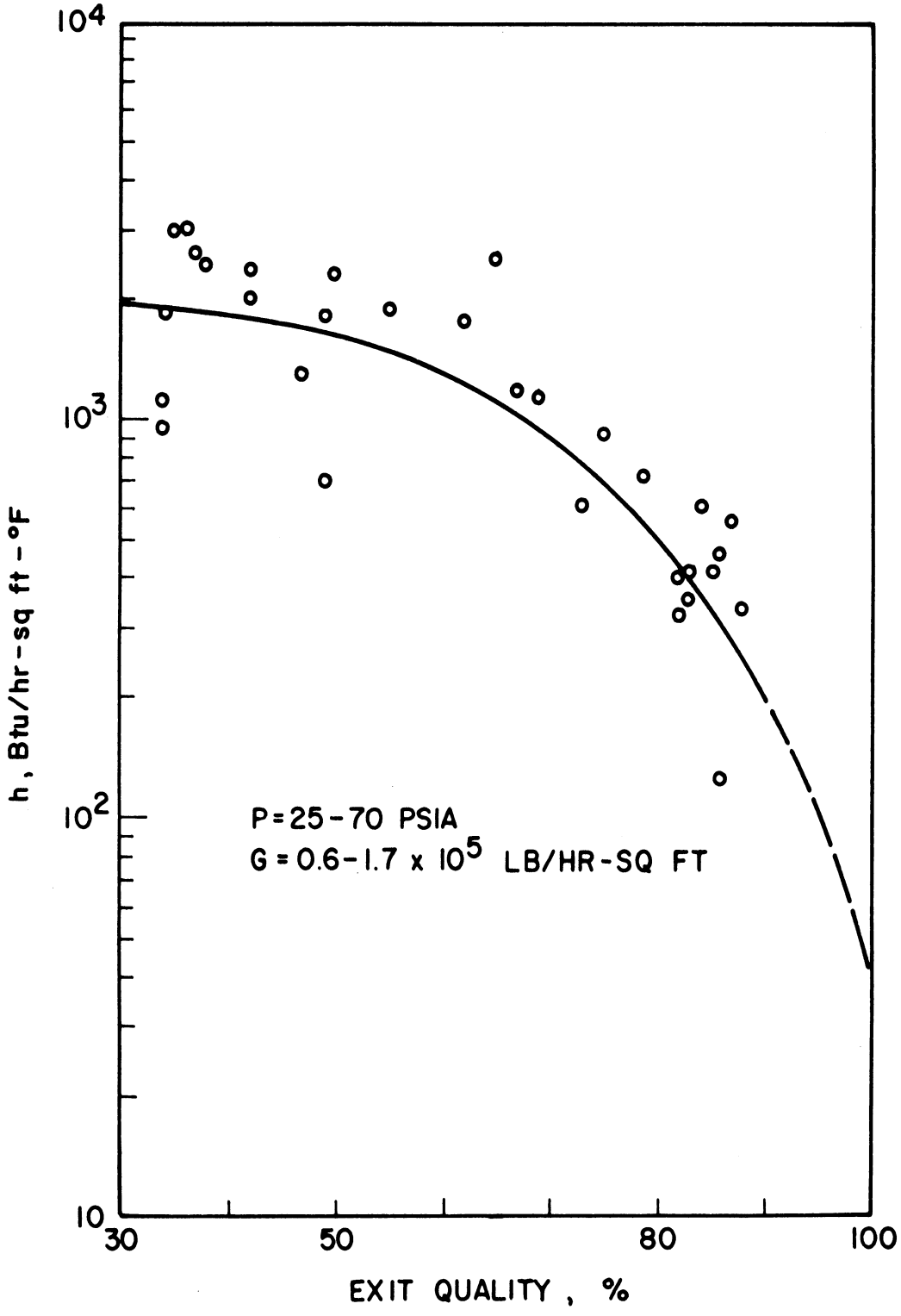

Figure 15 Data of the General Electric Company (69) for Average Transition and Film Boiling Coefficients of Potassium in Forced Convection.

the predicted curves. However, there is no reason to suspect a priori that potassium will also not agree with the available correlations. The droplet vaporization studies of Poppendiek (145) suggest that the film-boiling process for potassium is not much different from that of water, benzene, and Freon. The forced convection studies of the General Electric Co. show that the upper limit of the film-boiling coefficient for potassium is of the same order of magnitude as the coefficients of Hosler and Westwater for water and Freon 11.

DESCRIPTION OF EQUIPMENT

The most obvious method of obtaining film boiling, i.e., traversing the nucleate boiling curve and passing over the maximum heat flux, would require high capacity equipment. Since the flux levels in film boiling would probably be only a small fraction of the maximum heat flux, it was decided to adopt a technique used by Hosler and Westwater (79). This consisted of heating the dry boiler to a temperature above that required to obtain film boiling and then slowly charging liquid into the boiler, thus establishing film boiling directly without having to pass over the maximum heat flux. Hosler and Westwater found that a short free fall for that liquid return to the boiler of approximately 1-inch was necessary to avoid reverting to nucleate boiling. The appartus used in this investigation was designed using the above criteria.

A schematic diagram of the film boiling apparatus is shown in Figure 16. Figure 17 is a general view of the environmental vessel, potassium reservoir, instrument panel, vacuum system, and power supply.

Environmental Vessel

The environmental vessel consists of a 21-inch diameter by 27-inch long main section and a 13-inch diameter by 6-inch long top section. The main section is directly flanged to a Kinney PW 400 vacuum system which includes a 4-inch diffusion pump and a Welsch Duo-Seal vacuum pump. The top section contains a viewing port and six Conax glands for power leads and thermocouples. The flange for the top section has a 5 1/2-inch diameter opening through which the boiler assembly is lowered into the environmental vessel. The cooling coils around the main section are designed to keep the vessel cool but it was not found necessary to use them.

Boiler Assembly

The boiler assembly is shown in Figure 18 after it had been lowered into th 5 1/2-inch diameter opening in the flange to the top section of

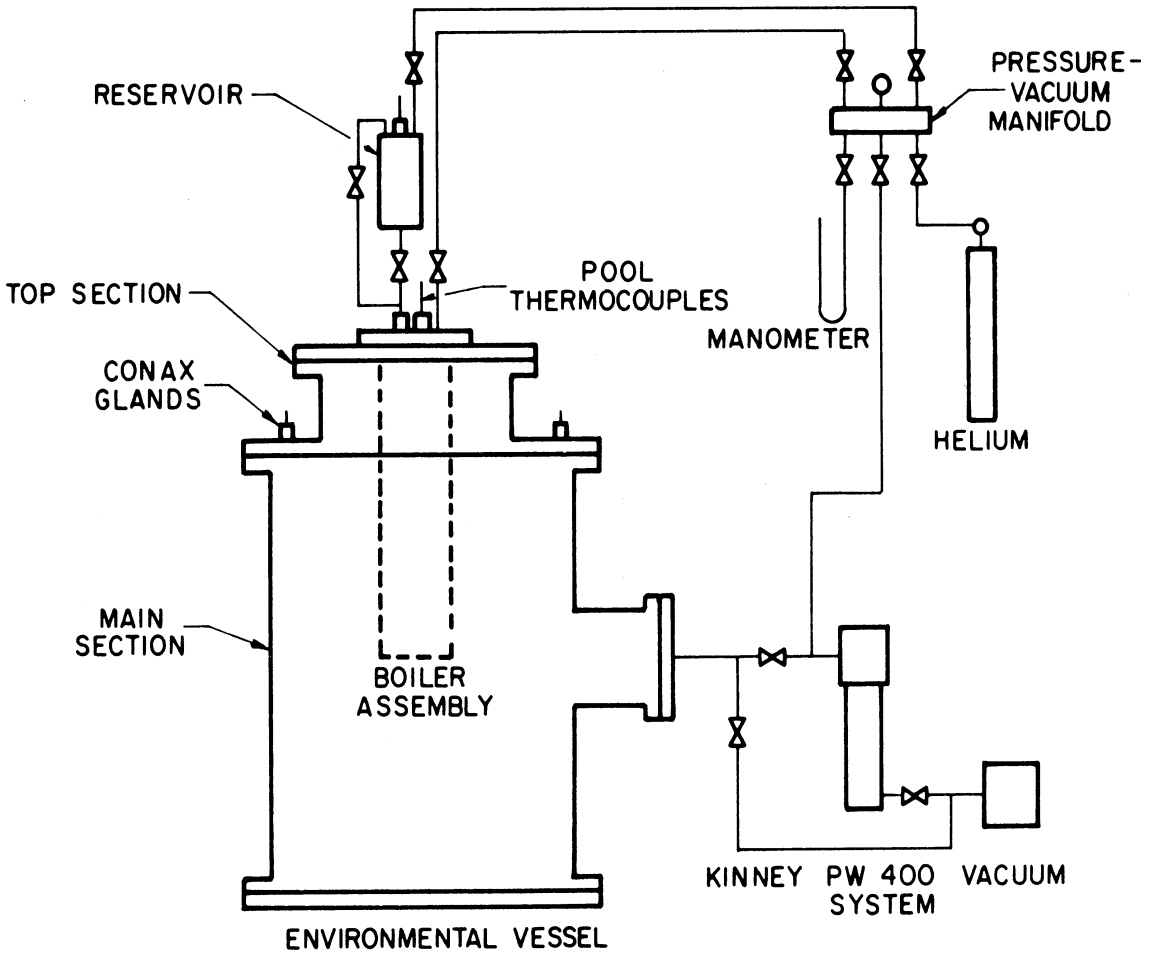

Figure 16 Schematic Diagram of Film Boiling Apparatus

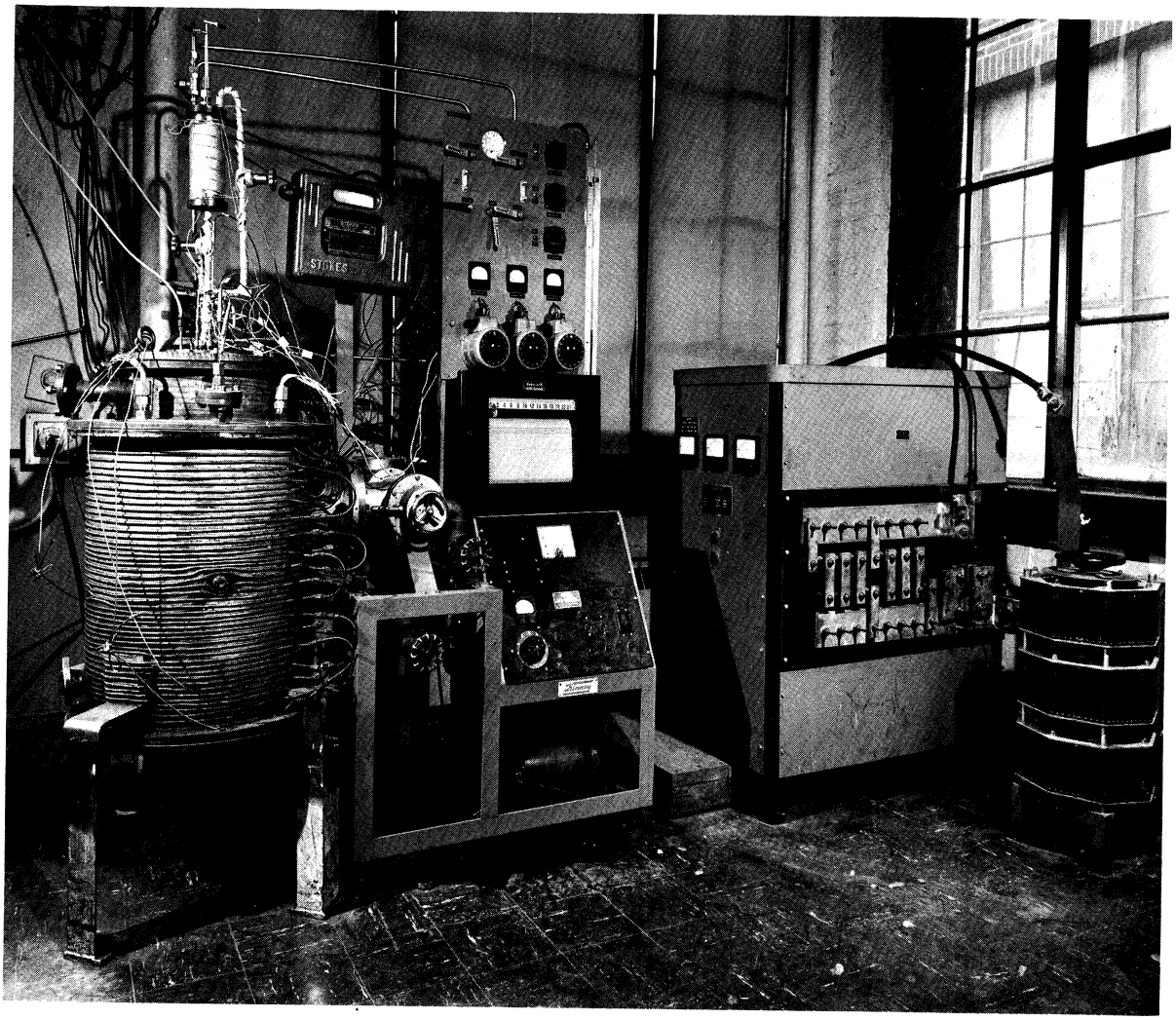

Figure 17 General View of Experimental Apparatus

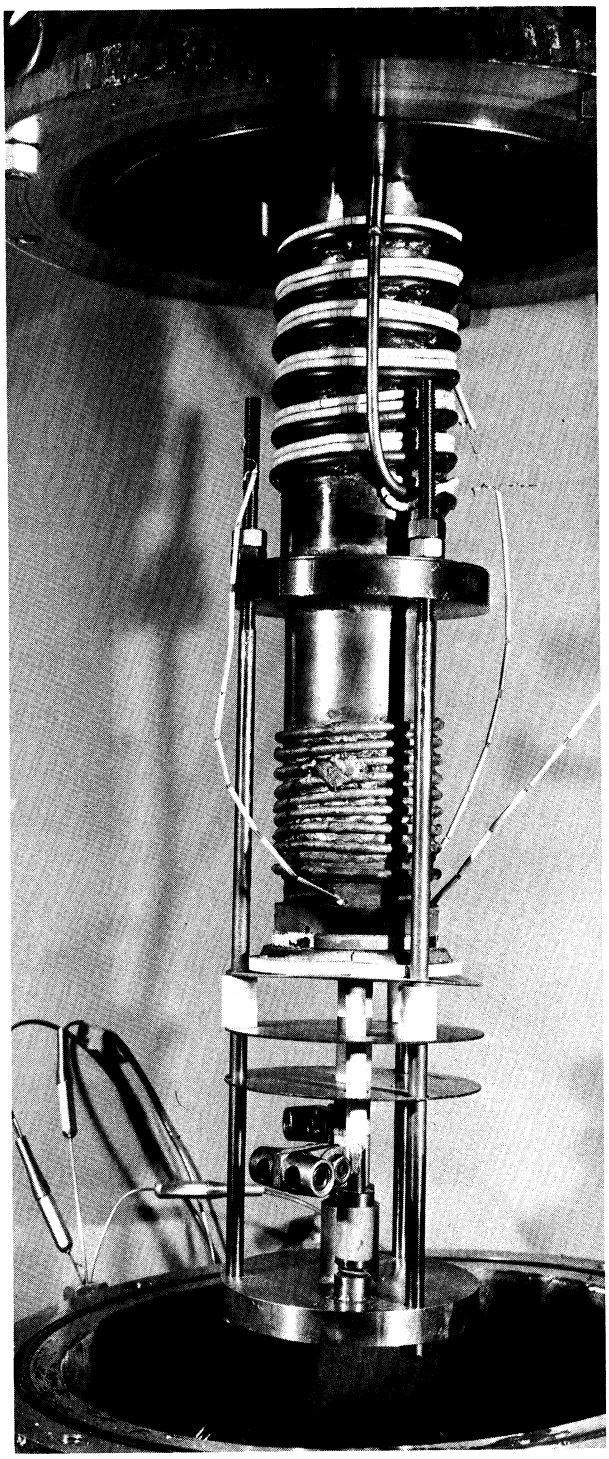

Figure 18 Boiler Assembly

the environmental vessel. It consists of the top flange through which the fill line and pool thermocouples are inserted, the condensor, the drip plate, the boiling chamber, the boiling plate, the main heater along with its bus bars and electrical insulators, and the compression plate with its spring for obtaining good electrical contact between the bus bars and the heater. Figure 19 shows the details of the boiling surface and heating elements.

The top flange is an 8-inch diameter by 3/4-inch thick plate of type 304 stainless steel. Eight equally-spaced Conax 3/16-inch OD MPG glands are silver-soldered to the flange around a 2-inch diameter. One of the glands is used for pressurizing and evacuating the condenser and the remaining seven are used for thermocouple wells to be lowered into the boiling chamber. At the center of the flange is a 3/8-inch OD Veeco gland welded to a 4-inch-long 3/4-inch OD extension. The gland, which allows the fill line to be raised and lowered, uses a Viton O-ring to insure that the fill line can be heated above the melting point of potassium during charging.

The condenser is a 9-inch-long section of schedule 40 Haynes 25 pipe. This portion of the boiler assembly would have normally been made of stainless steel, but the Haynes pipe was used because it was already available and could be readily welded to the other stainless steel components. The cooling coil welded to the outside of the condenser was made from 10 feet of 1/4-inch OD stainless steel tubing and is silver-soldered to the top flange. A 400-watt beaded Nichrome wire heater is wrapped around the condenser to insure that it can be always kept above the melting point of potassium.

Figure 20 is a section of the stainless steel drip plate. The purpose of the drip plate is to insure that all of the vapor generated in the boiling chamber reaches the condenser. An earlier design had indicated that liquid flowing down the walls of the boiling chamber may have disrupted the film boiling process. Liquid flowing down the walls of the condenser is prevented from dripping through the slots by 1/2-inch-high wires to avoid a high free fall. The condensate flows down the down-comer which ends one-inch above the boiling surface.

The boiling chamber is a 3 1/4-inch OD by 3-inch ID by 8-inch-long section of type 316 stainless steel tubing. A 3/16-inch OD by 93-inch long guard heater is Nicrobrazed to the boiler wall. The heater consists of two Nichrome wires insulated by magnesium oxide inside of a swaged Inconel sheath and is rated at 1 kilowatt at 115 volts AC.

The boiling plate is shown in Figure 21. To avoid a weld or undue thermal stress at the outer edge of the boiling surface, the plate was machined from solid bar stock 3 1/2-inch in diameter by 1 1/2-inch long of type 316 stainless steel. The plate section is 0.504-inch thick and

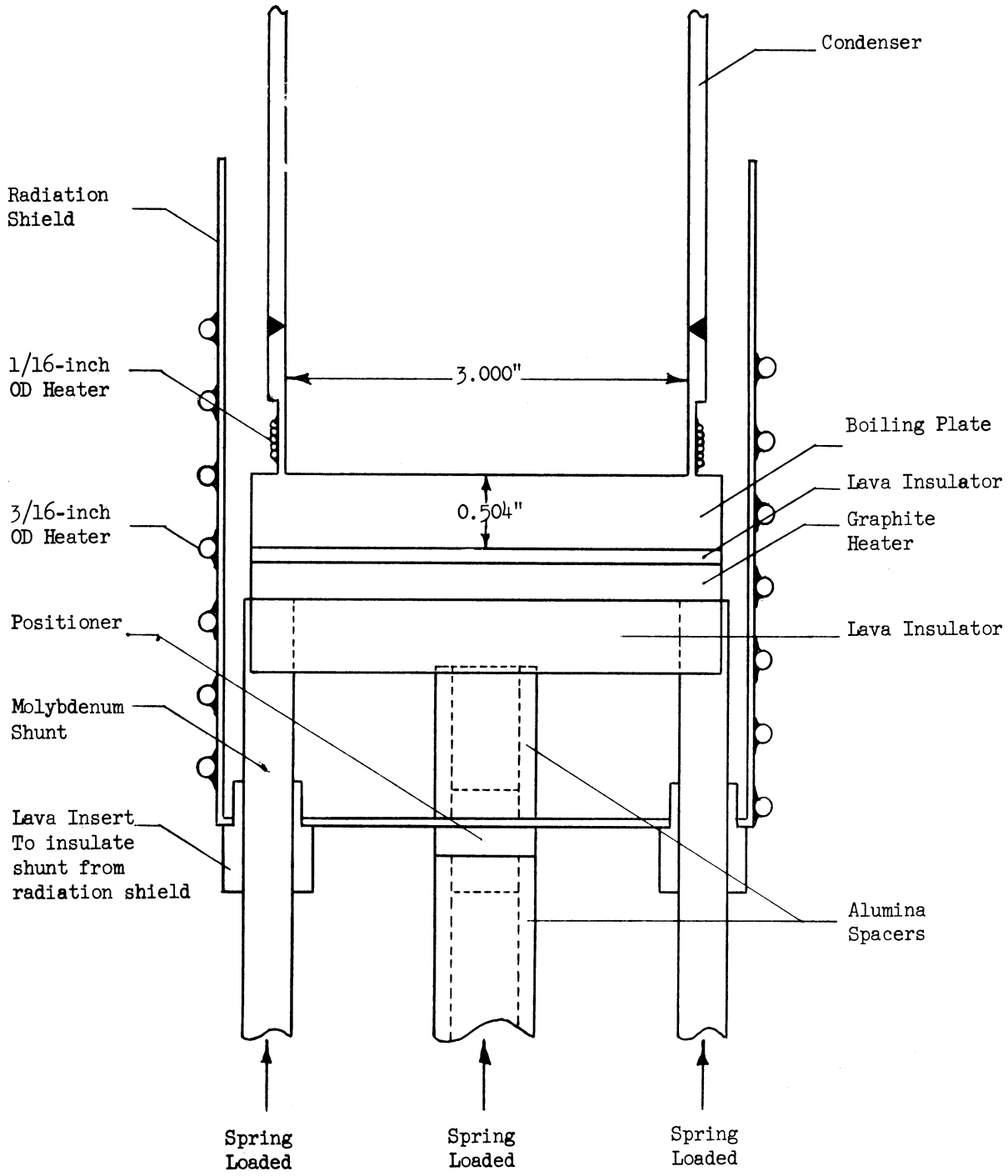

Figure 19 Boiler and Heater Assembly

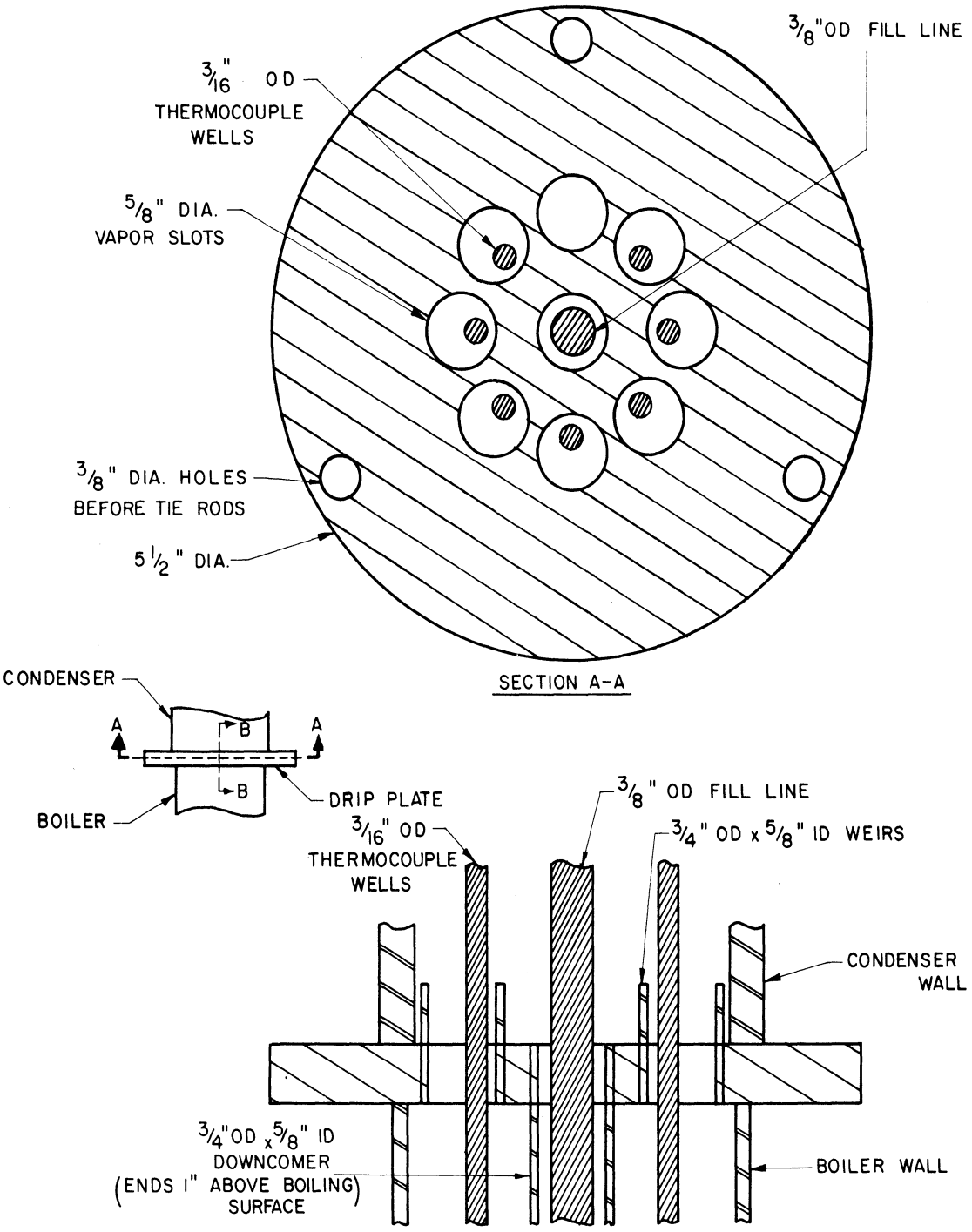

Figure 20 Diagram of Drip Plate

Figure 21 Boiling Plate

contains six 1/16-inch diameter holes for thermocouples. Figure 22 shows the location of the holes and their distance from the boiling surface. The 0.050-inch thick by 1/2-inch long thin-walled section above the boiling plate is designed to minimize heat conduction from the plate to the walls of the boiling chamber. The final preparation of the 3-inch diameter boiling surface consisted of polishing with 500 grit aluminum oxide cloth and then with 600 grit boron carbide powder.

Figure 23 shows the main heater which is made from a 3 1/2-inch diameter by 1/4-inch thick plate of National Carbon grade ATJ graphite. It has a measured resistance of approximately 0.14 ohm at room temperature. The heater is insulated from the boiling plate by a 1/32-inch-thick layer of alumina and was assembled according to the following procedure. High-purity alumina powder was mixed with water to trowelling consistency and allowed to stand for 24 hours in an airtight container. Spacers which consisted of 1/32-inch diameter alumina rods were placed on the bottom surface of the boiling plate and the thick alumina slurry was poured over the spacers. The graphite heater was then placed on the slurry and pressed down until contact was made with the spacers. The excess alumina slurry flowed out at the edges and through the slits in the graphite heater and were wiped off. Weights were then placed on the graphite heater until the alumina dried and hardened.

A 4 1/2-inch diameter zirconia crucible cover acted as the bottom insulator for the graphite heater and also as a guide for the two molybdenum bus bars. Copper strips are heli-arc welded to the bottom of the bus bars with Everdur filler and mechanical clamps are bolted to the copper strips for connection to the copper braid. The molybdenum bus bars are forced against the graphite heater by means of stainless steel springs to insure good electrical contact. Another spring allows the thermal expansion to avoid cracking the graphite heater. Compression of the springs is accomplished by tightening three 3/8-inch diameter stainless steel tie rods connecting the compression plate and the drip plate. The three radiation shields below the zirconia insulator are intended to keep the springs cool. Another radiation shield is placed around the graphite heater to cut down radial losses.

Figure 24 shows the boiler assembly with all the thermocouples and power leads hooked up prior to insulating the boiling chamber, boiling plate, and grahite heater assembly with several layers of Fiberfrax insulation. In Figure 25, the Fiberfrax insulation has been applied and the top section of the environmental vessel is ready to be lowered to the main section.

Charging System

Figure 26 is a schematic diagram of the charging system. The potassium reservoir consists of a 3 1/4-inch OD by 7-inch long stainless steel vessel

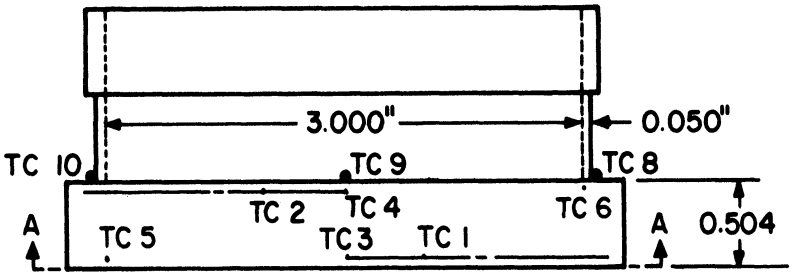

DISTANCE BETWEEN CENTERLINE OF THERMOCOUPLE HOLES AND BOILING SURFACE:

TC 1	.436"
TC 3	.438"
TC 5	.439"
TC 2	.072"
TC 4	.076"
TC 6	.072"

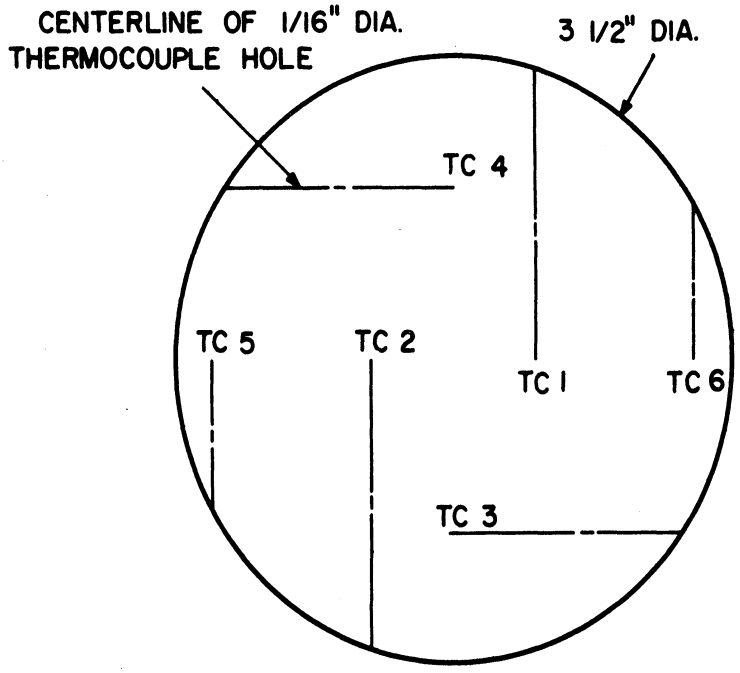

SECTION A-A

Figure 22 Location of Boiling Plate Thermocouples

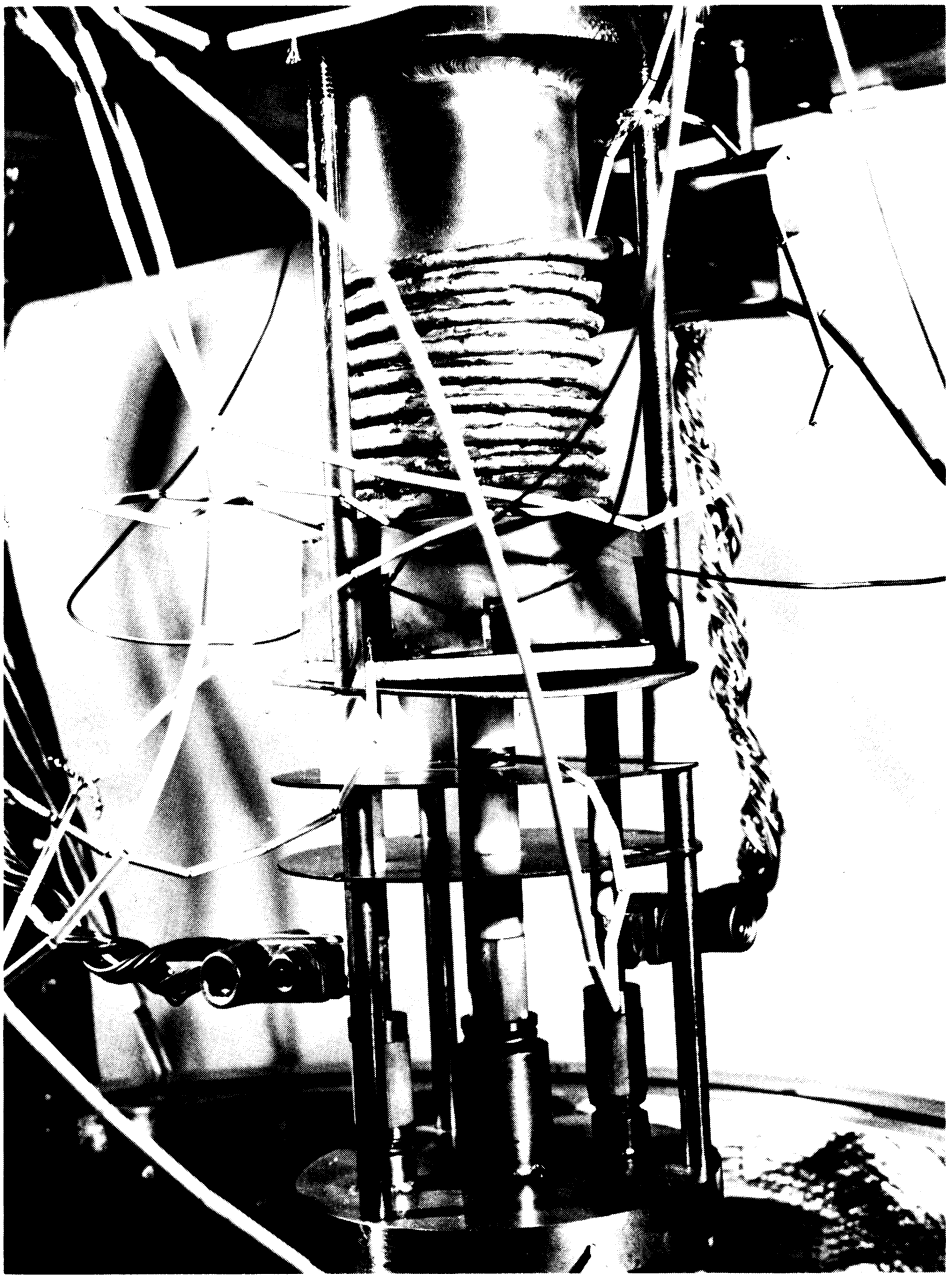

Figure 24 Instrumented Boiler Assembly

Figure 23 Graphite Main Heater

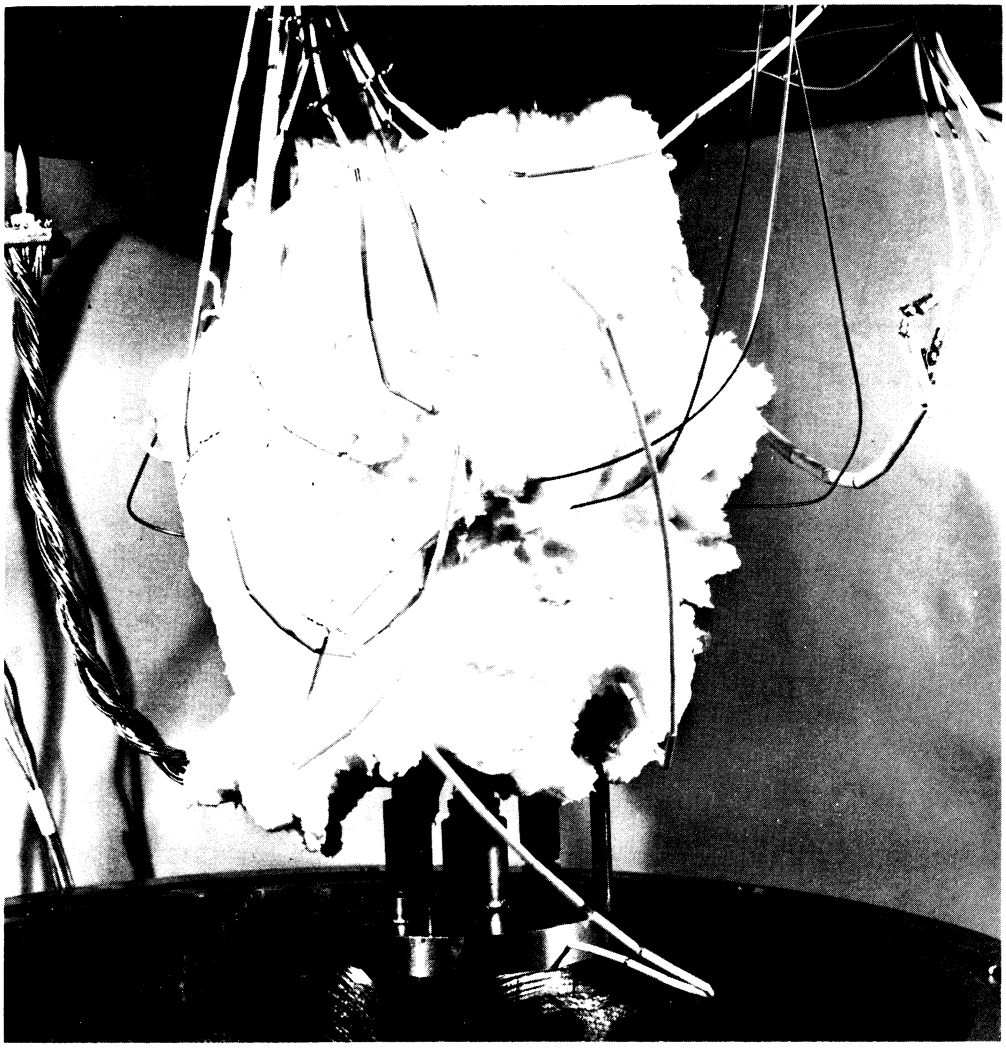

Figure 25 Instrumented and Insulated Boiler Assembly

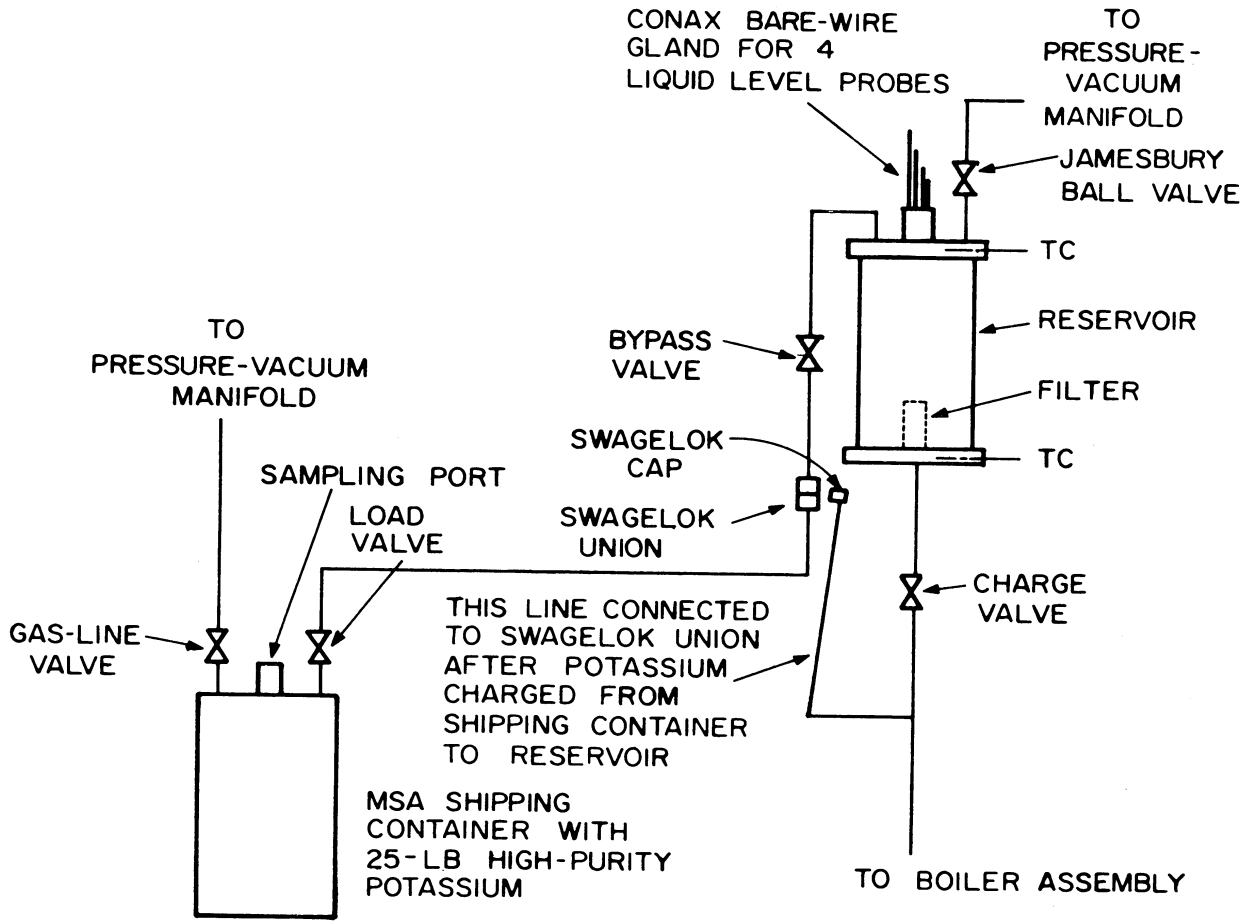

Figure 26 Diagram of Charging System

with a sintered stainless steel filter welded at the bottom for removing solid particles in the liquid. The filter is 1/2-inch OD by 1 1/2-inch high with a 12-micron porosity and is of the type used in Hoke in-line filters. The charge valve and bypass valve, as well as the two valves supplied with the 25-lb MSA shipping container, were Hoke TY 445 stainless steel bellows valves. A Conax gland at the top of the reservoir allowed for four 1/16-inch diameter stainless steel rods to be inserted into the reservoir to detect the liquid level. The rods were located just above the bottom (to detect the initial flow of potassium from the shipping container), and at 4, 4 1/4, and 4 1/2-inch above the bottom. Heating tapes were used on the reservoir, shipping container and lines to maintain the temperature approximately 100°F above the melting point of potassium during charging operations.

Instrumentation

Figure 27 is a schematic diagram showing the location of the temperature measurements made in the system. The six thermocouples in the boiling plate (see Figure 22 for location) and the thermocouple in the 3/16-inch OD well located 1/4-inch above the boiling surface, TC1 through TC7, were 1/16-inch OD, Inconel-sheathed, Pt-Pt 13% Rh swaged thermocouples with magnesium oxide insulation and grounded junctions made by the Claud S. Gordon Company. These seven thermocouples were hooked up to an 8-point thermocouple switch and utilizied a common cold junction, another swaged thermocouple immersed in an ice bath. The thermocouples located at the junction of the boiling plate and the 0.050-inch wall, TC8 through TC10, were made from 20-gauge Chromel-Alumel wire (Hoskins grade 3G-178) and were heli-arc-welded to insure good thermal contact. Pieces of stainless steel foil were placed around the junctions to avoid radiation error. These three thermocouples were hooked up to a second 8-point thermocouple switch and utilized a common cold junction, a thermocouple made from 24-gauge Chromel-Alumel wires (Hoskins grade 3G-178) immersed in an ice bath.

Each of the thermocouple switches was hooked up to a Leeds and Northrup Speedomax H Compact Azar recorder. A third thermocouple switch and recorder was available but was used only during the start-up phase. The output of any of the thermocouple switches could be switched to a Leeds and Northrup No. 8662 portable precision potentiometer. Hence, two temperatures could be monitored constantly until steady state conditions were achieved but only one temperature at a time could be taken using the potentiometer. A picture of the two recorders and the potentiometer is shown in Figure 28. The six thermocouples in 3/16-inch OD wells located between 1/2-inch and 4-inches above the boiling surface (TC11 through TC16) and the other check thermocouples located throughout the boiler assembly and potassium reservoir were made from 24-gauge Chromel-Alumel wires (Hoskins grade 3G-178) and were hooked up to a 12-point Brown Electronik recorder.

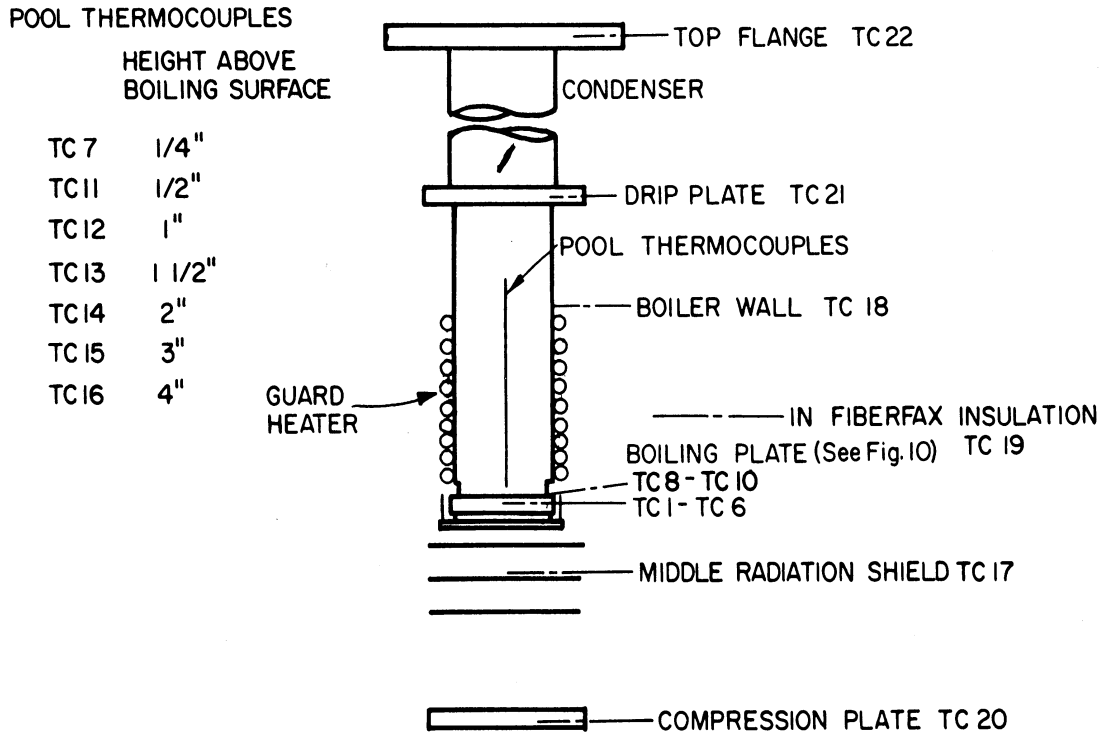

Figure 27 Location of Temperature Measurements

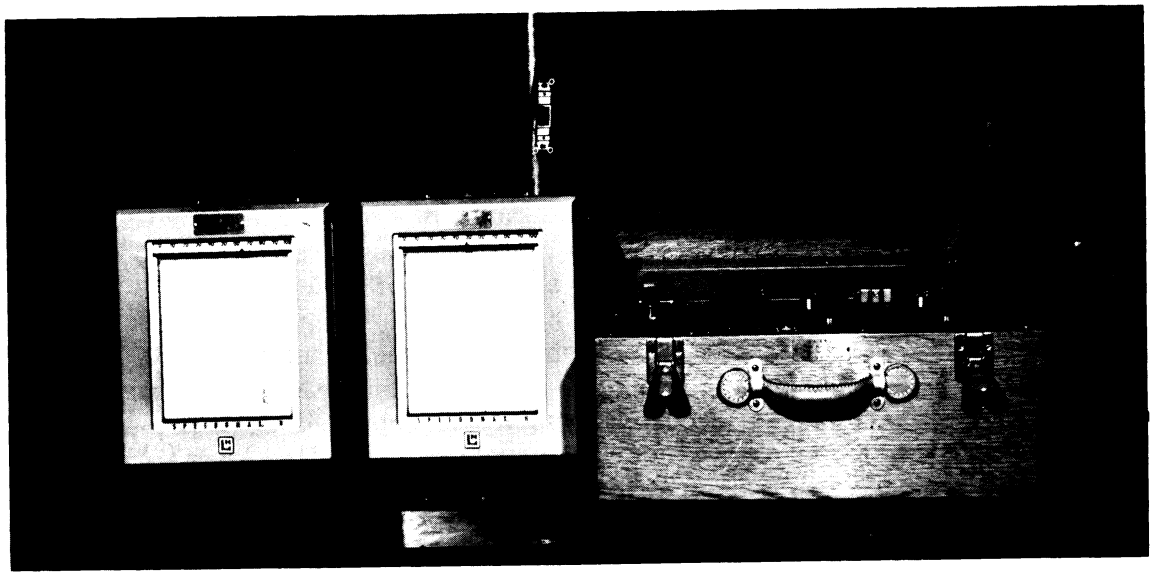

Figure 28 Temperature Recorders and Potentiometer

Pressure was measured with a U-tube manometer with a 100-cm scale graduated in millimeters. A Matheson gauge with a 30-inch vacuum to 15 psig range at the pressure-vacuum manifold was used primarily for outgassing and flushing with helium. Thermocouple vacuum gauges with 1 micron-1 atm ranges are located in the environmental vessel and just before the diffusion pump. A Stokes McLeod gauge with a pressure range of .03 to 5000 microns could be used just before the diffusion pump or could be hooked up to the pressure-vacuum manifold.

Power Supply

Power to the main heater (graphite heater) was furnished by a 12 KW, 3-phase, full wave Udylite rectifier with a rated output of 250-2000 amps at 48-6 volts DC respectively. The rectifier is supplied with a 0-75 v voltmeter, a 0-250 a ammeter and a 0-2000 a ammeter. Copper welding cables carried the current from the rectifier to the Conax electrode glands passing through the top section of the environmental vessel. The glands used 1/2-inch diamter copper bus bars and Teflon sealants. Inside the vessel, copper braid carried the current from the electrode gland to the mechanical clamps on the molybdenum bus bars. The copper power lead system was designed to carry a current of 200 amps.

Power to the guard heater (3/16-inch OD, Inconel-sheathed 1 KW Nichrome heater), the condenser heater (400-watt beaded Nichrome heater), and the heating tapes on the charging system was supplied by 1 KW, 110 volt AC powerstats. Simpson 0-10 amp AC ammeters were used on all three guard heater circuits.

Miscellaneous

All equipment coming into contact with potassium were made from stainless steel or Haynes 25. Type 316 stainless steel tubing was used for the 3/16-inch OD pool thermocouple wells and type-304 was used for gas lines. Hoke TY 445 bellows valves made from type-316 stainless steel were used on the potassium charging system but Jamesbury ball valves made from brass were used for the gas lines. Heli-arc welding between stainless steel or Haynes 25 components was utilizied whenever possible. Where welding was impractical, connections were made using Swagelok compression fittings made from type-316 stainless steel. Glands operating over 200°F used sealants made of Viton or Teflon; otherwise, neoprene sealants were used.

EXPERIMENTAL PROCEDURE

The MSA Research Corporation stainless steel shipping container with 25 lbs. of high-purity potassium (less than 10 ppm oxygen) was hooked up to

the reservoir just below the bypass valve (see Figure 26 for diagram of charging system). The entire system was then leak-checked under vacuum using a helium mass spectrometer. The reservoir and the lines between the reservoir and shipping container were then heated to approximately 250°F while under vacuum and then flushed three times with helium. The reservoir was back-filled with helium at 0 psig and slight helium pressure was then applied to the MSA shipping container to force the potassium liquid through the lines into the reservoir. The first liquid into the reservoir was detected by making electrical contact with the liquid level probe just above the bottom surface. The rising liquid level was detected by the probes at higher levels and the reservoir was filled to a level of 4 1/2 inches above the bottom surface. The load valve on the MSA shipping container was then closed and the lines allowed to cool to room temperature. The shipping container was disconnected from the reservoir under helium pressure to avoid introducing air into the system. This Swagelok connection below the bypass valve was then leak-checked using the helium mass spectrometer.

Before the commencement of boiling, a heat loss calibration was carried out. For various power settings of the main heater, the power to the guard heater was adjusted to minimize heat conduction from the boiling plate to the boiler wall and radiation from the boiling surface. The heat generated in the main heater would then consist mainly of radiation losses at the outer edge of the boiling plate and losses below the plate, including conduction down the molybdenum bus bars. It is assumed that these heat losses are approximately the same during boiling for the same boiling plate temperatures. The heat loss calibration data is presented in Appendix A and the heat loss curve is shown in Figure E-1 of Appendix E. The calibration was carried out with the system under vacuum to facilitate outgassing.

To obtain film boiling, the boiling plate was first heated up to approximately 1600°F under vacuum. The reservoir and charging lines were heated to approximately 250°F and the charge valve cracked to allow potassium liquid to drip slowly from the end of the fill line located 1/2-inch above the boiling surface. Since the low pressure in the boiler corresponded to a saturation temperature of approximately 700°F, film boiling was obtained directly. The boiling plate temperature was continuously monitored and the power was incremented to compensate for the drop in plate temperature due to the slowly increasing potassium level. Electrical contact with the liquid level probes in the potassium reservoir was monitored with an ohmeter to detect the falling liquid level. The charge valve was closed after approximately 1/4-inch of potassium had been charged to the boiler.

After film boiling was established, the system was allowed to come to steady state. The Chromel-Alumel check thermocouples throughout the system were monitored on the 12-point Brown Electronik recorder. Since this recorder was relatively slow (one point every 15 seconds), it was left on

continuously during operation. The boiling plate temperatures were checked periodically with the Speedomax recorders to determine whether steady state conditions had been achieved. Upon reaching steady state, the following data was recorded: the pressure from the mercury manometer, the amperage and voltage of the power from the rectifer to the main heater, the amperage of the power to the guard heater, and all the temperatures throughout the system. The thermocouples hooked up to the two 8-point thermocouple switches were read consecutively on the portable precision potentiometer and the check temperatures on the 12-point recorder corresponding to this time were later tabulated. The power to the main heater and guard heater were then changed and the system allowed to achieve steady state again.

The time required for the system to reach steady state after a change in the power level was approximately 30 to 60 minutes. Even after several hours of operation at the same power level, the boiling plate temperatures sometimes drifted very slowly due to changes in the line voltage of the power supply to the rectifier. This was evidenced by the fact that relatively large temperature shifts were encountered at approximately 8 a.m. and 5 p.m. The Speedomax recorders were used to insure that the boiling plate temperatures were not changing more than 1°F during the time that the temperatures could be read on the potentiometer.

The film boiling experimental data is tabulated in Appendix B. The first run was made at a constant pressure of 2 mm Hg and the measured liquid temperatures were between 983°F and 986°F. Almost half of the data points were taken while increasing the temperature. At a temperature difference of approximately 351°F, the boiling plate temperatures started to decrease rapidly but film boiling was maintained by quickly raising the power level of both the main heater and the guard heater. The third run consisted of increasing the pressure in small increments from 61 mm Hg to 300 mm Hg corresponding to liquid temperatures of 1011°F to 1243°F respectively. Data at higher pressure levels could not be obtained because it was decided to keep the boiling surface below 1700°F to avoid severe corrosion of the stainless steel by the potassium.

Nucleate boiling data was also obtained and is tabulated in Appendix C. Since it was unnecessary to charge the potassium on a hot surface, these runs started with an initial liquid level of 1/2-inch above the boiling surface. The charging procedure was to adjust the tip of the fill line at the 1/2-inch level and empty the contents of the reservoir into the boiler, which was maintained at approximately 400°F. The boiler was then pressurized and the excess liquid above the 1/2-inch level pushed back up into the reservoir. One of the purposes of these runs was to attempt to determine the critical heat flux at very low pressure. Another reason was to check the contention of Rallis and Jawurek (147) that a pressure exists below which the nucleate boiling regime cannot exist. They obtained data for ethanol where they were able to pass from natural convection directly into film boiling without experiencing the nucleate regime. However, nucleate boiling of potassium was obtained for pressures down to 1 mm Hg and heat fluxes up to 63,600 BTU/hr-sq ft were obtained at

this pressure without any indication that the critical heat flux was imminent. It was undesirable to go to very much higher fluxes because of the thermal stresses induced in the boiling plate by the large thermal gradient in the boiling plate. Nucleate boiling data was obtained at 1-2 mm Hg and 602-751 mm Hg.

During the nucleate boiling runs and for the film boiling data at the higher power levels, it was necessary to blow air through the cooling coils welded on the outside of the condenser. As the power level during film boiling was decreased, it was necessary to reduce gradually and then shut off the air to the condenser cooling coils in order to maintain the top flange of the boiler assembly above 148°F, the melting point of potassium. At the lowest power levels, the beaded Nichrome heater around the condenser had to be turned on. Through past experience in preliminary runs, it was found that all of the potassium eventually froze in the condenser leaving the boiling surface dry if the condenser was not maintained above the melting point of potassium.

In the tabulated data of Appendices A, B, and C, the temperature of one of the thermocouples is sometimes missing. During operation, this thermocouple sometimes developed an open circuit. However, when the thermocouple was working, its resistance was the same as the other Pt-Pt 13% Rh thermocouples and the sensitivity of the potentiometer when making a reading was not affected. This indicated that the circuit became interrupted by a break in only one leg of the thermocouple and that an emf when received corresponded to the emf of the hot junction rather than an intermediate point.

The experimental data above was taken using an apparatus on which refinements had been made. Preliminary data was obtained on the initial apparatus which did not include a downcomer for the liquid return from the condenser and whose guard heater on the walls of the boiling chamber had burned out during the start-up. Also, the three thermocouples at the edge of the boiling plate had not been welded on yet. This preliminary data is tabulated in Appendix D and is characterized by large radial gradients due to heat conduction from the boiling plate up the boiler walls. Reasonable data could be obtained only at relatively high temperature differences. At lower temperature differences, the boiling on the boiler walls reverted to the transition or nucleate regime and caused temperature distortions in the boiling plate such that one side of the plate was hotter than the opposite side. These distortions rendered the temperature differences in the plate meaningless. One of the thermocouples in the plate also displayed an erratic behavior by sometimes indicating an open circuit. When an emf signal was obtained, the resistance of the thermocouple was almost 20 times that of the other thermocouples in the boiling plate and a reading on the potentiometer was obtained with difficulty because of low sensitivity. Therefore, the temperature corresponding to this thermocouple was disregarded even for those cases where it was available.

EXPERIMENTAL RESULTS

Data on the film boiling of potassium was obtained for pressures between 2 mm Hg and 300 mm Hg, corresponding to liquid temperatures between 714°F and 1243°F. The data is tabulated in Appendix B and the method of treating the data is discussed in Appendix E. The results are tabulated in Table V and plotted in Figure 29 and 30.

The boiling curves (q/A vs. ΔT) for pressures of 2 mm Hg and 50 mm Hg are shown in Figure 29. The data for pressures between 61 mm Hg and 300 mm Hg do not determined a true boiling curve because the pressure was not held constant, but they were included to show the effect of pressure beyond 50 mm Hg. There appears to be a minimum in the heat flux at a temperature difference of 400°F for the 2 mm Hg film-boiling curve. For the 50 mm Hg curve, the trend at the lower temperature differences is not as well established but it appears that the minimum flux might occur at a higher temperature difference of 460°F although it may be as low as 351°F, the temperature at which the boiling plate temperatures started to fall rapidly. The heat transfer coefficient as a function of temperature difference is shown in Figure 30.

The effect of pressure on the heat flux at a constant temperature difference of 600°F is shown in Figure 31. The point at 170 mm Hg was obtained by interpolating the results for 61-300 mm Hg. Although there are not enough points at different pressures to accurately determine the dependency, it appears that the heat flux is proportional to the 1/4 to 1/3 power of the pressure.

The film boiling results for potassium obtained in this study agree with the potassium drop experiments of Poppendiek et al (145) and the high-quality forced convection data of the General Electric Co. (69). Poppendiek found that the process for the vaporization of potassium droplets was not different from that of water and Freon. Hosler and Westwater (79) obtained film-boiling coefficients of 28 to 40 BTU/hr-sq ft-°F for Freon-11 and water respectively at one atm. The present data indicates that the potassium film-boiling coefficient at one atm will be of the same order as that for water. The General Electric Co. data for forced convection of potassium at qualities approaching 100% indicate that the film-boiling coefficients at 25-70 psia would be in the range 30-70 BTU/hr-sq ft-°F. This is of the same order as that for water and again agrees with the present study.

Nucleate boiling data was obtained for pressures of 1-2 mm Hg and 602-751 mm Hg. The results are tabulated in Table VI and are plotted on Figure 32. Heat fluxes up to 63,600 BTU/hr-sq ft for temperature differences between 15°F and 49°F were obtained. There was essentially no difference between the low- and high-pressure data.

The experimental values of pressure and liquid temperature can be plotted to generate a vapor pressure curve for potassium. Figure 33 shows

TABLE V. Film Boiling Results

q/A (BTU/hr-sq ft)	ΔT (°F)	h (BTU/hr-sq ft-°F)	PRESSURE (mm Hg)
9,000	752	12.0	2
11,400	798	14.3	2
12,900	824	15.7	2
16,000	873	18.3	2
16,800	851	19.7	2
10,800	780	13.8	2
9,900	749	13.2	2
8,400	710	11.8	2
7,000	679	10.3	2
6,500	655	9.9	2
5,100	624	8.2	2
4,600	607	7.6	2
4,700	637	7.4	2
4,200	567	7.4	2
3,300	515	6.4	2
3,300	532	6.2	2
2,800	503	5.6	2
2,800	480	5.8	2
2,400	448	5.4	2
2,400	438	5.5	2
1,900	408	4.7	2
2,300	403	5.7	2
1,600	376	4.3	2
2,300	363	6.3	2
2,700	314	8.6	2
2,600	298	8.7	2
2,600	287	9.1	2
3,000	274	11.0	2
3,000	250	12.0	2
10,400	511	20.3	50
11,200	591	18.9	50
11,900	642	18.5	50
12,000	665	18.3	50
10,800	621	17.4	50
9,300	590	15.8	50
9,600	549	17.5	50
9,000	490	18.4	50
8,900	476	18.7	50
8,800	432	20.4	50
13,900	670	20.7	50

TABLE V.(continued)

q/A (BTU/hr-sq ft)	ΔT (°F)	(BTU/hr-sq ft-°F)	PRESSURE (mm Hg)
11,600	646	18.0	61
12,100	658	18.4	62
12,100	642	18.8	75
11,100	633	17.5	88
11,200	622	18.0	100
11,700	607	19.3	115
12,200	592	18.9	130
12,700	579	21.9	146
11,700	560	20.9	163
11,700	546	21.4	178
12,100	515	23.5	201
12,100	489	24.7	225
13,000	464	28.0	252
13,500	447	30.2	275
13,600	428	31.8	300

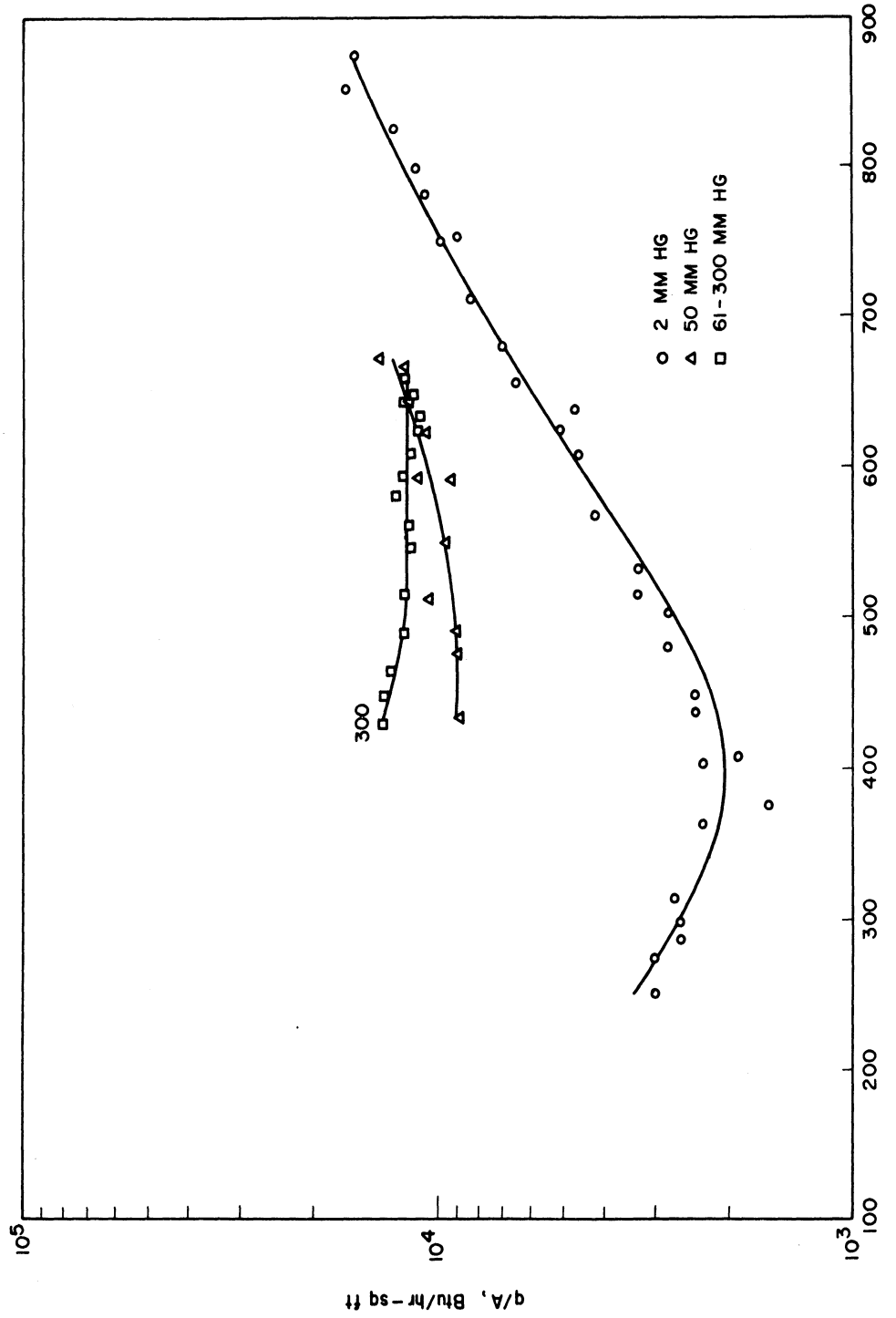

Figure 29 Heat Fluxes for Potassium in Film Boiling

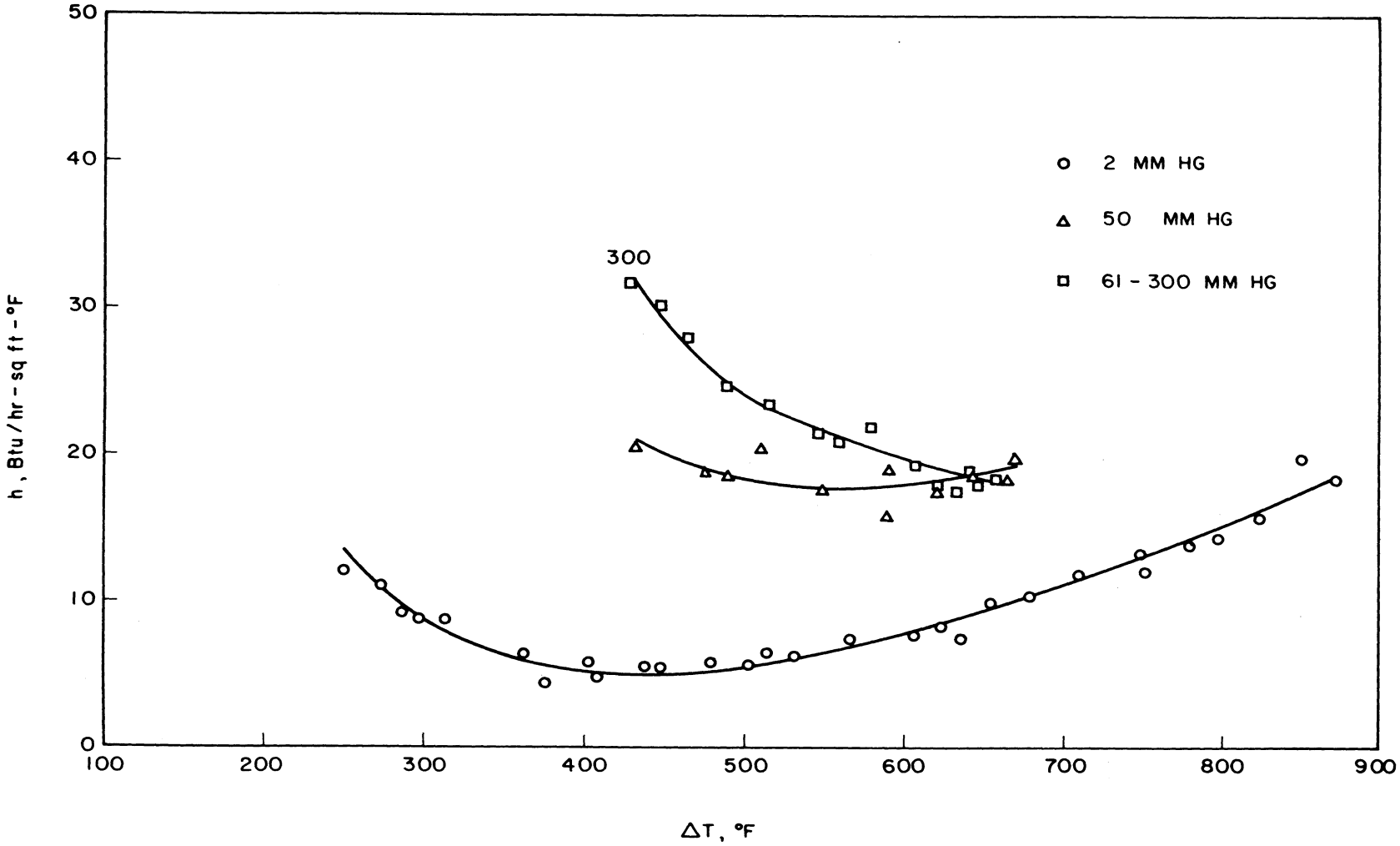

Figure 30 Heat Transfer Coefficients for Potassium in Film Boiling

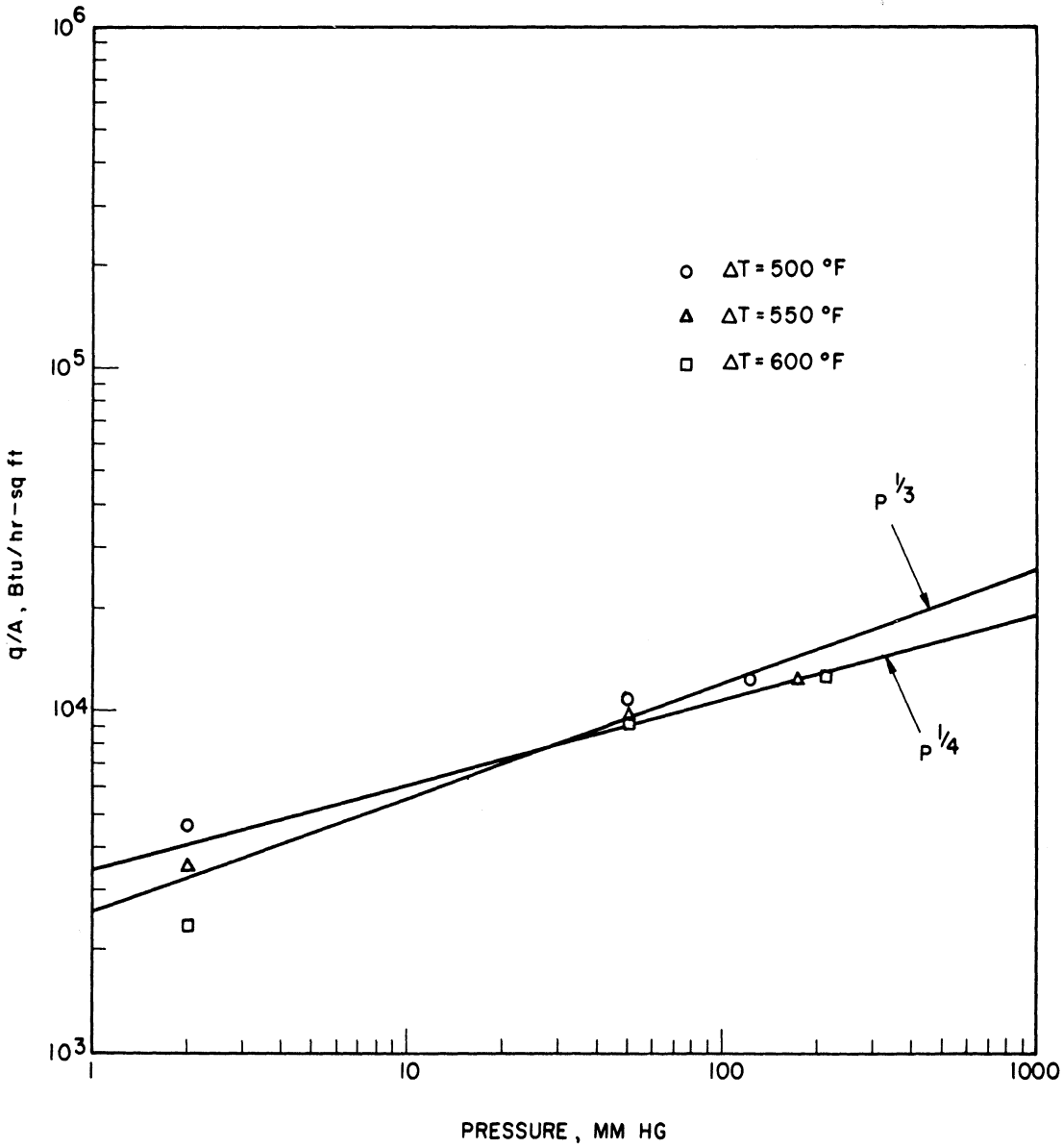

Figure 31 Effect of Pressure on the Heat Flux in Film Boiling

TABLE VI. Nucleate Boiling Results

Pressure (mm Hg)	q/A BTU/hr-sq ft	ΔT °F
2	7,000	14
2	4,000	2
1	47,400	32
1	47,700	29
1	26,200	20
1	58,700	33
2	5,700	10
2	13,900	17
2	20,600	17
2	25,600	19
2	32,500	25
2	40,000	28
2	47,200	28
709	18,000	20
659	23,200	24
684	29,200	26
704	36,000	30
728	46,600	37
707	36,900	35
721	46,600	38
736	53,700	49
751	63,600	44
730	46,600	44
717	41,200	39
724	32,900	31
723	26,000	24
708	21,000	20
640	13,400	15
602	9,600	31
680	17,400	19
707	21,900	24
700	28,300	32

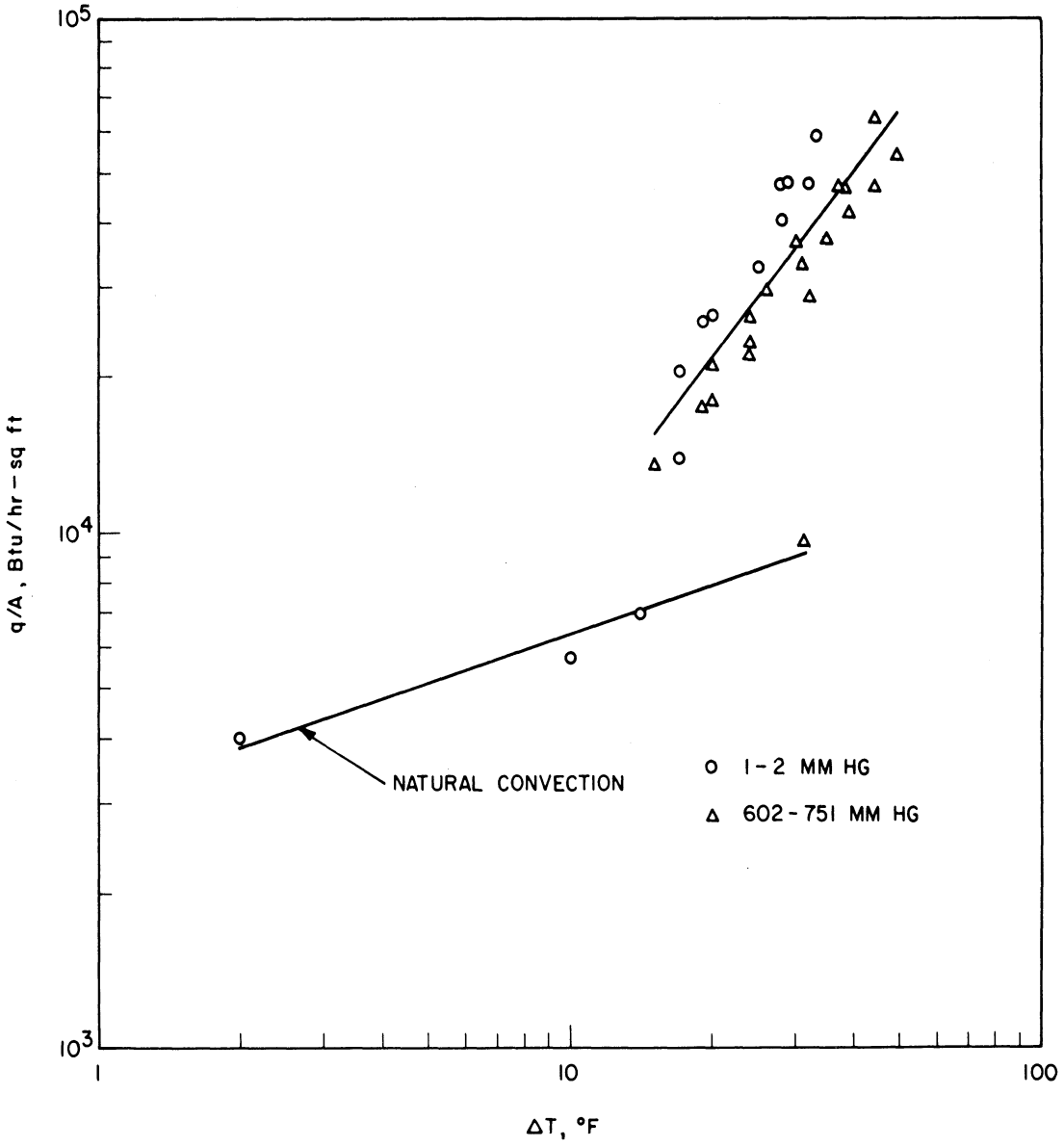

Figure 32 Heat Fluxes for Potassium in Nucleate Boiling

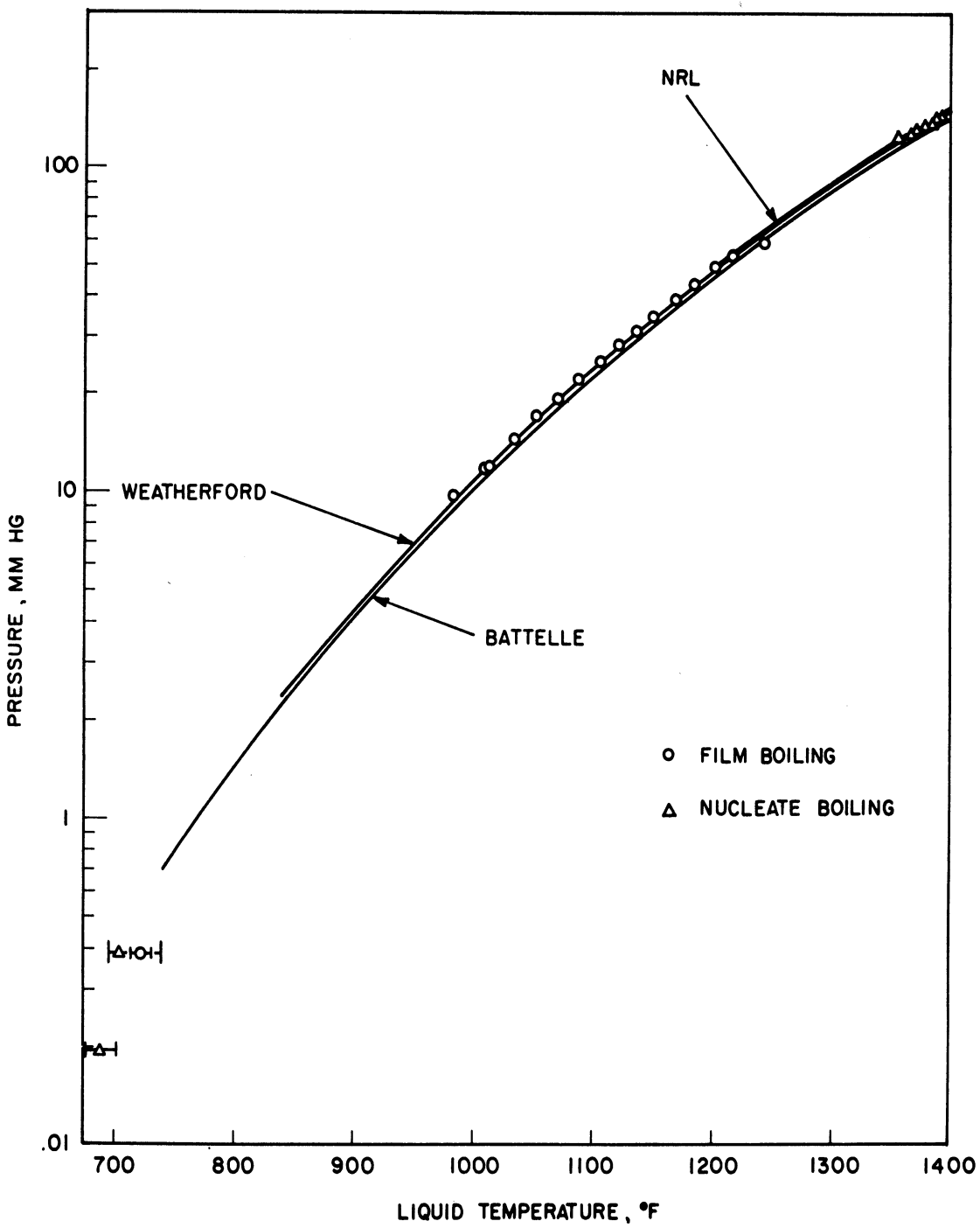

Figure 33 Vapor Pressure of Potassium

the vapor pressure data obtained in this study along with the curves from Weatherford (179), the Battelle Memorial Institute (103), and the Naval Research Laboratory (61). The data compares favorably with the curves indicating that saturated conditions prevailed during boiling.

DISCUSSION OF RESULTS

Comparison of Experimental Results with Theoretical Predictions

The heat transfer coefficients for the film boiling of potassium at 2 mm Hg and 50 mm Hg are plotted in Figure 34 along with the theoretical predictions of Berenson (18) at 0.1 and 1 atm, and of Frederking (65) at 0.1 atm. The basis for the physical properties of potassium used in evaluating the correlations is discussed in Appendix F. The experimental results uncorrected for radiation and other effects which might increase the heat transfer above that due to conduction and convection are about twice the predicted values. It is interesting to note that at 0.1 atm Frederking's prediction for spheres which assumes a turbulent, free convection process is very close to that of Berenson for horizontal surfaces which assumes that heat is transferred across the vapor film by pure conduction alone. From the predicted curves at 0.1 and 1 atm, the predicted effect of pressure on the heat transfer coefficient, and thus the heat flux, can be determined. The ratio of the heat transfer coefficient at 1 atm to that at 0.1 atm is relatively constant at 0.57. Using this value, the heat transfer coefficient is found to be proportional to the .244, or approximately 1/4, power of pressure. Hence, the heat flux is proportional to the 1/4 power of pressure for constant temperature difference. This agrees approximately with what was found experimentally. In Figure 31, the heat flux was found to be proportional to the 1/4 to 1/3 power of pressure at a temperature difference of 600°F.

The heat fluxes obtained experimentally at the minimum are substantially above the predictions of Berenson and Zuber. The comparisons are summarized in Table VII. It is seen that Berenson's equation for predicting the temperature difference at the minimum gives abnormally low values of 2°F and 36°F for film boiling at 2 mm Hg and 0.1 atm, respectively. An estimate of the minimum heat flux at one atm can be obtained by extrapolating to 760 mm Hg in Figure 31. This estimate is three times higher than Berenson's prediction but is not far from the upper limit of the range predicted by Zuber.

Effect of Radiation

At the high surface temperatures required for the film boiling of potassum, the radiative contribution to the heat flux can be significant. The heat transfer due to radiation can be estimated by assuming parallel plate geometry. The results are quite sensitive to values of the emissivities

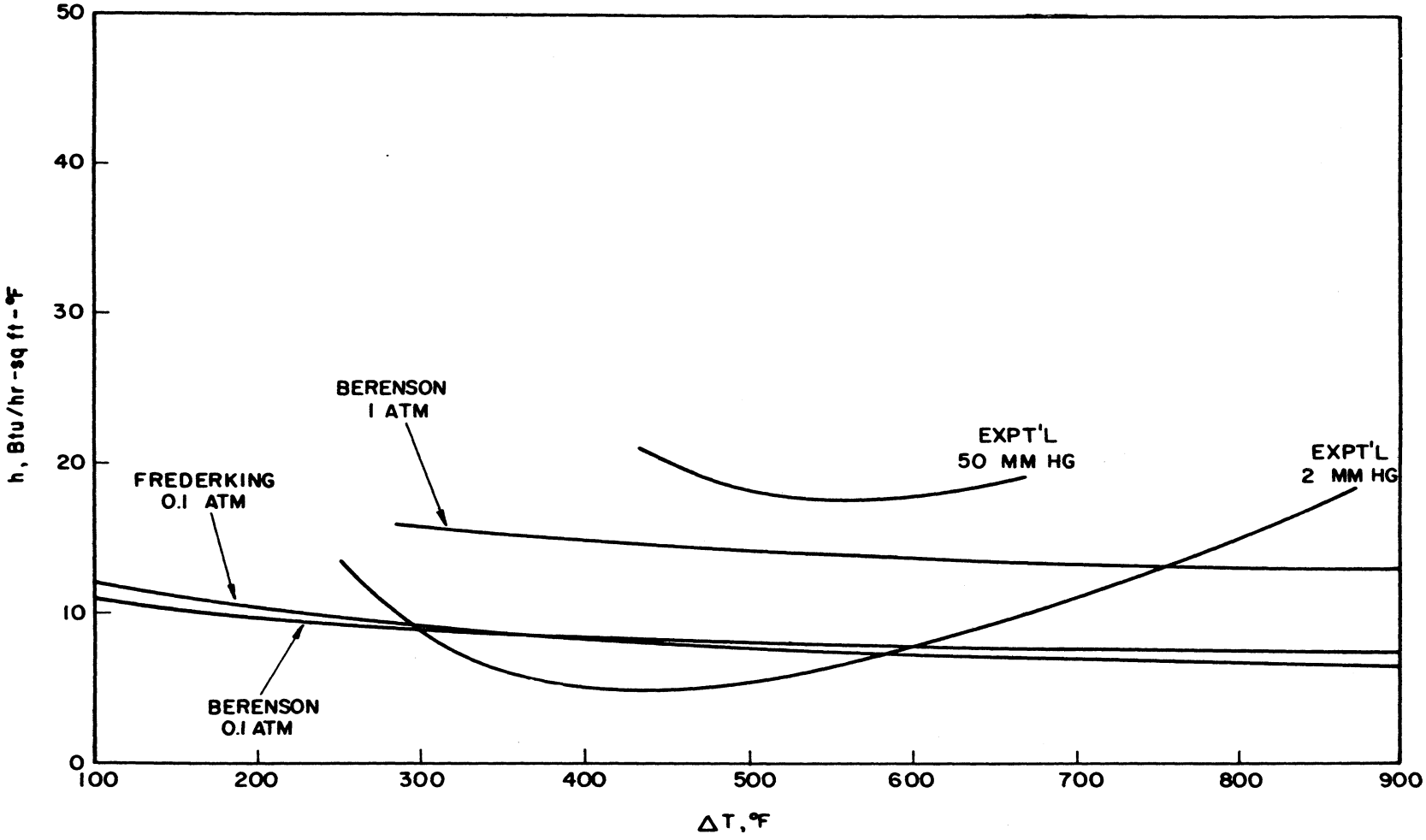

Figure 34 Comparison of Film Boiling Coefficients with Correlations

TABLE VII.

Comparison of Minimum Heat Fluxes
with Theoretical Predictions

	Minimum Heat Flux BTU/hr-sq ft	ΔT at Minimum Flux °F
Experimental (2 mm Hg)	2,000	400
Berenson (2 mm Hg)	200	2
Zuber (2 mm Hg)	222-518	
Experimental (50 mm Hg)	9,000	460
Berenson (0.1 atm)	513	36
Zuber (0.1 atm)	660-1,540	
Estimated from Figure 19 (1 atm)	15,000	
Berenson (1 atm)	4,810	287
Zuber (1 atm)	5,350-12,500	

used in the calculations. Experimental values for the emissivity of the stainless steel boiling surface were taken from the literature (70) and varied from .15 at 970°F to .58 at 1780°F. However, the emissivity of the liquid potassium surface was calculated using an equation suggestion by Jakob (90) based on the electrical resistivity.

$$\epsilon_o = 0.576 \sqrt{r_e T} + 0.124\, r_e T \qquad (30)$$

The normal emissivity ϵ_o is easily converted to the total emissivity by means of a table presented by Jakob. Using Equation 30, the theoretical predicition for the emissivity of a molten copper surface agrees with the experimental value given by Jakob within 10%. Using experimental data for the electrical resistivity of potassium obtained by the Battelle Memorial Institute (103), emissivities of 0.11 and 0.14 were calculated for film boiling at 2 mm Hg and 50 mm Hg respectively. The heat transfer due to radiation using the calculated potassium emissivities and assuming parallel plate geometry is shown in Figure 35. Since the emissivity of the potassium liquid is so low, the calculations are very sensitive to increases in its value. It is seen that doubling the potassium emissivity essentially doubles the heat flux due to radiation. The calculations were also done for an emissivity of 0.30 since this number is within the realm of possibility. Jakob notes an experimental emissivity of 0.31 for a molten iron surface.

The experimental values for the heat transfer coefficients in film boiling can be corrected for the effect of radiation by subtracting the radiative contribution corresponding to the heat fluxes in Figure 35. The results are shown in Figure 36 and comparison of the corrected curve for 50 mm Hg with Berenson's prediction for 0.1 atm shows that the predicted values are still about 40% lower than the experimental values. However, a higher potassium emissivity of 0.30 brings the corrected experimental curve to within 11% of the predicted curve. Thus, the effect of radiation is seen to be very significant but an accurate quanitiative measure of this effect is limited by uncertainties in the emissivity of potassium liquid. It is possible that radiation alone can account for the difference between the experimental and predicted values of the heat transfer coefficients in film boiling.

Effect of Vapor-Phase Dimerization Reaction

A process which could add to the heat transfer is a chemical reaction in the vapor between the solid heating surface and the boiling liquid. To illustrate the process involved, consider a gas which undergoes an endothermic dissociation reaction being heated by a solid surface. The molecules near the wall are heated and they dissociate, absorbing the energy associated with the endothermic heat of reaction. A concentration gradient in the gas

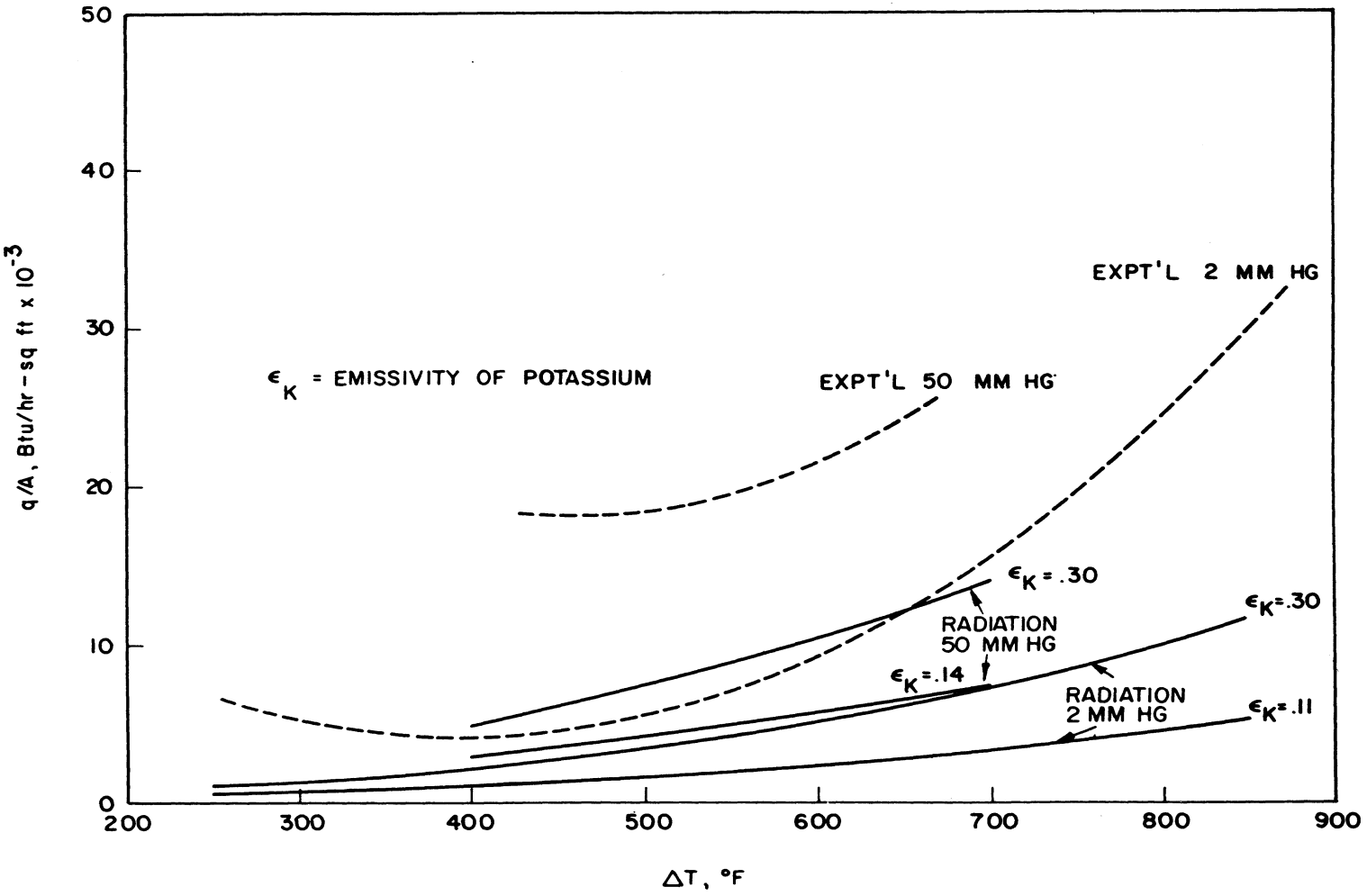

Figure 35 Heat Transfer Due to Radiation

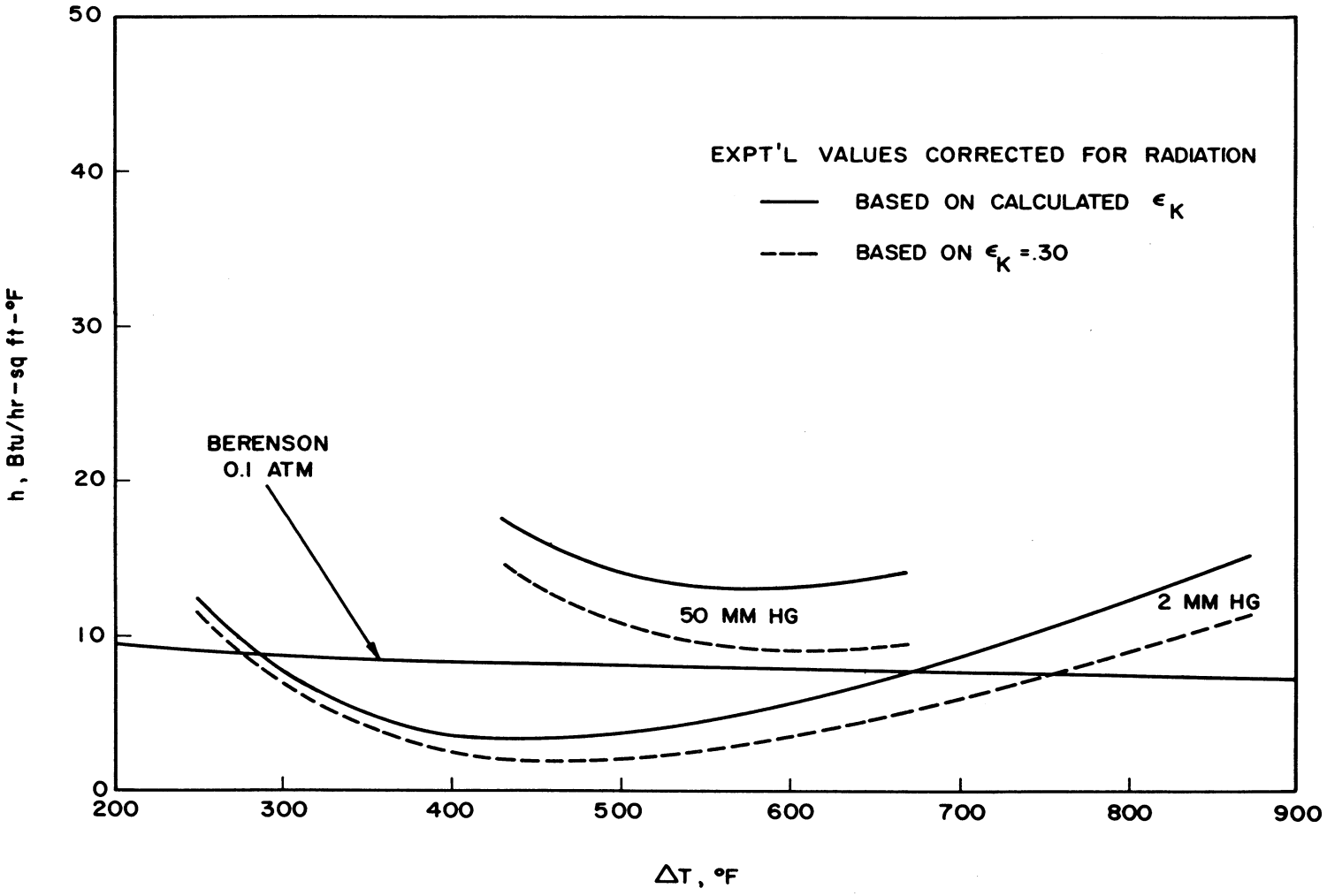

Figure 36 Correction of Film Boiling Heat Transfer Coefficients for Radiation

is established and the products of the dissociation reaction diffuse away from the wall. As they enter regions of lower temperature, the molecules begin to associate thereby releasing the heat of reaction to the new surroundings. Hence, heat is transferred by molecular diffusion in addition to the normal modes of conduction, convection , and radiation. This diffusional mechanism may be significant depending on the temperature level and the kinetics of the reaction.

The only type of reaction which has been treated extensively in the literature has been the "equilibrium" reaction in which the reaction rate is so high that the fluid may be assumed to have its equilibrium composition instantaneously after a change in temperature. A chemically reacting gas that has a temperature gradient across it, and whose local chemical composition can be described by the condition of local chemical equilibrium, can be considered as a non-perfect gas with temperature-dependent anomalies in its specific heat and transport properties. Use of the equilibrium theory corresponds to predicting the maximum effect of the chemical reaction on heat transfer.

Potassium vapor undergoes the dimerization reaction $K_2 = 2K$ in the vapor phase and the method of calculating the effect of this reaction is presented in Appendix G. In Figure 37, the effect of the dimerization reaction has been subtracted from the radiation-corrected experimental curve for 50 mm Hg. It is seen that the contribution from the reaction is relatively small, being a maximum of 10% at the lower temperature differences and decreasing as the vapor is superheated. Since the effect decreases with pressure, the experimental results for 2 mm Hg would not be expected to be significantly influenced.

Evaluation of Film-Boiling Correlations

The reliability of any correlation is proven by the accuracy with which it corresponds to actual experimental results regardless of whether it is applied in a range where some of the assumptions used in its derivation are known to be invalid. The results of the analyses of Zuber (186), Chang (40), and Berenson (18) for film boiling on a horizontal surface were presented in the Literature Review. Zuber predicts only the heat flux at the minimum. Chang obtained a relationship for the heat transfer coefficient as a function of temperature difference. Berenson derived an expression for the minimum heat flux identical in form to that of Zuber, and also predicted a functionality between the heat transfer coefficient and temperature difference. By dividing the two, he obtained an expression for predicting the temperature difference at which the minimum heat flux occurs. Berenson's correlation for the heat transfer coefficient is theoretically correct only near the minimum heat flux because he showed that the bubble spacing is unaffected by the vapor velocity and vapor film thickness only in the neighborhood of the minimum. Also, Berenson used his experimental results at the minimum to evaluate the

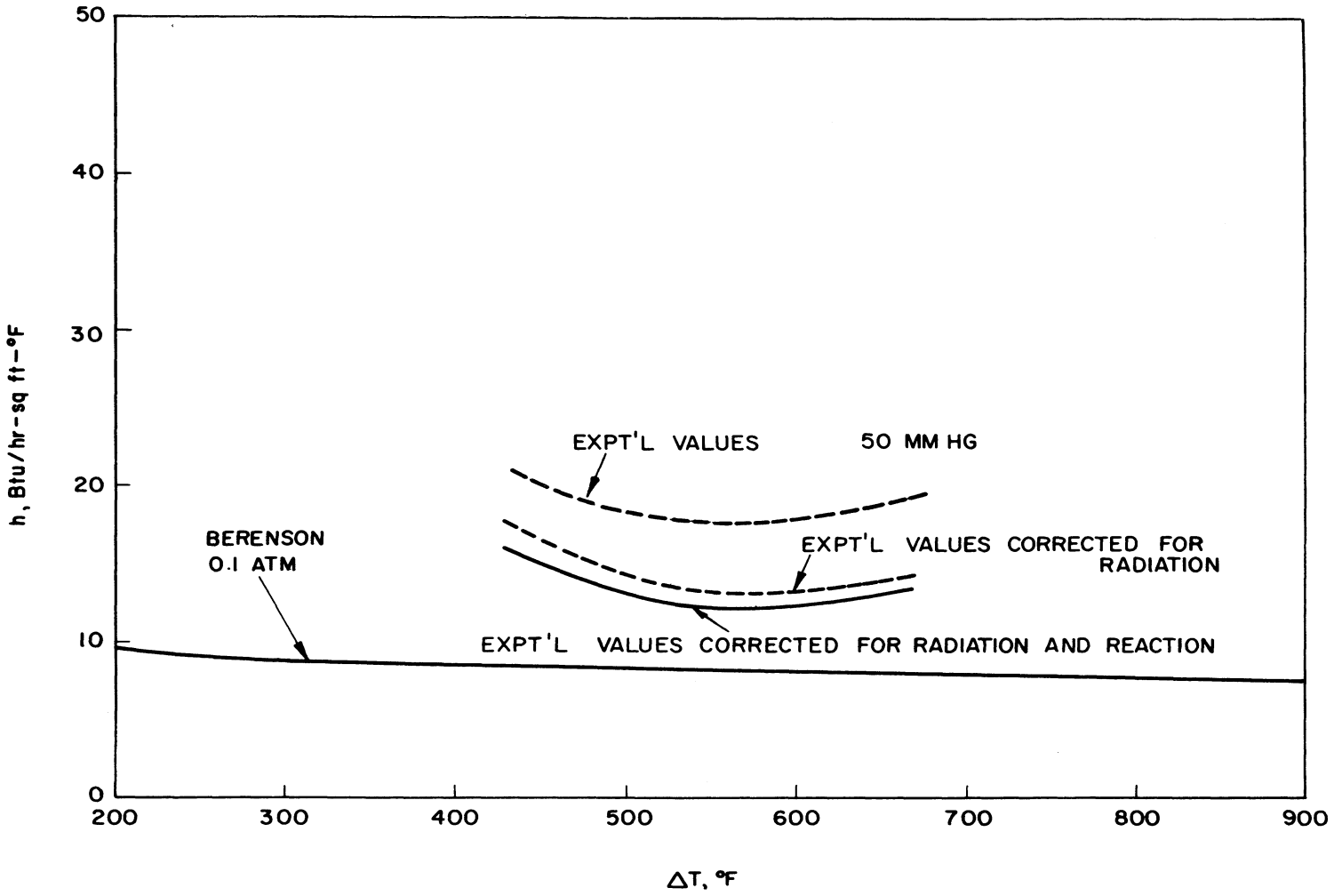

Figure 37 Correction of Film Boiling Heat Transfer Coefficients for Vapor Dimerization Reaction

constants in his expressions for the minimum heat flux and the heat transfer coefficient. Therefore, Berenson's equations agree well with his data for n-pentane and carbon tetrachloride at the minimum but not at higher temperature differences. However, the data of Hosler and Westwater (79) for film boiling of water and Freon-11 agrees with Berenson's correlation at the higher temperature differences but his predictions for the minimum heat flux were found to be seriously in error. The data for mercury do not seem to apply to any of the present correlations in that the heat transfer coefficients are about an order of magnitude higher than predicted at the lower temperature differences. Hosler and Westwater obtained heat transfer coefficients which were essentially constant with temperature difference whereas the results of Berenson and the present study yield coefficients which increase rapdily as a function of temperature difference.

Some clarification of the apparently contradictory experimental data can be obtained by considering the film-boiling correlations as expressions derivable from dimensional analysis and then applying all of the available data to evaluate the constants. In spite of the difference in flow characteristics, film boiling from horizontal tubes, vertical surfaces, spheres, and horizontal flat surfaces are described by equations of the same form providing the proper characteristic length is used:

$$Nu = a(Ra')^b = a(Gr'\ Pr)^b \qquad (31)$$

where Ra' and Gr' are modified Rayleigh and Grashof numbers, respectively. Some of the correlations are presented in Table VIII.

For film boiling on a horizontal flat surface, Equation (31) can be written in the form:

$$h = a\left[\frac{k_v^{\left(\frac{1}{b}-1\right)} \rho_v(\rho_l-\rho_v)g\ \lambda'}{\mu_v\ \Delta T\ D_b^{\left(\frac{1}{b}-3\right)}}\right] \qquad (32)$$

From the observed pressure effect in Figure 31 and noting the correlations in Table VIII, it would seem appropriate to assume a value of 1/3 or 1/4 for b. If b is 1/3, then there is no effect of the characteristic length, which does not seem reasonable. Therefore, let b be equal to 1/4. Then the coefficient a is given by:

$$a = h\left[\frac{\mu_v\ \Delta T\ D_b}{k_v^3 \rho_v(\rho_l-\rho_v)g\ \lambda'}\right]^{1/4} \qquad (33)$$

Values of the coefficient, a, can not be calculated from experimental data and plotted against some significant parameter to see whether it is actually a constant or whether any trends exist. Bromley (31) carried out a detailed analysis

TABLE VIII

FILM BOILING CORRELATIONS

Author	Geometry	Equation	Characteristic Length
Berenson	Horizontal flat surface	$Nu = 0.63(Ra')^{1/4}$	Bubble diameter
Bromley	Horizontal tube	$Nu = 0.62(Ra')^{1/4}$	Tube diameter
Bromley	Vertical tube or plate	$Nu = 0.62(Ra')^{1/4}$	Distance along tube of plate
Chang	Horizontal flat surface	$Nu = 0.43(Ra')^{1/3}$	Unspecified
Chang	Vertical surface	$Nu = 0.72(Ra')^{1/4}$	Distance along surface
Ellion	Vertical Surface	$Nu = 0.72(Ra')^{1/4}$	Distance along surface
Frederking	Sphere	$Nu = 0.14(Ra')^{1/3}$	Sphere diameter
Hsu	Vertical surface	$Nu = 0.943(Ra')^{1/4}$	Height of critical thickness

and concluded that if experimental values of the coefficient are plotted against the group $\Delta T\ C_p/\lambda'\ Pr$, the effect of the various assumptions in the analysis should be shown. In Figure 38, the experimental data of Berenson for n-pentane and carbon tetrachloride, that of Hosler and Westwater for water and Freon-11, that of Merte for mercury and that of the present study for potassium were used to calculate values of the coefficient, a, which were then plotted against the parameter $\Delta T\ C_p/\lambda'\ Pr$. The characteristic length used in the calculations was the bubble diameter as determined experimentally by Hosler and Westwater (73% of the most dangerous wavelength) rather than Berneson's prediction of 75% of the critical wavelength. The mercury data of Bonilla was not included since his results were inconsistent and incompatible with other data, showing an increase in the heat flux for a decrease in pressure and exhibiting abnormally high temperature differences in nucleate boiling. Instead of including all of the experimental points, only the values corresponding to the minimum heat flux and the highest temperature difference obtained experimentally were calculated but flags were used to indicate the limits of the coefficient due to scatter in the exper mental data. The values for potassium correspond to the experimental results which have been corrected for radiation and the effect of the dimerization reaction. The results of Figure 38 are summarized in Table IV for discussion purposes.

From Figure 38 and Table IX, the following conclusions can be drawn:

a. The data for mercury at the minimum heat flux do not conform to the rest of the experimental data. Clearly, the correlation does not correspond to the physical process taking place.

b. With the exception of Freon-11, the value of the coefficient increases with increasing temperature difference. This means that the experimental heat transfer coefficients are increasing the temperature difference more rapidly than can be accounted for by the assumed value of 1/4 for the power b in the equation $Nu = a(Ra')^b$.

c. The experimental results for potassium at high temperature differences give coefficients about four times higher than the rest of the data. However, the experimental results for n-pentane and carbon tetrachloride show that the heat transfer coefficients are increasing at such a rate that if data had been obtained at higher temperature differences, large values for the calculated coefficient in Figure 38 would also have been obtained. Figure 39 shows the heat transfer coefficients as a function of temperature difference for potassium, n-pentane and carbon tetrachloride. The heat transfer coefficients for the two organic fluids are increasing more rapidly at moderate temperature differences than those of potassium at high temperature differences.

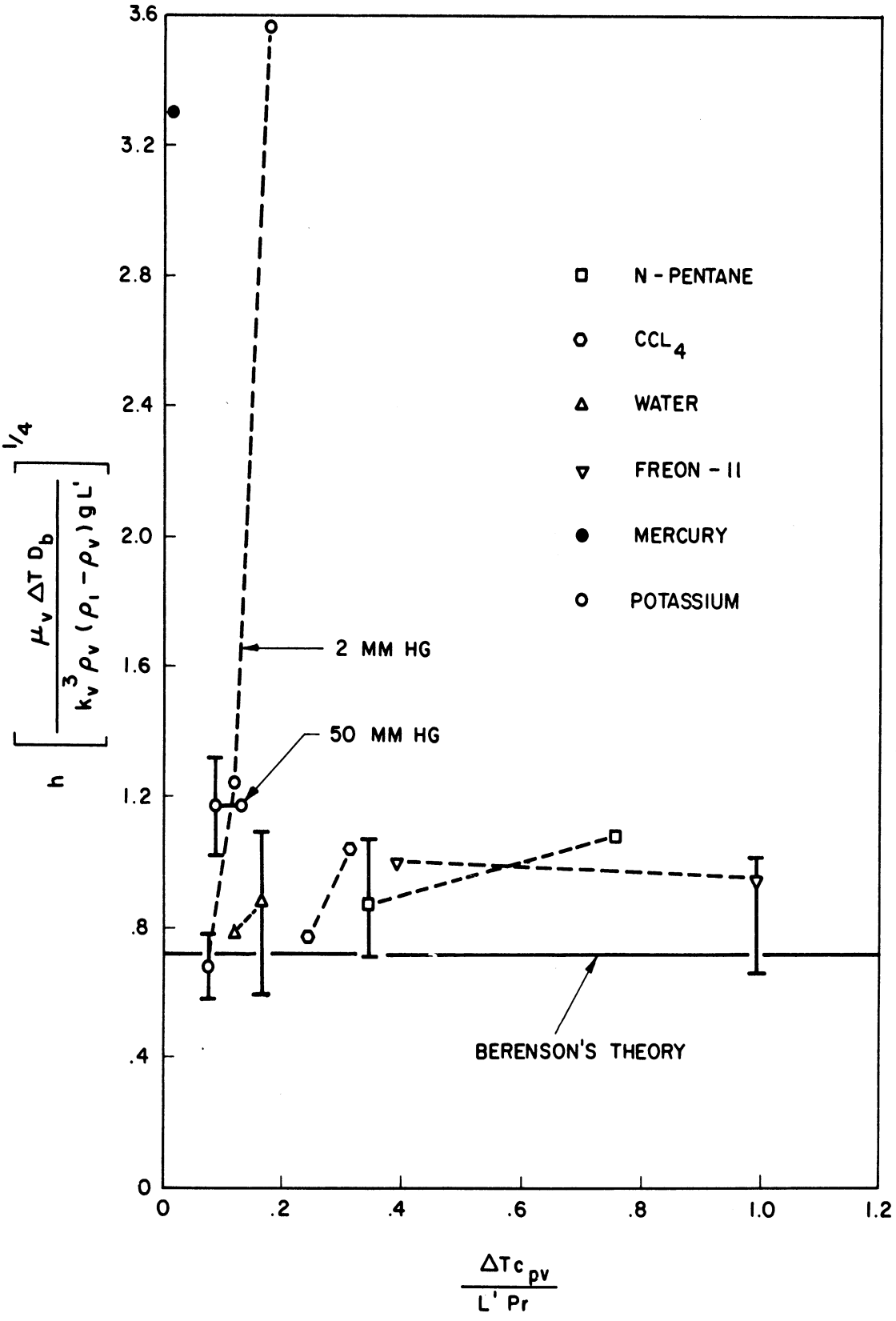

Figure 38 Correlation of Film Boiling Data for Horizontal Surfaces

TABLE IX

COMPARISON OF EXPERIMENTAL FILM BOILING DATA

		Value of Coefficient "a" in Equation 33		Deviation from Value of Berenson's Coefficient .72	
Fluid	ΔT Range	Minimum Heat Flux	Highest ΔT	Minimum Heat Flux	Highest ΔT
n-pentane	155°F	.87	1.08	21%	50%
CCl_4	52°F	.76	1.04	6%	44%
water	115°F	.79	.87	10%	21%
Freon-11	300°F	1.00	.95	39%	32%
Hg(1 atm)		6.11		749%	
Hg(80 psia)		3.33		362%	
K(50 mm Hg)	210°F	1.17	1.17	62%	62%
K(2 mm Hg)	473°F	.68	3.46	-6%	381%
K(2 mm Hg)	200°F	.68	1.22	-6%	69%

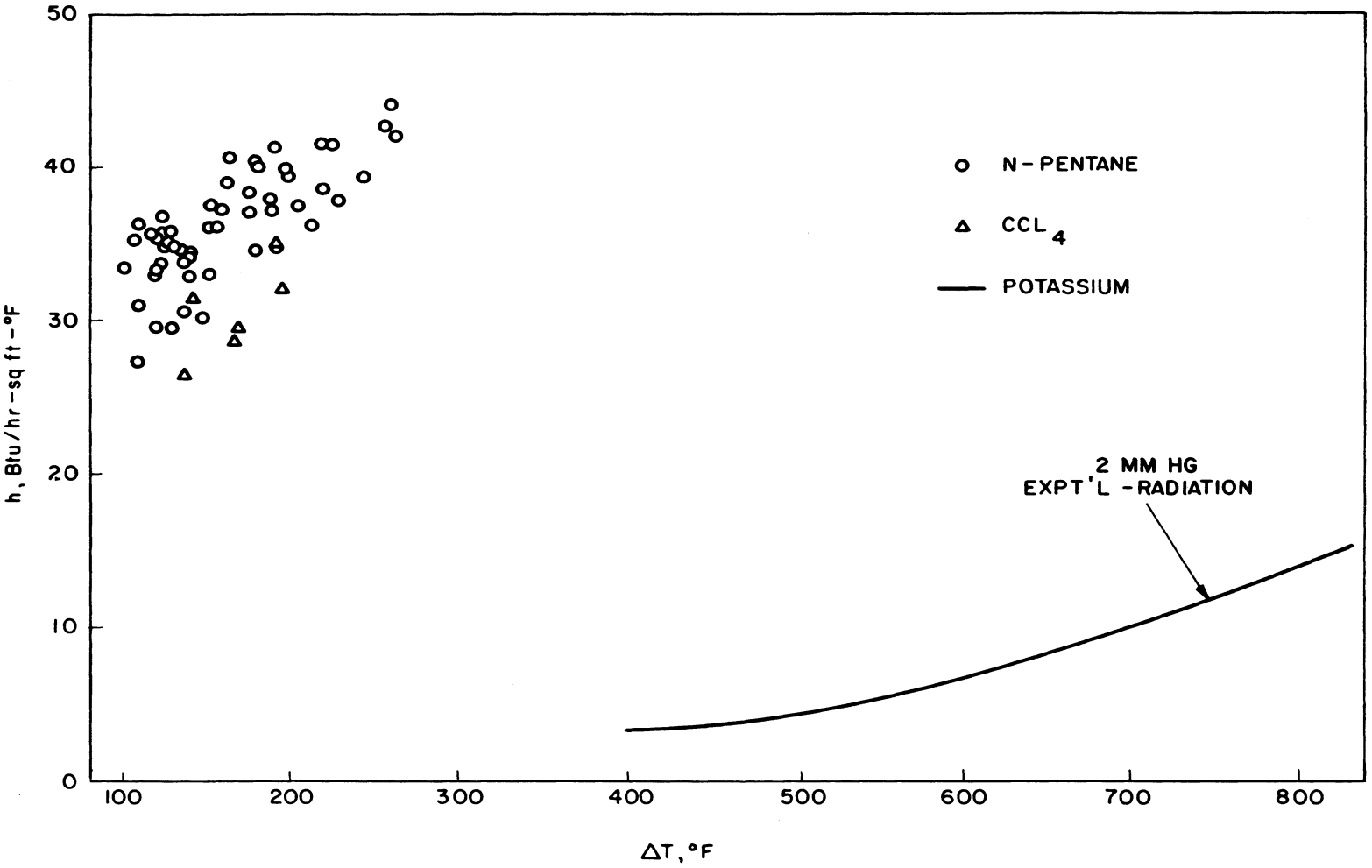

Figure 39 Rapidly Increasing Film Boiling Heat Transfer Coefficients

d. If the data for potassium is limited to a moderate range of temperature differences (last entry in Table IX), reasonable agreement is obtained with the other non-metallic data. Essentially all of the data are above the value of the coefficient assumed by Berenson although the flags showing the estimated scatter of the points indicate that some points will fall below Berenson's coefficient. The reason why Berenson's coefficient is below his points for n-pentane and carbon tetrachloride at the minimum is that the value assumed gave reasonable agreement with the data and also was within the theoretical limits set by his theory. Consideration of all of the non-metallic data gives an average value for the coefficient of 0.92 instead of Berenson's value of 0.72. Including the potassium data for a moderate range of temperature differences gives only a slightly higher coefficient of 0.97 since the potassium results bracket the non-metallic data. Therefore, the equation for the heat transfer coefficient which gives the best fit to all the experimental data is:

$$h = 0.97\left[\frac{k_v^3 \rho_v (\rho_l - \rho_v) g\, \lambda'}{\mu_v\, \Delta T\, D_b}\right]^{1/4} \tag{34}$$

$$D_b = 4.7\sqrt{\frac{3 g_c \sigma}{g(\rho_l - \rho_v)}} \tag{35}$$

Equation 34 predicts the heat transfer coefficient up to moderate temperature differences (200°F) from the minimum flux but does not account for rapdily increasing coefficients at high temperature differences exhibited by some of the experimental data.

In Table VII, it was shown that the minimum heat fluxes obtained for boiling of potassium of 2 mm Hg and 50 mm Hg were an order of magnitude higher than Berenson's and Zuber's predictions. The equation for the minimum heat flux is:

$$(q/A)_{min} = a'\, \rho_v \lambda' \left[\frac{g(\rho_l - \rho_v)}{(\rho_l + \rho_v)}\right]^{1/2} \left[\frac{g_c \sigma}{g(\rho_l - \rho_v)}\right]^{1/4} \tag{36}$$

The value of the coefficient a' assumed by Berenson was 0.09 and was evaluated from his experimental data at the minimum. Zuber predicts a range of values for a' of 0.10 to 0.233 because of uncertainties in the assumptions used in the analysis. The coefficient a' is given by:

$$a' = \frac{(q/A)_{min}}{\rho_v \lambda'} \left[\frac{(\rho_l+\rho_v)}{g(\rho_l-\rho_v)}\right]^{1/2} \left[\frac{g(\rho_l-\rho_v)}{g_c\sigma}\right]^{1/4} \qquad (37)$$

Similar to the treatment of the relationship for the heat transfer coefficient, experimental data for various fluids on horizontal surfaces can be used to calculate the coefficient, a', to see whether it is truly a constant. The results are summarized in Table X. The potassium values used for 2 mm Hg and 50 mm Hg were corrected for radiation and vapor dimerization reaction. The minimum heat flux for potassium at one atm was estimated by Figure 31, giving $(q/A)_{min}$ = 15,000 BTU/hr-sq ft.

From Table X, it is apparent that the minimum heat flux data for potassium at low pressures does not agree with the rest of the data. It is also seen that Berenson's value of 0.09 for the coefficient is much too low for the average of all the experimental data presented. The average value for the coefficient for water, organics, and mercury is 0.140, which is more than 50% above Berenson's value but well within the theoretical range predicted by Zuber. Including the estimated value for potassium at one atm, raises the average value to 0.164. However, the estimated minimum does not include corrections for the effects of radiation and vapor dimerization reaction, which would probably bring the calculated value for the coefficient down close to 0.2. Hence, it is concluded that the equation for the minimum heat flux is best represented by:

$$(q/A)_{min} = 0.14\ \rho_v\lambda'\left[\frac{g(\rho_l-\rho_v)}{\rho_l+\rho_v}\right]^{1/2}\left[\frac{g_c\sigma}{g(\rho_l-\rho_v)}\right]^{1/4} \qquad (38)$$

It is felt that this equation is not valid at low pressures, although more data is needed to substantiate this contention.

Berenson obtained an expression for the temperature difference at the minimum merely by dividing his equation for the minimum heat flux by his expression for the heat transfer coefficient. In Table VII, it was shown that this method predicts unreasonably low minimum temperature differences of 2°F and 36°F for potassium at 2 mm Hg and 0.1 atm, respectively. Although this approach can be followed using the modified equations, it is felt that very large errors might result. The scatter in the experimental data produces an already large uncertainty in the expressions for the minimum heat flux and the heat transfer coefficient and dividing one by the other may compound the uncertainty. However, it is the only available method for estimating the location of the minimum heat flux and thus it may have to be used to see whether a reasonable value is obtained.

In the comparisons between experimental data and correlations, deviations might occur due merely to the uncertainties in determining the physical properties of the various liquid. The properties for n-pentane and carbon tetrachloride were taken from Berenson's report, those for Freon-11 were given

TABLE X

COMPARISON OF MINIMUM HEAT FLUX DATA

Fluid	Coefficient a' (Equation 36)
n-pentane	.134
CCl_4	.091
water	.189
Freon-11	.167
Mercury (Merte)	.119
Potassium (2 mm Hg)	6.74
Potassium (50 mm Hg)	1.16
Potassium (est., 1 atm)	.285

by Hosler and Westwater in their paper, and those for water were taken from McAdams (121). The properties for mercury were taken from Weatherford (178). The properties of potassium were obtained from Weatherford (178), the Naval Research Laboratory Report 6233, the Battelle Memorial Institute Report 4673 and Coe (45). Values for the liquid and vapor densities, latent heat of vaporization and specific heat were taken from the Battelle Report. The density and latent heat values given by NRL were for higher pressures, but agreed well with the Battelle values. The surface tension was taken from Coe. The viscosity of potassium vapor was calculated theoretically (178) and then used along with calculated values of the specific heat to estimate the vapor thermal conductivity. A constant value of the Prandtl number equal to 0.73 was assumed in this calculation. There is no experimental evidence to sbustantiate these values although work is currently in progress at MSA Research Corporation (vapor thermal conductivity), Aerojet-General Nucleonics (vapor thermal conductivity and viscosity) and the University of Michigan (vapor thermal conductivity). Previous experimental work had been carried out by Battelle but the contract was terminated before results could be obtained. The apparatus for determining thermal conductivity gave values for nitrogen which agreed well with published values, thereby providing a check on the experimental technique. However, anolmalous results were obtained for potassium vapor which could not be reconciled within the time allowed for the experimental work. On the other hand, no proof exists for the validity of the technique and apparatus for determining the vapor viscosity. Hence, the conformity of potassium and other alkali metals to the film boiling correlations cannot be more accurately determined without precise values for the transport properties of their vapors.

A by-product of the calculations to determine whether potassium film boiling agrees with correlations proven for non-metallic fluids is the estimation of the bubble diameter. Using Equation 35, which predicts values for the bubble diameter approximately 80% larger than Berenson's equation, the bubble diameter for potassium in film boiling is found to be of the order of one inch. The boiling surface used had a diameter of just three inches and hence edge effects may be significant.

Effect of Radial Gradients in the Boiling Plate

In the present experimental system, the heat flux at the boiling surface must be calculated by measuring the temperature at several points in the boiling plate using thermocouples. The temperature measurements are then used with the known distance between thermocouples and the thermal conductivity to establish the heat flux across the plate. This heat flux is equal to the flux at the boiling surface only if there are no radial gradients. The boiling plate is connected to a tube which serves as the containment vessel for the boiling liquid. The flux lines in the boiling plate depend on the relative resistances to heat flow of the boiling surface and conduction up the tube wall. If the boiling coefficient is very low, as in film boiling, then

conduction up the tube wall can severely distort the flux lines in the plate. Because of this radial heat flow, the temperature gradient in the plate is no longer an accurate measure of the flux occurring at the boiling surface. Because of this radial heat flow, the temperature gradient in the plate is no longer an accurate measure of the flux occurring at the boiling surface. The relationship between the boiling surface flux and the flux calculated by measuring the temperature gradient on the plate in the presence of radial gradients requires a knowledge of the entire temperature field in the boiling plate.

In order to assess the effect of radial gradients, a computer simulation of the boiling plate was carried out. Figure 40 is a diagram of the boiling plate and the model used for the analysis. Finite difference techniques were applied to Laplace's equation in cylindrical coordinates assuming polar symmetry and the resulting system of equations were then solved on the IBM 7090 digital computer.

As an extreme condition, consider the case where the guard heater on the boiler wall was inoperative and thus there was no method of limiting heat flow from the boiling plate up the boiler wall. A set of temperature measurements actually obtained during the preliminary film boiling runs is shown in Figure 41. Because of the assumption of polar symmetry, the experimentally obtained temperatures in the boiling plate are shown as if they were all located along a radius. The thermocouples along the bottom of the boiling plate were used to specify the bottom boundary condition. A thermocouple on the outside of the tube wall approximately 1/16-inch above the level of the boiling surface indicated that the radial gradient from the center of the boiling surface to the tube wall was of the order of 100°F. Another thermocouple located on the radiation shield opposite the boiling plate indicated that the radiation was flowing from the shield to the boiling plate. The temperature of the liquid was 691°F, indicating that boiling was indeed in the film regime. Various values for the boiling coefficient (assumed constant along the boiling surface) were then assumed until reasonable agreement was obtained between the experimental temperatures along the top of the boiling plate and the calculated isotherms in the boiling plate. Figure 41 shows that the isotherms are severely distorted indicating the existence of large radial gradients even near the center of the plate. The heat flux along the boiling surface can be obtained from the computer results and compared with the heat flux which would be calculated by the thermocouple measurements in the boiling plate:

	Heat Flux Btu/hr-sq ft	
	1/2" radius	1" radius
Experimental heat flux	6,500	8,900
Heat flux at boiling surface obtained from computer simulation	3,930	3,870
Experimental error	65%	130%

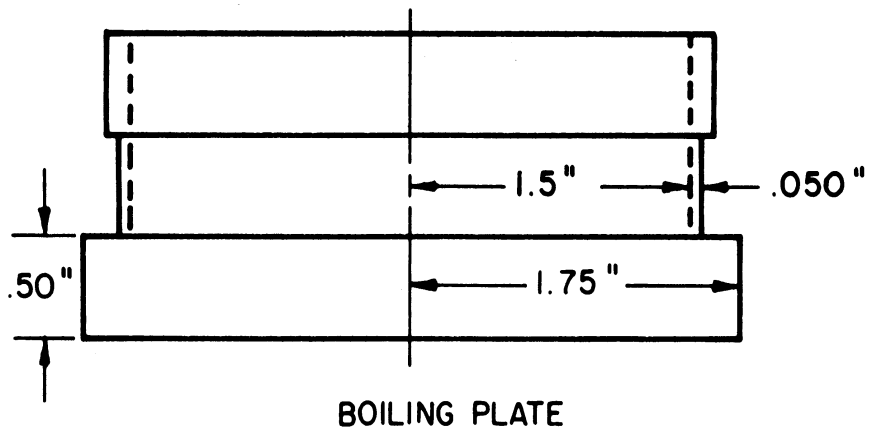

BOILING PLATE

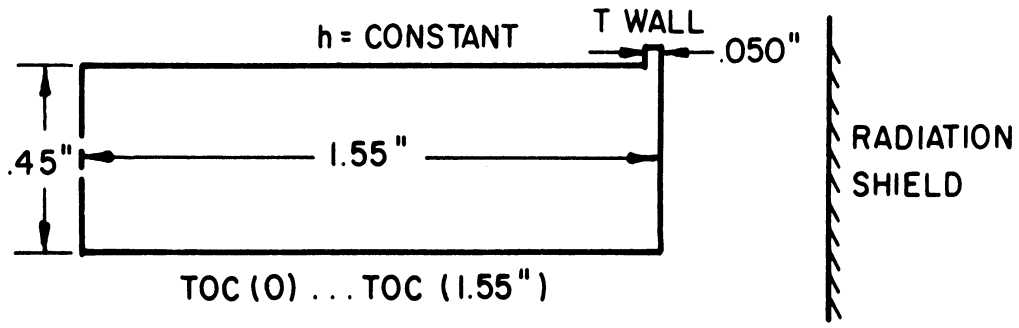

MODEL FOR COMPUTER SIMULATION

Figure 40 Model for Computer Simulation of Boiling Plate

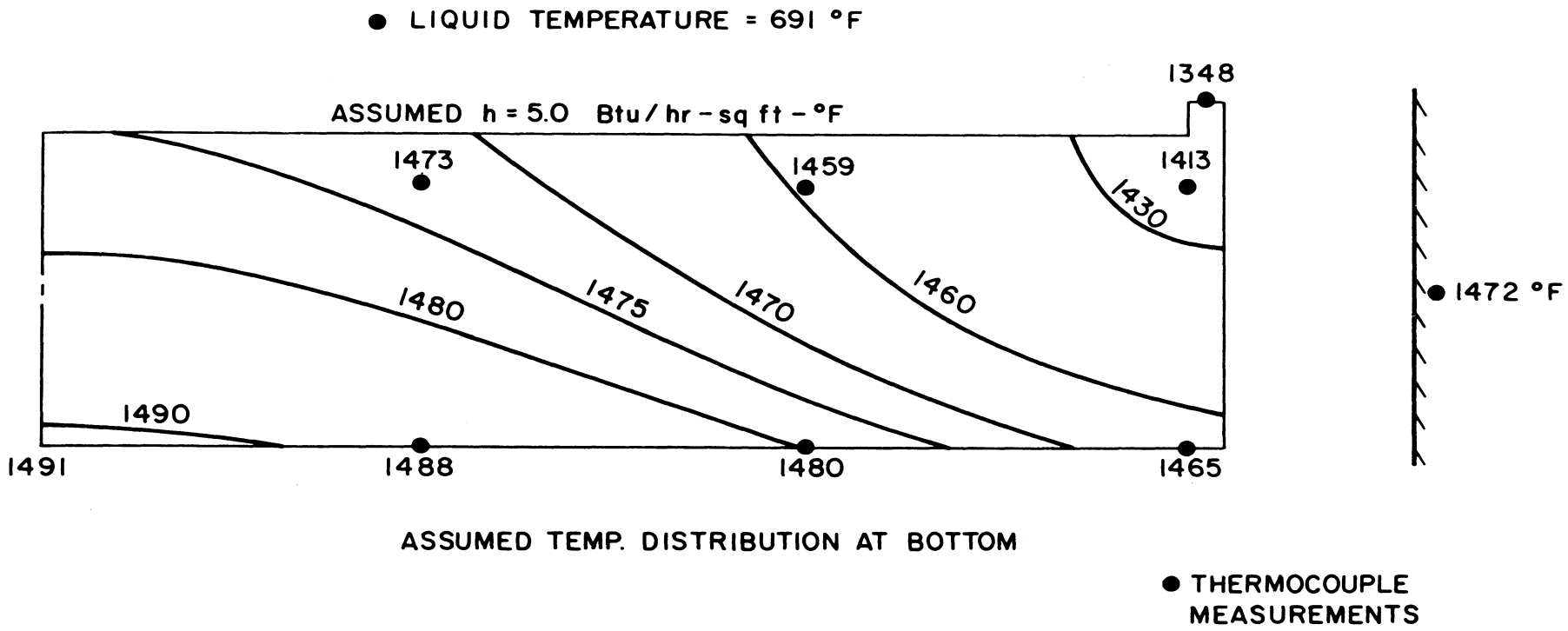

Figure 41 Temperature Distribution in Boiling Plate Obtained by Computer Simulation

Hence, using the 1/2-inch radius thermocouples to calculate the heat flux would result in a value 65% higher than the flux which would be actually occurring at the boiling surface.

The results of the analysis can be used to determine what the difference in the experimental heat flux and the heat flux at the boiling surface would be as a function of radius. In particular, would there be an error if thermocouples were placed in the center of the boiling plate? Using the temperatures corresponding to the depths of the top and bottom thermocouples below the boiling surface, a "calculated flux" can be obtained. The radial variation of this calculated flux is compared with that of the heat flux at the boiling surface in Figure 42. It is seen that if thermocouples were located in the center of the boiling plate, they would calculate a heat flux 55% higher than that occurring in the middle of the boiling surface.

The magnitude of the distortion of the isotherms is highly dependent on the boiling coefficient. Figure 43 shows the effect of varying the boiling coefficient for the same set of boundary conditions. Very little error over a substantial distance from the center of the plate would result for the high coefficients associated with nucleate boiling.

When the guard heater on the boiler wall was replaced, it was possible to adjust this heater during operation so that the difference between the temperature at the outer edge of the boiling plate was within a few degre s of the temperature in the interior of the plate. Under these conditions, the error in the experimentally calculated heat fluxes due to radial gradients would be negligible according to the type of analysis described above. However, the heat loss calibration and the film boiling data indicate the existence of two isolated cold spots at the outer edge of the boiling plate above the location of the bus bars to the graphite heater. The calibration data also show that the interior of the boiling plate at least out to a radius of 1/2-inch is not affected by this heat drain. The effect during film boiling would be expected to be even less, since the heat flow would help to smooth out the isotherms in the region above the bus bars. The maximum effect of the bus bar effect can be obtained by assuming that the heat drain is occurring over the entire outer edge in an annular ring rather than at two circles. Figure 44 shows that the isotherms are almost horizontal out to a radius of 1/2-inch. Hence, the thermocouples at 1/2-inch radius can still be used to calculate the heat flux with negligible error due to radial gradients.

Accuracy of Heat Flux Calculations

The uncertainty in the experimental results lies mainly in the heat flux. The temperature difference between the boiling surface and the liquid is known to within a few percent because this quantity, although it is obtained by taking the difference between two large numbers, is also large. However, the heat fluxes during film boiling were calculated with temperature gradients in the boiling plate of 30°F or less thereby introducing the possibility of a relatively large error. This uncertainty can be discussed in terms of random

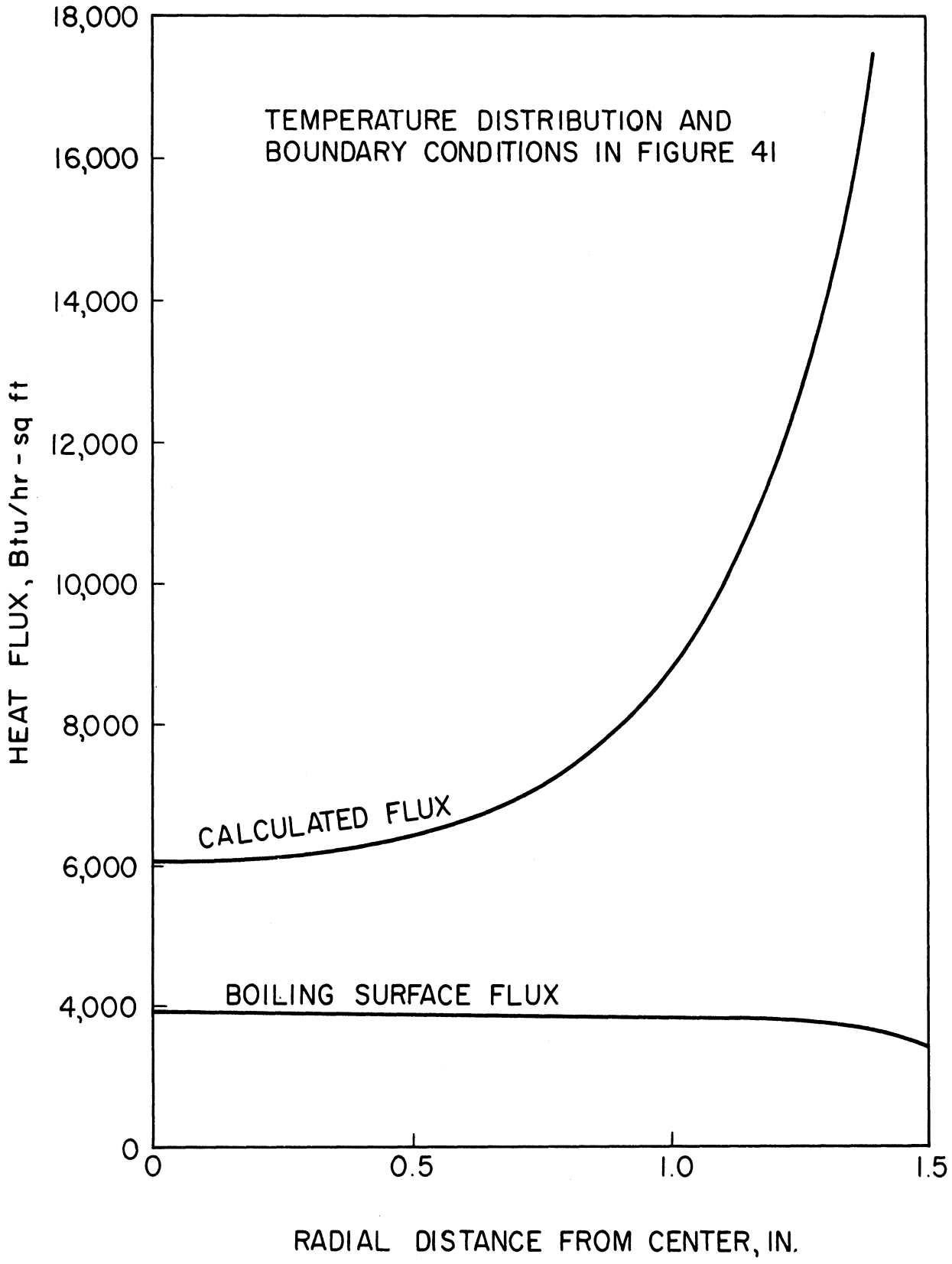

Figure 42 Comparison Between Boiling Surface Flux and Flux Calculated from the Temperature Distribution Obtained by Computer Simulation

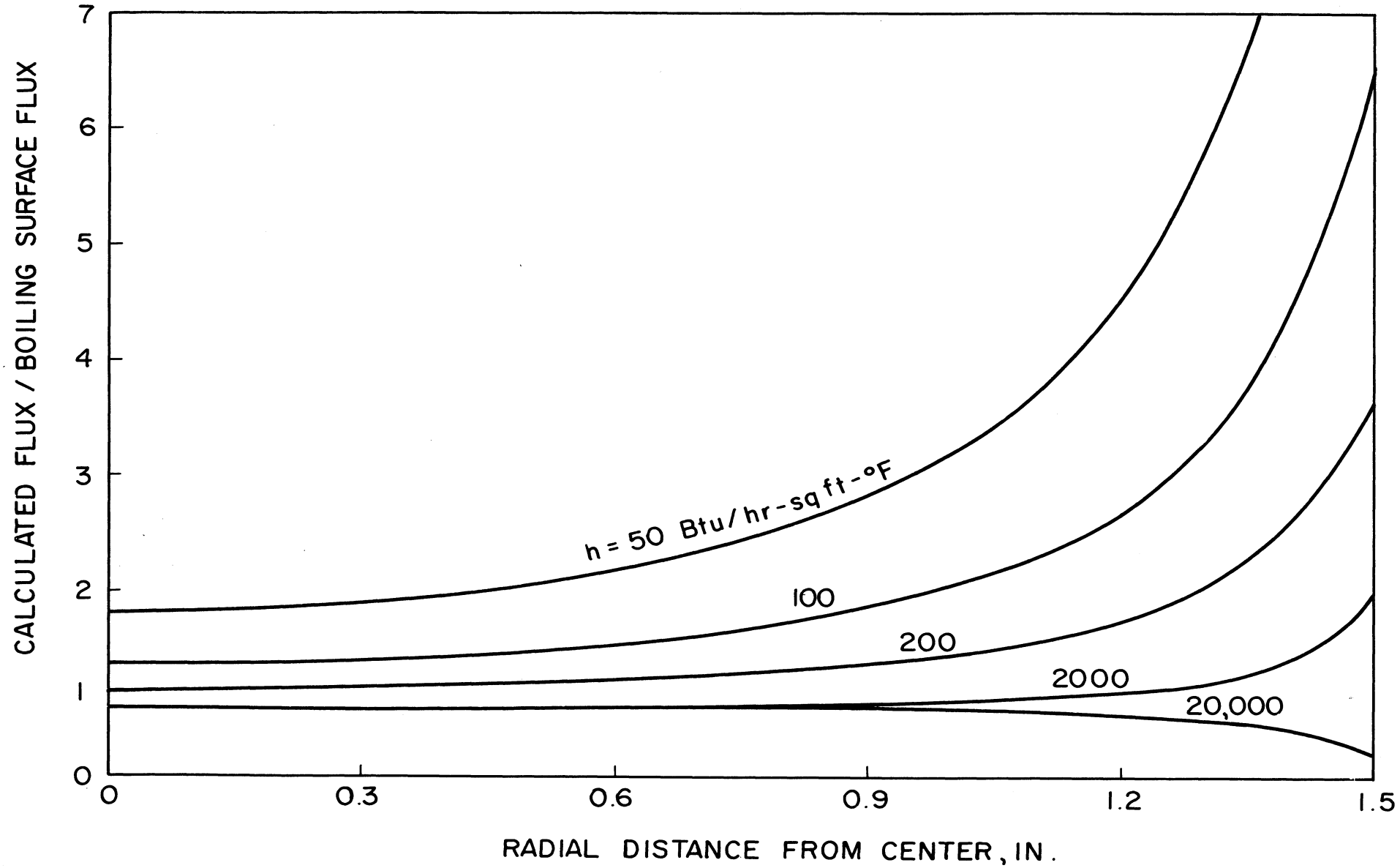

Figure 43 Effect of Boiling Coefficient on Edge Effect Due to Radial Gradients

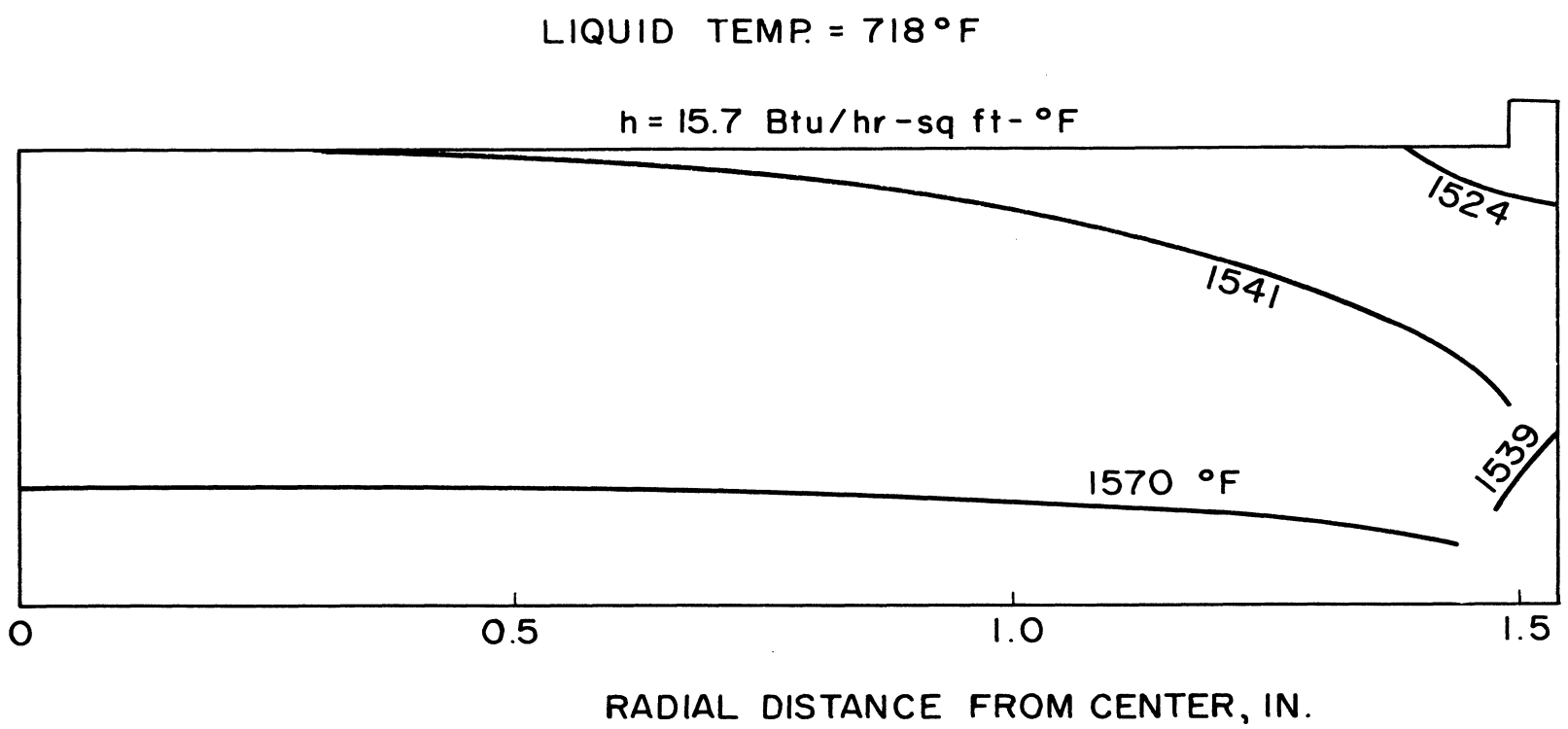

Figure 44 Temperature Distribution in Boiling Plate for Computer Simulation to Determine Maximum Effect of Heat Drain Down Busbars

or accidental errors, systematic or constant errors, and errors of method.

An error of method can arise as a result of approximations and assumptions made in the theoretical development of an equation used to calculate the desired result. It can be assumed that the Fourier equation of heat conduction used to calculate the heat flux is theoretically accurate as long as the correct average thermal conductivity is used and the flow is unidirectional. For the temperature gradients in the boiling plate encountered during film boiling, the thermal conductivity varies a fraction of a percent. It was shown in the previous section on the discussion of radial gradients that the guard heater could be adjusted during operation such that the effect of radial gradients at the location of the thermocouples used to calculate the heat flux would be negligible. Hence an uncertainty in the heat flux due to an error of method can be neglected.

A systematic or constant error arises when some factor operates to continually bias the results. Such errors can be detected by performing the experiment with a number of different apparatus or by calculating the results by several independent methods. Two factors which might introduce systematic errors into the calculation of the heat flux are the thermal conductivity and the distance between the two temperatures used in the Fourier equation. In Figure E-1 in Appendix E, the thermal conductivity of stainless steel as obtained by several researchers agree within 5 percent. Assuming that each of the thermocouple holes were drilled to within .010-inch and that the hot junction of each of the thermocouples is off by one-half the diameter of the thermocouple introduces a possible uncertainty of 23% in the distance used in the Fourier equation. These two factors could combine to give a maximum systematic error in the heat flux of 28%.

Random or accidental errors are inevitable in all measurements and result from errors of observation due to variation in the sensitivity of measuring instruments and the keenness of the senses of perception. They produce expermental scatter but a reliable average value can be calculated statistically if enough measurements are obtained. The actual scatter of the experimental results shown in Figure 29 is relatively low. More than 80% of the points fall within one standard deviation of the curves fitted to the data and only one point falls outside the 95% confidence limits.

The only significant factor which contributed to experimental scatter is the precision with which the temperature measurements are made. It is important that the difference between the thermocouples used to calculate the heat flux is known accurately. All of the 1/16-inch OD Pt-Pt 13% Rh thermocouples were calibrated before use. The equipment and procedures used for the calibration are discussed in Appendix H. The thermocouples TC1 and TC2 were calibrated only to 1480°F, the maximum anticipated saturation temperature of potassium, because they were originally used in the preliminary runs to measure temperatures in the liquid pool. They were used in the boiling plate after modification of the apparatus because the thermocouples used initially could no longer

be inserted into the holes. The thermocouple calibration data in Table H-1 in Appendix H shows that the agreement between TC1 and TC2 is very good and their average difference is 0.3°F over the calibration range 430-1480°F. After they had been in operation in the boiling plate for awhile, they were essentially re-calibrated during the heat loss calibration. The heat loss data in Appendix A shows that TC1 and TC2 agree to within 1°F in the range 997-1632°F. These thermocouples were not re-calibrated in the constant-temperature furnace described in Appendix H since there was a high probability that they would develop open circuits if they were straightened. The two thermocouples that TC1 and TC2 replaced had developed open circuits after they were removed from the system and straightened.

Since the same potentiometer and the same observer were used in both the calibration and data runs, an estimate of the uncertainty in the temperature measurements during film boiling can be obtained from the statistical analysis of the thermocouple calibration data. From Table H-1, the standard deviations of the curves fitted to the calibration data for TC1 and TC2 are 0.9°F and 0.4°F respectively. The 95% confidence limits for TC1 and TC2 would be approximately 1.8°F and 0.8°F respectively, thus giving an uncertainty in their difference of 2.6°F. This corresponds to a maximum uncertainty of 43% which occurs at the lowest heat fluxes encountered during film boiling, whereas the data shows an acutal scatter of 20% at the minimum for the 2 mm Hg results.

An independent method for calculating the heat flux to check that of using the temperature measurements in the boiling plate consisted of subtracting an experimentally-determined heat loss from the power input to the main heater and dividing by the area of the boiling surface. The heat loss calibration ucrve is shown in Figure E-2 in Appendix E and it is seen that all of the points fall within 10% of the best line through the data. The comparison between the heat fluxes calculated by the two methods is shown in Figure 45. Except for two points, the heat flux calculated by the heat loss method is always lower than that obtained by Fourier's equation and the average deviation is 19%.

When one considers all of the possible factors which might introduce systematic or random errors, the maximum uncertainty in the calculated heat flux may be as high as 70%. However, the actual scatter of the data indicates that the uncertainty may be much less. Factors of unknown magnitude may bias the results upward or downward by almost 30% but an independent method of calculation agrees with 19%. It is felt that the present experimental results are accurate to within 30%.

CONCLUSIONS

1. In stable film boiling, the heat flux increases with increasing pressure at a given temperature difference.

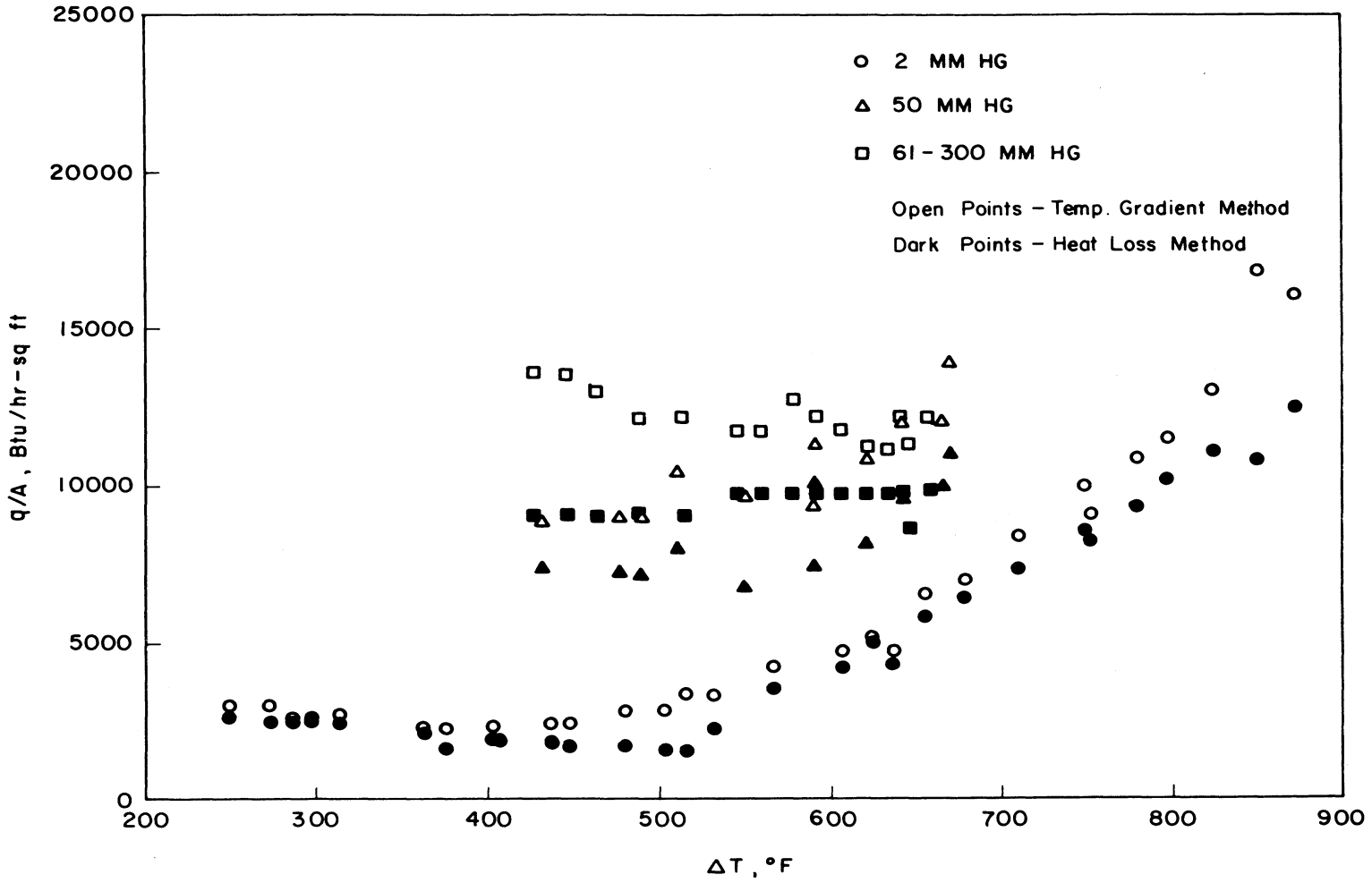

Figure 45 Comparison of Temperature Gradient Method and Heat Loss Method for Calculating the Heat Flux

2. The heat fluxes encountered during film boiling of potassium are substantially above the theoretical predictions. However, the contributions to the heat flux of radiation and the vapor-phase dimerization reaction are significant. After correction for these two factors are made, the experimental results at moderate temperature differences can be correlated to within 22% by the equation,

$$h = 0.97\left[\frac{k_v^3 \rho_v (\rho_l - \rho_v) g\, \lambda'}{\mu_v\, \Delta T\, D_b}\right]^{1/4} \qquad (34)$$

where D_b is the bubble diameter given by the expression,

$$D_b = 4.7\sqrt{\frac{3 g_c \sigma}{g(\rho_l - \rho_v)}} \qquad (35)$$

The constant 0.97 in Equation (34) gives the best fit to the present results and to all of non-metallic data for film boiling from a horizontal surface at moderate temperature differences. Film boiling data for mercury does not agree with Equation (34) nor to most of the other correlations currently available.

3. The present results at low pressure do not agree with present correlation for predicting the minimum heat flux. However, the data indicates that the prediction of Zuber might be in agreement at higher pressures near 1 atm. The best fit to all of the metallic and non-metallic data is given by the correlation,

$$(q/A)_{min} = 0.14\, \rho_v \lambda' \left[\frac{g(\rho_l - \rho_v)}{\rho_l + \rho_v}\right]^{1/2} \left[\frac{g_c \sigma}{g(\rho_l - \rho_v)}\right]^{1/4} \qquad (38)$$

4. No reliable method for predicting the location of the minimum heat flux for all fluids is currently available.

5. The film boiling heat transfer to potassium, as well as to some non-metallic fluids, increases more rapidly at high temperature differences than can be accounted for by available correlations.

LIQUID METAL BOILING IN AGRAVIC FIELDS

Herman Merte, Jr.

INTRODUCTION

Test apparatus was designed and constructed to obtain data on the influence of increased body forces, up to a/g = 20, on nucleate boiling of liquid metals. Mercury was selected as the initial fluid, and the flat heating surface is oriented such that the body forces are perpendicular to it. The test vessel is shown in Figure 46 and the centrifuge schemtic in Figure 47. Detailed descriptions are given in Reference (8).

The heater surface initially consisted of a 0.001 inch thick foil of 347 stainless steel attached to a copper heater block containing cartridge-type electrical heaters. Some data obtained with this surface are presented below, but difficulties arose in maintaining a sufficient degree of wetting to produce nucleate boiling. Early operation gave consistent nucleate boiling, but as time progressed the boiling mode would vary unpredictably between nucleate and film boiling on startup. Trace additives of Mg and Ti were of assistance for short periods of time only.

The stainless steel foil was removed and replaced with C-1010 carbon steel sheet 0.005 inches thick. This was assembled to the copper heater block in the same manner as the stainless steel foil. Prior to assembly the surface to be in contact with the mercury was given a thin plating of copper to promote initial wetting by the mercury. Nucleate boiling was then obtained fairly consistently.

TEST CONDITIONS AND PROCEDURES

The independent variables in the data presented below consisted of pressure P(20, 80, 300 psia, nominal), heat flux q/A (18,000 to 405,000 BTU/hr-ft^2), and effective gravitational acceleration a/g (= 1, 5, 10, 15).

A liquid depth of 1/2 inch was used for all the tests reported here. The nominal pressure measured and listed is that at the liquid free surface. For determination of the saturation temperature at the heat surface, $T_{sat.}$ H.S. corrections in pressure due to changes in hydrostatic head with acceleration were applied. Argon was used as the pressurant, and once operation began an inert atmosphere was maintained at all times.

Figure 48 is a schematic of the test vessel identifying the location of the various thermocouple temperature measurements made, and is included for reference.

The bulk subcooling of the liquid could not be controlled, and varied from -5°F (superheat) to 8°F for nucleate boiling, depending on the heat flux level

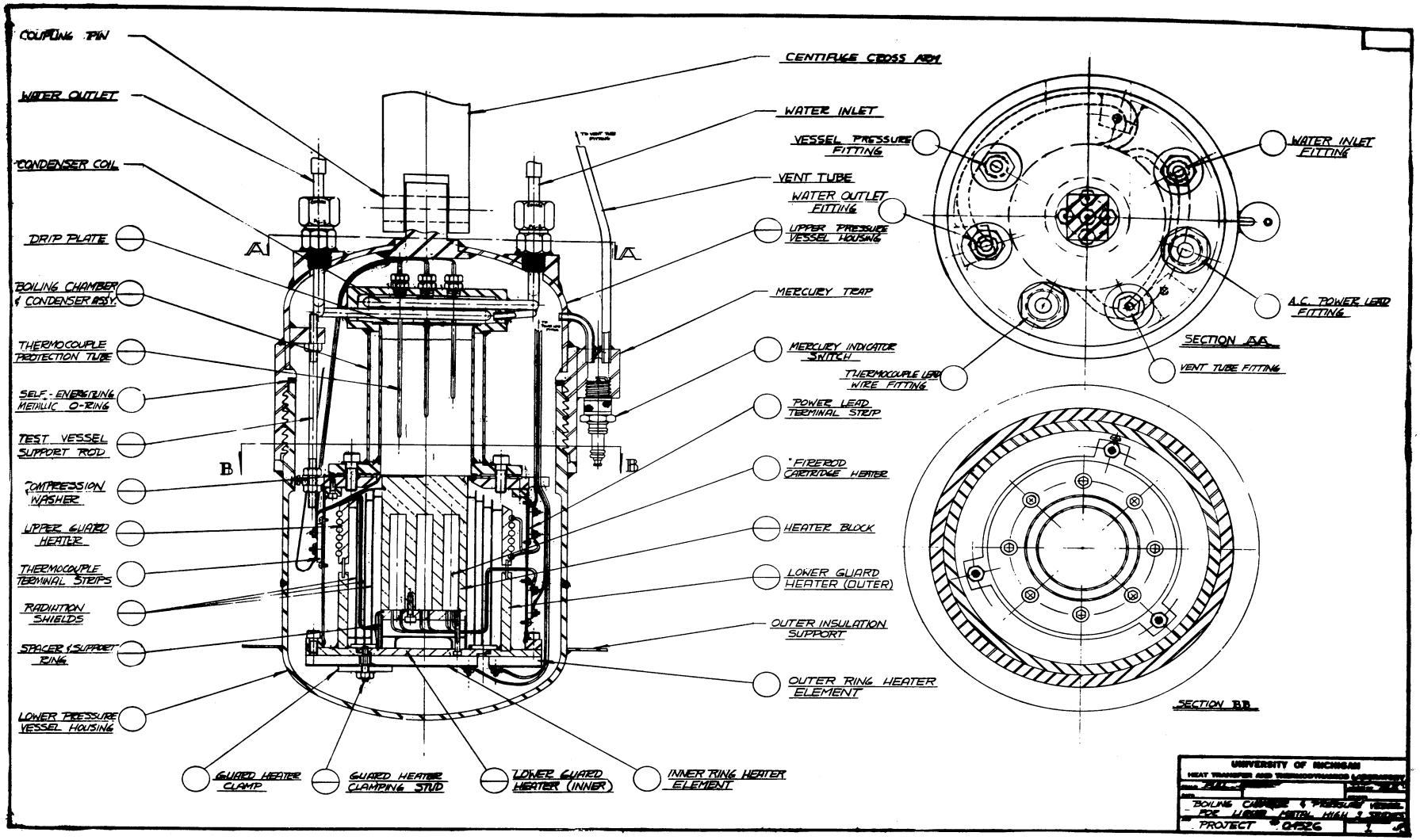

Figure 46 Test Vessel for Boiling Mercury Study Under High Gravity.

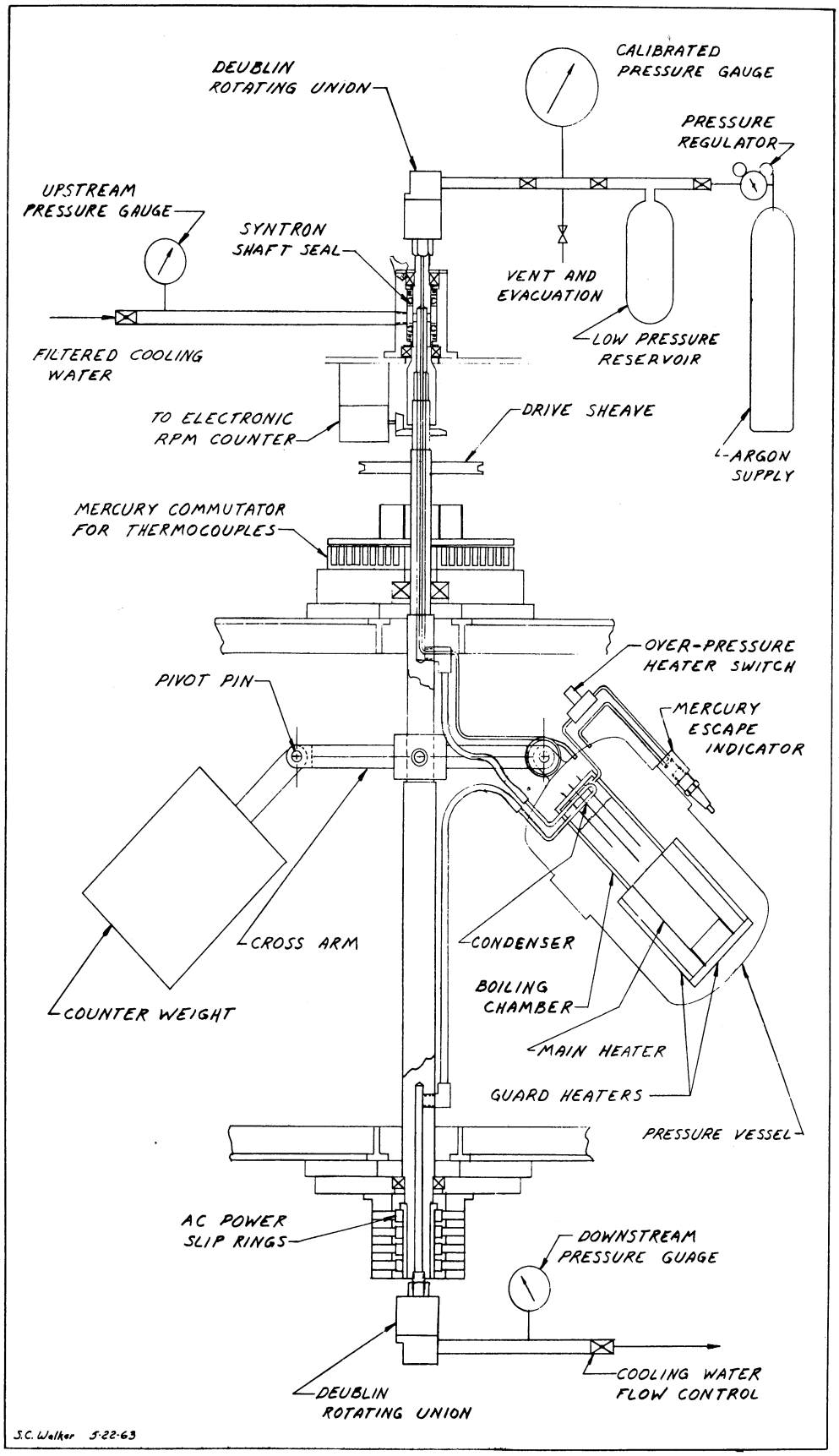

Figure 47 Mercury Boiling Test Vessel in Centrifuge

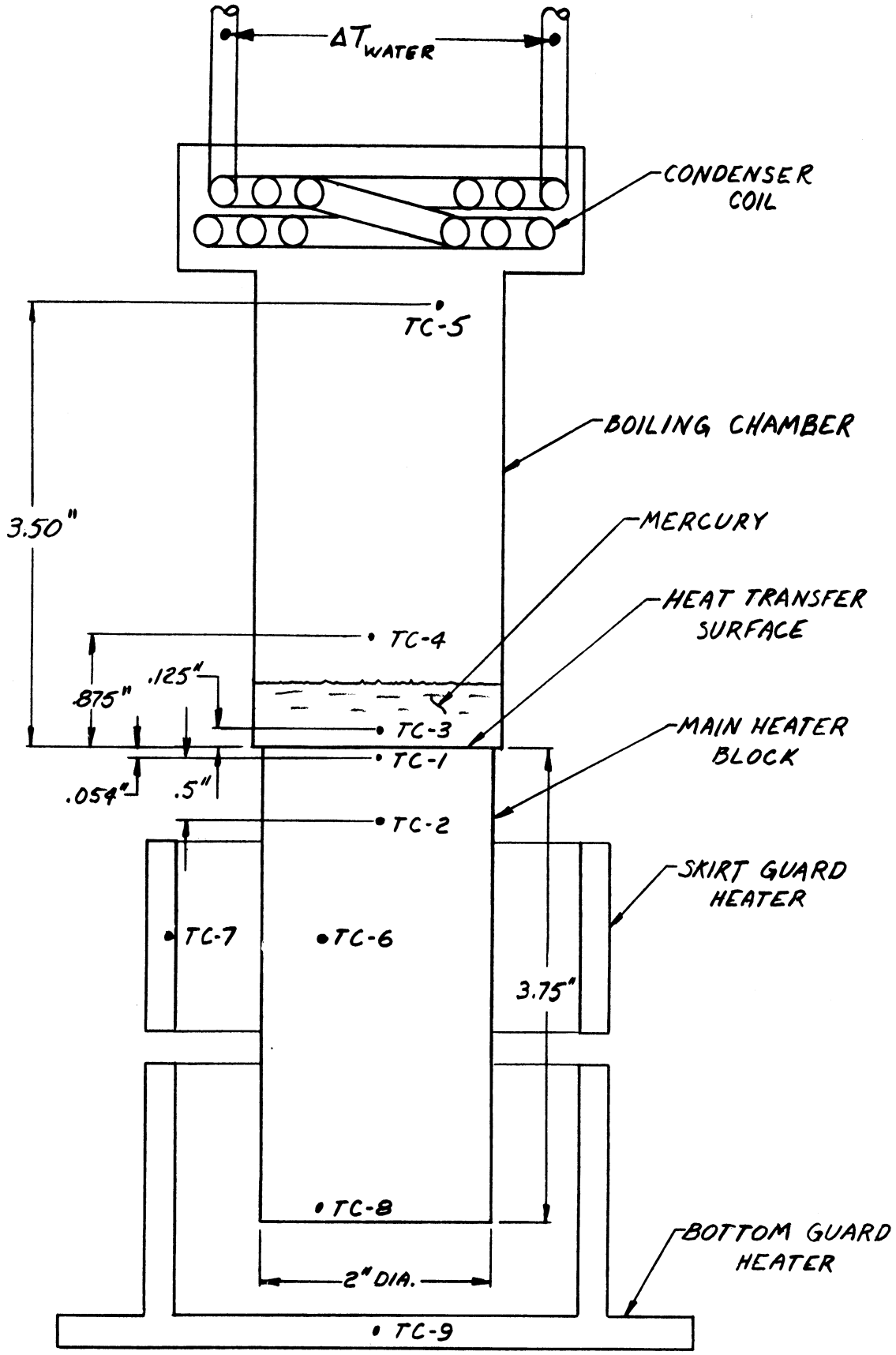

Figure 48 Thermocouple Locations for Reference

and acceleration, and on how it is defined. This latter point will be clarified below.

The significant parameters for all the tests conducted are listed in Appendix I. It is appropriate to describe the headings in the table at this point. The run numbers indicate the sequence in which the data were obtained. The pressure at the liquid free surface, the heat flux, and acceleration level are self-evident.

$T_{H.S.}$ is the heat transfer surface temperature and is computed by extrapolating the temperature measured approximately 1/32 inch below the heater surface (TC-1 in Figure 48).

$T_{sat.\ H.S.}$ is the saturation temperature at the heat surface, determined from the measured free liquid surface and the appropriate hydrostatic head.

$\Delta T_{sat.}$ is the difference between the above two quantities ($T_{H.S.}$-$T_{sat.\ H.S.}$), and might be termed the heater surface superheat.

T_B is the temperature of the liquid as measured 1/8 inch above the heater surface at the center. This is the only temperature measurement in the liquid, and no specification can be made concerning the temperature distribution within the liquid. However, with boiling of mercury at standard gravity in another work (26), it was found that the bulk mercury temperature was essentially that of the saturated liquid at the liquid-vapor interface, hence somewhat subcooled at the heating surface. This will be seen to be the case for the most part in the present work when the heat flux is sufficiently large. With the lack of other information it will be assumed that, with the relatively small liquid depth involved and the intense fluid notion arising with higher acceleration, the liquid is uniform in temperature. Measurements with water under similar circumstances (28) indicated this type of behavior.

ΔT_B is the difference between the heater surface and measured liquid temperature ($T_{H.S.}$-T_B). This parameter is of significance in non-boiling convection. The difference between $\Delta T_{sat.}$ and ΔT_B is of course the same as the difference between $T_{sat.\ H.S.}$ and T_B, and indicates the local liquid subcooling at the heater surface. This quantity is tabulated in the next-to-last column as Subc. at H.S.

T_{VI} is the measured temperature in the vapor space about 3/8 inches above the free liquid interface (TC-4 in Figure 48) and T_{V2} is the measured vapor temperature just below the condenser coils (TC-5 in Figure 48).

$T_{sat.\ F.S.}$ is the saturation temperature corresponding to the measured system pressure, and is thus the saturation temperature at the free liquid surface.

The difference between the saturation temperature at the free surface $T_{sat.\ F.S.}$ and the bulk temperature T_B is the subcooling at the free surface

and is tabulated as Subc. at F. S. in the last column (= $T_{sat.\ F.S.}-T_B$). It should also be noted that the difference ($T_{sat.\ H.S.}-T_{sat.\ F.S.}$) is equal to the difference in subcooling between the heat surface (H.S.) and liquid free surface (F.S.), and represents the change in saturation temperature within the liquid due to the hydrostatic head. It will be noted that in several cases that the liquid will be superheated somewhat with respect to the free surface but still subcooled at the heater surface.

The last column in Appendix I, Subc. at F.S., provides an indication as to how closely the bulk liquid temperature approaches the saturation temperature corresponding to the free surface. It is noted that in general this quantity decreases as heat flux is increased, and also as acceleration is increased.

At high levels of heat flux, where large quantities of vapor are leaving the liquid surface, it might be expected that the measurement of this vapor temperature, T_{V1}, should be quite close to the $T_{sat.\ F.S.}$ if the original calibrations of the thermocouples were made with accuracy. Comparing these at levels of heat flux q/A = 100,000 BTU/hr-ft^2 and above, one notes the maximum difference varies between 0.2 and 1.4°F, and verifies the accuracy of the level of temperature measurements.

Before the data obtained were considered as valid, the system was operated at a minimum of 1/2 hour at each condition. The independent variables were P, q/A and a/g. P and q/A were held constant for each test in the majority of cases, and a/g varied.

Test Run numbers 6, 7 and 17 correspond to the type 347 S.S. heat surface, whereas all subsequent tests were conducted with the carbon steel (C-1010) surface.

EXPERIMENTAL ACCURACY

Heat Flux

The heat flux was computed in three ways: (a) from the electrical power input to the main heater, (b) from the enthalpy rise of the coolant, (c) from the temperature gradient within the heater block. In general, when water was used as a coolant, (a) and (b) were in excellent agreement for steady-state conditions. Although guard heaters were installed around and under the main heater block, these could not always be controlled to match the heater temperatures closely. It is estimated that a conservative accuracy of heat flux level is ± 5 percent.

Acceleration

The equivalent acceleration at the heater surface is calculated from the measured rotational speed and the geometry of the system, and is known within

± 1 percent.

Pressure

At pressure levels of 80 and 300 psia a precision pressure gage was used, having an overall uncertainty of ± 1/4 psi. This pressure was used to determine the saturation temperature, and at a pressure level of 80 psia, the uncertainty in $T_{sat.\ H.S.}$ and $T_{sat.\ F.S.}$ is ± 0.5°F. At a pressure level of 300 psia these uncertainties are ± 0.2°F. At a pressure level of 20 psia a mercury manometer was used, which could be read to ± 0.05 "Hg. This corresponds to an uncertainty in $T_{sat.\ H.S.}$ and $T_{sat.\ F.S.}$ of 0.1°F.

At various pressure levels, and hence saturation temperature levels, the density of the mercury changes. At any given acceleration level, however, the hydrostatic head at the heater surface, in psi, is independent of this density change since a fixed and known amount of liquid is present.

Temperature

The chromel-constantan thermocouples were "aged" 24 hours at 1200°F, and then calibrated from ambient to 900°F by comparison with a platinum resistance thermometer in a large constant temperature block. Using a type K-3 L & N potentiometer, it is estimated that levels of temperature are measured with ± 0.5°F accuracy while relative temperatures can be measured within ± 0.1°F. The rotating mercury slip ring assembly was found to introduce signal errors of less than 5 microvolts.

The maximum uncertainty of temperature measurement of ± 0.5°F, combined with the maximum uncertainty of $T_{sat.\ F.S.}$ of ± 0.5 arising from the uncertainty in pressure measurement combine to give a total uncertainty of ± 1.0°F when comparing the measured vapor temperature T_{V1} with the saturation temperature. As pointed out earlier the largest difference observed was 1.4°F, well within the 2°F possible difference.

EXPERIMENTAL RESULTS

The results are tabulated in Appendix I. To facilitiate observing the influence of a/g, with P and q/A held constant for each test, the data are plotted as measured temperatures versus a/g for each test. These are referred to individually below, with remarks as appropriate. Composite plots for overall behavior are then presented later.

Run Number 6 (Figure 49)

a/g = 1 ; P = 80 psia; q/A = 23,000 BTU/hr-ft^2

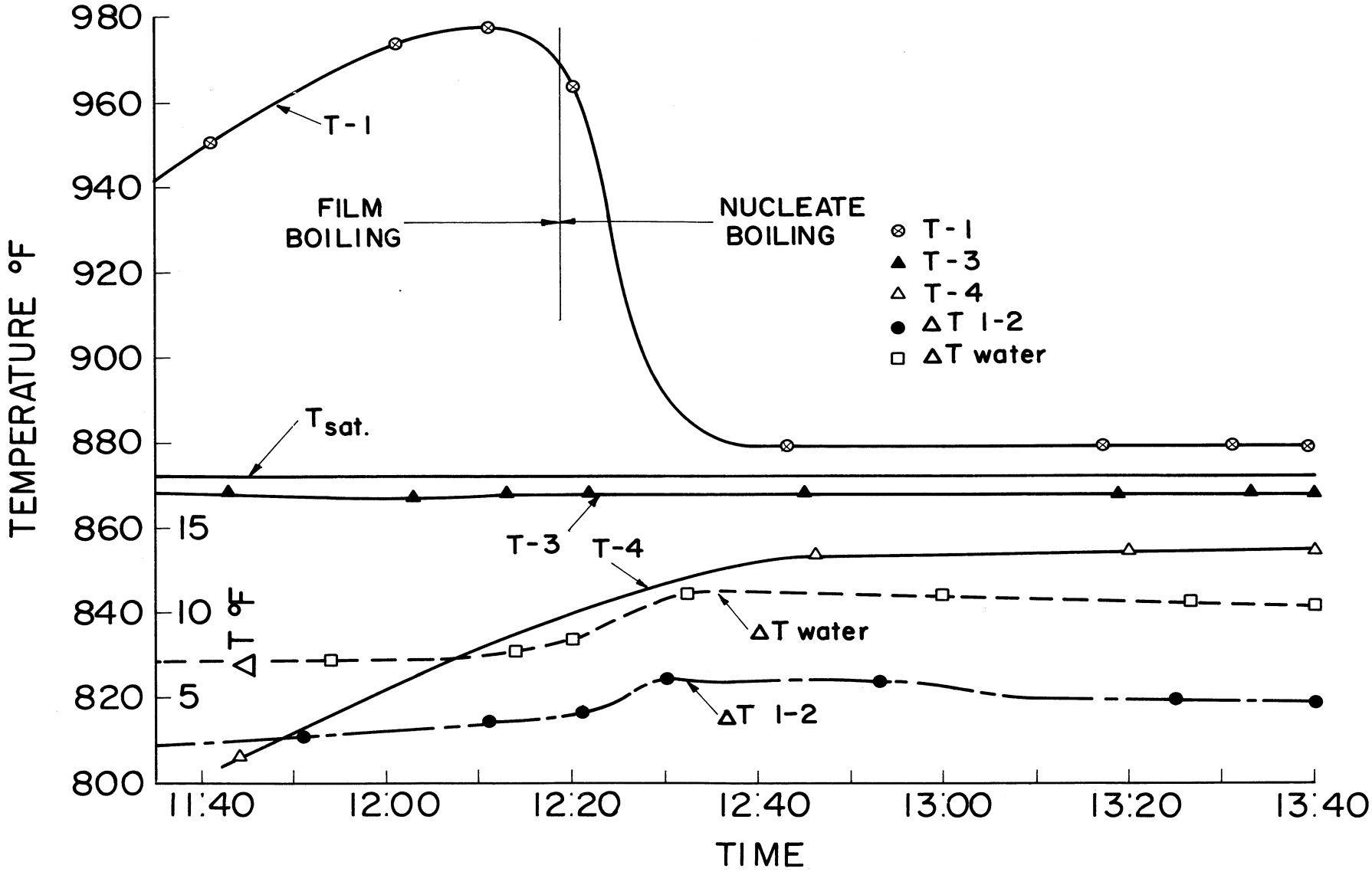

Figure 49 Time-Temperature Data for Run No. 6

This shows the time-temperature data in the later heatup and steady-state stages. The bulk liquid temperature (T-3) remains constant, being about 4°F subcooled, while the heater surface temperature rises and then suddenly drops. The power input to the heater was constant in this period, being equivalent to a heat flux of q/A = 23,000 BTU/hr-ft^2 at the heat transfer surface. It is believed that at some time prior the boiling mode went directly into film boiling from natural convection, and spontaneously reverted to nucleate boiling. While in film boiling a significant portion of the power input was going into heating of the copper block, rather than in producing vapor. This is supported by the behavior of the temperature in the vapor space (T-4), which rises suddenly with nucleate boiling, and the increase in ΔT(1-2) and ΔT_{water}, which are proportional to the rate of heat transfer to the mercury.

Similar behavior was observed by other workers (26) where apparent premature film boiling was attributed to the non-wetting characteristics of mercury. When suitable "conditioning" of the surface had taken place, the system reverted to nucleate boiling. In Figure 49, it appears that with the initial startup the mercury was not wetting the stainless-steel surface to a sufficient degree until after some period of operation.

Run Number 7 (Included in Figure 51)

a/g = 1 ; P = 80 psia ; a/A = 46,900 BTU/hr-ft^2

No tendency for film boiling was observed.

Run Number 8 (Figure 50)

a/g = 1 ; P = 80 psia ; a/A = variable

In initiating this test at q/A = 100,000 BTU/hr-ft^2 film boiling set in. It was then conducted to find the order of magnitude of the maximum heat flux for this system with nucleate boiling at a/g = 1. This was accomplished by raising the power level in small increments. In order to do so in a reasonable length of time it was not possible to wait for true steady-state at each level. Thus, some care should be exercised in comparing these results to steady-state results. Figure 50 shows the data for the entire period, along with indications of the regimes of boiling present. The transition from nucleate to film boiling, or the maximum heat flux, is fairly well defined, and is accompanied by a pronounced increase in temperature level of the heater, even with a large decrease in heat flux. The temperature measurement in the vapor region near the cooling coil (T-5) dropped off scale on the recorder, as might be expected with the decrease in vapor generation rate. To determine the approximate region of the minimum heat flux for film boiling, the heat flux was then reduced in small increments until the system reverted to nucleate boiling, as is indicated in Figure 50.

A summary of the results for periods closet to steady-state are given below:

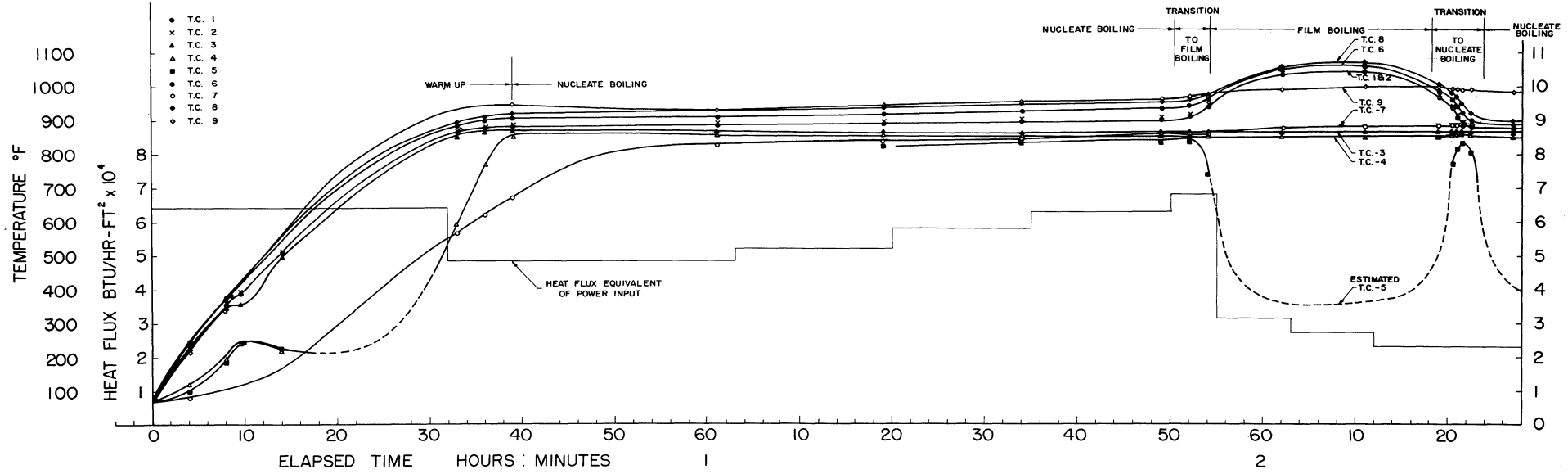

Figure 50 Time-Temperature Data for Run No. 8

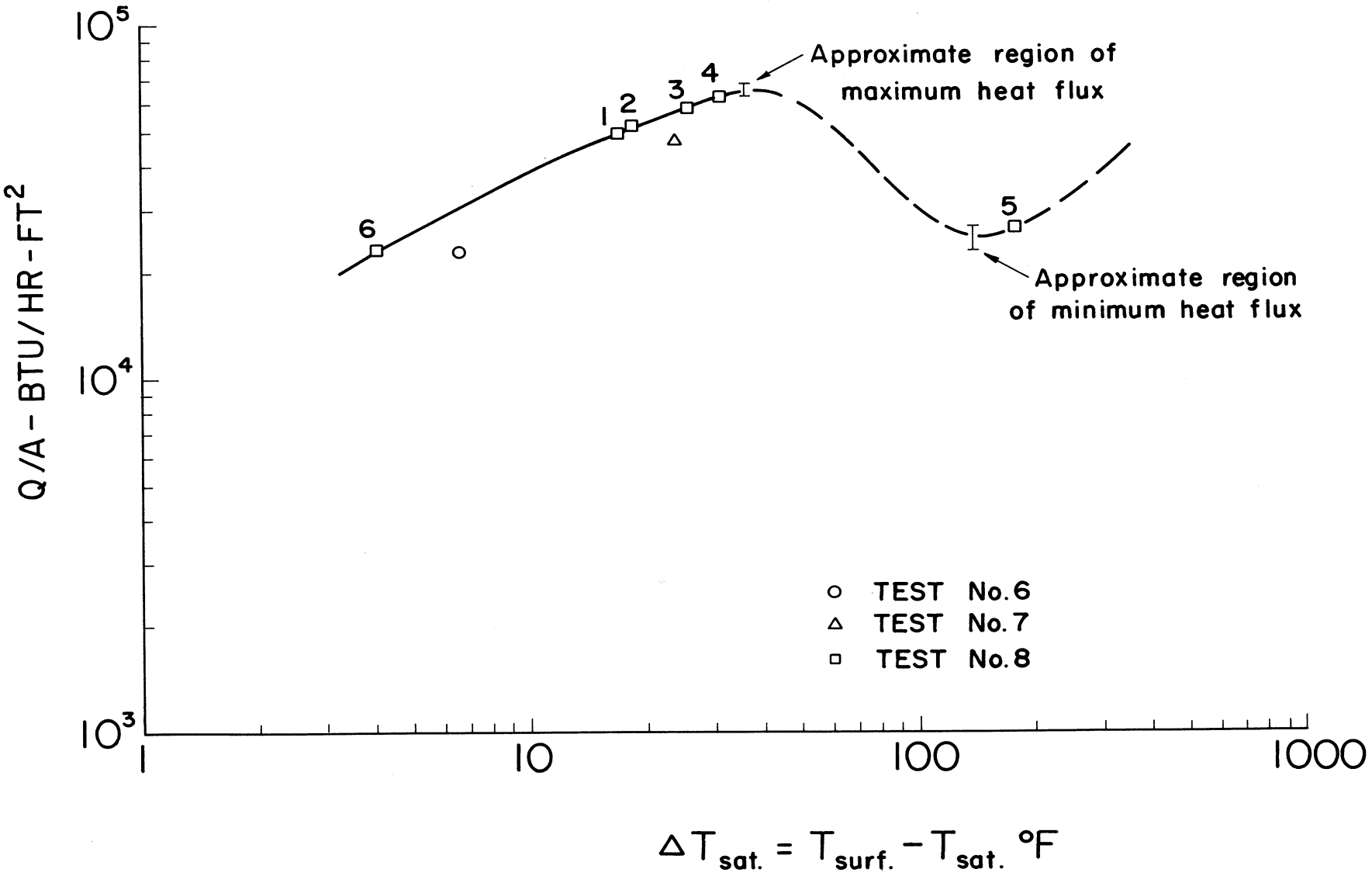

Figure 51 Boiling Data for Mercury

TABLE XI

Test Run No. 8 a/g = 1

P = 78.2 psia Mercury Depth = 1/2" T_{sat} = 871.6°F

Time	Data No. Fig. 50	q/A $\frac{BTU}{hr \cdot ft^2}$	T-1	T-3	T_{surf} °F (Estim.)	ΔT_{sat} °F	Remarks
1:01	1	48,500	890.0	868	888.6	17.0	Nucleate Boiling
1:19	2	52,000	891.3	867	889.8	18.2	Nucleate Boiling
1:34	3	58,000	898.4	867	896.8	25.2	Nucleate Boiling
1:49	4	63,000	904.0	866	902.2	30.6	Burnout occurs within this region of heat flux.
1:53		68,000	B.O. ≈910	866		B.O. ≈36	
2:11	5	27,000	1051.3	866	1050.7	179.1	- Stable Film Boiling. Transition from minimum film to nucleate.
2:19		23,000	Min. ≈1010	867		Min. ≈140	
2:27	6	23,000	876.1	867	875.6	4.0	Nucleate Boiling

The maximum heat flux occurs within the region q/A = 63,000 - 68,000 Btu/(hr)(sq ft) with ΔT_{sat} 36°F, and the minimum film boiling heat flux occurs within the region q/A = 23,000 - 27,000 Btu/(hr)(sq ft) with ΔT_{sat} 140°F. For comparison with the steady-state data of Runs 6 and 7, the data above are plotted on Figure 51.

The correlation of Noyes (136) based on Na data predicts a maximum heat flux for mercury of $(q/A)_{max} = 2.6 \times 10^6$ Btu/(hr)(sq ft) for the tes conditions here. The gorss discrepancy with the experimental results here may well be a consequence of the poor wetting of mercury with the type 347 stainless steel heating surface used.

Run Number 17

a/g = 1, 5 ; P = 80 psia ; q/A = 18,000 BTU/hr-ft^2

With subsequent tests it was not possible to obtain nucleate boiling at all. Small amounts of Mg were added to the mercury, which was successful in producing nucleate boiling for short periods of time only. It was then planned that data for film boiling at high acceleration be obtained, with the view that this may assist in producing nucleate boiling again. The cooling system was modified to use air as well as water, so the liquid could be maintained at saturation conditions with the low heat flux associated with film boiling. The results for one run are tabulated below:

TABLE XII

Test Run No. 17

P = 80.3 Mercury Depth = .55" $q/A = 18{,}000$ Btu/hr-ft^2

	a/g = 1	a/g = 5
T_{sat} (at Heater Surface)	875.3	877.2
ΔT_{sat} - °F	282	101
T_{liq} - °F	873.7	874.8
h - Btu/hr-ft^2 - °F	64	178

The increase in the heat transfer coefficient by a factor of almost 3 for a 5-fold increase in a/g is noted, although any general conclusions must await the availability of more data.

Run Number 19 (Figure 52)

a/g = 1, 5 ; P = 80 psia ; $q/A = 18{,}500$ BTU/hr-ft^2

For this and all subsequent tests the type 347 stainless steel heating surface was replaced by a C-1010 carbon steel surface. On initial heat-up, film boiling was established, even at this low flux. Steady conditions were not reached, but the centrifuge was rotated at a/g = 5 to break down the vapor film. Once this occurred it is noted from the data in Table I that boiling was completely suppressed at a/g = 5. Upon return to a/g = 1, boiling did not return but ΔT_B

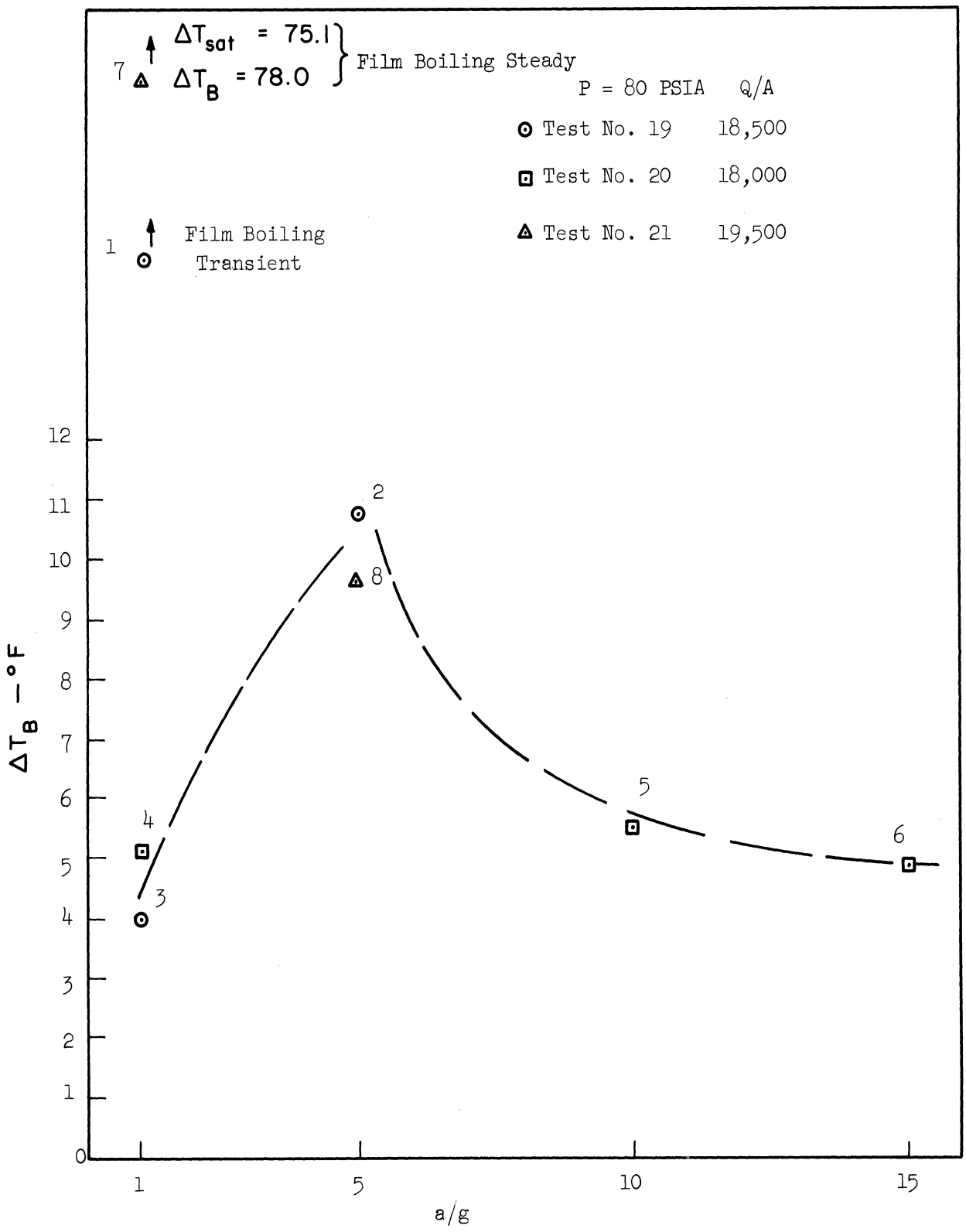

Figure 52 Non-Boiling Natural Convection Data for Mercury Under High Gravity

reduced below that observed at a/g = 5, from ΔT_B = 10.8°F at a/g = 5 to ΔT_B = 4.0°F at a/g = 1. This unexpected behavior was reproduced in the following two independent tests.

Run Number 20 (Figure 52)

a/g = 1, 10, 15 ; P = 80 psia ; q/A = 18,000 BTU/hr-ft^2

In this test no boiling was present, even at the initial a/g = 1, with ΔT_B being close to that for the previous run, although these tests were conducted several days apart. At a/g = 10, ΔT_B rose somewhat and then decreased at a/g = 15. It appears that with extremely good wetting that buoyant forces are not controlling in heat transfer between the solid surface and the mercury.

Run Number 21 (Figure 52)

a/g = 1, 5 ; P = 80 psia ; q/A = 19,500 BTU/hr-ft^2

The two previous runs were repeated once more to check reproducibility, and on start up film boiling again occurred. Upon rotation to a/g = 5, boiling was again suppressed completely as seen in Figure 52, with ΔT_B close to that for Run Number 19.

The strange pattern of non-boiling convection shown in Figure 52 is most interesting and as yet unexplained. It may be the manifestation of some type of critical instability in the vicinity of a/g = 5, and may warrant further investigation.

Run Number 22 (Figure 53)

a/g = 1 - 15 ; P = 80 psia ; q/A = 34,000 BTU/hr-ft^2

Both $\Delta T_{sat.}$ and ΔT_B decrease as acceleration increases, and the value of $\Delta T_{sat.}$ is lower at a/g = 1 after being subjected to the higher acceleration. This will be noted to occur quite regularly, and most likely is an effect of a surface "conditioning" arising from operation at the higher accelerations. If the bubble sizes are decreased with acceleration, it is possible that additional nucleating sites are activated and remain active after return to a/g = 1.

The subcooling at the liquid free surface decreases between a/g = 1 and a/g = 5, and then remains fairly constant, whereas the subcooling at the heater surface first decreases and then increases. This behavior will also be observed in a number of subsequent tests, and it may bear some relation to the behavior noted in Figure 52. Since the heat flux is imposed, the temperature level of the liquid will be determined in part by the relative thermal resistance between the heater surface and the liquid, compared to an equivalent thermal resistance between the liquid and the coolant fluid in the condenser coils. The latter type of heat transfer is a complex phenomena involving evaporation, diffusion through an inert gas, and natural convection.

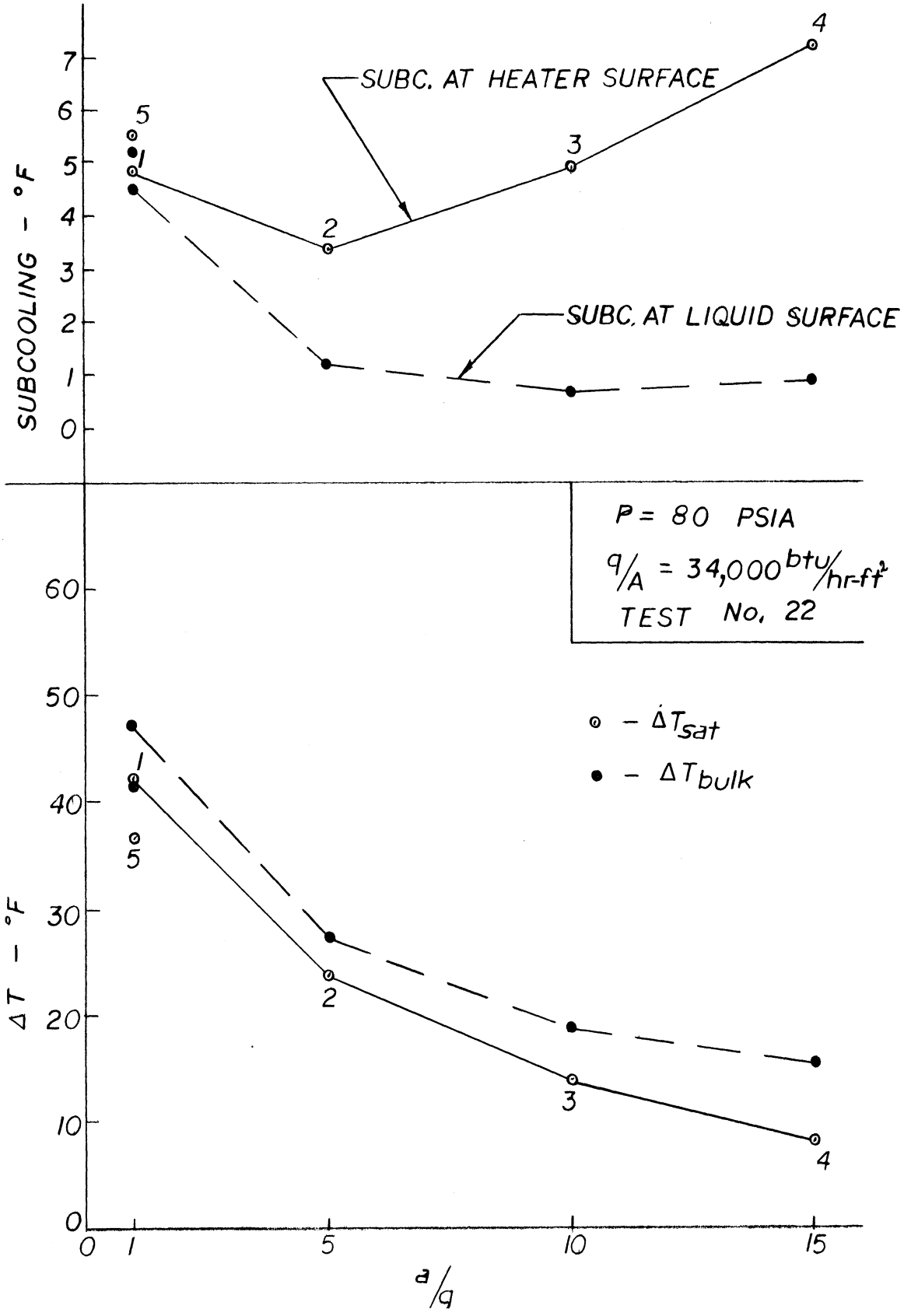

Figure 53 Mercury Boiling Data under High Gravity, Run Number 22

Run Number 23 (Figure 54)

$a/g = 1 - 15$; $P = 80$ psia ; $q/A = 46{,}000$ BTU/hr-ft^2

The behavior is similar to that of Run Number 22. Quite a pronounced change in $\Delta T_{sat.}$ takes place between $a/g = 1$ and $a/g = 5$. At $a/g = 5$, the liquid free surface is at saturation.

Run Number 24 (Figure 55)

$a/g = 1\text{-}15$; $P = 80$ psia ; $q/A = 61{,}000$ BTU/hr-ft

Although conducted at a higher heat flux than the previous test, the $\Delta T_{sat.}$ at $a/g = 1$ is lower, indicating non-reproducibilities at $a/g = 1$ conditions. As acceleration is increased, however, the decrease of $\Delta T_{sat.}$ is less pronounced than in Run Number 23, and it might be expected that results obtained at higher acceleration will be more consistant. This will be examined more closely in the composite comparison of results.

The subcooling at the heater surface increases linearly, and the subcooling at the liquid free surface becomes negative. Either the temperature distribution within the liquid is not uniform, as postulated, or it has become superheated.

Run Number 25 (Figure 56)

$a/g = 1\text{-}15$; $P = 80$ psia ; $q/A = 78{,}000$ BTU/hr-ft^2

The change in $\Delta T_{sat.}$ between $a/g = 1$ and $a/g = 5$ is smaller than previous tests.

Run Number 26 (Figure 57)

$a/g = 1 - 15$; $P = 80$ psia ; $q/A = 98{,}300$ BTU/hr-ft^2

This is the highest heat flux employed at this pressure, and it is noted that the decrease in $\Delta T_{sat.}$ with increasing acceleration is smaller than at the lower levels of heat flux. This is consistent with the behavior observed with water (128).

The next four tests were repeats of several of the above, again to check reporducibility.

Run Number 27 (Figure 58)

$a/g = 1, 5$; $P = 80$ psia ; $q/A = 32{,}000$ BTU/hr-ft^2

After a period of inactivity of 7 weeks the above test was conducted. Film boiling set in initially and then reverted to nucleate boiling. $\Delta T_{sat.}$ at $a/g = 1$ was close to that for Run number 22 (Figure 53) but the decrease at $a/g = 5$ was not

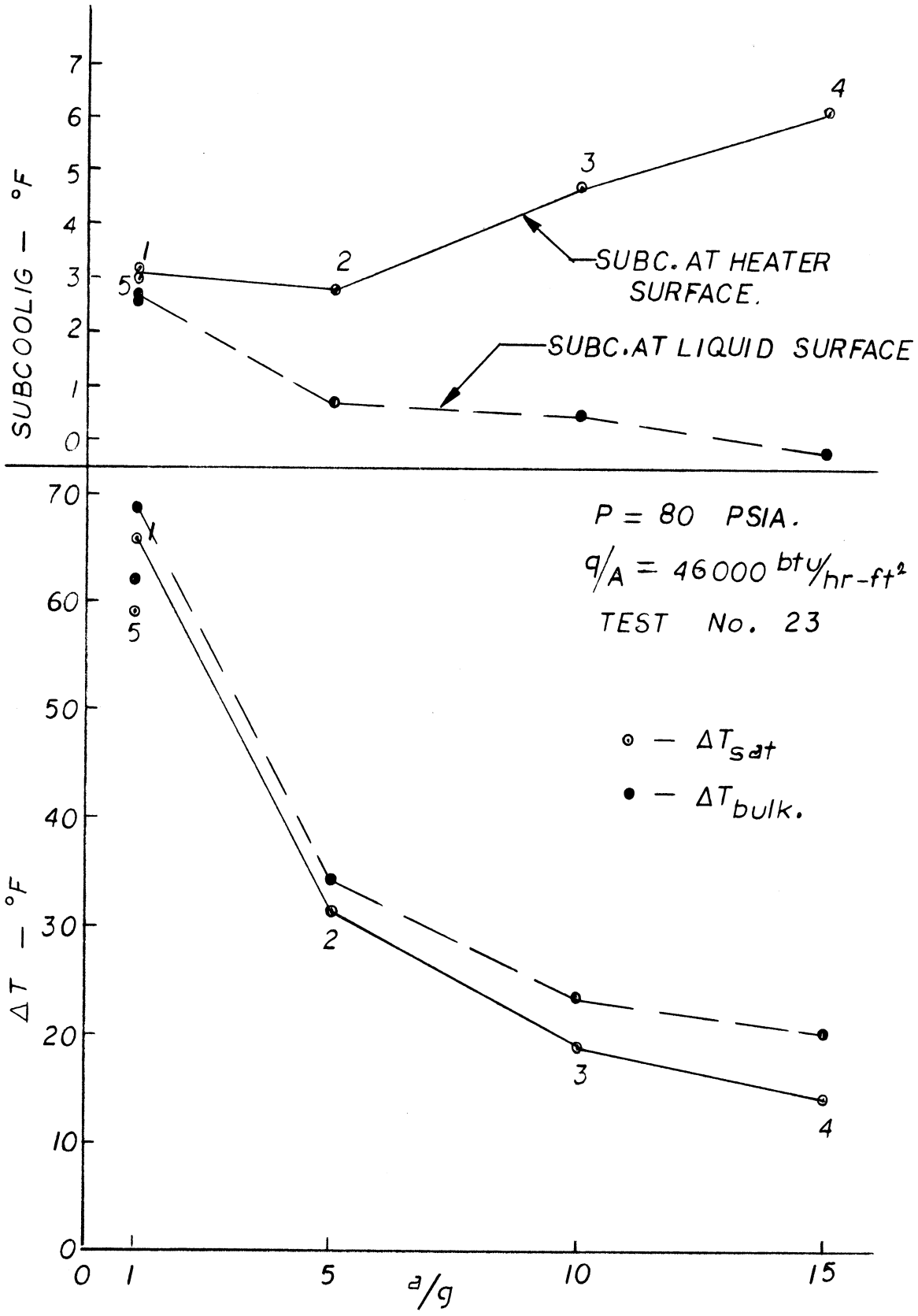

Figure 54 Mercury Boiling Data under High Gravity, Run Number 23

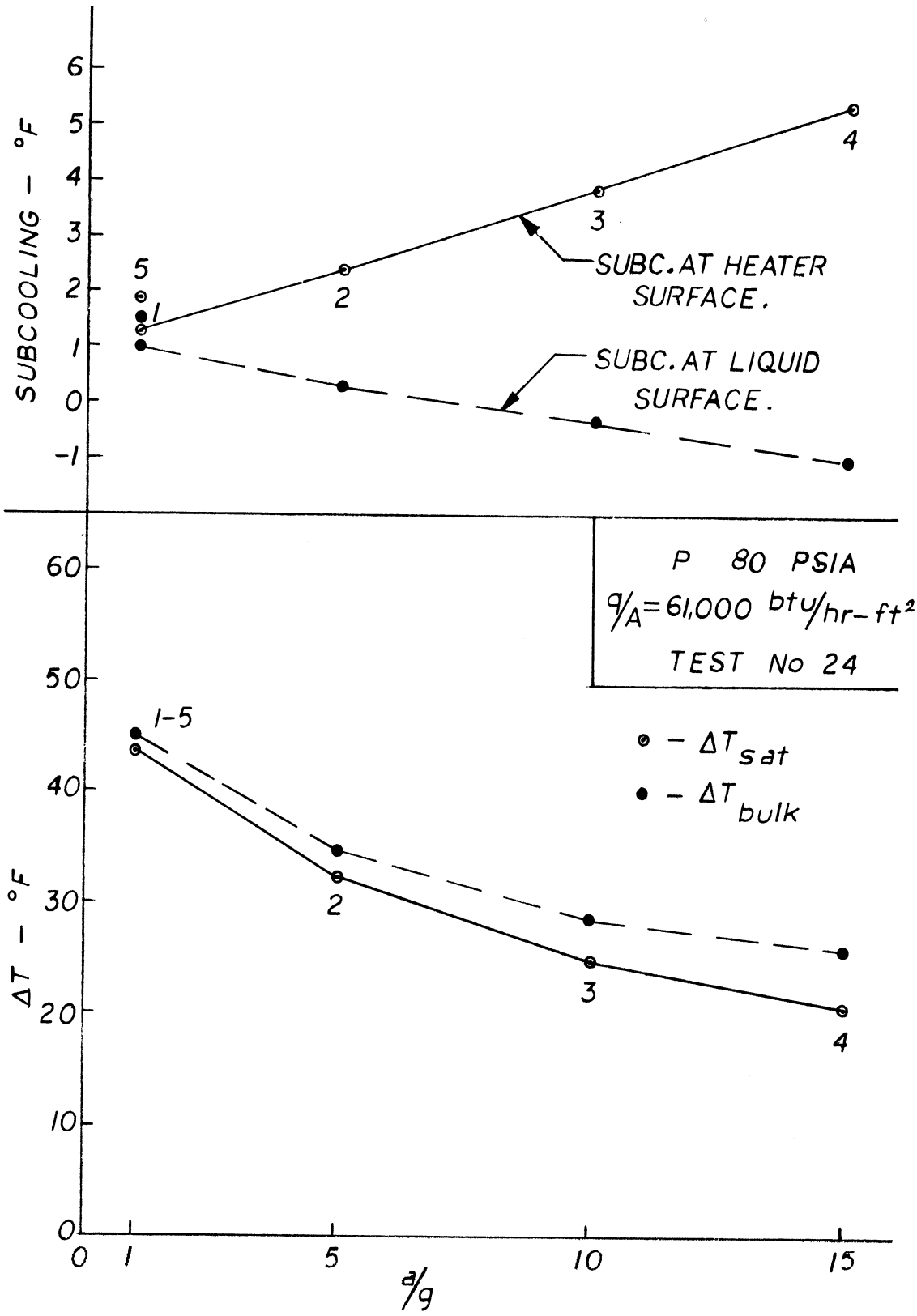

Figure 55 Mercury Boiling Data under High Gravity, Run Number 24

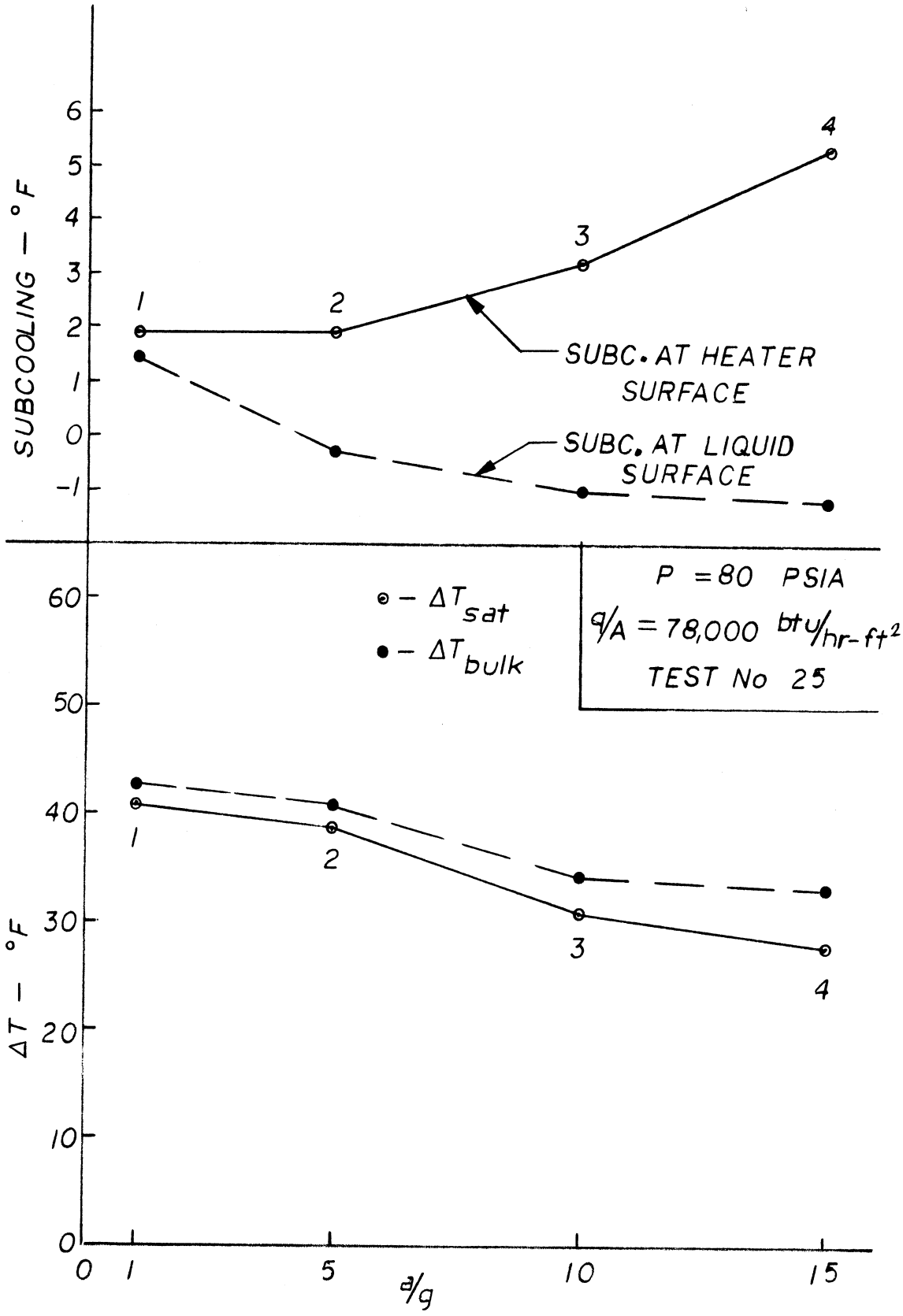

Figure 56 Mercury Boiling Data under High Gravity, Run Number 25

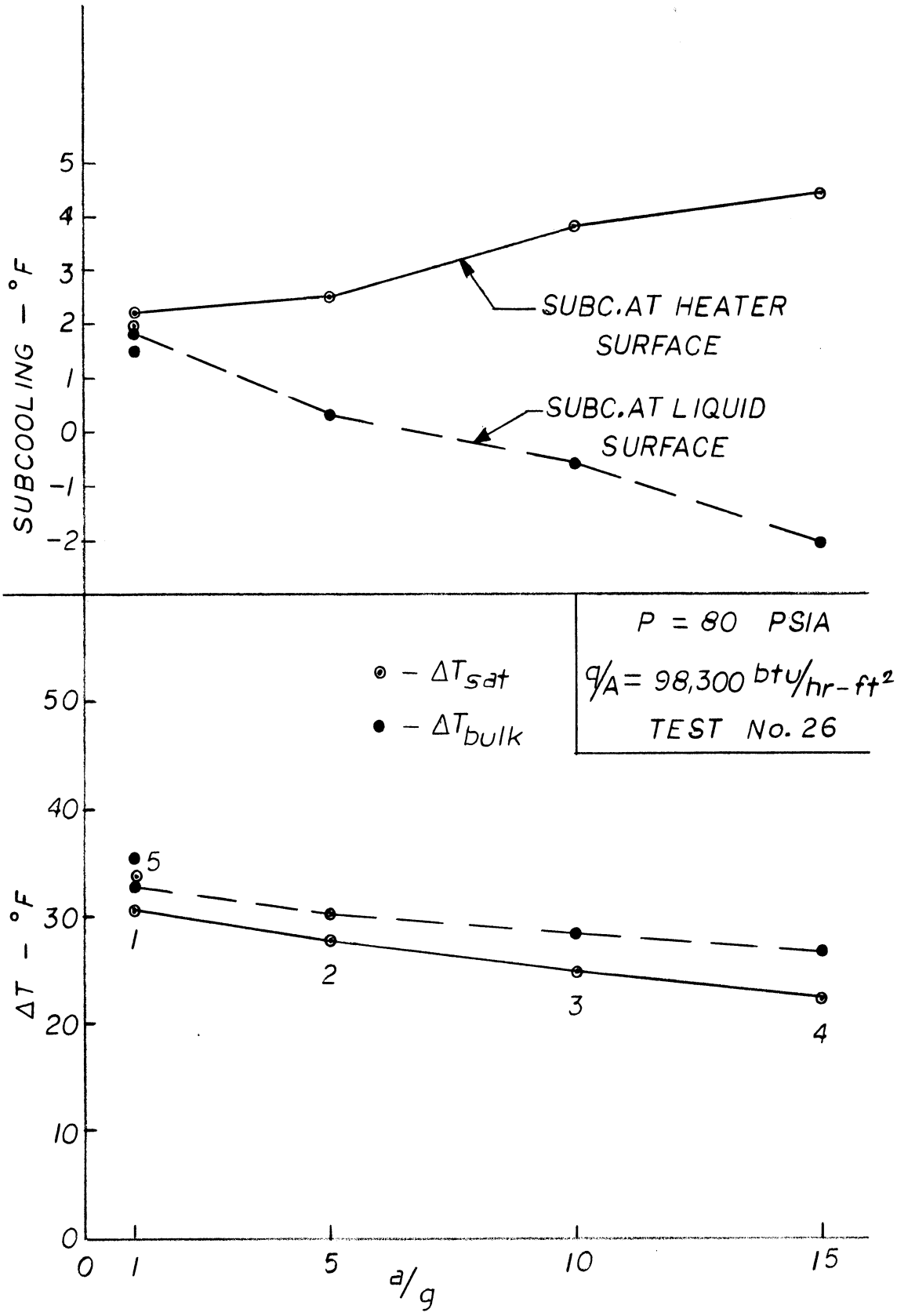

Figure 57 Mercury Boiling Data under High Gravity, Run Number 26

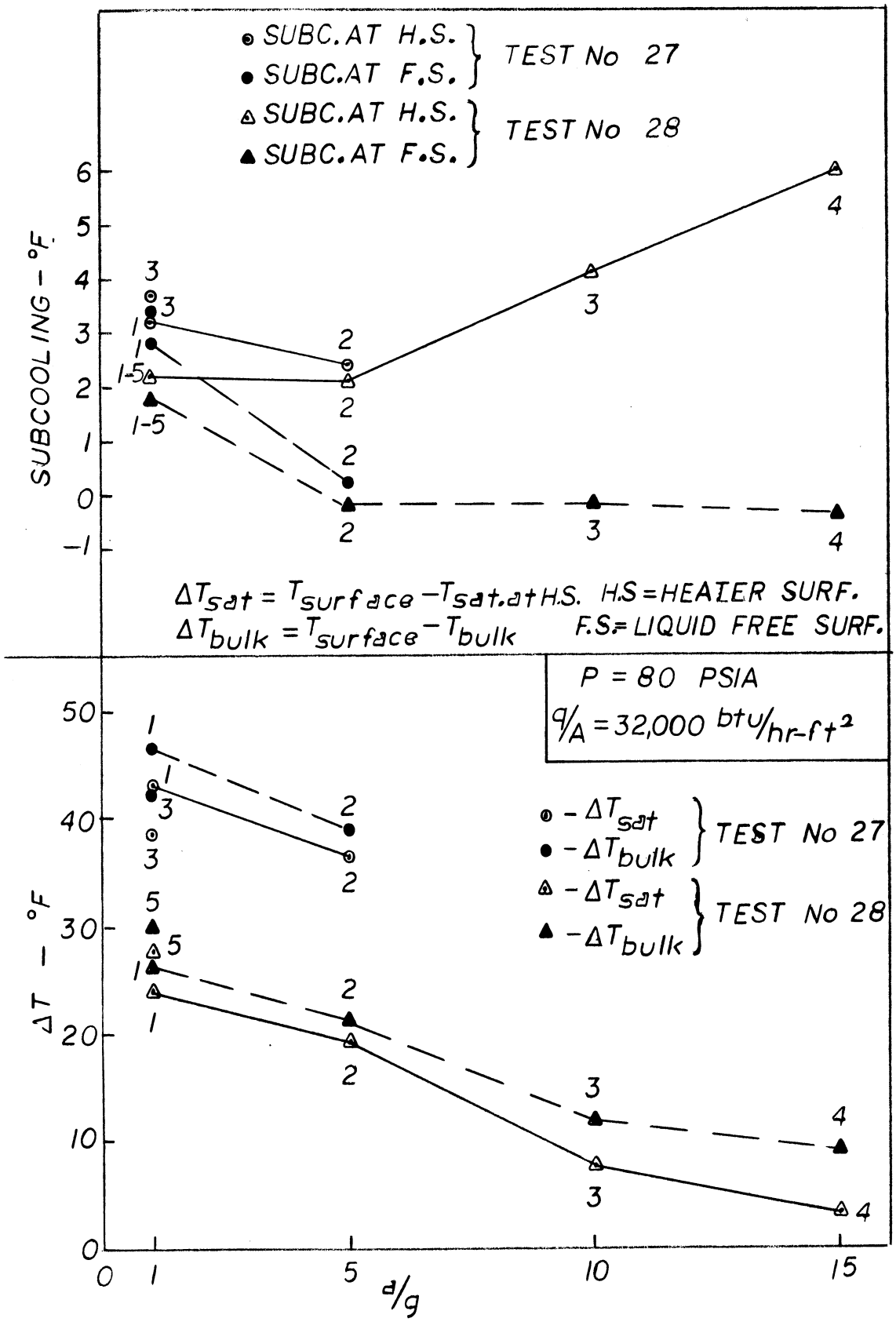

Figure 58 Mercury Boiling Data under High Gravity, Runs Number 27 and 28

as pronounced. This test was repeated again several days later, below.

Run Number 28 (Figure 58)

$a/g = 1 - 15$; $P = 80$ psia ; $q/A = 32{,}000$ BTU/hr-ft^2

$\Delta T_{sat.}$ at the initial $a/g = 1$ was considerably lower than previous observations, and the value at the final $a/g = 1$ increased somewhat, in opposition to the behavior in all other tests conducted.

Run Number 29 (Figure 59)

$a/g = 1 - 15$; $P = 80$ psia ; $q/A = 60{,}000$ BTU/hr-ft^2

This is a repeat of Run Number 24 (Figure 55), and the values of $\Delta T_{sat.}$ are somewhat lower, moreso at $a/g = 1$ than at higher acceleration levels. The subcoolings, however, are almost identical.

Run Number 30 (Figure 60)

$a/g = 1 - 15$; $P = 80$ psia ; $q/A = 100{,}000$ BTU/hr-ft^2

This is a repeat of Run Number 26 (Figure 57), and the behavior is quite similar.

This concluded all the data obtained at the nominal pressure $P = 80$ psia. In an effort to discover any possible overall patterns of the influence of heat flux on subcooling of the liquid at the various accelerations, a composite of all the subcoolings were made as shown in Figure 61. It appears that increasing heat flux results in lowered subcoolings, that the liquid free surface becomes essentially saturated at the higher accelerations, and the subcooling at the heater surface increases with acceleration. A definite lower limit on subcooling exists at the heater surface, dictated by the liquid depth, and could be decreased at the higher accelerations only by decreasing the liquid depth, as was discussed in Reference 8. To determine the influence of subcooling requires further work with liquid depth as a variable.

Figure 62 is a composite of the various tests at $P = 80$ psia, showing the overall influence of a/g on $\Delta T_{sat.}$ for the various levels of heat flux. The behavior becomes more consistent at the higher levels of acceleration, which tends to point to the decreasing effects of surface conditions as body forces increase. This is shown more clearly in Figure 63, which is a cross-plot of the data in Figure 62. The results at the highest level of heat flux, however, remain somewhat anomalous.

Figure 64 is a plot of $\Delta T_{sat.}$ normalized to the value at the initial level of $a/g = 1$ for the various levels of heat flux, which tends to eliminate the differences in surface conditions which may exist between the various tests. The values shown at $a/g = 1$ which are different from unity are those corresponding

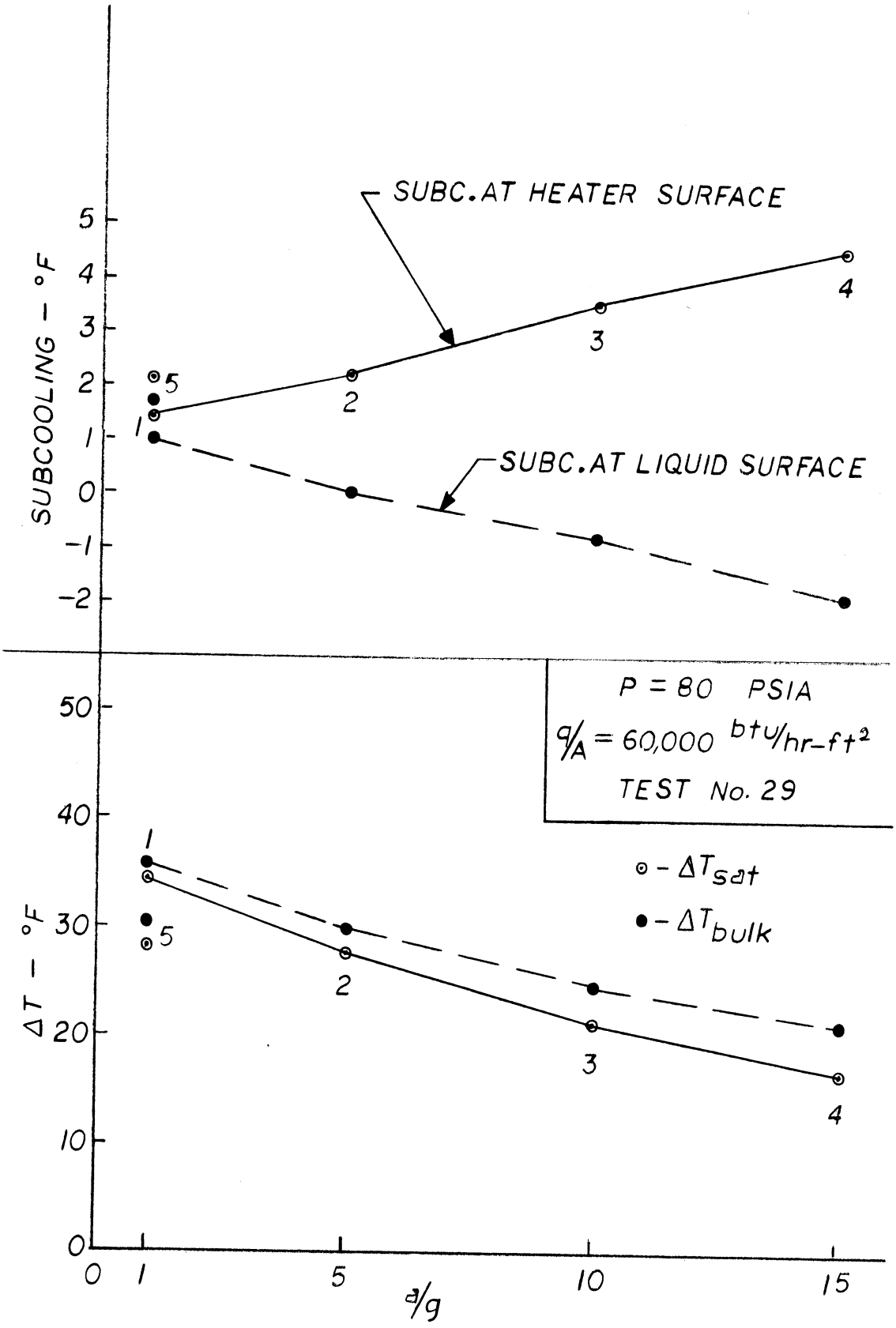

Figure 59 Mercury Boiling Data under High Gravity, Run Number 29

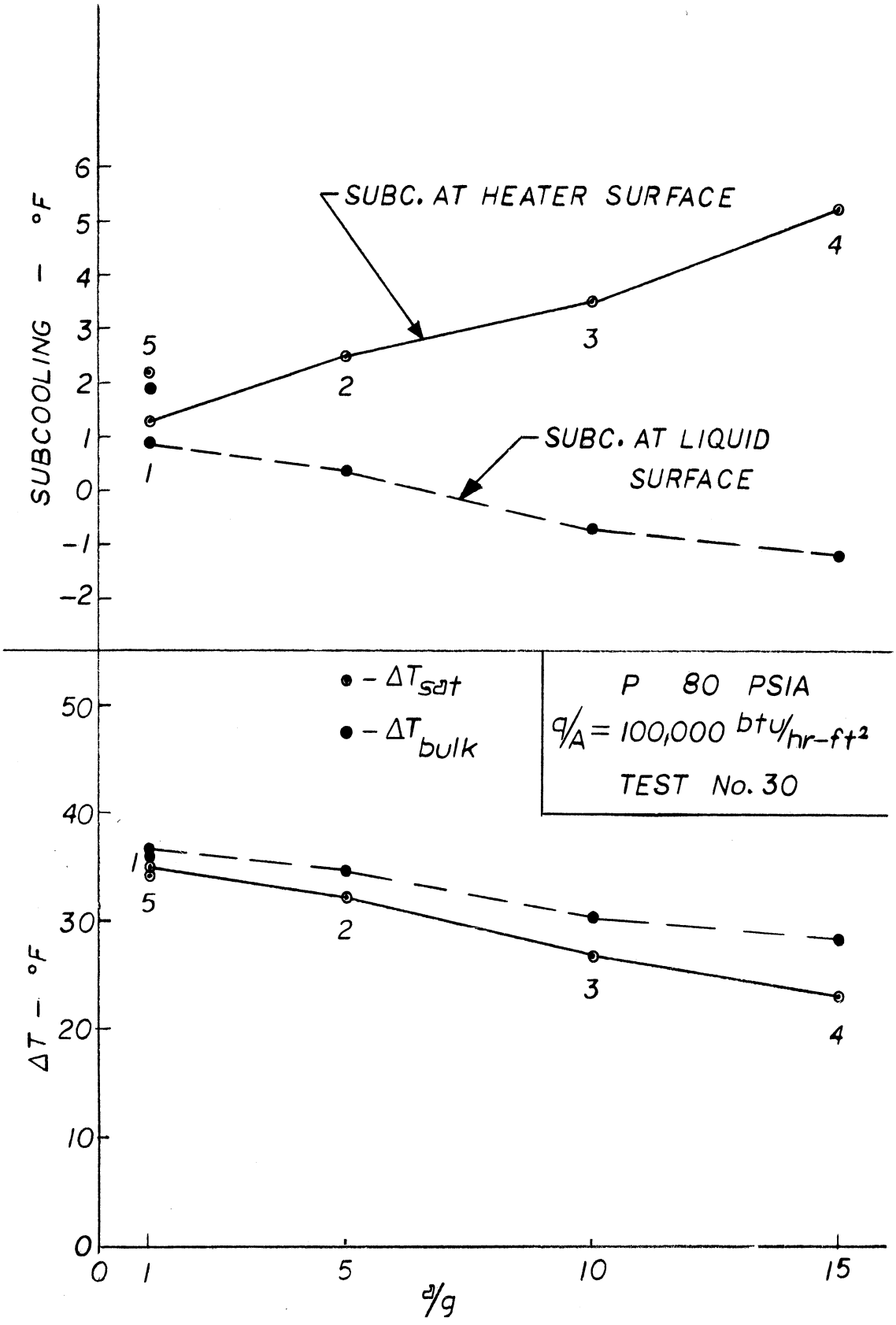

Figure 60 Mercury Boiling Data under High Gravity, Run Number 30

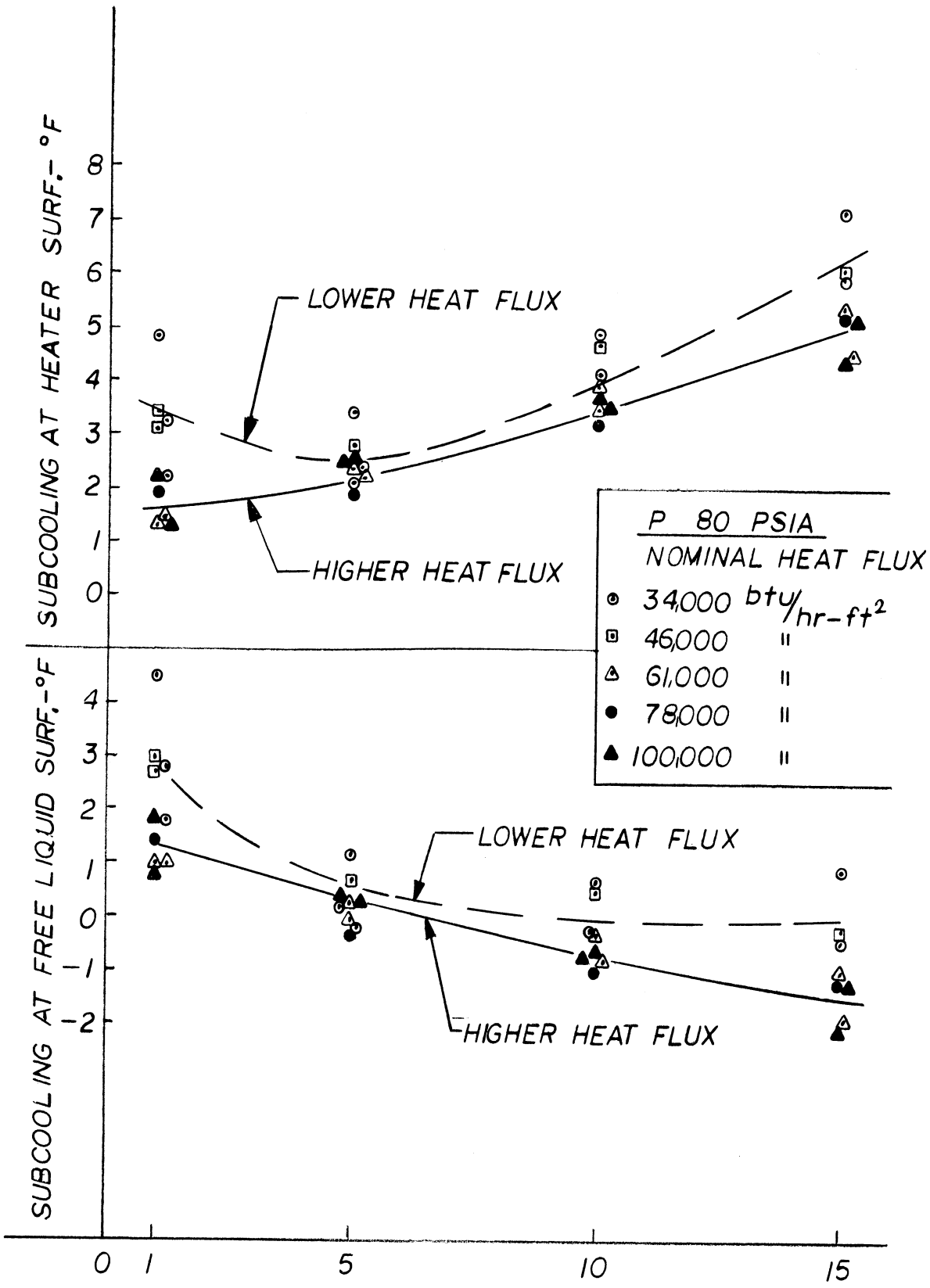

Figure 61 Composite of Influence of High Gravity on Subcooling for P = 80 psia

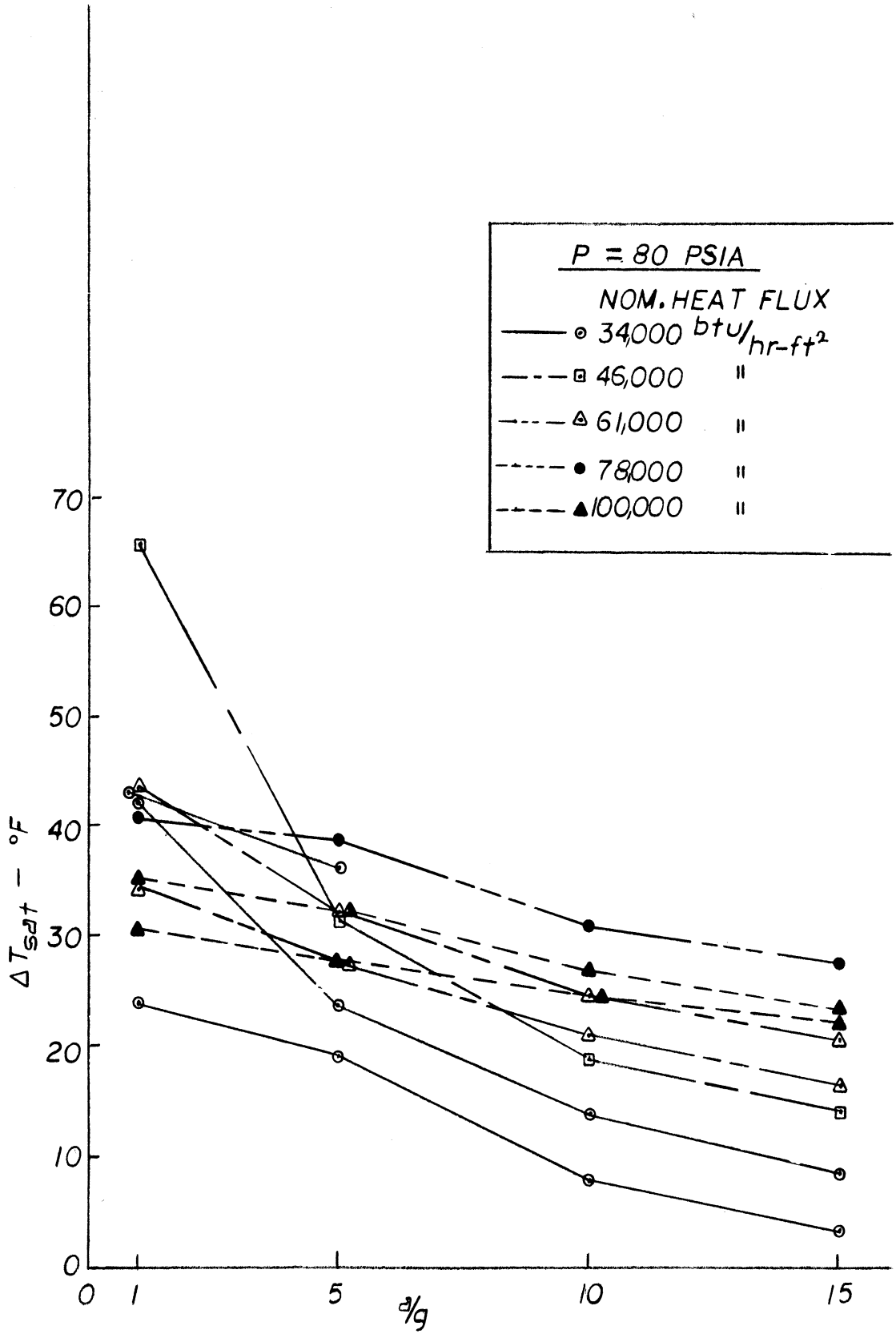

Figure 62 Composite of Influence of High Gravity on ΔT_{sat} for P = 80 psia

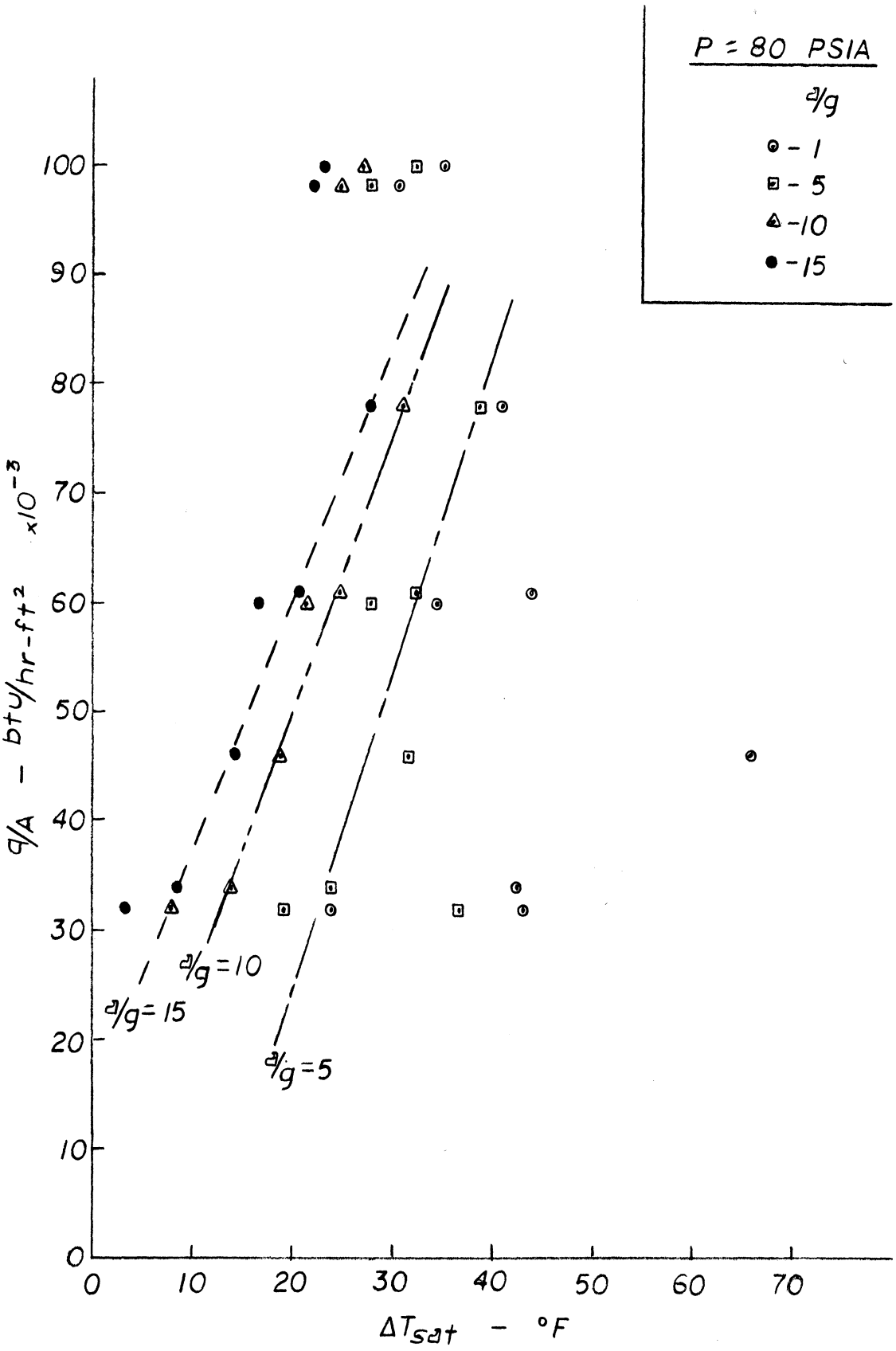

Figure 63 Heat Flux versus ΔT_{sat} for levels of Acceleration for P = 80 psia

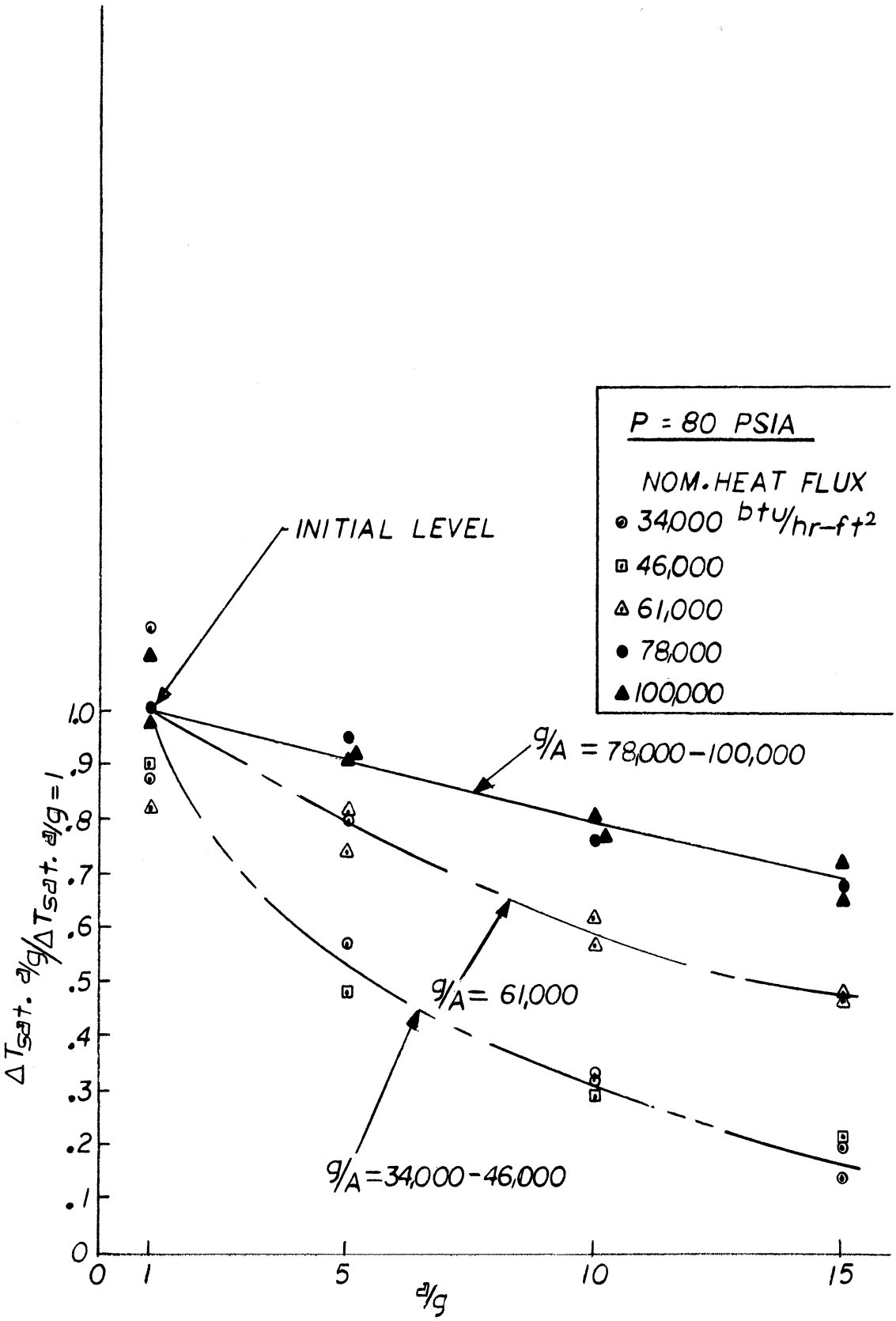

Figure 64 Influence of High Gravity on Normalized ΔT_{sat} for P = 80 psia

to a/g = 1 after operation at higher accelerations, and serve to indicate the effect of surface conditioning by operation at high accelerations. The influence of acceleration is decreased as heat flux increases, perhaps due to the decreasing contribution of non-boiling convection. Figure 64 may also serve to indicate that with sufficiently high heat flux, the nucleate boiling process will not be significantly influenced by operation at body force levels below standard gravity until very low levels are reached.

The following three tests were conducted at a pressure of 20 psia with several levels of heat flux.

Run Number 31 (Figure 65)

$a/g = 1 - 15$; P = 20 psia ; $q/A = 32{,}000$ BTU/hr-ft^2

As acceleration increases, $\Delta T_{sat.}$ decreases and then becomes negative, indicating that nucleate boiling has ceased. This is also indicated by the behavior of ΔT_{BULK}, which first decreases and then increases to a constant value at the two upper acceleration levels. This latter behavior is interesting in that it suggests that for mercury under these conditions that the "natural convection" heat transfer is now independent of further changes in body forces. The large differences in subcooling between the heater surface and the free liquid surface might also be noted. This arises from the larger change in $T_{sat.}$ with pressure at this lower level of pressure.

Run Number 32 (Figure 66)

$a/g = 1 - 15$; P = 20 psia ; $q/A = 60{,}000$ BTU/hr-ft^2

$\Delta T_{sat.}$ decreases appreciably between a/g = 1 and a/g = 5, with small subsequent changes. ΔT_{BULK} first decreases and then increases, as acceleration increases, as contrasted to the continual decrease at the higher pressure level.

Run Number 35 (Figure 67)

$a/g = 1 - 15$; P = 20 psia ; $q/A = 100{,}000$ BTU/hr-ft^2

A large change in $\Delta T_{sat.}$ again takes place between a/g = 1 and a/g = 5, whereas no change takes place between a/g = 10 and a/g = 15. It is possible that were the acceleration to be increased further, that $\Delta T_{sat.}$ would undergo an increase. This possible effect may be a function of pressure also. At the end of operat on at high acceleration, $\Delta T_{sat.}$ at a/g = 1 is significantly lower than the initial value, pointing to a possible surface "conditioning" by the boiling phenomena. This is a generally observed effect.

Figure 68 shows the composite influence of acceleration on the subcooling for the above three tests, with just very slight differences with heat flux. The effect of acceleration is quite pronounced as compared to that at a higher pressure, as might be noted by comparing Figures 61 and 68. As pointed out earlier, this is a consequence of the differences in the change of saturation temperature with

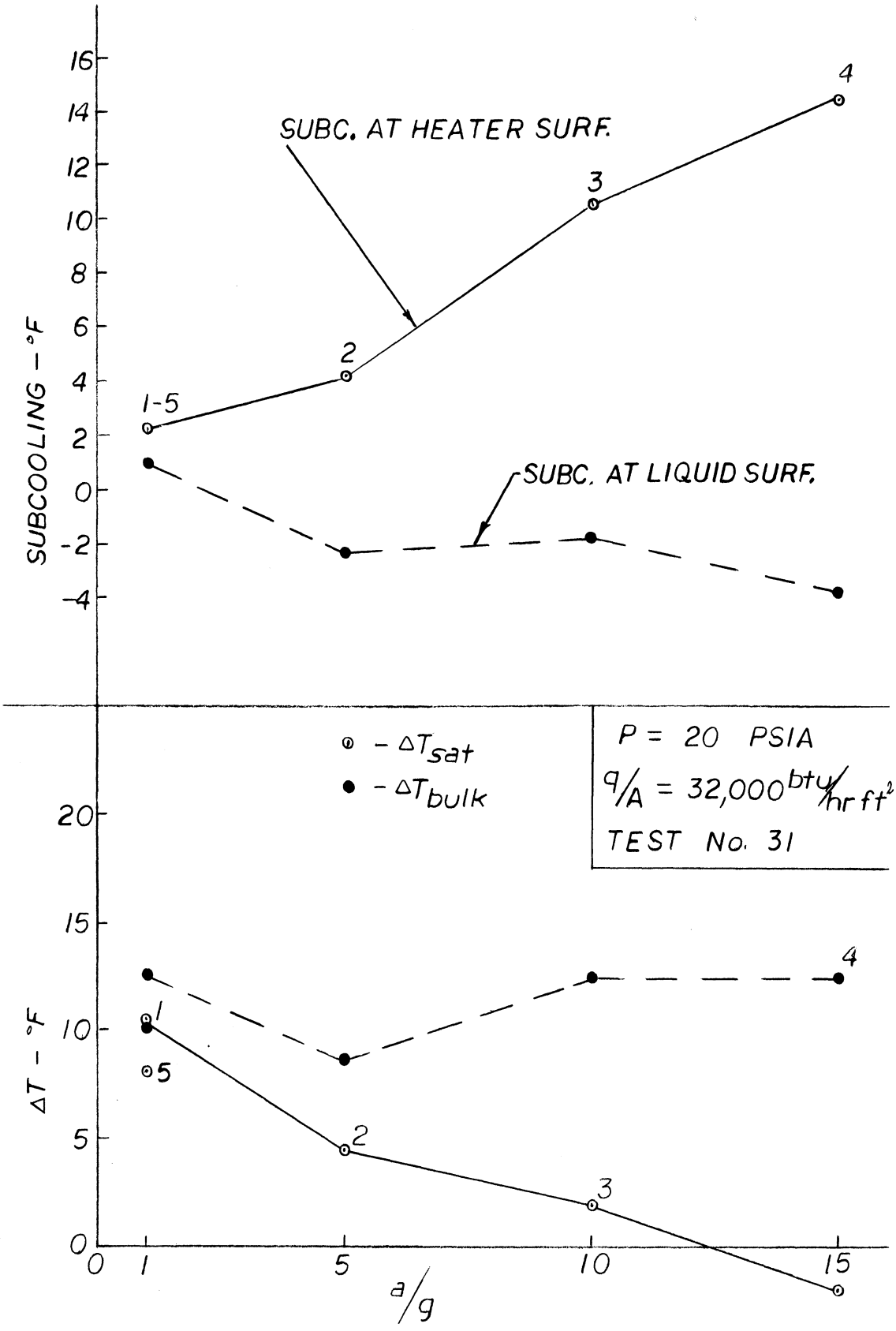

Figure 65 Mercury Boiling Data under High Gravity, Run Number 31

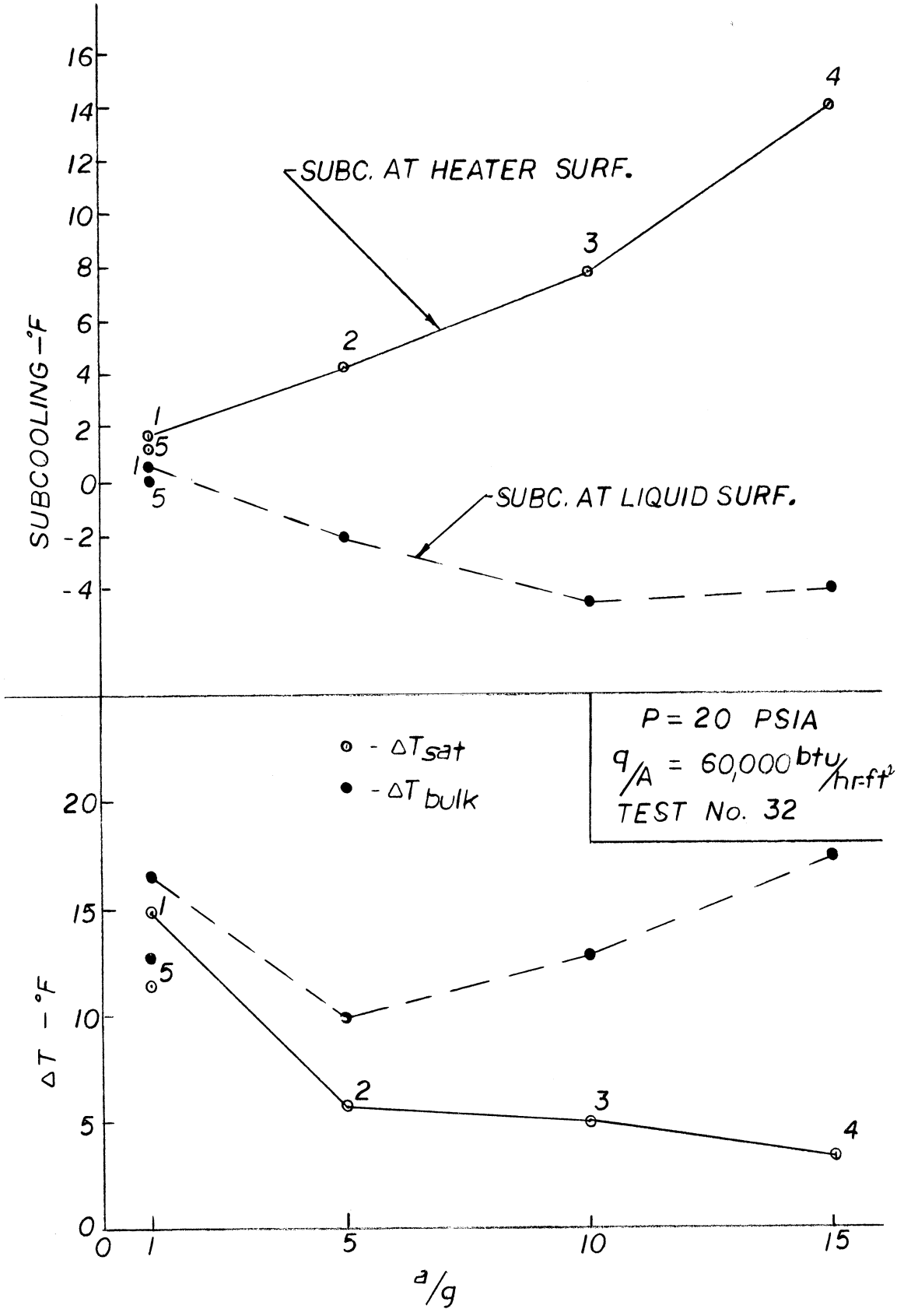

Figure 66 Mercury Boiling Data under High Gravity, Run Number 32

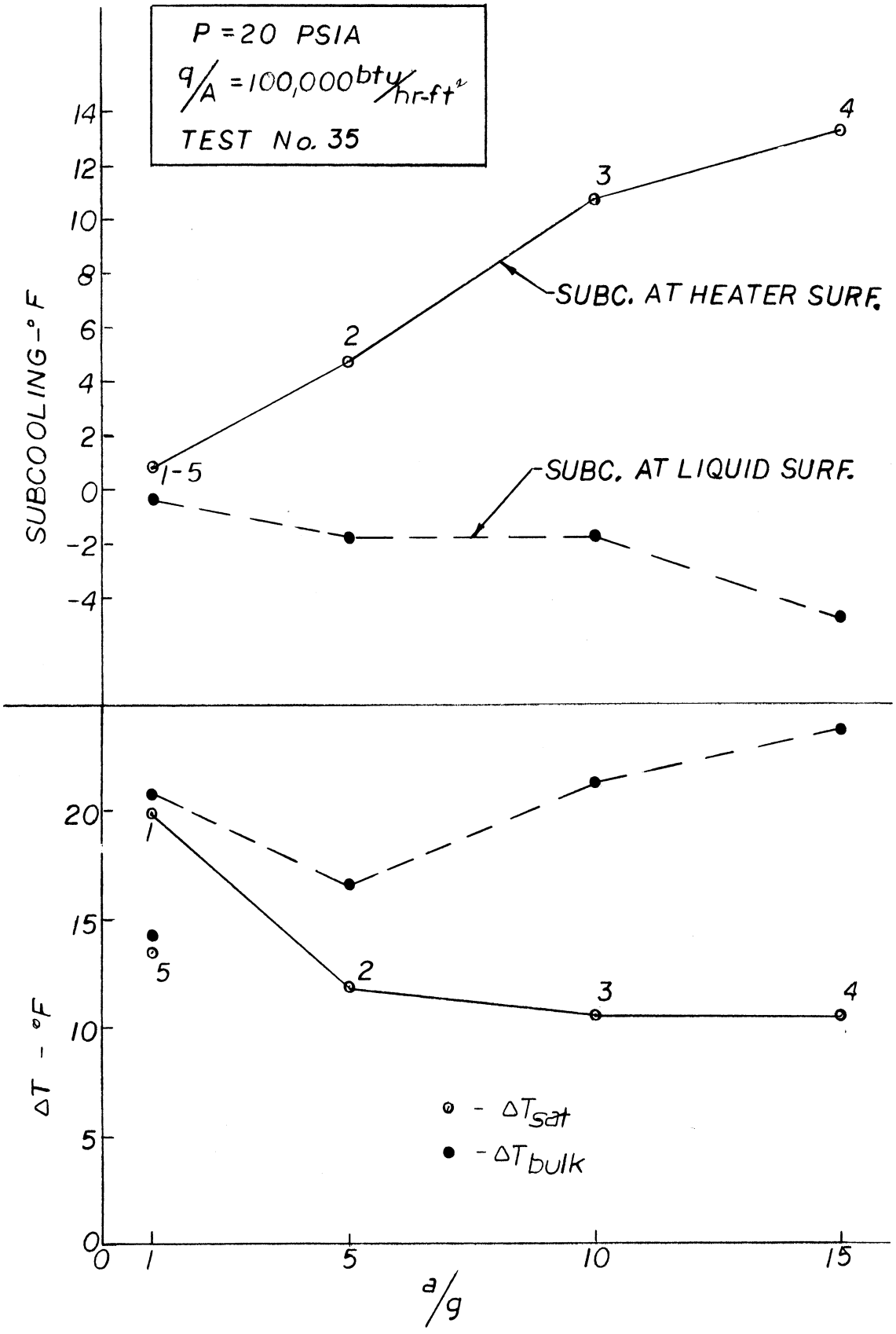

Figure 67 Mercury Boiling Data under High Gravity, Run Number 35

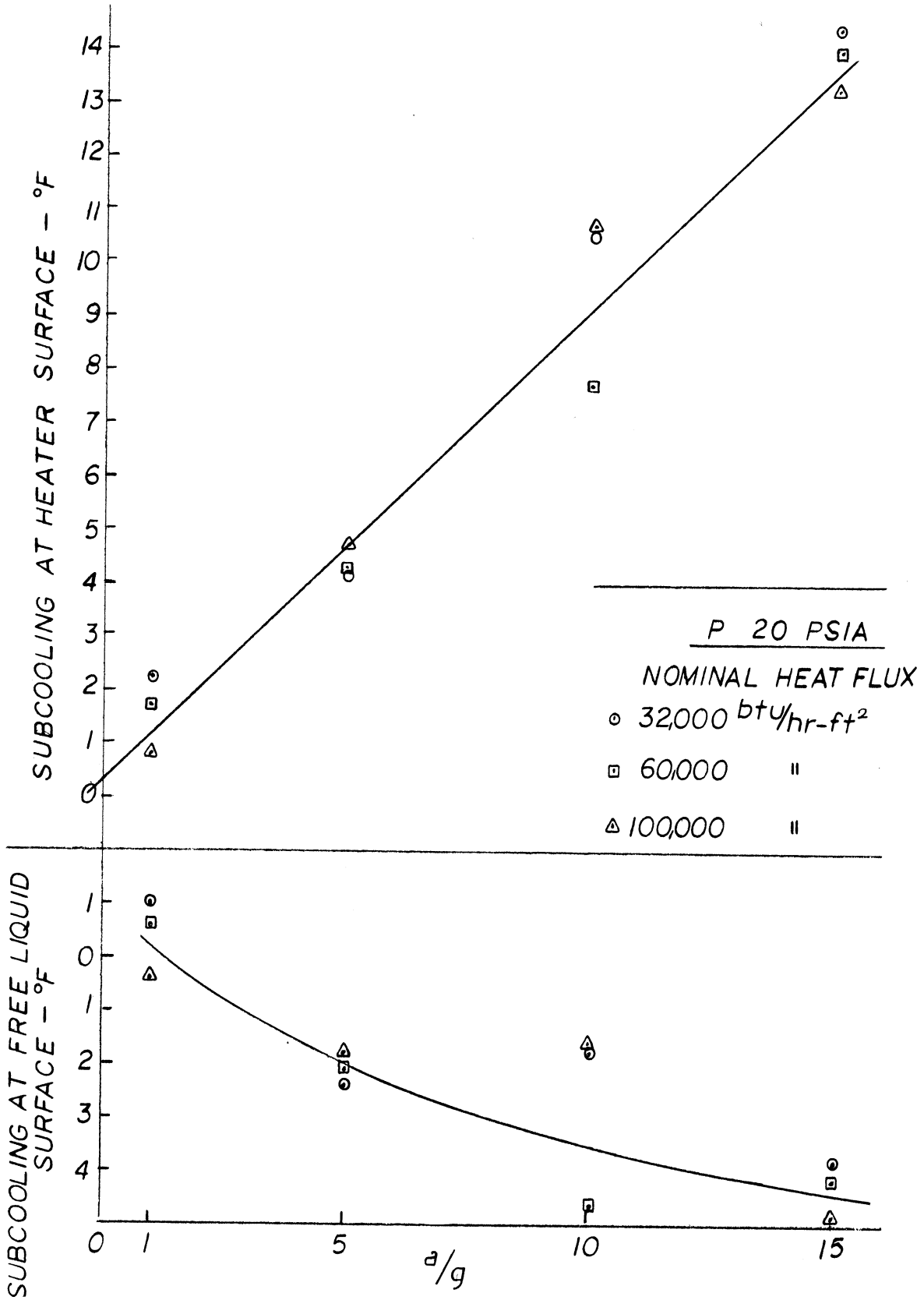

Figure 68 Composite of Influence of High Gravity on Subcooling for P = 20 psia

pressure due to a/g at the different pressure levels.

Figure 69 is a composite plot of the influence of a/g on $\Delta T_{sat.}$ and ΔT_{BULK} at the three levels of heat flux for P = 20 psia as compared to Figure 62 for P = 80 psia. Figure 70 is the plot of heat flux versus $\Delta T_{sat.}$ for the various levels of acceleration at P = 20 psia as compared to Figure 63 for P = 20 psia, and the greater consistency of the results is noted. Figure 71 shows the influence on the normalized $\Delta T_{sat.}$ for the several levels of heat flux. The decreasing influence of acceleration is clearly seen at the higher levels of heat flux.

The following tests were conducted over a wide range of heat flux levels for P = 300 psia.

Run Number 37 (Figure 72)

a/g = 1 - 15 ; P = 300 psia ; q/A = 34,000 BTU/hr-ft^2

At this level of heat flux nucleate boiling is completely suppressed at acceleration levels above a/g = 1, most likely because of the large subcooling which arises from the decreased effective thermal resistance in the vapor space at this high pressure. It is interesting to note that the value of ΔT_{BULK}, and thus a heat transfer coefficient which might be based on this, is not influenced by a/g. In fact, ΔT_{BULK} increases slightly with a/g. Upon the final return to a/g = 1, ΔT_{BULK} decreases considerably, even though the liquid temperature has returned to its original level. The heater surface superheat is quite small, 0.6°F, and no nucleate boiling is believed present. This behavior is opposite to that which would be normally expected. Readings at the final condition of a/g = 1 were taken over a 20- minute period and no changes occurred in this interval, indicating that steady-state conditions existed.

Run Number 38 (Figure 73)

a/g = 1 - 15 ; P = 300 psia ; q/A = 63,000 BTU/hr-ft^2

The decrease in $\Delta T_{sat.}$ with acceleration is relatively small, and the value at the final a/g = 1 is just slightly smaller than the initial one. The difference in subcooling between the heater surface and liquid free surface is smaller than at the lower levels of pressure because of the decreasing change of saturation temperature with pressure at this level of pressure.

Run Number 39 (Figure 74)

a/g = 1 - 15 ; P = 300 psia ; q/A = 100,000 BTU/hr-ft^2

$\Delta T_{sat.}$ appears to change more from a/g = 1 to a/g = 5 than in the previous run, and the value at the final a/g = 1 is decreased to some extent.

Run Number 40 (Figure 75)

a/g = 1 - 15 ; P = 300 psia ; q/A = 205,000 BTU/hr-ft^2

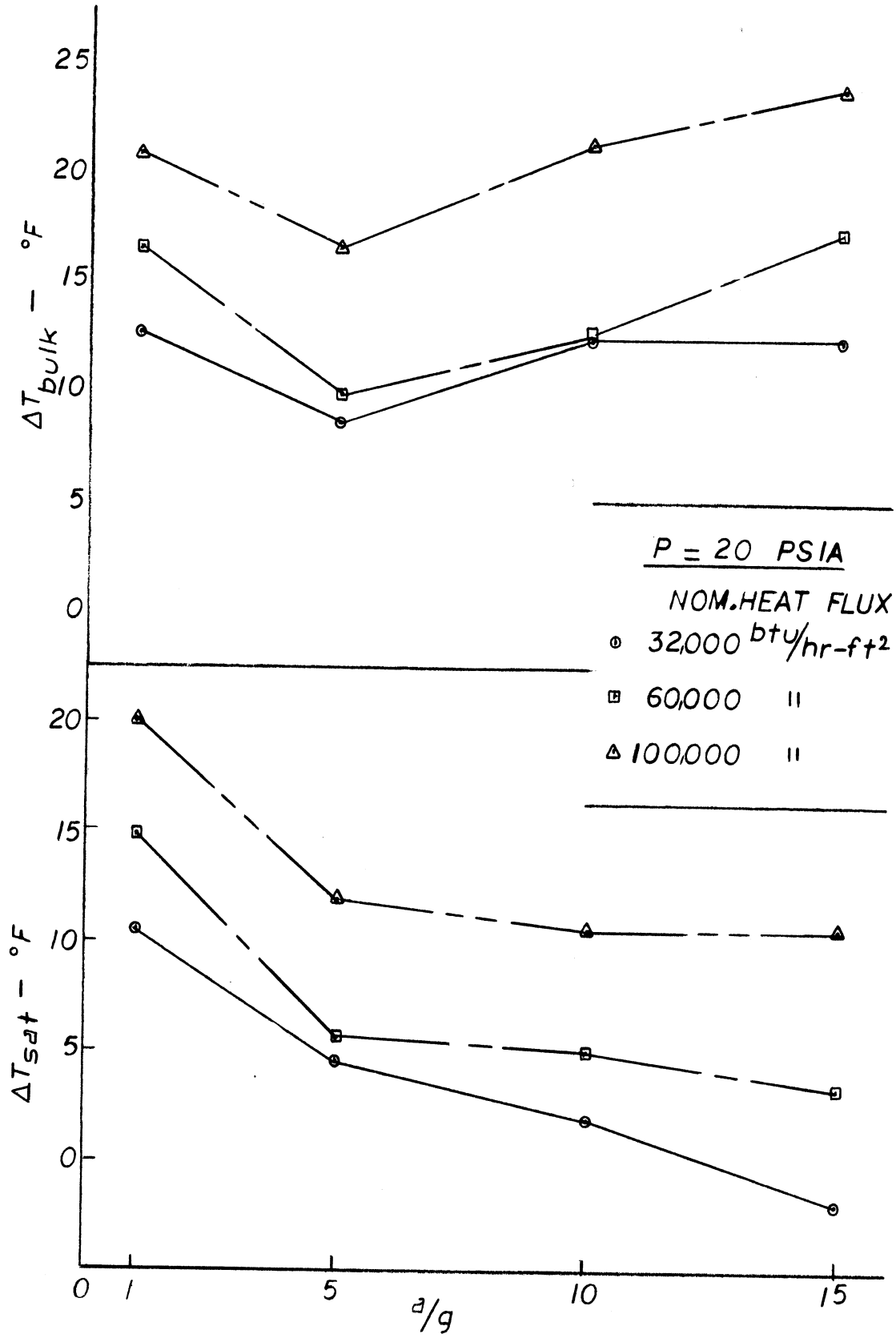

Figure 69 Composite of Influence of High Gravity on ΔT for P = 20 psia

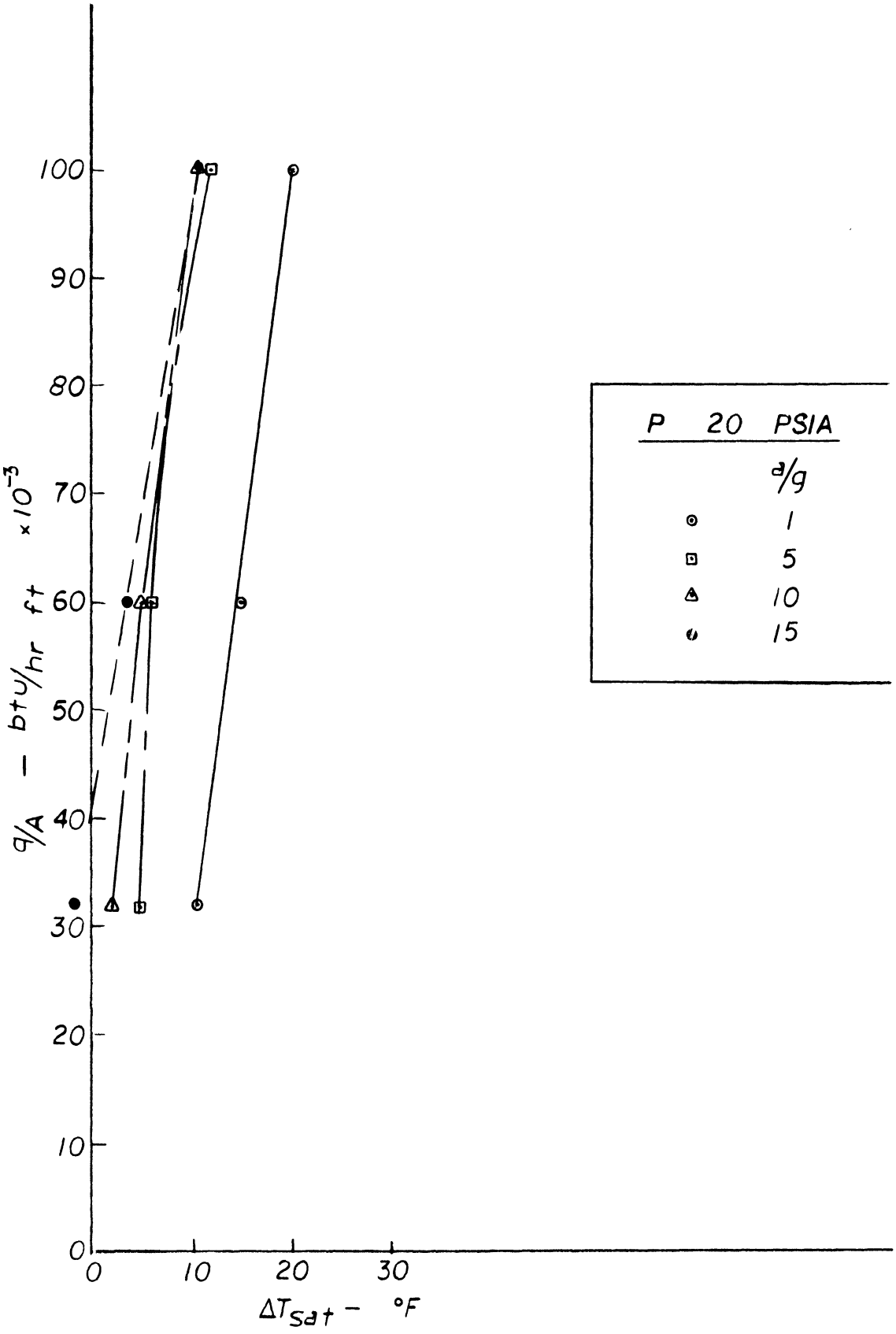

Figure 70 Heat Flux versus ΔT_{sat} for Levels of Acceleration for P = 20 psia

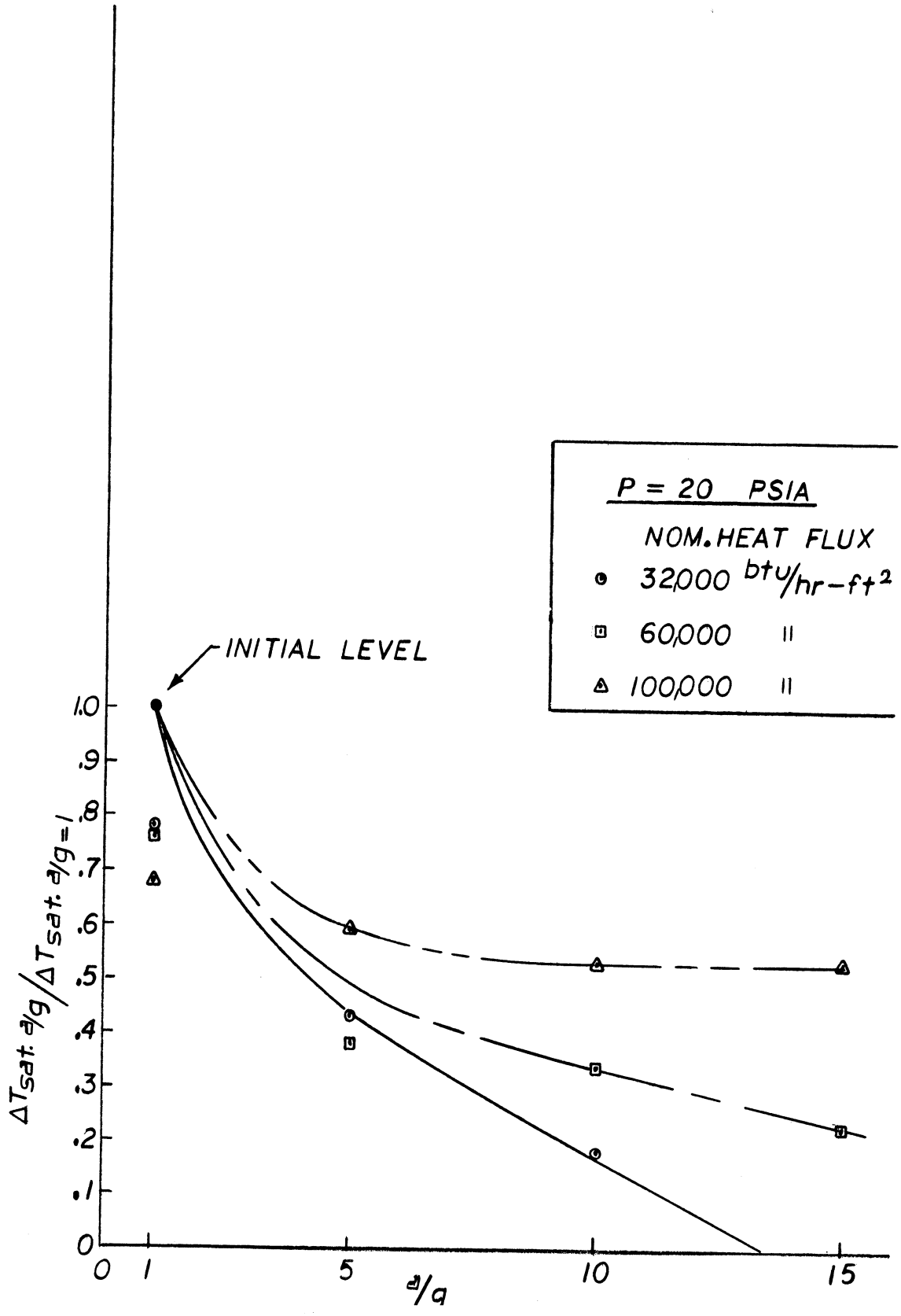

Figure 71 Influence of High Gravity on Normalized ΔT_{sat} for P = 20 psia

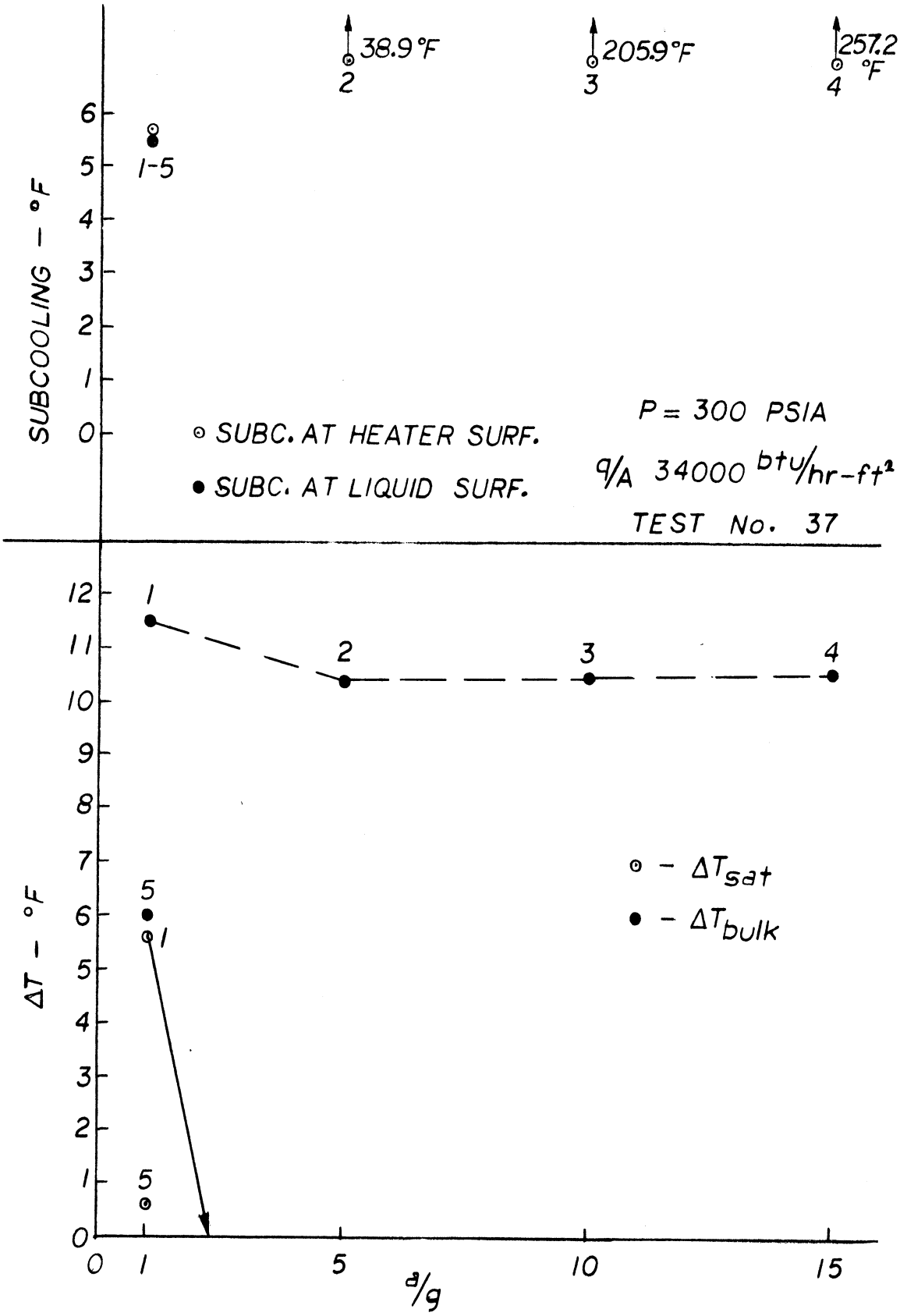

Figure 72 Mercury Boiling Data under High Gravity, Run Number 37

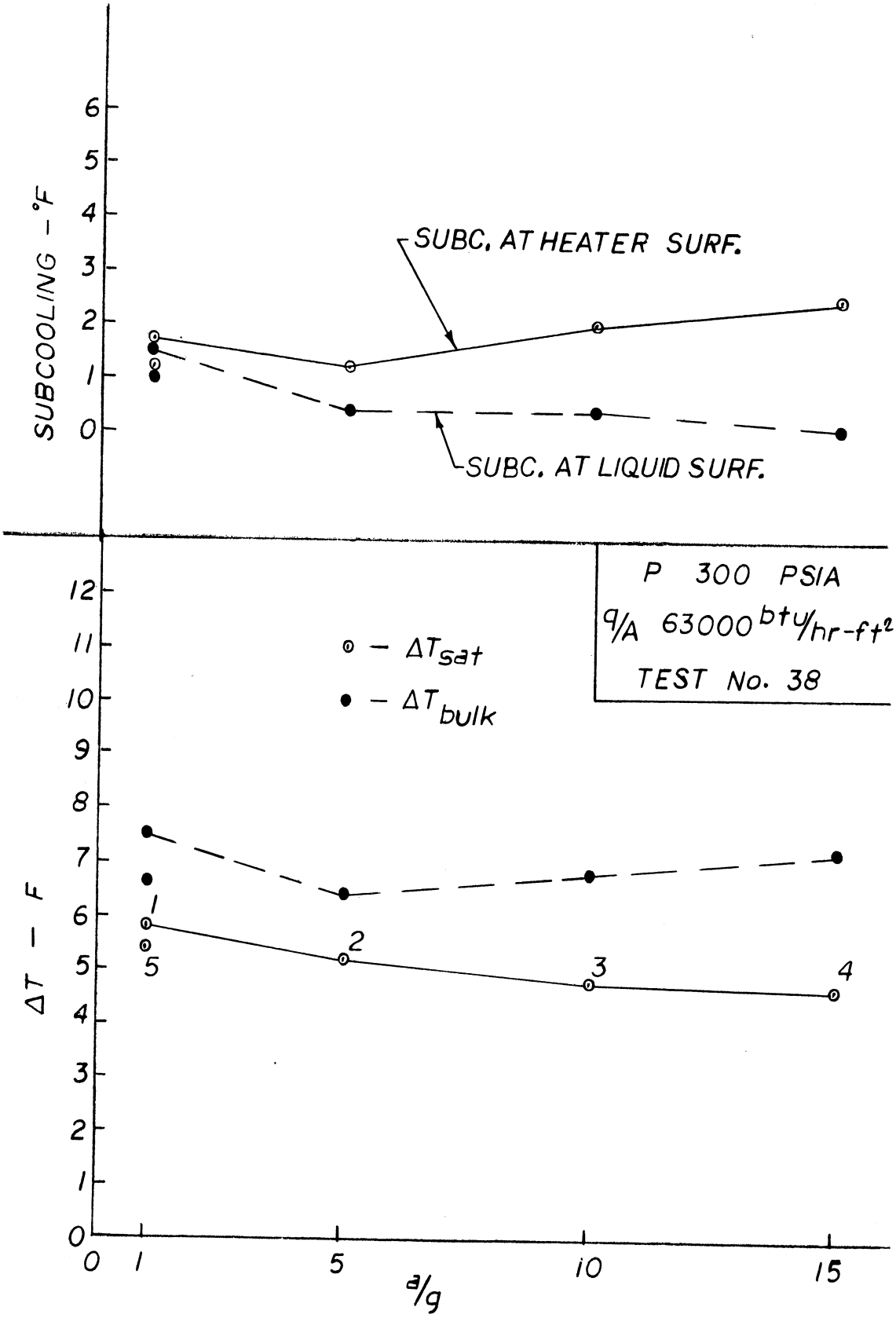

Figure 73 Mercury Boiling Data under High Gravity, Run Number 38

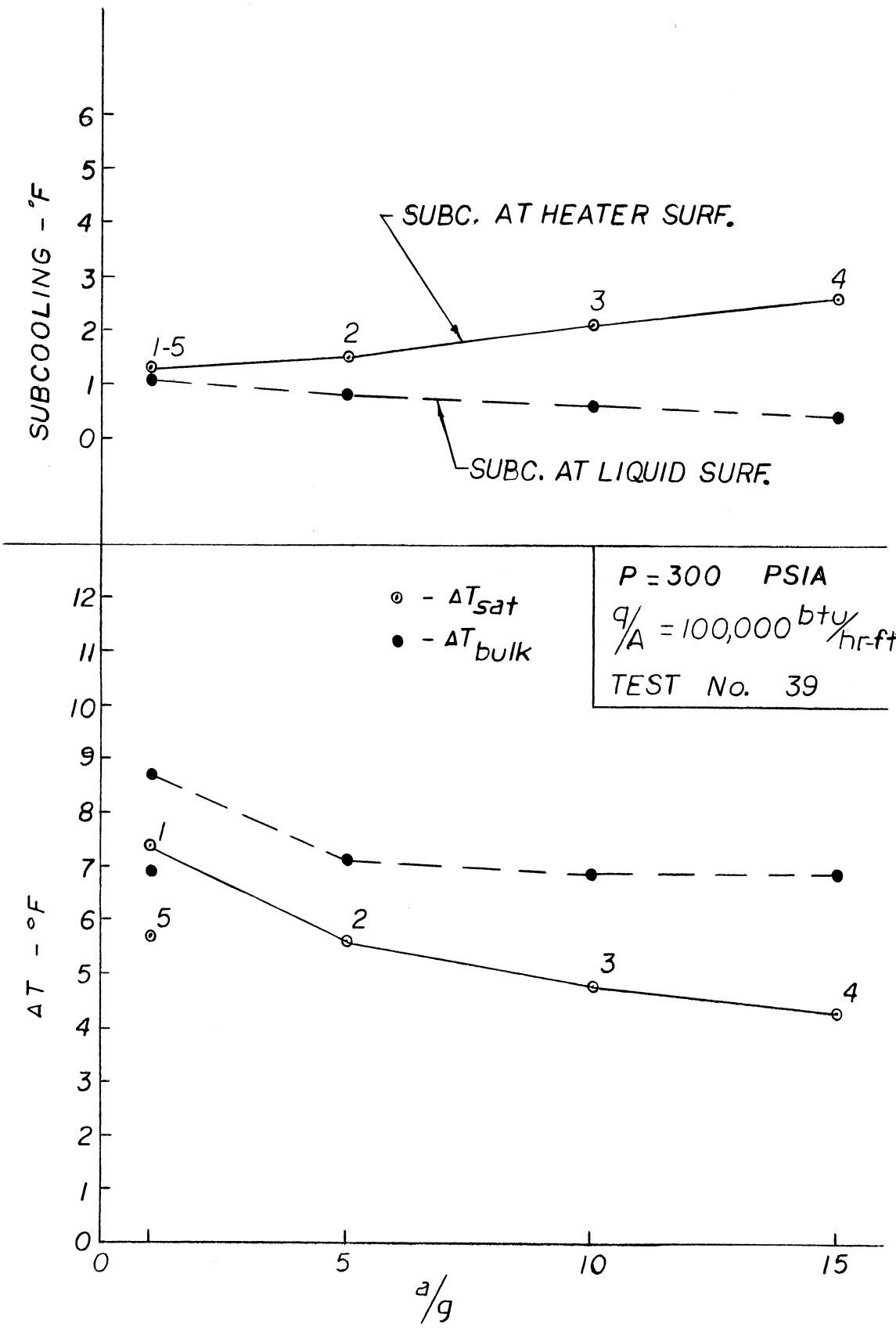

Figure 74 Mercury Boiling Data under High Gravity, Run Number 39

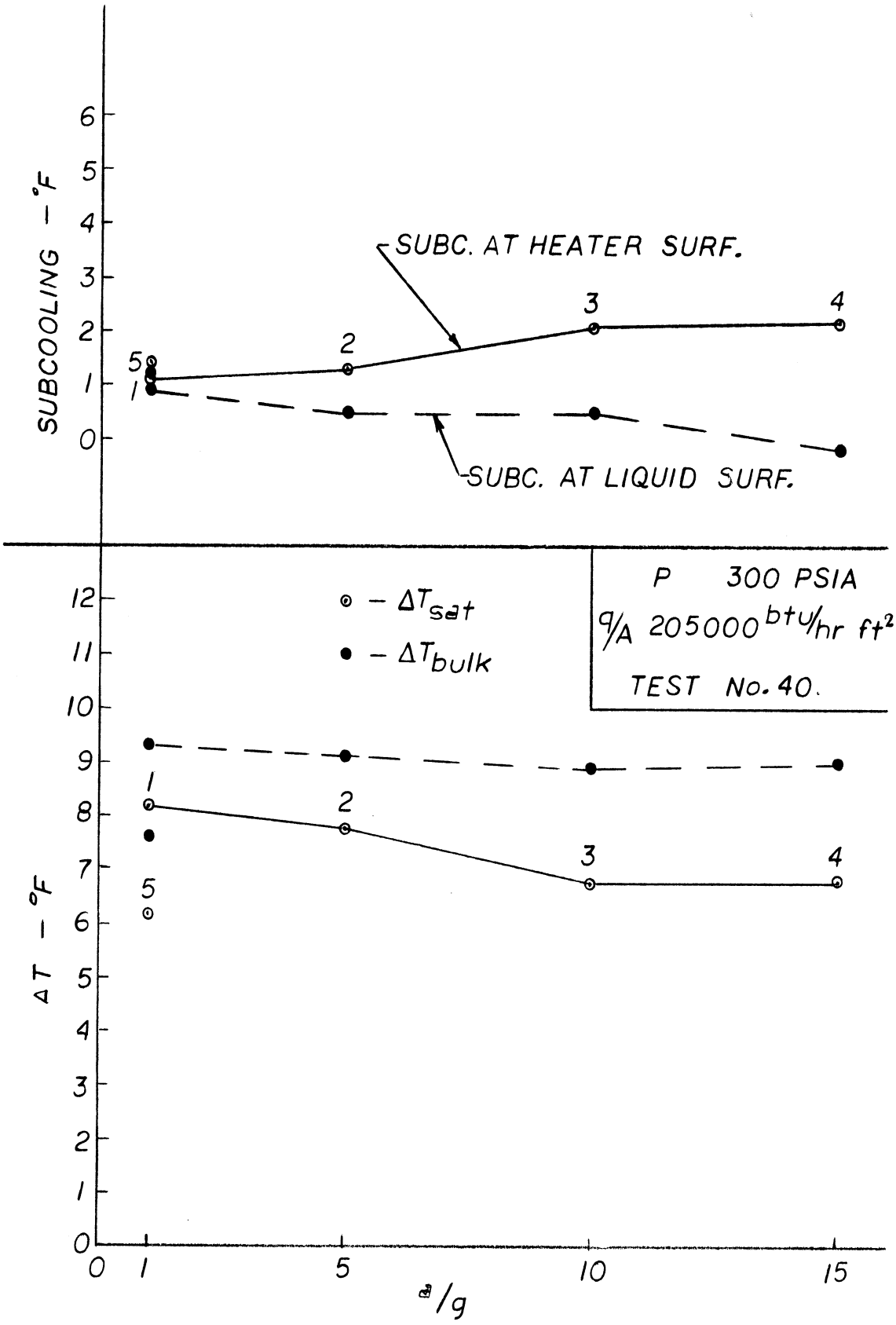

Figure 75 Mercury Boiling Data under High Gravity, Run Number 40

$\Delta T_{sat.}$ again decreases between a/g = 1 and a/g = 10, and then remains constant to a/g = 15, and then decreases to the final level of a/g = 1. The significance of the changes in $\Delta T_{sat.}$ at a/g = 1 before and after operation at higher accelerations was not evident at the time the tests were being conducted. It might have been of interest to pass through further cycles of operation at the higher accelerations to observe the nature of subsequent changes.

Run Number 41 (Figure 76)

a/g = 1 - 15 ; P = 300 psia ; q/A = 405,000 BTU/hr-ft^2

It is noted that $\Delta T_{sat.}$ increases with acceleration up to a/g = 5, then decreases. A similar increase was observed with water (Reference 128) at the higher levels of heat flux and acceleration, although the subsequent decrease was not present. This may be a consequence of the density differences between water and mercury vapor and liquid, along with the heat flux and acceleration levels. Further analytical work relating buoyant and dynamic forces with nucleate boiling are required to establish criteria for the differences in behavior observed.

The subcoolings at the heater surface and free liquid surface are plotted in Figure 77. No changes are observed due to heat flux, and the effect of a/g is small at this level of pressure. Furthermore, the liquid appears to be at the saturation temperature for the free surface.

In Figure 78 the composites of $\Delta T_{sat.}$ and ΔT_{BULK} are plotted versus a/g for the various levels of heat flux and the cross plo of q/A versus $\Delta T_{sat.}$ with a/g as the parameter is given in Figure 79. Figure 80 shows the influence of a/g and q/A on $\Delta T_{sat.}$ normalized to those at a/g = 1.

After completion of all the testing the vessel was disassembled and the heater surface examined. The heater surface appeared in good condition with a small amount of erosion indicating the location of the nucleate boiling sites. These markings on the surface indicated that a large number of uniform nucleation sites had existed over approximately 80 percent of the surface.

CONCLUSIONS

Only a small amount of data was obtained with non-boiling conditions, but that which was obtained are interesting. From Figure 52 at P = 80 psia the ΔT_B increases at a/g = 5 and then decreases with higher acceleration, but with only small changes between a/g = 10 and a/g = 15. From Figure 65 and 72 increasing acceleration has no influence on ΔT_B, indicating that buoyant forces have no influence on the heat transfer coefficient defined in terms of this ΔT_B. It is possible that the small liquid depth (1/2-inch) has some bearing here.

It was desired to eliminate subcooling as a variable with nucleate boiling, but this was possible only at the higher levels of pressure. To maintain constant

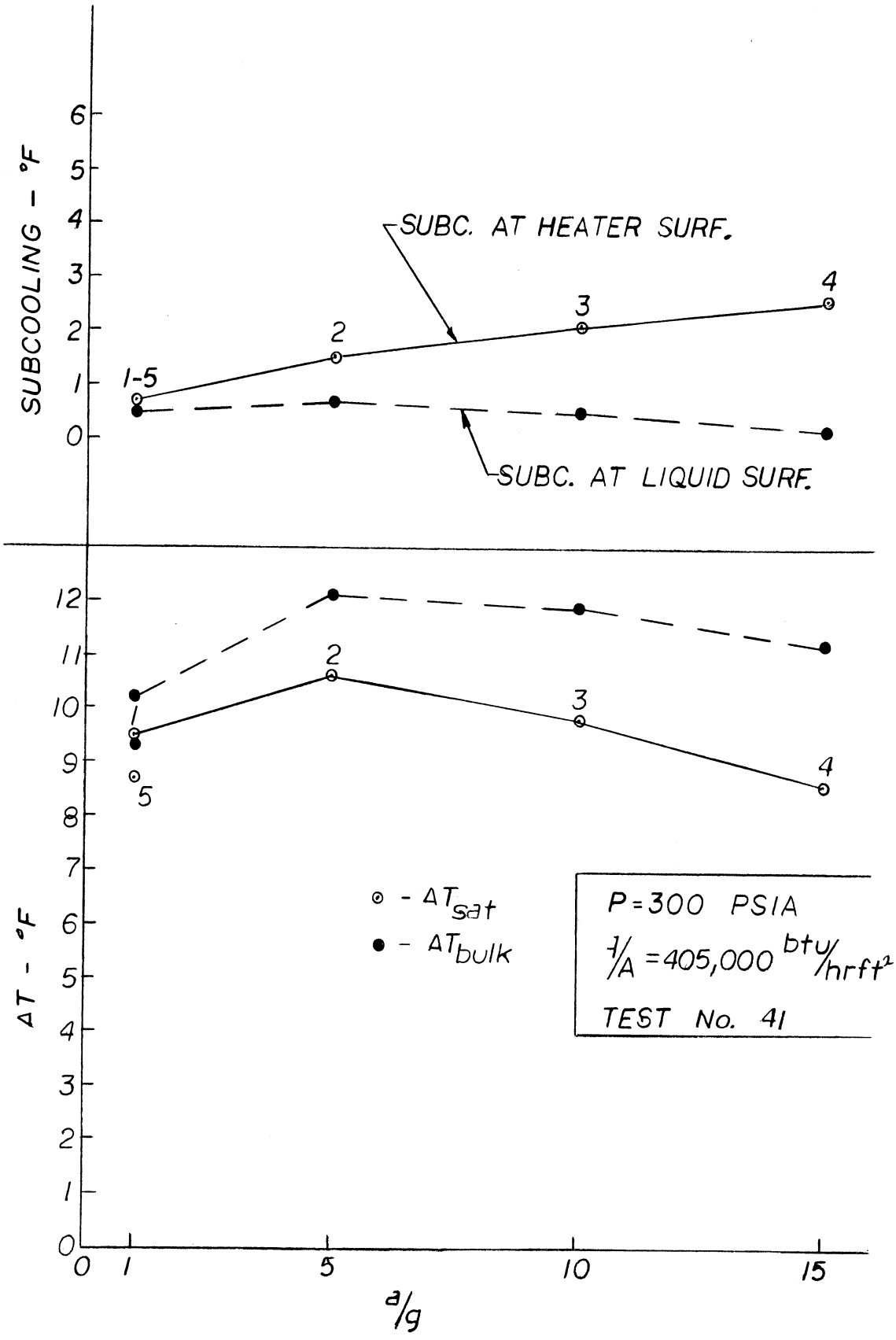

Figure 76 Mercury Boiling Data under High Gravity, Run Number 41

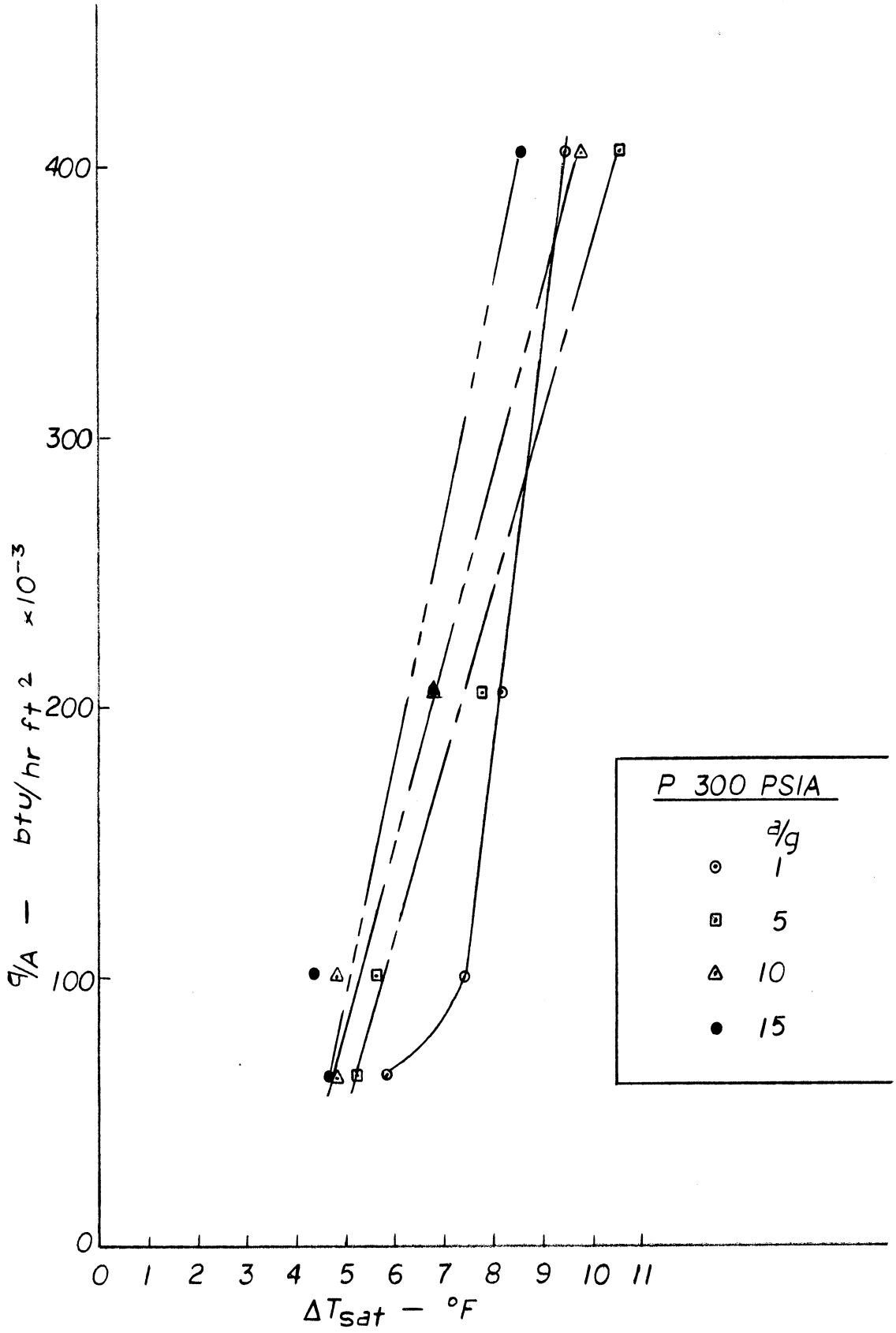

Figure 77 Composite of Influence of High Gravity on Subcooling for P = 300 psia

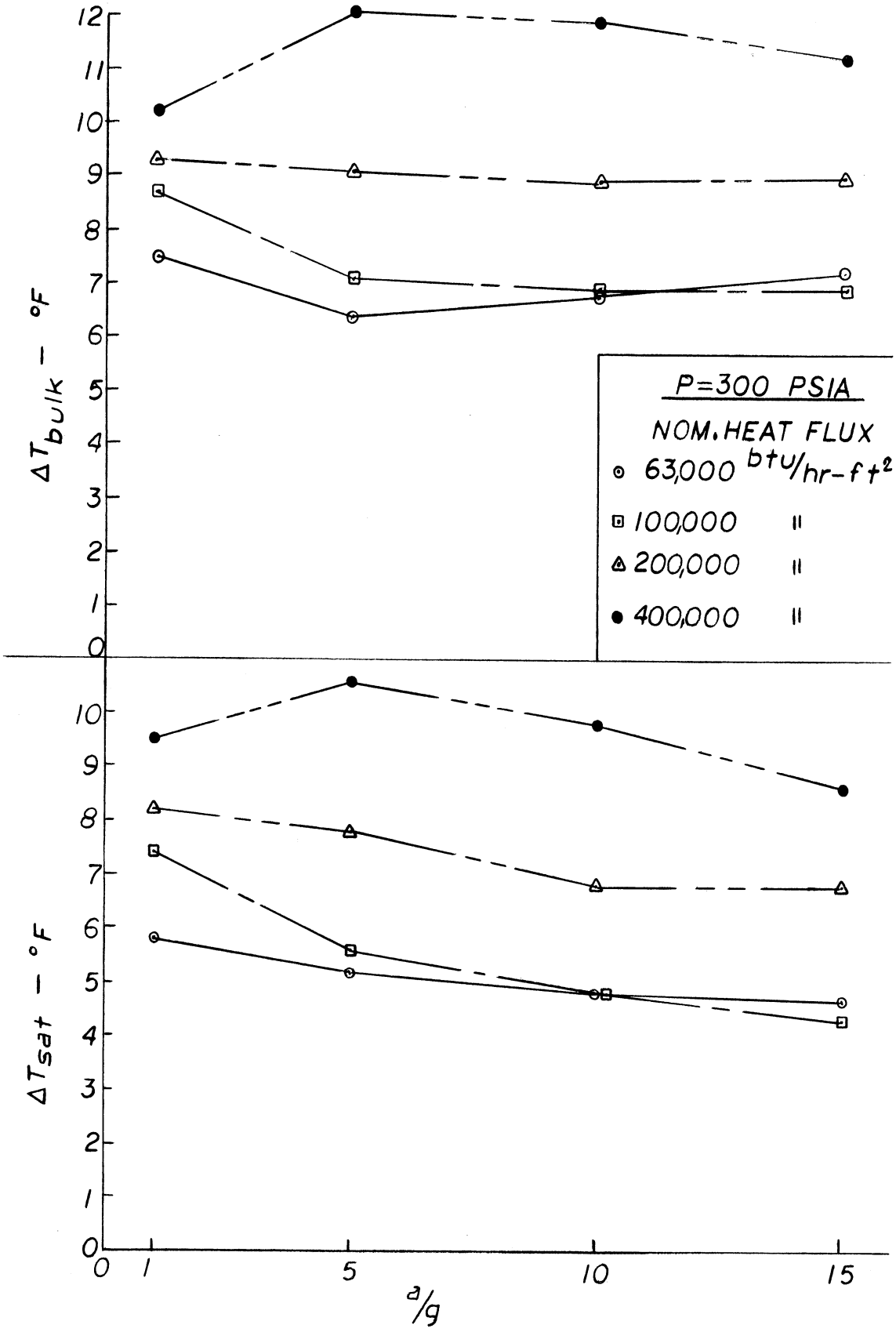

Figure 78 Composite of Influence of High Gravity on ΔT for P = 300 psia

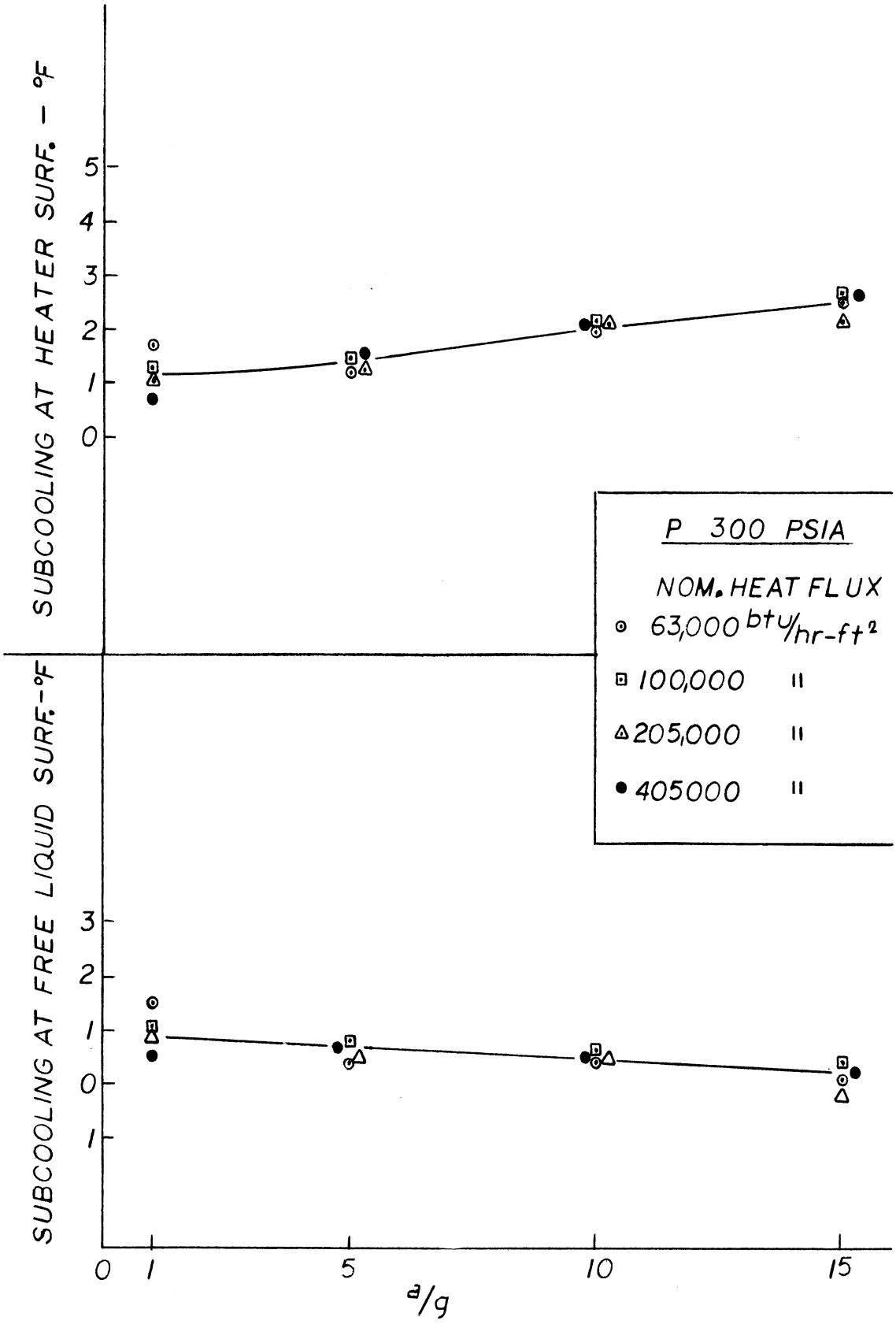

Figure 79 Heat Flux versus ΔT_{sat} for Levels of Acceleration for P = 300 psia

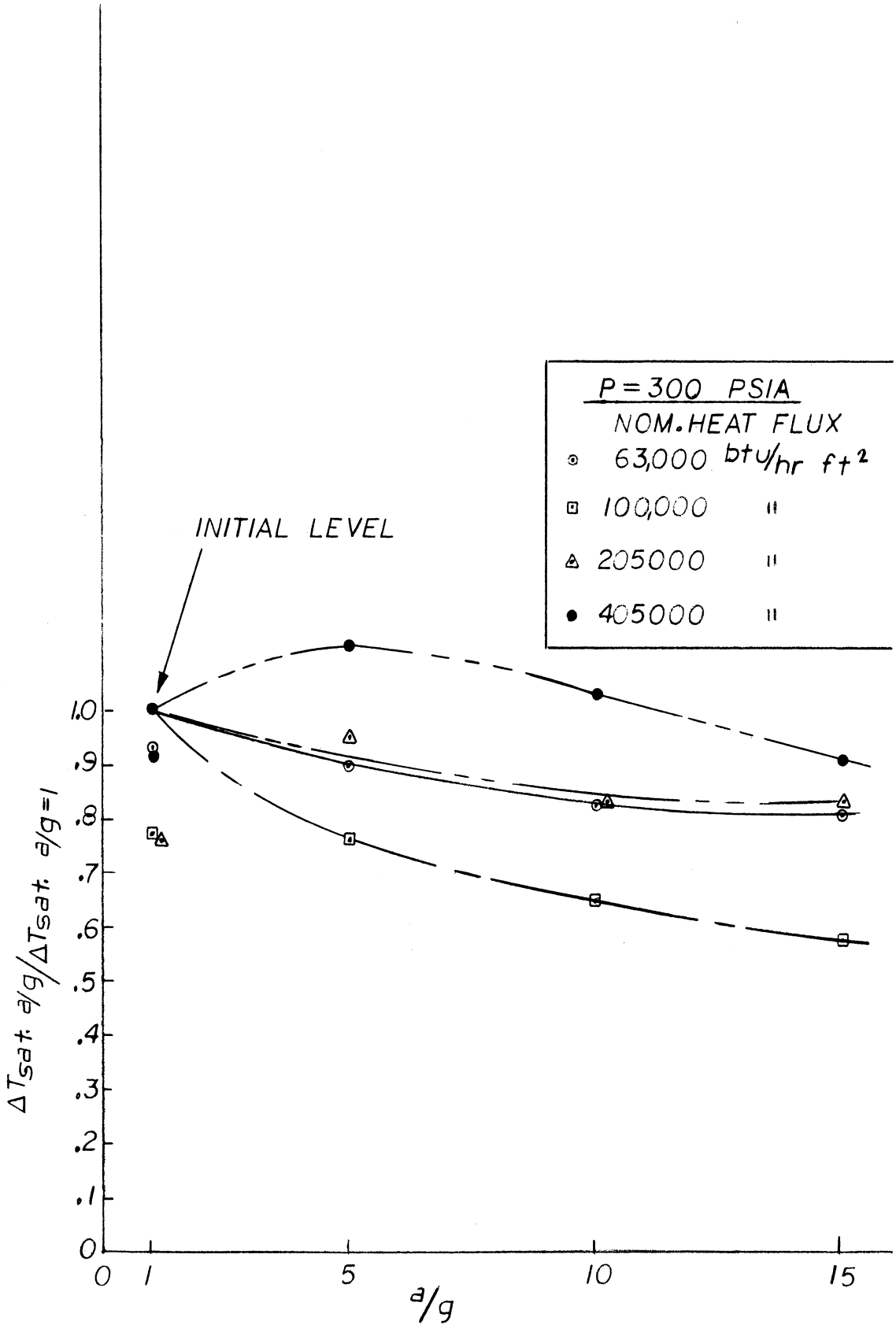

Figure 80 Influence of High Gravity on Normalized ΔT_{sat} for P = 300 psia

subcooling it would be necessary to vary the liquid depth as acceleration level is changed.

The influence of acceleration and pressure on nucleate boiling is best observed by referring to the plots of the normalized $\Delta T_{sat.}$ for each pressure level, Figures 64, 71 and 80. Generally speaking, as heat flux is increased, the changes of $\Delta T_{sat.}$ with acceleration become smaller. Also, as the pressure level is increased, the changes of $\Delta T_{sat.}$ with acceleration become smaller. This may be due to the decreasing density difference between the liquid and vapor. At the highest level of pressure and heat flux, Figure 80, $\Delta T_{sat.}$ first increases with increasing acceleration. This phenomena may also occur at sufficient levels of heat flux at the lower levels of pressure. The trends in that direction appear to be present in bubble sizes and frequency with acceleration, and the motion induced within the liquid near the heating surface by the bubbles moving through the liquid at high velocities.

The results obtained indicate a prior history effect on nucleate boiling due to operation at high gravity levels. $\Delta T_{sat.}$ at $a/g = 1$ was most generally lower after operation at high acceleration. This may be due to the activation of additional nucleation sites during the high acceleration periods, some of which then remain active. The reproducibility of the absolute values of $\Delta T_{sat.}$ was not as good as might have been desired in some cases. This is believed due to the relatively poor wetting characteristics of mercury. It would be desirable to obtain the above corresponding data with Na or K, which have more reproducible wetting characteristics.

The expected behavior of nucleate boiling under reduced gravity conditions might be determined by extrapolating the results in Figure 64, 71 and 80 to low gravity. These indicate that $\Delta T_{sat.}$ should not change drastically at sufficiently high pressure levels. The extent to which this extrapolation could be carried is, however, not known at this time, and would require experimental data.

SODIUM CONDENSING STUDIES

Robert E. Barry

Anthony J. Sartor

INTRODUCTION

The use of liquid metals in heat transfer systems offers several advantages to the equipment designer. In particular, at a given temperature, the vapor pressure of liquid metals is substantially lower than that of water or organic heat transfer fluids. This low vapor pressure permits the use of light weight designs for high temperature heat transfer systems. Liquid metals are also noted for their high thermal conductivity which offers the potential of higher heat transfer rates for a given temperature difference and, for some applications, a substantial reduction in the required heat transfer area. Table XIII compares the physical properties of several liquid metals with those of water at their normal boiling points.

In the foreseeable future, high power levels will be required for the operation of auxiliary equipment in space vehicles. The use of nuclear energy, with its limited fuel requirements, to operate a thermal energy conversion cycle appears to be the only feasible choice as an energy source for this application. Since radiation is the only method of heat rejection in space, such cycles must operate at relatively high temperature levels, and liquid metals appear to be an excellent choice for the working fluid. The Department of Defense and the National Aeronautics and Space Administration are sponsoring research for this application.

Central station power plants utilizing mercury have been in use since 1922. In such plants, mercury is vaporized in the boiler, expands through a turbine, and is liquified in the condenser. Condensing mercury has also been used for the distillation of crude oil and as a temperature control in catalytic converters.

It was primarily in connection with power generation in space, however, that the recent increased interest in the condensing heat transfer rates of liquid metals developed. Weight is a prime consideration in the design of a space vehicle and the efficient design of the heat rejection system requires a precise knowledge of the condensing heat transfer coefficient for liquid metals.

Thus, it has only been within the last fifteen years that experiments were devised with the primary aim of determining the condensing heat transfer coefficient of a liquid metal vapor. These experiments have been concerned with the condensation of mercury, cadmium, sodium, rubidium and potassium on a cool surface and under conditions such that predictions of the condensing heat transfer coefficient from a film theory of condensation would be expected to apply.

TABLE XIII - PHYSICAL PROPERTIES FOR SATURATED LIQUIDS AND VAPORS AT 1 ATM

	H_2O	Hg	Cs	Rb	K	Na	Li	Ga
Melting Point °F	32	-38	83	102	145	208	357	86
Boiling Point °F	212	674	1260	1295	139	1630	2440	3601
Tc °F	705	2659		3032	3095	4166	4135	
Pc psia	3200	15,000		2790	2500	4409	11,850	
Vapor press. psia at 2000°F		~5000	200	200	150	70	2.5	<1mm
Latent Heat Btu/#	970	126	211	348	850	1662	8300	1830
ρ #/ft^3	60	794	105	81.9	41.45	46.25	26	300
k Btu/hr ft °F	.39	7.11	10.7	11.65	17.98	32	29.6	30
μ #/ft hr	.72	2.15	.5	.36	.3	.36	.4	1.6 (800°C)
C_p Btu/#°F	1.0	.032	.057	.0877	.187	.307	.98	.09
Pr	1.85	.0097	.003	.003	.003	.0034	.013	.0048
α ft^2/hr	.0078	0.28	2	1.77	2.38	2	1.2	~1
σ #/ft	.0041	.027		.004	.005	.007	.0295(MP)	~.04
ρ_v #/ft^3	.0373	.244	.114	.071	.031	.016	.004	
μ_v #/ft hr	.0311	.1475	.065	.06	.047	.0551	.0473	
Cp_v Btu/# °F	.35	.025	.037	.06	.126	.213	.708	
k_v Btu/hr ft °F	.0035	.005	003	005	.008	.0161	.0459	

However, the general observation from all these experiments has been that the measured values of liquid metal condensing heat transfer coefficients are much lower than would be predicted from film theory. The film theory assumes that the major resistance to heat transfer lies within the liquid film and can be predicted from the physical properties of the condensed liquid.

It should be noted, however, that the experimental results for the condensing heat transfer coefficient are widely scattered, due primarily to the difficulties of making precise measurements at high temperatures in corrosive media. This has so far precluded the development of any adequate theory or empirical formula for the prediction of the condensing heat transfer coefficient.

The object of this investigation was to determine experimentally the condensing heat transfer coefficient for sodium at temperatures up to 1500°F and heat fluxes exceeding 1/2-million BTU/(hr)(sq ft). Such values cover the range of operating conditions that might be used in a space power cycle and the heat flux extends, by a factor of five, the range of previous experimental data for any alkali metal. In order to test the concept of a resistance to heat transfer in the vapor phase, it was also planned to vary the vapor temperature while maintaining a constant temperature difference between the vapor and the cooled wall. The data would then be compared with film theory and with predictions from the kinetic theory of condensation for the purpose of defining the mechanism of the resistance to heat transfer.

The experiment was conducted by condensing sodium on the outside of a vertical tube through which potassium was flowing. The advantage of this technique was that it permitted the independent variation of the vapor temperature and the flux.

REVIEW OF THE LITERATURE

1. Condensation

It is convenient to classify the condensation of a species from the vapor phase as occurring in one of three modes: (a) condensation within the bulk vapor, (b) dropwise condensation on a cool surface, and (c) film condensation on a cooled surface.

Condensation within the bulk vapor can occur by the formation of droplets on foreign bodies such as dust or it can occur in a sub-cooled vapor in the absence of foreign bodies. This phenomenon can be observed in the formation of clouds or in supersonic wind tunnels.

Dropwise condensation involves the impingement of molecules upon a cooled wall, subsequent liquification, and coalescence with nearby droplets. The larger drops thus formed run down the surface, sweeping it clean, and permit the cycle to occur again. The heat transfer coefficient in dropwise condensation is usually much ligher than that observed in film condensation due to the

absence of a continuous film through which the heat must be transferred (121). The occurrence of dropwise condensation is usually attributed to the existence of high interfacial energies between the liquid and the cooled wall. In other words, the liquid fails to wet the wall.

Film type condensation occurs when the liquid wets the wall forming a continuous film of condensate which is continually being replenished by the condensation of the vapor. The thickness of the film depends upon the slope of the cooled wall, the motion of the wall, and the velocity of the vapor relative to the film.

Mercury has been observed in dropwise condensation upon stainless steel tubes, in dropwise condensation succeeded by film type condensation after several hours on carbon steel tubes, and in film type condensation upon copper or nickel tubes (130). The condensation of the alkali metals has never been visually observed but from indirect evidence, it can be said that at temperatures exceeding 600°F, alkali metals wet the surface of the structural metal. This conclusion can be inferred from the output of electromagnetic flowmeters which approaches the theoretical value as the temperature is increased. Furthermore, the alkali metals are excellent "getters" of surface contaminants, thus serving to insure a "clean" surface.

The existence of a non-condensible gas in the vapor space can seriously lower the condensing heat transfer coefficient. This is because the vapor molecules must diffuse through the non-condensible gas in order to reach the condensate surface thus introducing a resistance to mass transfer.

2. Theory of Film Condensation

Studies of film condensation have heretofore been based upon the theory of Nusselt (141) or refinements thereof. Nusselt's development considers the laminar film condensation of a vapor on an isothermal wall. The only forces acting on the film are gravity and the shear stress at the wall. Acceleration of the film and shear at the vapor-liquid interface are neglected and it is assumed a) that the temperature drop through the film is linear, b) that the surface temperature of the film corresponds to the saturation temperature of the vapor and c) that the physical properties of the film are constant. This analysis results in the following equation for the average condensing heat transfer coefficient on a vertical wall.

$$h_m \left(\frac{\mu^2}{k^3 \rho^2 g} \right)^{1/3} = 1.47 \, (Re_f)^{-1/3} \qquad (39)$$

where $Re_f = \frac{4\Gamma}{\mu}$ (40)

The corresponding equation for condensation on a horizontal cylinder is:

$$h_m\left(\frac{\mu^2}{k^3\,\rho^2 g}\right)^{1/3} = 0.5\,(Re_f)^{-1/3} \qquad (41)$$

These equations successfully describe film condensation of steam and organic vapors within engineering accuracy (90, 121).

More recently several investigators have extended the theory to account for the assumptions in Nusselt's analysis. Colburn (47) and Seban (162) considered turbulent flow in the film. Sparrow and Gregg (166) utilized a boundary layer treatment of the film to examine the effects of acceleration of the film, Bromley (30) and later Rohsenow (152) studies the effects of non-linearity in the film temperature distribution, and Koh (96) investigated the effect of shear stress at the vapor liquid interface.

Sukhatme and Rohsenow (169) showed that these corrections were small when considering the condensation of a metal vapor under conditions corresponding to present engineering design, and that analyses based upon the structure of the liquid film did not explain the low heat transfer coefficients which have been observed.

The results of several investigations of liquid metal condensation are shown in Figure 81 where they are compared with Nusselt's theory. It can be seen that the observed coefficients fall far below the prediction of the theory, sometimes by more than two orders of magnitude.

There remains one more assumption of Nusselt's theory to be examined. Namely, that the surface temperature of the film is equal to the saturation temperature of the vapor. If the film surface temperature were much lower than the vapor temperature, the low heat transfer coefficients could be explained. This effect can be examined by use of the kinetic theory of condensation.

3. The Kinetic Theory of Condensation

Consider a vapor at pressure, P_v, and temperature T_v condensing on a liquid film whose surface temperature is T_s corresponding to a saturation pressure, P_s. Under the assumption of an ideal gas having a Maxwellian velocity distribution, it can be shown from the kinetic theory of gases that, at equilibrium, the flux of molecules in any one direction is given by:

$$\frac{W}{A} = P\sqrt{\frac{M}{2\,\pi\,R\,T}} \qquad (42)$$

In accordance with Schrage (160), where there is a net motion of the molecules, the flux of vapor molecules impinging on the liquid surface is:

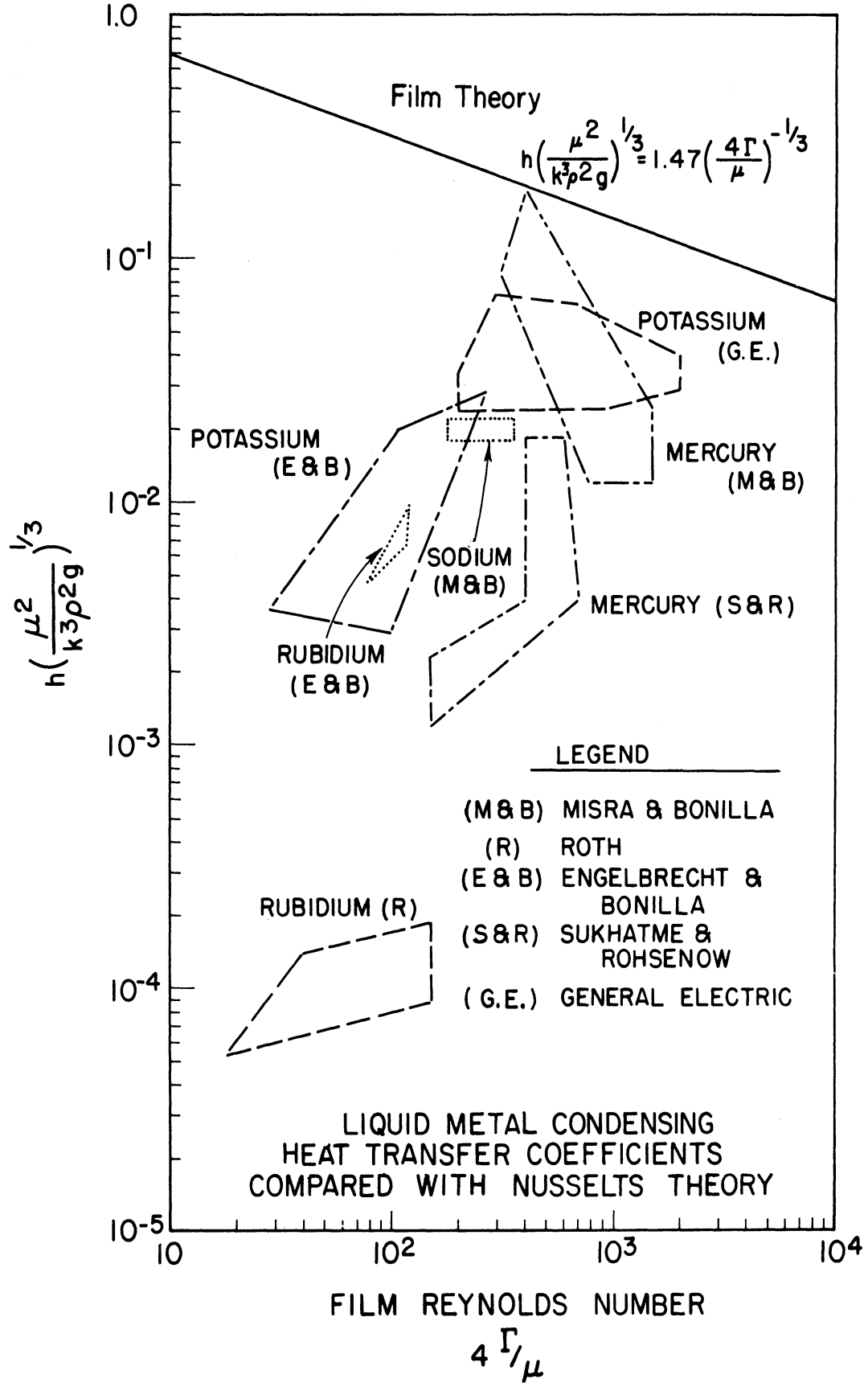

Figure 81 Liquid Metal Condensing Heat Transfer Coefficients Compared with Nusselt's Theory

$$\frac{W}{A} = \Gamma_1 P_v \sqrt{\frac{M}{2 \pi R T_v}} \tag{43}$$

where

$$\Gamma_1 = e^{-\varphi^2} + \varphi \pi^{1/2} (1 + \text{erf } \varphi) \tag{44}$$

and

$$\varphi = \frac{W/A}{\rho (2 R T_v/M)^{1/2}} \tag{45}$$

But, it is possible that not all the molecules that strike the surface actually condense and consequently, an accommodation coefficient σ_c is introduced to account for this. Thus, the flux of condensing molecules at the liquid surface is given:

$$\left(\frac{W}{A}\right)_c = \sigma_c \Gamma_1 P_v \sqrt{\frac{M}{2 \pi R T_v}} \tag{46}$$

and, of course, the flux of reflected molecules is given by:

$$\left(\frac{W}{A}\right)_r = (1 - \sigma_c) \Gamma_1 P_v \sqrt{\frac{M}{2 \pi R T_v}} \tag{47}$$

The absolute rate of evaporation of a liquid into a high vacuum is given by:

$$\left(\frac{W}{A}\right)_e = \sigma_e P_s \sqrt{\frac{M}{2 \pi R T_s}} \tag{48}$$

where again, an evaporation coefficient σ_e has been introduced to account for the deviation of experimental results from the kinetic theory of gases.

Finally, the expression for the net flux of condensation is given by:

$$\left(\frac{W}{A}\right)_{net} = \left(\frac{W}{A}\right)_c - \left(\frac{W}{A}\right)_e = \sigma_c \Gamma_1 P_v \sqrt{\frac{M}{2 \pi R T_v}} - \sigma_e P_s \sqrt{\frac{M}{2 \pi R T_s}} \tag{49}$$

The value of σ_e may approach unity when evaporation is taking place in a high vacuum, but when condensation is taking place, it is evident that σ_e could have values much less than unity due to the interference of the condensing molecules with the evaporation molecules. In the absence of specific knowledge about

the evaporation coefficient, certain assumptions may be made.

The assumption which has been most often used in the study of condensation is that $\sigma_e = \sigma_c$. Actually, there is no physical reason why this should be so. In utilizing this assumption, the usual method of correlation is to determine T_S (and hence P_S) by a measurement of the wall temperature coupled with the use of Nusselt's film theory to determine the temperature difference between the wall and the surface of the condensate film. T_V is measured directly and either P_V is measured or it is assumed equal to the saturation pressure corresponding to T_V. The condensing mass flux is determined from a heat balance on the coolant and then σ_c can be solved for and correlated with the parameter of the experiment The recent studies of Labuntsov and Smirnov (102), and Aladyev (4), utilized the kinetic theory of condensation to correlate their results. They found a linear relation between log σ_c and log pressure.

Wilhelm (183) solved the equations of momentum, mass and energy transfer applying to the kinetic theory of condensation using several different arbitrary assumptions concerning the value of σ_e and the velocity distribution of the reflected molecules. He stated that these solutions failed to yield results that "are considered physically consistent and systematic".

One observations can be made regarding Equation (49); namely, for a given temperature difference $T_V - T_S$, the net condensing flux depends uniquely upon σ_c, σ_e and T_V. If σ_c and σ_e are constants, and if there were a resistance to mass transfer in the vapor phase, the net condensing flux should depend only upon T_V. Results to date do not support such a conclusion.

4. Liquid Metal Condensing Experiments

Meaningful experiments in liquid metal condensation began with the work of Misra and Bonilla (130) which was reported in 1956. Mercury vapor was condensed at pressures ranging from 0.1 to 15 psia on the outside of a vertical 1/2-inch diameter tube using water or air as the coolant. Several tube materials were used: carbon steel, copper plated steel, nickel and stainless steel. A composite condenser tube was also used, constructed of a length of nickel between two lengths of stainless steel, thus forming a thermocouple by which the average wall temperature could be determined. Motion pictures, still photographs and visual observations showed dropwise condensation on the stainless steel tubes, dropwise succeeded by film type condensation on carbon steel tubes and film type condensation on the copper plated and nickel tubes. The heat flux was determined by a heat balance on the coolant. The vapor temperature was measured directly. The wall temperature was computed from the coolant temperature and the predicted temperature drops through the coolant film and the metal wall. When the composite condenser tube was used, the wall temperature could be determined directly. The temperature difference across the condensate film was measured in some of the runs by employing a differential thermcouple consisting of a tiny stream of mercury in contact with a wire of the same material as the condenser tube and barely touching the condensate surface. A second method of determing the surface temperature was to barely touch the condensate

film with a wire of the same material as the condenser tube, thus forming a differential thermocouple.

The heat flux varied from 25,000 BTU/(hr)(sq ft) with air cooling to 750,000 BTU/(hr)(sq ft) with water cooling. The heat transfer coefficients shown in Figure 81 range from 3,000 to 50,000 BTU/(hr)(sq ft)(°F).

Misra and Bonilla examined their data from the viewpoint of the kinetic theory of condensation and concluded that this theory could not explain the low heat transfer coefficients. Wilhelm (183) also examined the data of Misra and Bonilla from this standpoint assuming that the accommodation coefficient for condensation σ_c, equaled the evaporation coefficient σ_e. Using Equation (49), Wilhelm (38) calculated values of σ_c ranging from a .02 to .61 but offered no explanation for this variation.

Misra and Bonilla also obtained heat transfer coefficients for sodium vapor condensing on a 1/2-inch tube inclined at an angle of 45 degrees. The vapor temperature was around 1500°F and the heat flux ranged from 60,000 to 100,000 BTU/(hr)(sq ft). The resulting heat transfer coefficients of 11,000 to 15,000 was shown in Figure 81 and represent about 8 percent of the value derived from Nusselt's theory.

In 1959, Cohn (46) in order to expand the available data on liquid metal condensation, studied the condensation of mercury inside a vertical 10-inch long, 1/2-inch diameter, stainless steel tube cooled by nature convection. A thermocouple in the wall served to determine the temperature difference. Heat fluxes up to 51,000 BTU/(hr)(sq ft) were obtained at vapor temperatues up to 725°F. The calculated heat transfer coefficient varied from 2300 to 60,000 BTU/(hr)(sq ft)(°F). As can be seen from Figure 81, these values are well below Nusselt's predictions.

In 1962, Roth (156) condensed rubidium at low heat fluxes on the outside of a vertical air-cooled U-tube inserted in the vapor space of a boiler. The program was admittedly a preliminary one, designed to gain experience in handling alkali metals at high temperatures, obtain corrosion information and to observe visually the mode of condensation. Thermocouples imbedded in the wall of the tube and in the vapor space gave the temperature difference. The heat flux was obtained by a heat balance on the coolant. Vapor temperatures ranged from 940°F to 1618°F and the maximum heat flux was 9,000 BTU/(hr)(sq ft). The calculated heat transfer coefficients are very low, ranging from 10 to 53 BTU/(hr)(sq ft)(°F).

Roth offers no explanation for these low values but Sukhatme and Rohsenow (153) suggest that heat conduction along the thermocouple leads could account for errors in the wall temperature measurement. They support this premise by noting that the air side coefficient seems to vary haphazardly with the air flow rate. However, Roth reported vapor to wall temperature differences of up to 314°F and it is difficult to see how an error of this magnitude could be introduced. As is seen in Figure 81, Roth's data fall far below the other data for alkali metals. There is no trend in the reported heat transfer

coefficient with respect to either the vapor temperature or the heat flux. Attempts to observe the condensation of sodium through a sapphire window in an earlier experiment failed when the window cracked.

In 1963, the data of Engelbrecht and Bonilla (171) for condensing potassium and rubidium were reported. Two apparatus were used in these experiments. The first consisted of a cylindrical pot type boiler with a 13-inch long, 1/2-inch diameter condenser, mounted at an angle of 45 degrees. The tube was a nickel-stainless steel composite and served as one junction of a differential thermocouple which determined the wall temperature. The second apparatus was a 21-inch long 1 3/4-inch diameter tube in which the bottom six inches served as the boiler and the remaining 15 inches served as the condenser. Both apparatus were air cooled and condensation occurred inside the tube.

Potassium was condensed at temperatures ranging from 714°F to 1042°F and heat fluxes from 2300 to 23,000 BTU/(hr)(sq ft) were obtained. The calculated heat transfer coefficients, shown in Figure 81, ranged from 480 to 9300 BTU/(hr)(sq ft)(°F) and tend to support the sodium data of Misra and Bonilla (130).

Rubidium was condensed inside the 1 3/4-inch tube at temperatures of 636°F, 714°F, and 877°F. The corresponding heat fluxes were 82,000, 12,700 and 12,180 BTU/(hr)(sq ft) and the heat transfer coefficients were 1550, 3160, and 2220 BTU/(hr)(sq ft)(°F). These three values are 30 times higher than the heat transfer coefficients reported by Roth.

In 1964, Sukhatme and Rohsenow (169) reported the results of condensing mercury at low pressures (.02 to .33 psia) on the outside of a vertical 3/4-inch diamter nickel tube extending into the mercury vapor space. The pressures correspond to vapor temperatures of 260°F to 390°F and this temperature range is lower than that for any other investigation of liquid metal condensation. The wall temperature was determined by measuring the electrical resistance of a selected length of the nickel condensing tube and the heat flux was determined from a heat balance on the coolant. Water and silicone oil were used as coolants in order to obtain different heat fluxes at the same vapor temperature. They measured condensate film thicknesses by means of gamma-ray attenuation at several heat fluxes and found that the thickness of the condensate film was resonably close to the thickness predicted by simple hydrodynamic theory. Therefore, the low heat transfer coefficients obtained could not be attributed to a thicker film than would be predicted by Nusselt's theory. Heat fluxes from 34,000 to 101,000 BTU/(hr)(sq ft) were obtained at temperature differences ranging from 11°F to 234°F. As indicated in Figure 81, the resultant heat transfer coefficients of from 190 to 3100 BTU/(hr)(sq ft)(°F) fall far below Nusselt's theory and are lower than the results obtained by Misra and Bonilla (130) for mercury.

The significant finding of the investigation by Sukhatme and Rohsenow was that the heat transfer coefficient increased as the vapor pressure increased. The data were correlated on the basis of Schrage's kinetic theory of condensation using Equation (49) and assuming that σ_c equals σ_e. It was found that a

value for the condensing accommodation coefficient, σ_c, of 0.45 successfully correlated the condensing heat transfer coefficient and explained the variation of heat flux with pressure.

Based upon these findings, Sukhatme and Rohsenow concluded that the previous data for film condensation of metal vapors, contained errors due either to the presence of non-condensible gases or to inaccurate wall temperature determinations. It is worthwhile digressing for a moment to discuss this point.

Misra and Bonilla (130) tested for the effect of non-condensibles by deliberately introducing a steady flow of inert gas into the system. They then plotted the observed heat transfer coefficient against the flow rate of the inert gas and extrapolated the curve to the y=axis, assuming that the heat transfer coefficient thus obtained was for the case of no non-condensibles. Sukhatme and Rohsenow point out that this technique is questionable since the pertinent quantity is the actual amount of non-condensibles present in the system and not the rate of leakage or removal. On the other hand, the data of Misra and Bonilla show a slight drop with increasing vapor pressure and if there were non-condensibles present, it would be expected that higher heat transfer coefficients would be obtained at higher pressures. In the absence of further data, it is impossible to make a judgment as to whether or not the data of Misra and Bonilla contained errors due to non-condensibles.

Sukhatme and Rohsenow questioned the data of Cohn (46) and it must be admitted that the anomalous results obtained for condensing steam in his apparatus indicate that Cohn's data for mercury is questionable.

The use of an accommodation coefficient of 0.45 by Sukhatme and Rohsenow to correlate their data was questioned by Wilhelm (183). Wilhelm pointed out that the accommodation coefficient obtained in this experiment varied from .368 to .605 under conditions such that the use of an "average" accommodation coefficient would be physically meaningless and that such usage could only be a correlating device.

Sukhatme and Rohsenow demonstrated that large percentages of non-condensible gases added to the system appreciably lowered the heat transfer coefficient but did not make any quantitative measurement of the amount of gas actually present in the system.

In 1965, the General Electric Company (69) reported the results of condensing a two-phase potassium flow inside a vertical 5/8-inch diameter tube cooled by liquid sodium on the outside. The vapor temperature ranged from 1130 to 1312°F and local condensing coefficients were obtained at two points along the length of the tube; at length to diameter ratios of 13 and 46. The vapor temperature at these two points was not measured directly but calculated from the inlet temperature and a calculated pressure drop. As the authors recognized, this technique can lead to serious error. Thermocouples in the wall gave the temperature difference and the heat flux was obtained from a heat balance on the coolant.

The vapor quality in these experiments varied from 25 to 87 percent and the vapor velocity was varied over a wide range. Large disturbances in the film structure would be expected under such conditions and the actual area upon which condensation was taking place could be substantially different than the area of the tube wall. The heat flux was varied from 17,000 to 84,000 BTU/(hr)(sq ft)(°F) and the heat transfer coefficients shown in Figure 81 averaged about 20 percent of the prediction from Nusselt's theory. The heat transfer coefficients reported in this reference show no variation with respect to the vapor temperature. The results reported in previous reports have been recalculated on a different basis in this reference.

Labuntsov and Smirnov (102), in a paper presented at the Third International Heat Transfer Conference in August 1966, report on experimental data which they obtained by condensing potassium and sodium on a vertical stainless-steel tube 30 mm in diameter. Vapor and wall temperatures were measured at distances of 2.26 mm, 10.01 mm and 17.97 mm from the condensing surface.

The experiments were carried out at pressures ranging from 18.7 mm Hg to 900 mm Hg for potassium and from 17.1 mm Hg to 248 mm Hg for sodium. Air was used as a coolant, and heat fluxes varied from 31,800 BTU/(hr)(sq ft) to 63,500 BTU/(hr)(sq ft). The values of the heat transfer coefficient obtained ranged from approximately 5290 BTU/(hr)(sq ft)(°F) to 20,600 BTU/(hr)(sq ft)(°F) for potassium and from 4900 BTU/(hr)(sq ft)(°F) to 19,400 BTU/(hr)(sq ft)(°F) for sodium. These values are substantially lower than the values postulated by Nusselt's theory. The data were correlated on the basis of the kinetic theory of condensation using Equation (49), and it was found that a dependency of the accommodation coefficient on the saturation pressure existed, as shown in Figure 82.

In another paper presented at the Third International Heat Transfer Conference in August 1966, Aladyev et. al. (4) presented the results of condensing potassium inside a vertical stainless steel tube 4 mm in diameter and 50 mm in length. The pressures at which they conducted their work varied from 30 mm Hg to 76 mm Hg. Water was used as a coolant and the flux variation was from 60,400 BTU/(hr)(sq ft) to 700,000 BTU/(hr)(sq ft). The vapor temperature ranged from approximately 600°F to 1450°F and the condensing coefficient varied from 7050 BTU/(hr)(sq ft)(°F) to 17,600 BTU/(hr)(sq ft)(°F). In this investigation they found, as did Labuntsov and Smirnov (102), that the heat transfer coefficient increased as the vapor pressure increased. The data were again correlated on the basis of the kinetic theory of condensation using Equation (49), and it was found that a variation in accommodation coefficient occurred as the saturation pressure changed. (see Figure 83)

There is enough data to state that Nusselt's theory of film condensation does not predict condensing heat transfer coefficients for liquid metals. Measured coefficients are much lower than predicted and do not follow any trend suggested by film theory.

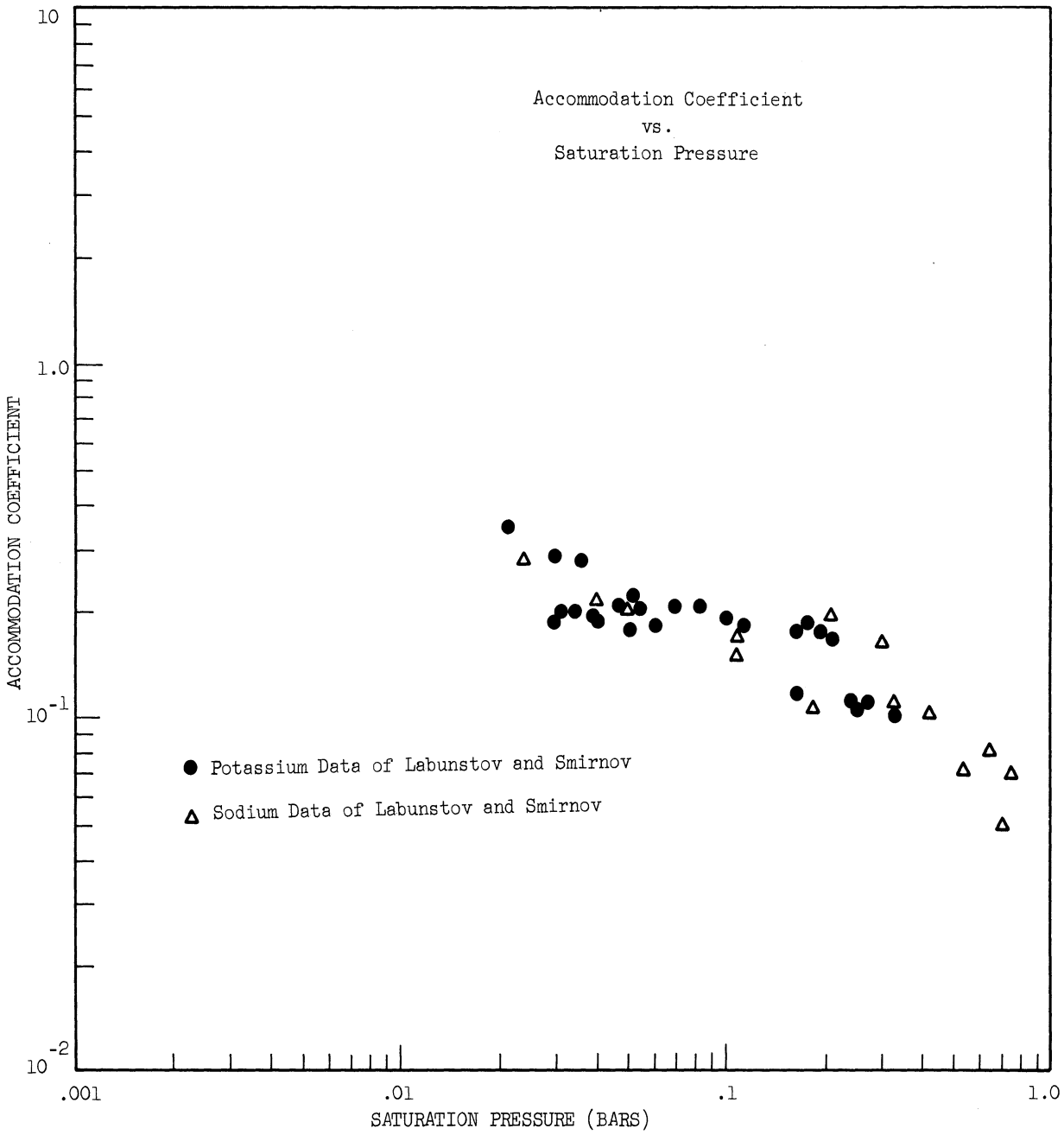

Figure 82 Sodium and Potassium Data of Labuntsov and Smirnov (102)

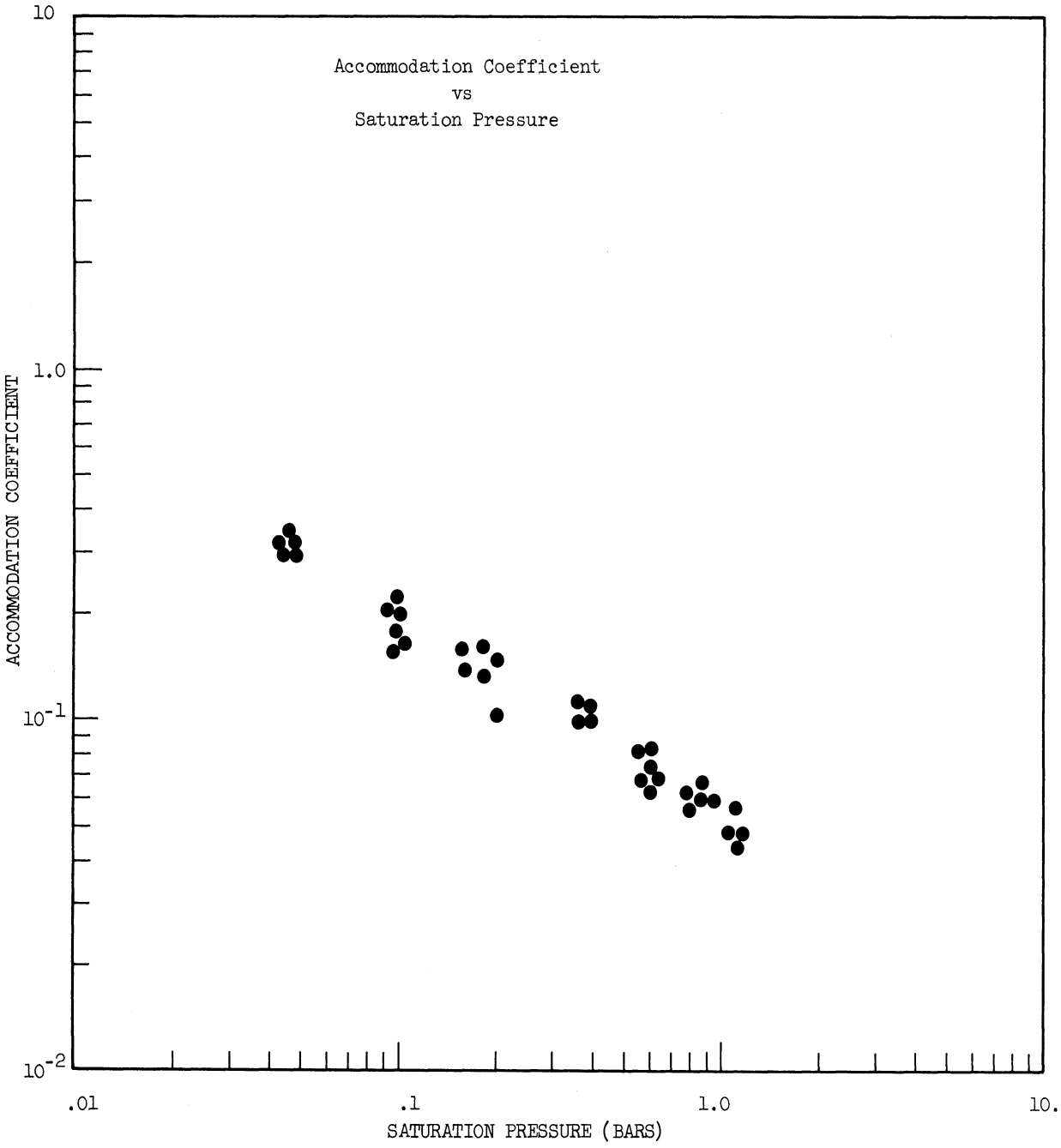

Figure 83 Potassium Data of Aladyev, et al. (4)

Sukhatme and Rohsenow (169), Labuntsov and Smirnov (102), and Aladyev et. al. (4), indicate an increase of the heat transfer coefficient with increasing pressure. This data was taken over a wide range of pressures. The data of Misra and Bonilla (120) show a slight decrease with increasing pressure, and the other data are too scattered to determine an effect. Sukhatme and Rohsenow (169) indicate that they have correlated their mercury data using the kinetic theory of condensation and an accommodation coefficient of 0.45. However, from the recent work of Labuntsov and Smirnov (102) and Aladyev et. al. (4), it would appear that a correlation based on the kinetic theory of condensation may be possible, but not with a constant value of accommodation coefficient as suggested by Sukhatme and Rohsenow (169). The two Russian papers indicate that the accommodation coefficient varies with the saturation pressure and that this observation permits correlation of much of the most recent liquid metal data.

The most reliable data for mercury appears to be that of Misra and Bonilla (130) and Sukhatme and Rohsenow (169). Unfortunately, these two sets of data produce a range of two orders of magnitude in the reported heat transfer coefficient.

Except for the results of Roth (156) which are so low as to lack credibility, the alkali metal data of Misra and Bonilla (130), Engelbrecht and Bonilla (171), and the General Electric Company (69) show slightly better agreement. The data of Labuntsov and Smirnov (102) and Aladyev, et. al. (4) cover a wide range of pressures and heat fluxes and appear to agree with each other. Their recommendation that the accommodation coefficient varies with pressure deserves further consideration. The majority of the reported heat transfer coefficients range from about 1000 to 19,000 BTU/(hr)(sq ft)(°F).

DESCRIPTION OF EQUIPMENT

The sodium condensing heat transfer experiments were conducted on a boiling liquid metal test loop constructed for the University of Michigan by the MSA Research Corporation of Callery, Pennsylvania. This loop consists of two separate fluid circuits: the primary circuit contains potassium which is circulated by a pump through a preheat section, a heat transfer test section, a condenser, and a cooler; the secondary circuit, which is a natural circulation boiling and condensing loop, contains sodium.

1.3 Summary of the Loop Circulation Mode

A schematic diagram of the loop is shown in Figure 84. The potassium in the primary circuit is pumped by an electromagnetic pump through a throttle valve and an electromagnetic flowmeter. The flow is then equally distributed into the three parallel heated tubes of the preheater and exits into a common heater at the test section inlet.

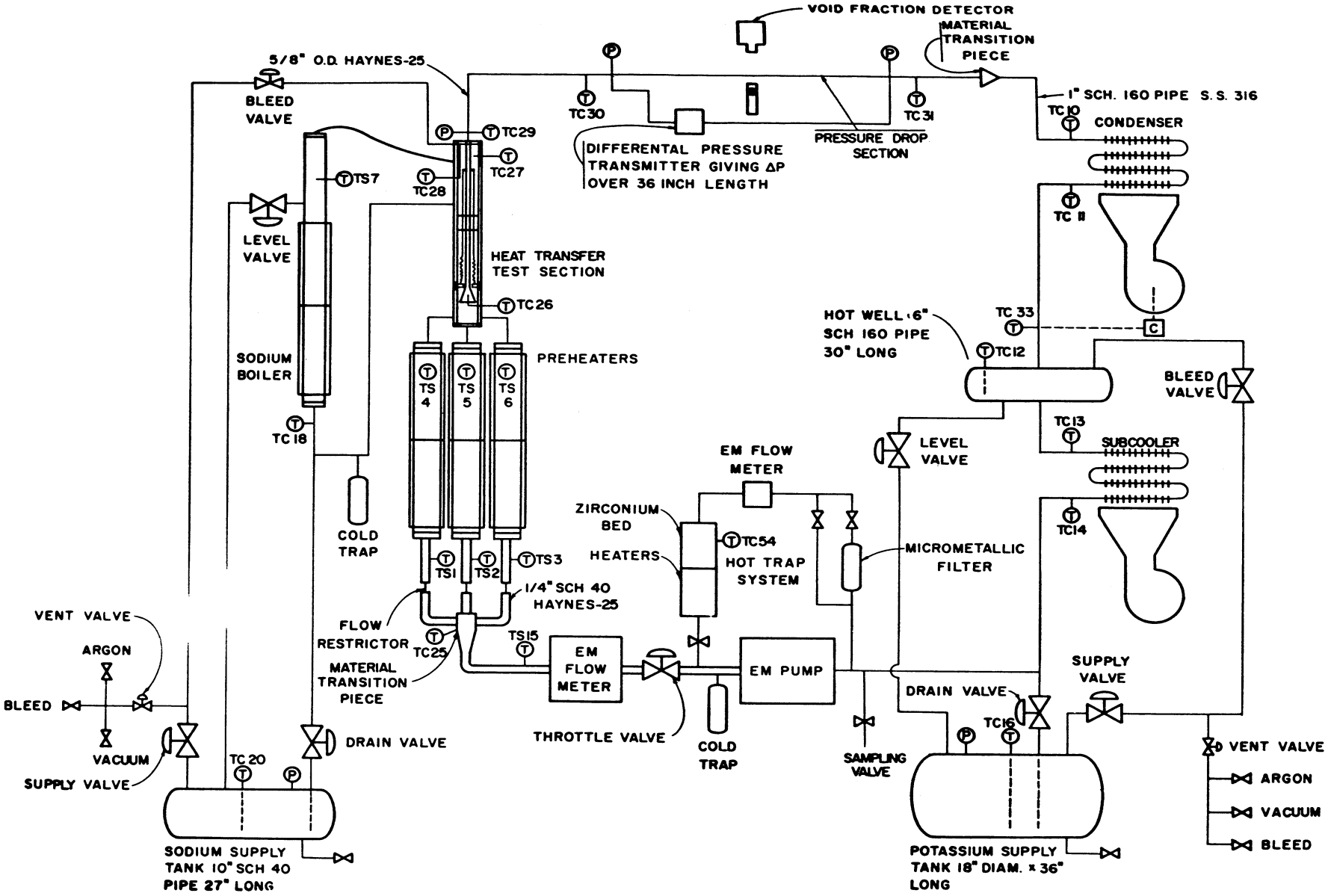

Figure 84 Flow Schematic-Boiling Liquid Metal System

By control of the pressure of the inert gas in the primary circuit and the power input to the preheater, the potassium may exit the preheater either as a liquid or as a liquid-vapor mixture. In the sodium condensing heat transfer experiments the potassium was maintained as a liquid.

The potassium then flows into a 1/2-inch tube within the test section. Heat is transferred to the potassium along the top 2-inches of this tube by sodium vapor condensing on the outside of the tube. The potassium is then passed through a horizontal straight section of tube in which pressure drop and void fraction measurements can be made. The flow then continues into a condenser, through a hot well and into a subcooler from whence the flow is returned to the pump.

In the secondary circuit, sodium is vaporized in the boiler, condensed in the shell side of the test section, and returned by gravity to the boiler.

Each circuit is equipped with a supply tank from which the system can be charged and into which the liquid metal can be dumped. The supply tanks may be evacuated or pressurized with argon. Each circuit is also equipped with a diffusional cold trap for the maintenance of low oxide concentration. Valves and auxiliary lines are located in each circuit for pressurizing, venting, leveling and draining. The argon used in the system is purified by passing it through a NaK bubbler.

2. Major Loop Components

The major components of the loop are shown in Figure 85, 86 and 87.

Pump: This is an MSAR Style II electromagnetic conduction pump. The pumping section consists of a 1-foot length of 3/8-inch stainless tube flattened so as to provide flow channel 1/16-inch wide. The developed pressure is rated at 100 psi at no flow and 80 psi at 2 GPM. The flow rate is controlled by varying the applied voltage from 0 to 270 V with a variable transformer or by regulating the throttle valve. A 10 KVA capacitor is connected across the pump to correct the power factor and reduce the line current. The pump is equipped with two blowers for cooling the coils.

Throttle Valve: This valve is a General Kinetics Corporation 1/4-inch Hi-100 stainless steel valve with a bellows seal. A ball whose position is controlled by an air operated cylinder floats in the fluid between the inlet and outlet seats. The valve provides a linear response to the air signal.

Flowmeter: The flow rate in the primary circuit is measured by a MSAR Style FM-2 magnetic flowmeter. This consists of two voltage taps diametrically mounted on a 3/8-inch stainless tube and perpendicular to the field of a permanent magnet.

Preheater: The preheater consists of three sections of 4-inch OD by 3-inch ID by 45-inch long Haynes-25 pipe mounted in parallel. Approximately 3 feet of

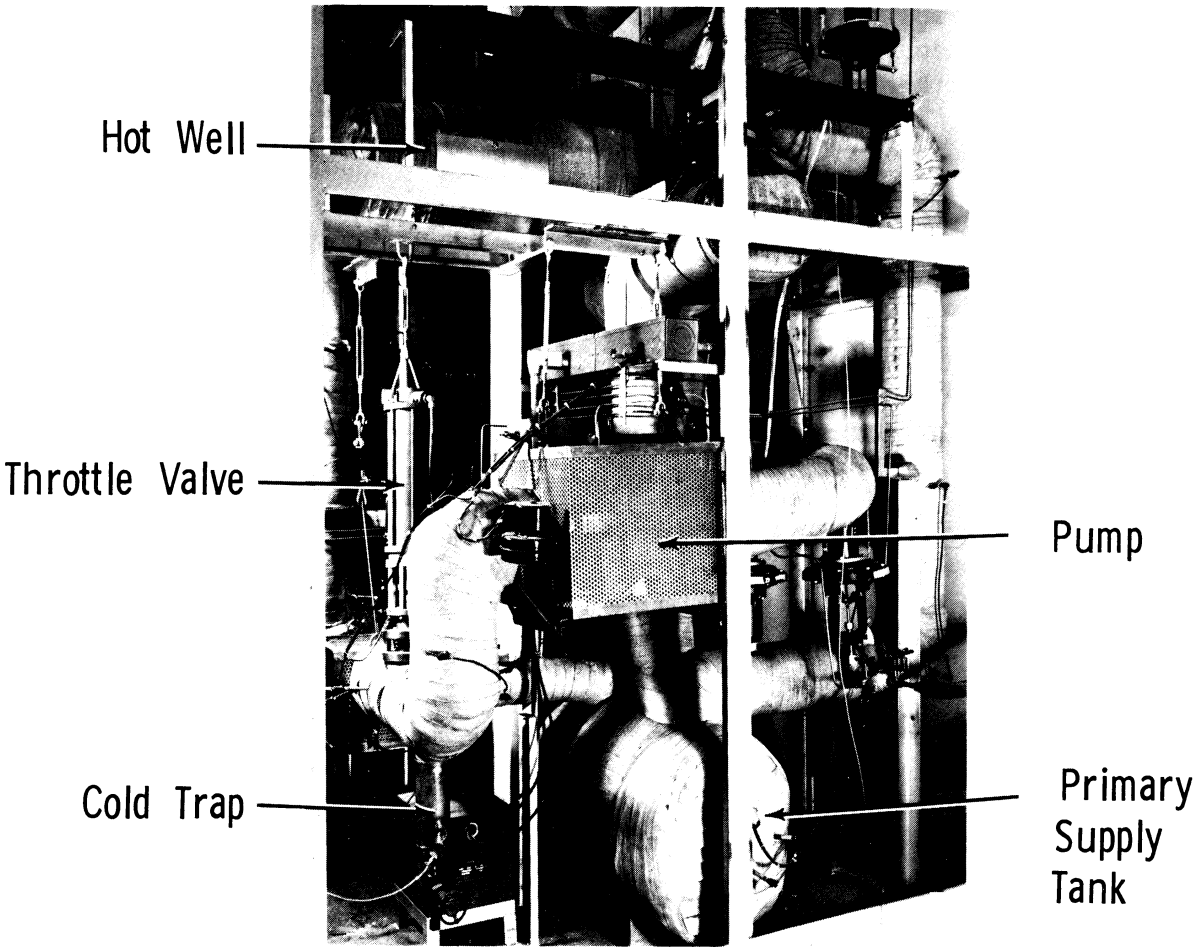

Figure 85 Potassium Boiling heat Transfer Test Loop, North Elevation

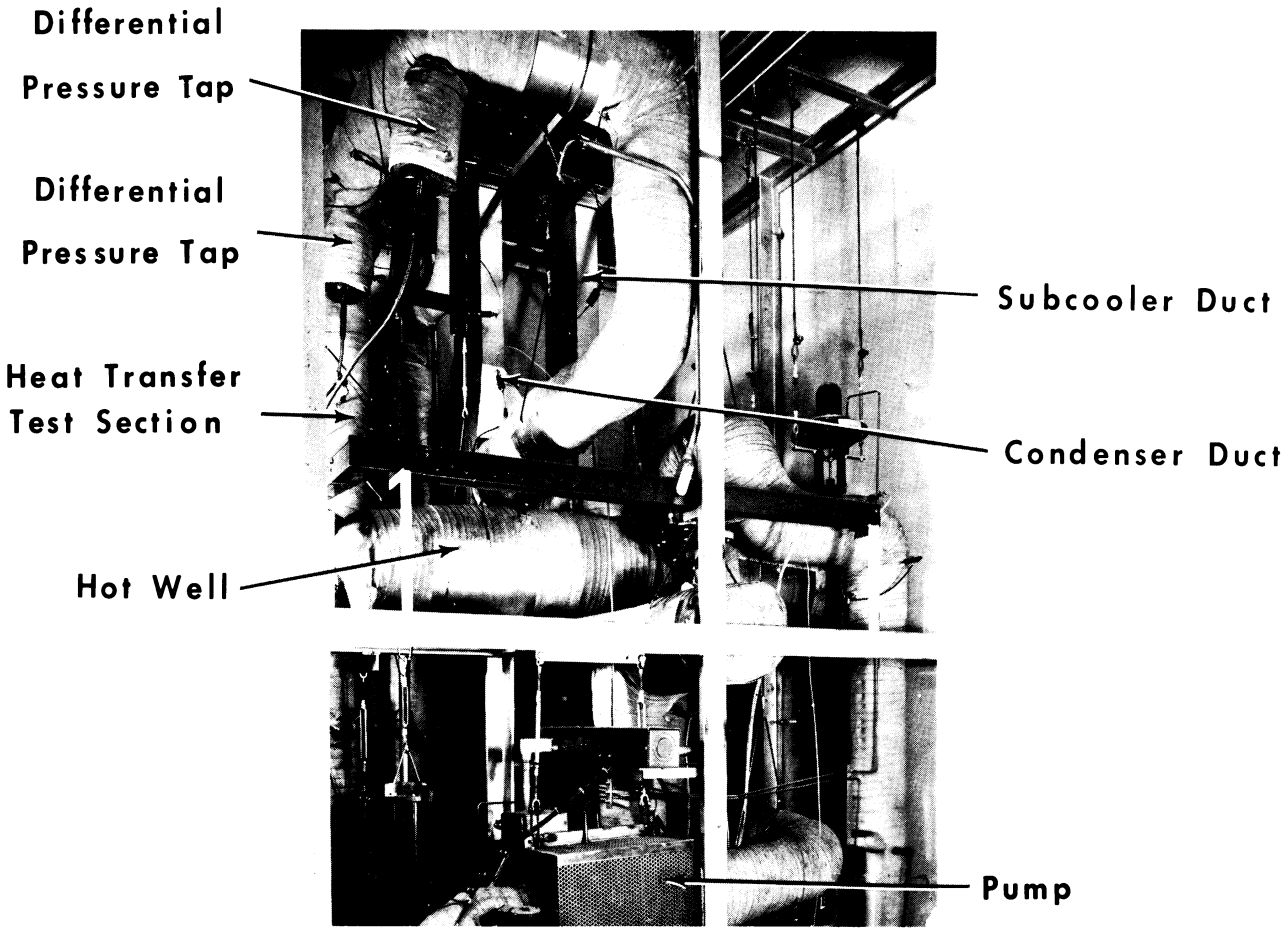

Figure 86 Potassium Boiling Heat Transfer Test Loop, North Elevation

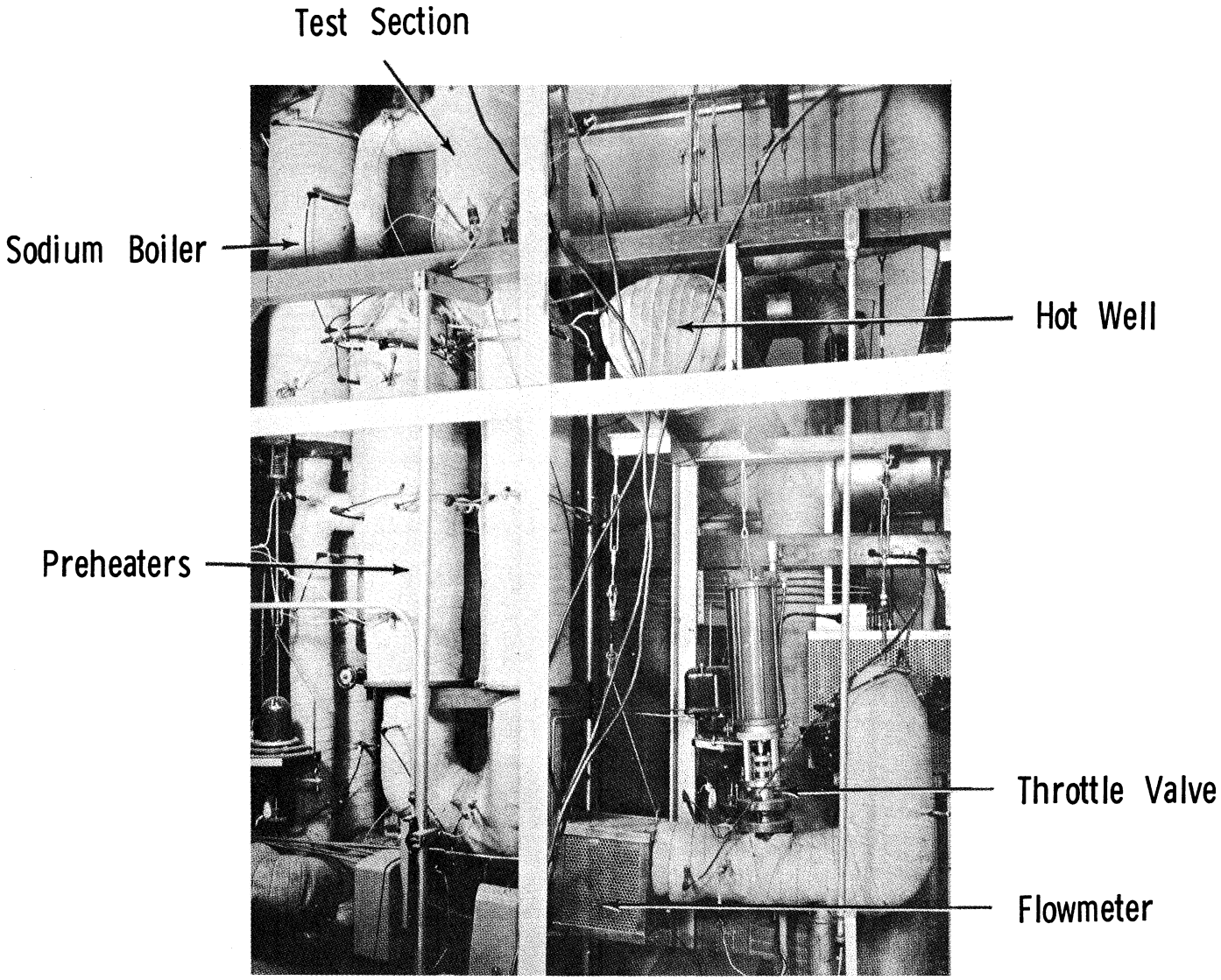

Figure 87 Loop, East Elevation.

each section is heated by four radiant clam shell heaters. These heaters were manufactured by Electro-Applications Incorporated and are rated at 2.8 KW at 230 V, with an allowable element temperature of 2000°F. The twelve heaters provide for a total of about 34 KW rated power. An orifice is located in the entrance line of each of the preheaters to help maintain uniform flow in the three sections. Each section is provided with a 40-inch long rod upon which are welded 1/8-inch Swagelok nuts at 1 1/2-inch intervals with the open end downward. These nuts served as vapor traps to enhance stable boiling in the preheater during potassium boiling studies. The entrance, exit, exterior wall and heating element temperatures were monitored.

Heat Transfer Test Section: The main features of this section are shown in Figure 88. The Heat Transfer Test Section was deisnged to deliver heat fluxes in excess of 500,000 BTU/(hr)(sq ft) to a two inch long section of 1/2-inch OD by .012-inch wall Haynes-25 tube. The flows from the preheater (which may be two-phase or single-phase) tangentially enter the bottom of a 4-inch OD by 3-inch ID by 36 1/2-inch long Haynes-25 pipe. The fluid next enters a funnel leading to a 23-inch length of the 1/2-inch OD tube. All but the top 2 inches of this tube are enclosed in a heat shield consisting of 1-inch pipe welded to the 1/2-inch tube at the top and connected to the 4-inch pipe at the bottom by means of a bellows assembly. The exposed two inches of the 1/2-inch tube functions as the heat transfer test section. The 21-inch length prior to entering the test section serves to provide a fully developed velocity profile. As shown in Figure 88, this 21-inch length is enclosed by 1-inch pipe, a loose fitting cylinder containing thermocouples, the test section wall, guard heaters and insulation, all of which serve to provide essentially adiabatic flow during the development of the velocity profile.

In operation, sodium vapor tangentially enters the top of the 4-inch pipe and condenses on the exposed 2-inches of tubing. The condensate exists through the overflow pipe and returns by gravity to the sodium boiler.

The test section is monitored for heat losses by means of chromel-alumel thermocouples while the readings pertinent to the determination of heat transfer parameters are made by platinum/platinum-10% rhodium thermocouples located at the test section inlet and outlet and in the sodium vapor space. In addition, a thermocouple located beyond the exit of the test section after the flow turns a corner is used as a check on the mixed mean temperature of the fluid exiting the test section.

Absolute pressure is read at the test section outlet by means of a Taylor Instrument Company diaphragm type sensing element, back filled with NaK leading to a pneumatic transmitter.

Pressure-Drop Measurement Section: This section consists of a horizontal 3-foot length of 5/8-inch OD by .495-inch ID Haynes-25 tube. Differential pressure across this length is read by two diaphragm sensing elements, back filled with NaK which are connected to each side of a diaphragm in a pressure

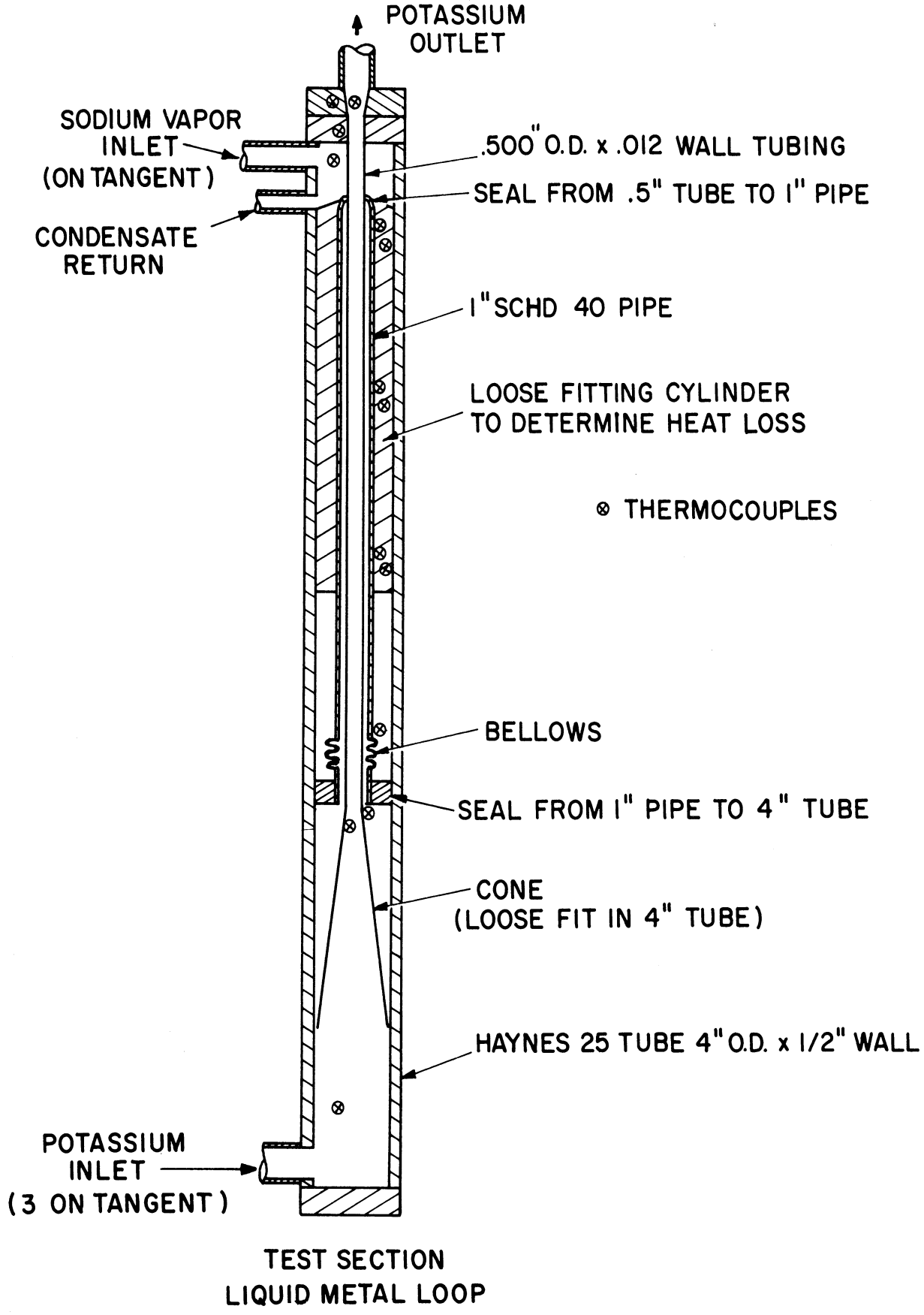

Figure 88 Heat Transfer Test Section

transmitter. The transmitter has three ranges; 100, 300, and 600 inches of water. Thermocouples are located upstream and downstream of this section.

Condenser: The condenser consists of 5-feet of 1-inch, Sch 160 stainless steel finned tube encased in a blower duct. Air is supplied by an 800 cfm blower and the condenser is rated at 60,000 BTU/(hr). The air flow is controlled by louvres at the blower discharge and the louvre position is controlled by an air signal.

Hotwell: The hotwell is a horizontal 54-inch long section of 6-inch Sch 160 stainless steel pipe. It is located between the condenser and subcooler and serves a number of purposes. Primarily, it assures an all-liquid flow through the subcooler and thus a liquid level above the pump in the event of large flow instabilities. It also acts as a accumulating chamber for non-condensibles and as an expansion tank for liquid, the total volume of which may vary with temperature changes and vapor fraction changes in the loop.

As indicated in Figure 84, the primary loop may be pressurized with argon in the hot well, by means of the primary vent and bleed valves, for non-boiling operation. The loop may also be evacuated in this way. Other auxiliary piping connects the hot well with the supply tank via two separate routes. The bleed line runs from the top of the hotwell to the bleed valve then down to the supply valve and the supply tank. The level line, which extends 1 inch up from the hotwell bottom, runs straight down to the level valve and continues to the supply tank.

Hot Trap System: Considerable difficulties were experienced in the operation of the potassium loop due to oxide plugging. The hot trap assembly shown in Figure 84 was installed to "getter" the oxygen from the potassium.

The hot trap consists of a 4-foot bed of zirconium chips connected across the inlet and outlet of the pump. A portion of the loop flow can be recycled through the hot trap at 1200°F (heating accomplished by heaters similar to those in the preheater) where the zirconium removes the oxygen from the potassium. The hot trap system includes a MSAR magnetic flowmeter and a micrometallic filter. The filter is used to remove entrained particles from the flow.

Sodium Boiler: The sodium boiler consists of a 4-inch OD by 3-inch ID by 54-inch long section of Haynes-25 pipe. The bottom 3 feet are heated by four clam-shell heaters of the same type as in the preheater with a rated power of 11 KW. The boiler is provided with four vapor trap assemblies similar to those in the preheater. The sodium loop auxiliary lines serve a similar function to those of the primary loop with the sodium bleed line exiting from the top of the vapor space in the test section. The location of this bleed line permitted non-condensibles to be removed from the area around the test section.

Valves: There are ten air-operated valves, the primary and secondary circuit each having a bleed, vent, level, supply and drain valve. These are 1/2-inch bellows sealed globe valves Model HY 473, manufactured by Hoke, Incorporated. They are designed for liquid metal service at 1500°F and 50 psig. The valves added after the system was built are Hoke HY 477B. These valves are manually

operated and located on the hot trap inlet and outlet and on a filter between the primary supply tank and the primary circuit. This latter filter is used to filter the potassium as it comes from the supply tank.

Piping: The preheater, heat transfer test section, sodium boiler, vapor and condensate lines, and pressure drop section are constructed of Haynes-25 alloy. From the pressure drop section to the subcooler, 1-inch, schedule 160, 316 stainless steel is used. From the subcooler to the preheater inlet, 1/2-inch schedule 80, 316 stainless steel is used. All lines are traced with electrical warm-up heaters which are controlled by switches at the loop panel. All lines and components are insulated with 1-inch of Johns-Manville Cerafelt insulation, and 1-inch of Johns-Manville Banroc insulation and covered with asbestos tape. Surface thermocouples to measure system temperatures during heat-up and operation are provided at many points in the system.

3. Control and Safety Features

The loop control panel, shown in Figure 89 was assembled by R. T. Brokaw and Company, Ann Arbor, Michigan, using instruments supplied by the University of Michigan. It is located in an adjoining room. In normal circumstances, the control panel has all facilities necessary for complete remote operation of the loop.

Superior Electric Company Powerstat variable transformers control the voltage to the preheaters, sodium boiler and the pump. Electrical power to the preheaters and sodium boiler are read on General Electric AC kilowatt meters. All the air operated valves (including the drain valves) are operated by solenoids actuated by switches on the control panel. A 48-point Brown Recorder monitors the chromel-alumel thermocouples used for loop operation.

The temperatures of the preheater heating elements and the sodium boiler heating elements are read on Wheelco Limitrols which automatically cut off the power to their respective unit in the event of a temperature excursion. The millivolt signal from the flowmeter is read on a Wheelco Limitrol. If the flow falls below a certain preset value, power to the preheaters, sodium boiler and the pump is cut off. A time delay switch is used to monitor power failures. In the event of a total power failure of less than 10 seconds duration, all power circuits return to their previous setting. If the power failure is of longer duration, the alarm buzzer will ring and power to the preheaters, boiler and pump will not be restored unless positive action is taken by the loop operator.

The positions of the throttle valve, subcooler louvre, condenser louvre, and both drain valves are controlled by manually actuated air pressure regulators. A Taylor Transcope Recorder monitors any one of the seven platinum/platinum-10% rhodium thermocouples used in heat transfer calculations, the absolute pressure above the heat transfer test section, and the differential pressure in the pressure drop section. The platinum/platinum-10% rhodium thermocouples are

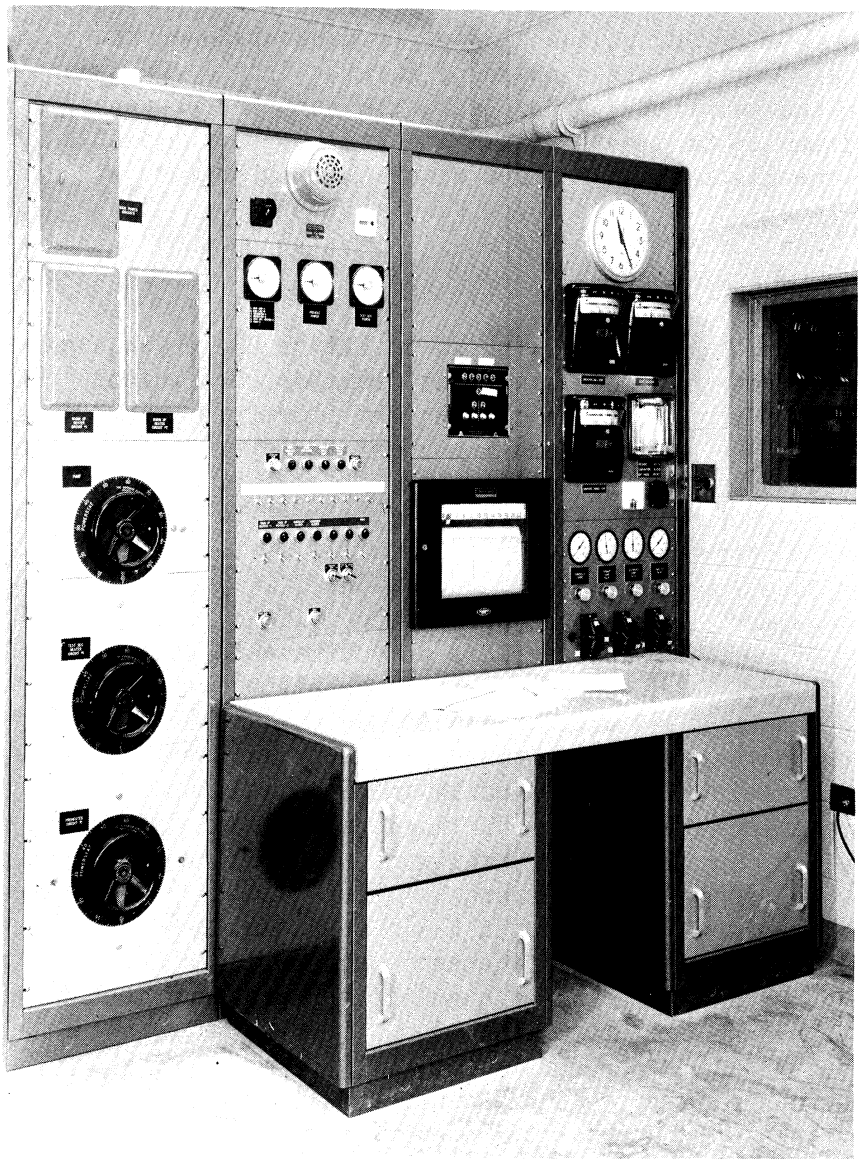

Figure 89 Liquid Metal Loop - Control Panel

usually read on a Leeds and Northrup K-2 potentiometer. If a serious emergency should occur (such as a leak accompanied by fire), use of a scram buttom will immediately drain the contents of both circuits to their respective supply tanks and cut off all electrical power to the loop.

Molten potassium and sodium at high temperature when in contact with concrete will spall, giving off showers of burning drops. To prevent this added difficulty in the event of a major leak, the loop was housed in a sheet steel enclosure and on top of a metal pan. The pan not only prevents spalling but also aids in the disposal of residue after such an emergency.

4. Temperature Measurement

There are six thermocouples, shown in Figure 84, which are important to the determination of the condensing heat transfer coefficient. TC 25 measures the temperature of the potassium exiting the flowmeter. This temperature is used in combination with a calibration chart to determine the potassium flow rate. TC 26 and TC 29 at the heat transfer test section inlet and outlet provide, in conjunction with the flow rate, a heat balance on the potassium flow and hence a determination of the heat flux at the test section. TC 27 in the sodium vapor space, in conunction with TC 26 and TC 29 is used to determine a log-mean temperature difference. TC 28 located in the end closure of the test section vapor space allows an estimate to be made of the condensing rate at this point. TC 30, located beyond an elbow above the test section serves as a check on TC 29 with regard to the exit bulk temperature of the potassium. These thermocouples were calibrated against a secondary standard which had been previously calibrated by the National Bureau of Standards. They are platinum/platinum-10% rhodium Thermoelectric Model CEI-18-P10 couples, mounted in wells. In the experimental runs, the millivolt signal from these thermocouples was read on a Leeds and Northrup type K-2 potentiometer which had been previously calibrated against a K-3 potentiometer so that a signal of 0.1 microvolt could be read with confidence. Calibration charts for the thermocouples were constructed by use of a multiple regression technique and the temperatures could be read to 0.1°F.

That thermocouples in high temperature environments tend to age is a well known circumstance. Throughout the operation of the loop this possibility was examined and the loop was operated at various times under substantially isothermal conditions with the thermocouples interchanged in their location. The emf signals from these thermocouples were found to agree within 1°F. These results indicated that the thermocouples were at least giving accurate temperatures within 1°F relative to each other. A discussion of the effect of such errors in temperature measurement may be found in Appendix M.

5. Flow Measurement

The calibration curves supplied with the flowmeter were checked by filling the known volume in the preheaters at various constant flow rates. The average

meter calibration factor from eight determinations fell within 1.7 percent of the curve value. This result indicated that the theoretical curve was quite satisfactory. At various periods, this calibration was checked by single determinations and found not to have changed.

EXPERIMENTAL PROCEDURE

Before the condensing runs were begun, a series of operations were followed to insure the absence of non-condensible gases in the sodium vapor space.

The sodium boiler, vapor and condensate lines were evacuated through the bleed and vent lines to a pressure of 10 microns and the evacuation was continued while the boiler and associated lines were heated to 700°F. The system was then cooled to 200°F while a vacuum of 10 microns was maintained. All valves were closed and the boiler allowed to sit for five days, at which time the pressure had risen to 20 microns. The non-welded connections in the sodium boiler system were then checked by a helium leak detector and found to be leak tight.

The boiler was charged with sodium by opening the drain valve and the excess of liquid above the level line was drained through the level line by equalizing the pressure between the boiler and the supply tank and opening the level valve. In this way, approximately 1.8 gallons of sodium were charged.

The sodium boiler was again evacuated to 10 microns and then heated to 600°F during further evacuation. By these operations, it was felt that non-condensibles were substantially removed from the system. A further test for the presence of non-condensibles is described later.

Since it requires about eight hours to bring the loop from a standby condition to operating temperatures, the condensing experiments were run continuously for six days.

The potassium in the primary supply tank was melted and heated to 200°F. The preheaters were heated to 1000°F and 8 gallons of potassium charged. The primary circuit was pressurized to 20 psia to prevent local boiling and circulation was begun by applying voltage across the pump. After 24 hours of operation, at 1000°F the power to the sodium boiler was gradually increased until there was evidence of heat transfer in the test section as indicated by a rise in temperature of the potassium.

While holding the sodium vapor temperature at 1300°F, the potassium inlet temperature at 1100°F, and the potassium flow rate at 1.5 GPM, the following procedure was carried out: The sodium vent line was opened to a vapor trap whose capacity was roughly equal to the vapor volume in the sodium circuit. The vapor trap was being continuously evacuated to a pressure of 15 microns. The valve between the vapor trap and the vacuum pump was closed, and the sodium bleed valve opened allowing sodium vapor (and presumably any non-condensibles present)

to sweep through the bleed line into the vapor trap. The vapor pressure of sodium at this temperature is 2 psia affording a substantial driving force. During this operation, the vapor temperature would drop about 10°F after which the bleed line was closed and the vapor trap re-evacuated. In about ten minutes, the vapor temperature would rise to its former value. The overall heat transfer coefficient was calculated before the bleed and after the bleed.

After the first two bleeding operations a rise in the overall coefficient was noted; from 1600 to 2300 to 2400 BTU/(hr)(sq ft) (°F). A third bleed brought no further change. During the next several days, the bleeding procedure was followed at different conditions and the coefficient before and after such operations remained the same. By such intermittent bleeding, it is believed that all non-condensibles were removed from the sodium system.

Further runs were carried out in such a manner as to cover a sodium vapor temperature range of 1240 - 1525°F at constant heat fluxes ranging from 250,000 to 575,000 BTU/(hr)(sq ft) and at constant temperatures while varying the flux. The vapor temperature was controlled primarily by the preheater power setting which controlled the potassium temperature. The flux was controlled by varying the sodium boiler power setting. A given set of conditions was held for as long as it took to determine that the loop had reached steady state. The criterion for this condition was the constancy of temperature and flux which were taken hourly. At least two readings at each setting were taken. The following list summarizes the readings essential for the determination of the condensing heat transfer coefficient.

a) Temperatures indicated by TC 25, 26, 27, 28, 29.

b) Flowmeter signal in millivolts.

In addition to the above, the temperatures in the cylinder surrounding the 1/2-inch diameter tube prior to the heat-transfer test section were monitored to determine that the length of tube between TC 26 and the heat transfer section was in fact adiabatic. Some 50 thermocouples located around the loop were also monitored hourly.

EXPERIMENTAL DATA

The experimental data taken by Barry (15) in March of 1965 and the results calculated from these data are tabulated in Table A, Appendix J. Subsequent experimental data taken by Balzhiser, Gahman and Sartor in January of 1966 along with the calculated results from these data are tabulated in Table B of Appendix J. The sodium vapor temperature was varied from 1240°F to 1525°F and the heat flux was varied from 215,000 to 583,000 BTU/(hr)(sq ft). Heat fluxes substantially below 215,000 BTU/(hr)(sq ft) and vapor temperatures below 1240°F were obtained but are not reported since unstable boiling commenced in the sodium boiler at lower values of these parameters. At the high end, the flux was limited to 583,000 BTU/(hr)(sq ft) and the vapor temperature to 1525°F to avoid operating

at conditions that might damage the bellows.

The physical properties for potassium and sodium were taken from Weatherford (179) except for the thermal conductivities of the liquid which were taken from Roehlich (151). The values from both these references were verified by recent work at Battelle Memorial Institute (103). The thermal conductivity of the .012-inch test section wall was taken from the manufacturer's literature.

The potassium inlet temperature ranged from 1060°F to 1316°F and the temperature rise of the potassium varied from 52°F to 139°F. The temperature difference between the sodium vapor and the potassium outlet ranged from 65°F to 171°F.

The potassium inlet and outlet temperatures and the potassium flow rate were used to calculate the heat flux. The log-mean temperature difference between the sodium vapor and the potassium was calculated and used in conjunction with the flux to determine the overall heat transfer coefficient. The potassium physical properties were evaluated at the average of the inlet and outlet temperature.

The overall heat transfer coefficient was used in conjunction with the known tube wall resistance and the predicted potassium coolant film coefficient to determine the sodium condensing heat transfer coefficient. It would have been useful to have a measurement of the wall temperature and thus obtain a direct determination of the condensing heat transfer coefficient. However, the tube wall was too thin to permit the placement of a thermocouple and the measurement of the electrical resistance of the tube wall was impractical because of the difficulty of insulating the electrical leads from the condensing chamber walls. The thin wall was necessitated by the requirements of operating over a wide range of heat fluxes at a particular vapor temperature and yet maintaining a reasonably low temperature difference between the condensate film and the potassium to avoid severe thermal stresses. There are some definite advantages in the use of the thin wall in that it eliminates errors due to inaccurate thermocouple placement and reduces end effects to a negligible value.

In evaluating the sodium condensing heat transfer coefficient, the following equation was used.

$$\frac{1}{U} = \frac{1}{h_c} + \frac{t}{k} + \frac{1}{\alpha h_k} \qquad (50)$$

The overall coefficient, U, was determined by the experiment. The wall thickness, t, thermal conductivity, k, and ratio of cooling to condensing area, α, were known. It was necessary, then, to determine the potassium film coefficient, h_k, in order to calculate the sodium condensing transfer coefficient, h_c.

Since the 1/2-inch diameter test section is only 2-inches long, it is evident that the test section constitutes a thermal entrance region for the potassium and the potassium film coefficient, h_k, can be expected to be higher (because of the thin developing thermal boundary layer) than it would be for long tubes (where the thermal boundary layer is fully developed). There is a good deal of experimental data for heat transfer to liquid metals in long tubes, but very little for heat transfer in tubes where the ratio of length to diameter is small. If a reasonable criterion could be found to evaluate h_k, then h_c, the condensing coefficient could be evaluated. The establishment of such a criterion is the subject of Appendix K.

The sodium condensing heat transfer coefficient ranged from 7280 to 14,700 BTU/(hr)(sq ft)(°F) and the calculated temperature differences between the vapor and the test section wall varied from 22°F to 68°F. A sample calculation is presented in Appendix L and an error analysis is presented in Appendix M.

In Figure 90, the dimensionless sodium condensing heat transfer coefficient is plotted against the condensate film Reynolds number. On this plot, no trend for the variation of the heat transfer coefficient with film Reynolds number is apparent and it would be reasonable to state that over the range of conditions studied, the condensing heat transfer coefficient for sodium is about 10,800 BTU/(hr)(sq ft)(°F).

Figure 91, a plot of the heat transfer coefficient versus the difference in temperature between the vapor and the wall, includes the data of Misra and Bonilla (130) and Aladyev et al (4). Misra and Bonilla's data were taken for sodium condensing on a 6-inch long tube inclined at an agle of 45 degrees. Aladyev et al (4) condensed potassium in a vertical stainless steel tube 4 mm in diameter and 30 mm in length. The data of this investigation agrees with the data of the above two investigations and show that the condensing heat transfer coefficient for both potassium and sodium vapor is much lower than would be predicted by the film theory. The film theory predicts differences across the film on the order of 2°F to 5°F. It does not appear that any correlation of the data is likely to be obtained using the classical film theory.

The next attempt to correlate the data was to compare it with the predictions of the kinetic theory of condensation by utilizing Equation 49 and assuming σ_c equal to σ_e. As shown in Figure 92 and 93, it is impossible to pick a single value of σ_c which corresponds to the data. However, as shown in Figure 94, if the data of this study is plotted as suggested by Aladyev et al (4) and Labuntsov and Smirnov (102) a linear variation appears to exist between log σ_c and log pressure. Thus, it appears that the kinetic theory of condensation will adequately describe the condensation of alkali metal vapors if a pressure dependent accommodation coefficient is utilized.

In Figure 95, the data of Figure 92 and 93 are collected and it appears that in the particular temperature range at which this investigation was carried

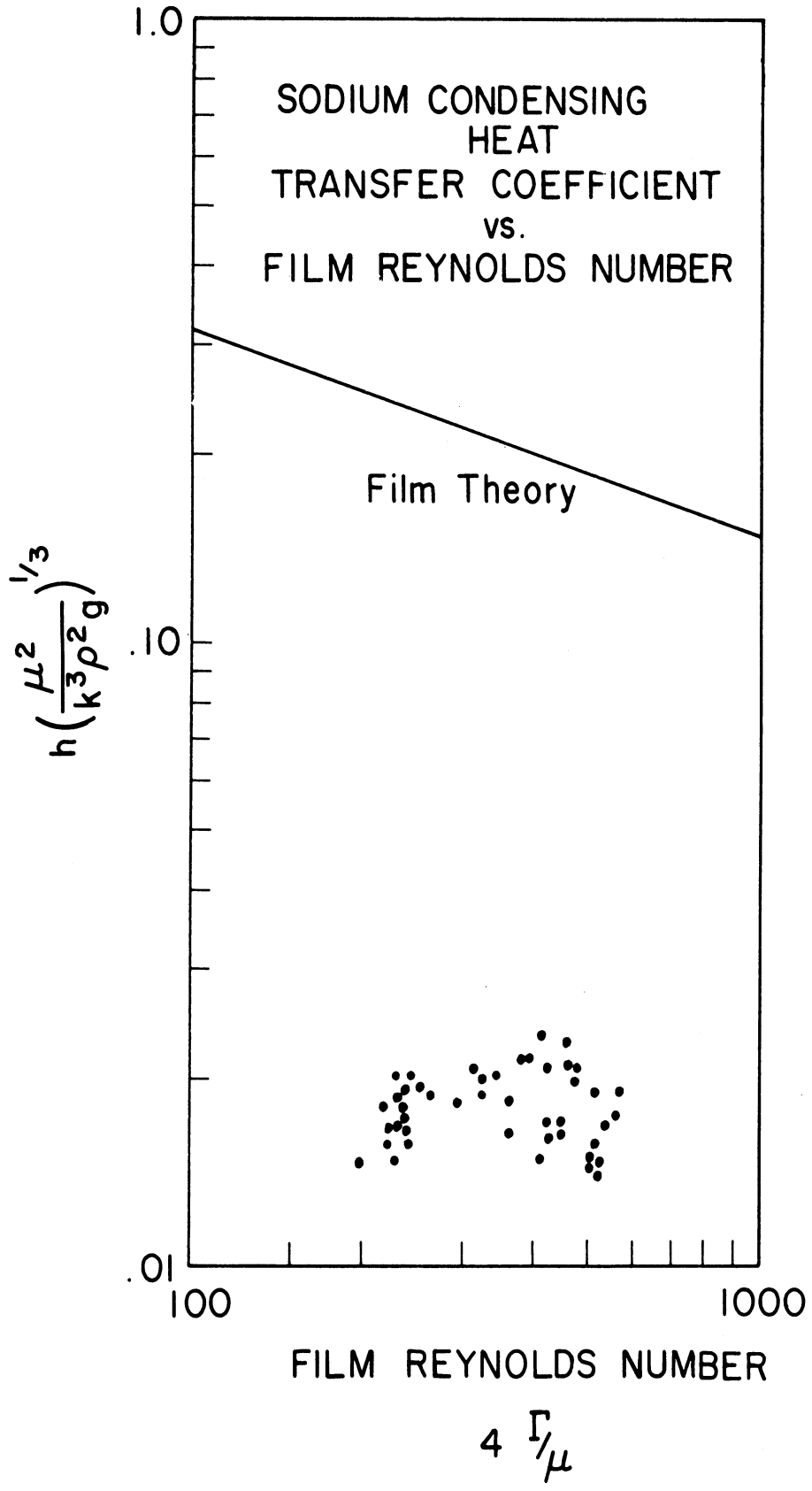

Figure 90 Sodium Condensing Heat Transfer Coefficient vs. Film Reynolds Number

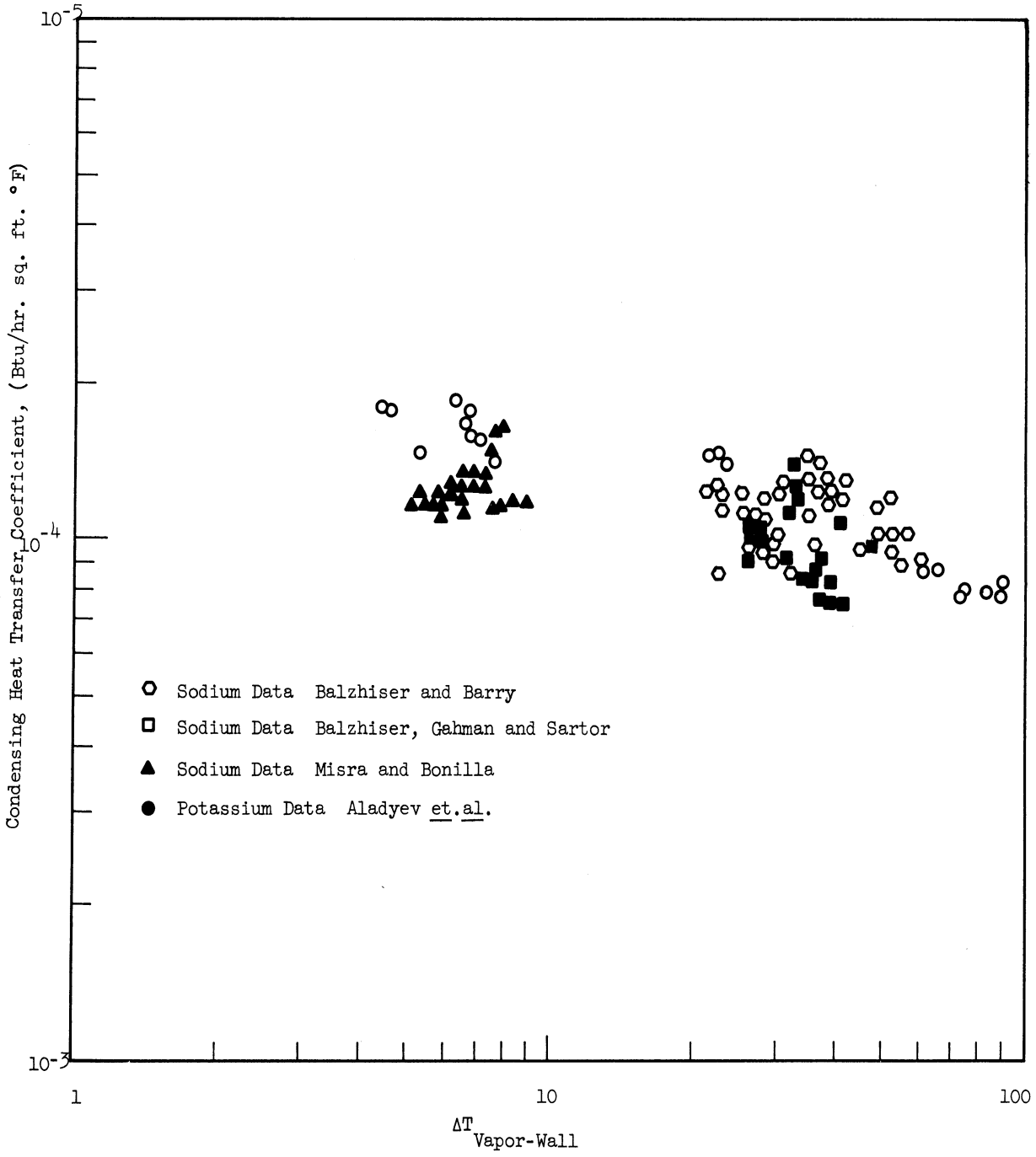

Figure 91 Condensing Heat Transfer Coefficient Versus $\Delta T_{Vapor-Wall}$

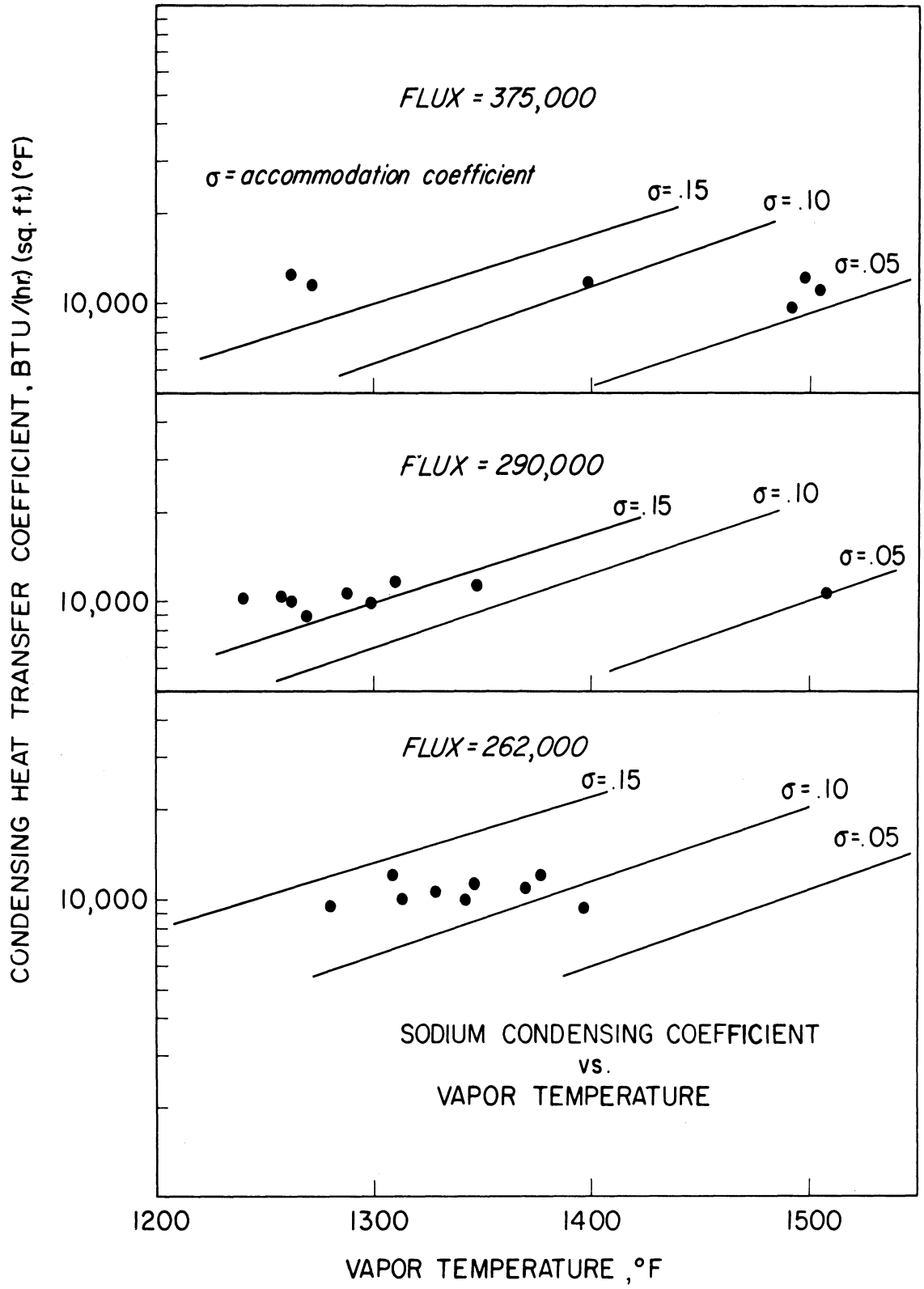

Figure 92 Sodium Condensing Heat Transfer Coefficient vs. Vapor Temperature

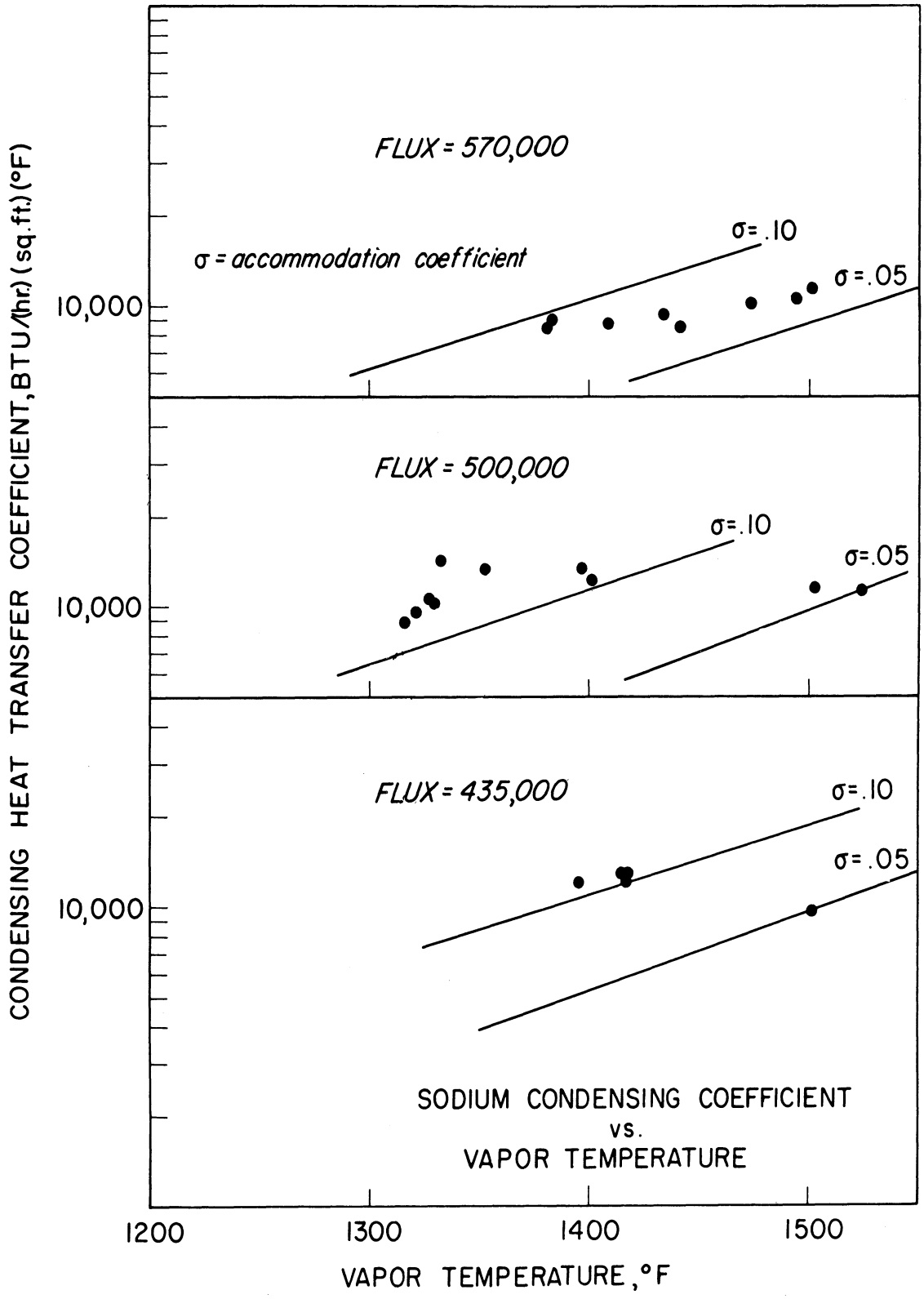

Figure 93 Sodium Condensing Heat Transfer Coefficient vs. Vapor Temperature

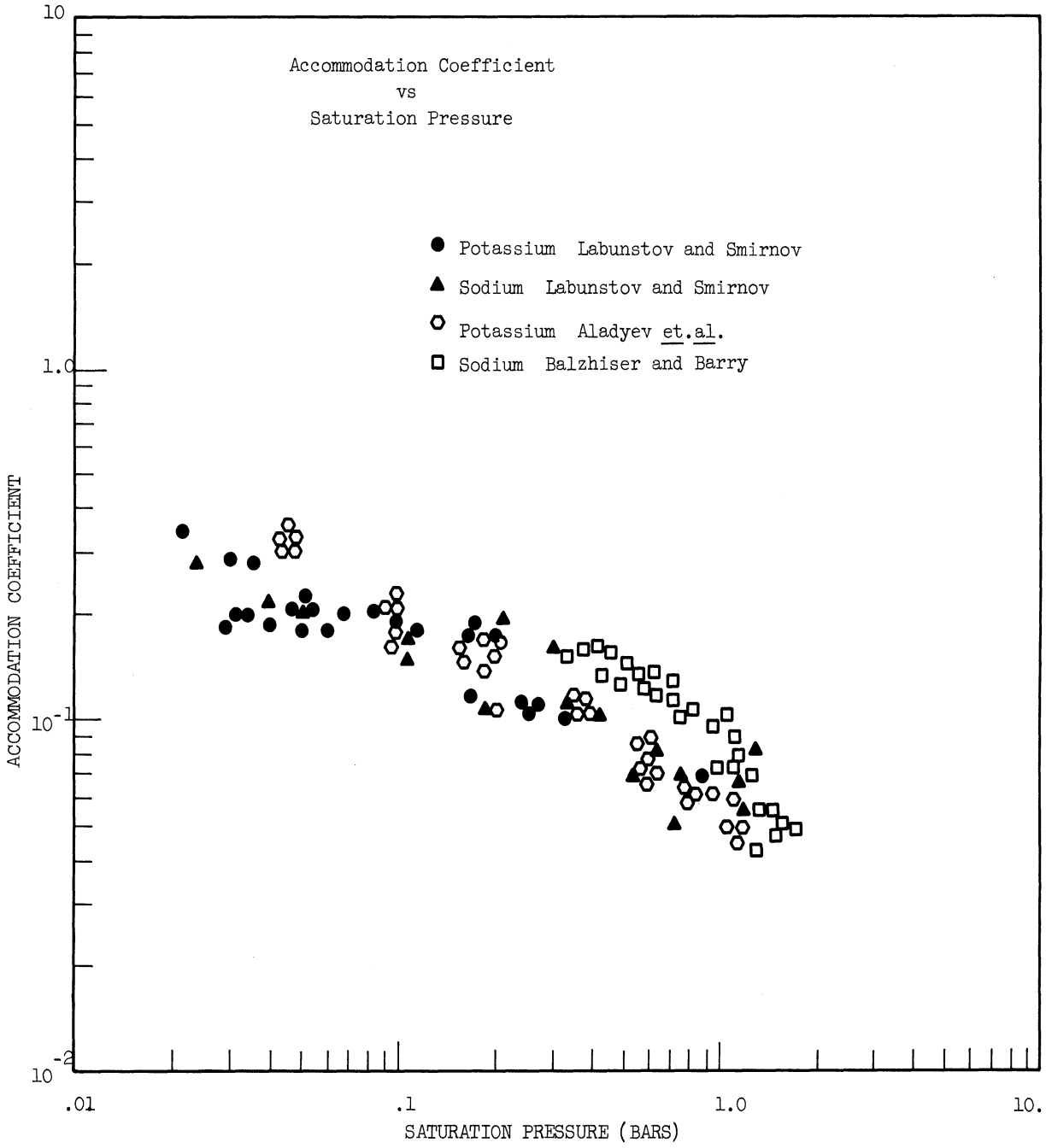

Figure 94 Accumulated Data Indicating Variation of Accommodation Coefficient with Saturation Pressure

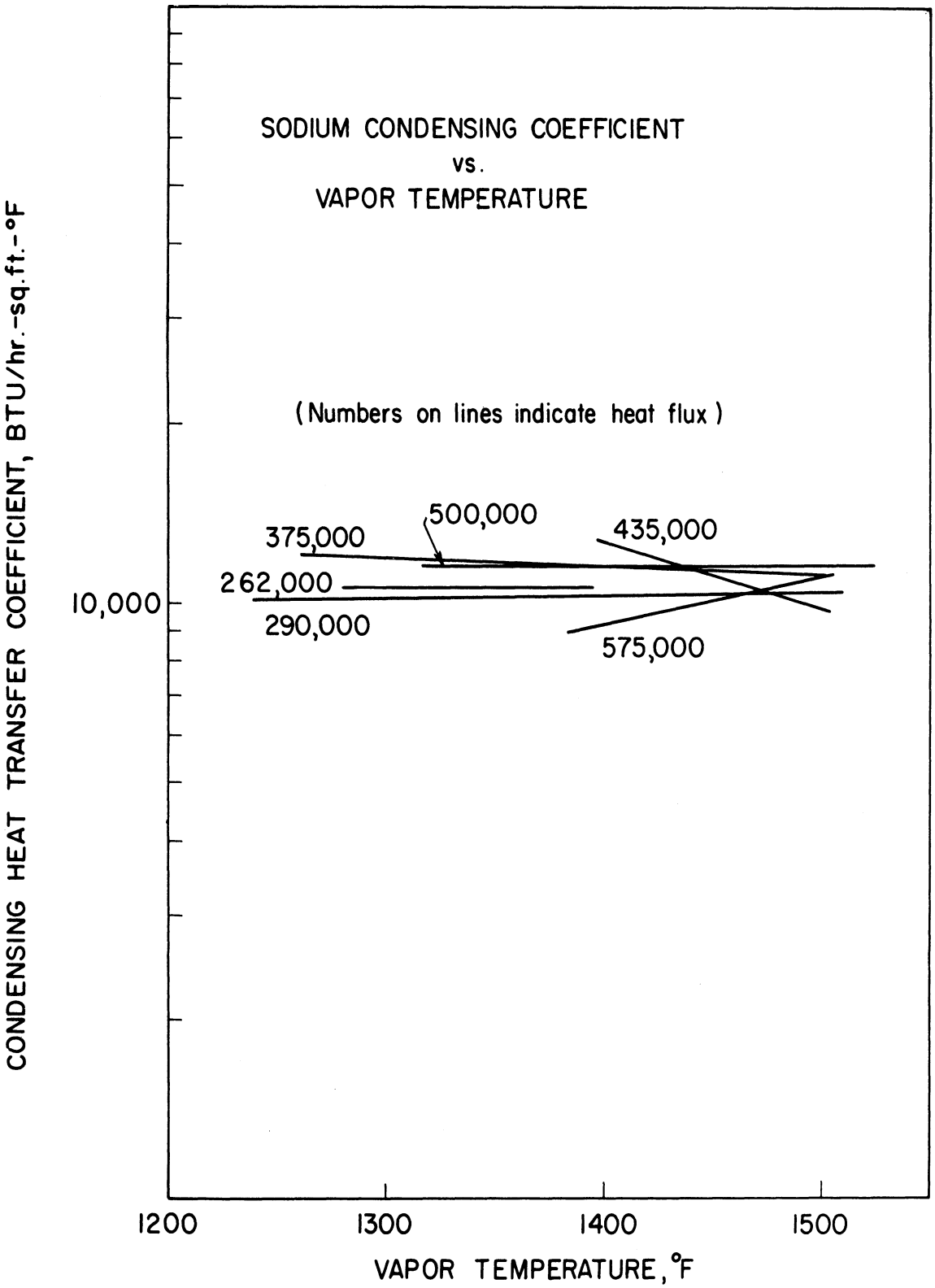

Figure 95 Sodium Condensing Heat Transfer Coefficient vs. Vapor Temperature

out, no trend exists for the heat transfer coefficient with regard to either the vapor temperature or the heat flux. However, Figure 96, which includes the Aladyev et al data (4) suggests a decreasing coefficient with increasing heat flux.

DISCUSSION OF RESULTS

As shown in Figure 97, there are seven resistances to heat transfer which were considered in the interpretation of the results of this experiment. They are:

(a) The resistance of the vapor phase

(b) The resistance of the vapor-liquid interface

(c) The resistance of the condensate film

(d) The resistance at the condensate film - tube wall interface

(e) The resistance of the tube wall

(f) The resistance at the tube wall - potassium coolant inferface

(g) The resistance within the potassium coolant

The first four resistances, the vapor phase, the vapor-liquid interface, the condensate film, and the condensate film-tube wall interface are considered as contributing to the sodium condensing heat transfer coefficient. In this discussion, these resistances will also be stated in terms of the observed or calculated temperature drops for ease in visualizing the relative magnitudes of these resistances to heat transfer.

As previously explained, the experimental data consisted of the measured heat flux which ranged from 215,000 to 583,000 BTU/(hr)(sq ft) and the overall temperature difference between the sodium vapor and the potassium coolant which ranged from 86°F at the lower flux to 224°F at the higher flux. From this data and the calculated resistances of the tube wall and of the potassium coolant, the sodium condensing heat transfer coefficient was determined. These calculations will now be examined in some detail.

It was assumed that the resistance to heat transfer at the condensate film-tube wall interface is negligible as is the temperature drop at the tube wall-potassium coolant interface. Significant surface contamination would be required to have a substantial temperature drop at these liquid-solid interfaces. As already noted, the alkali metals are excellent cleaners of metal walls and the high temperatures involved in this experiment (a minimum of 1040°F on the potassium side) would facilitate the removal of any surface contamination.

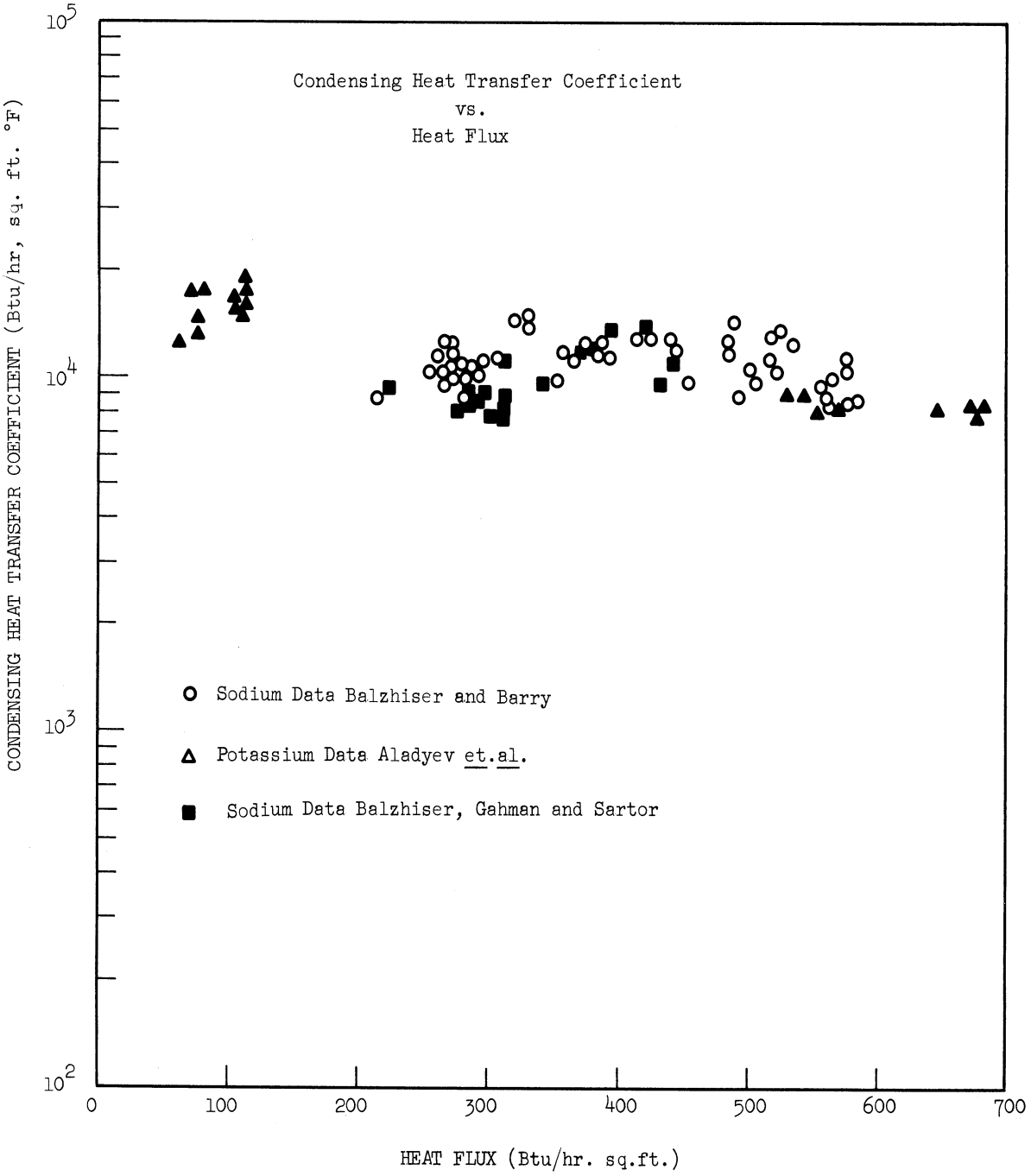

Figure 96 Condensing Heat Transfer Coefficient Versus Heat Flux

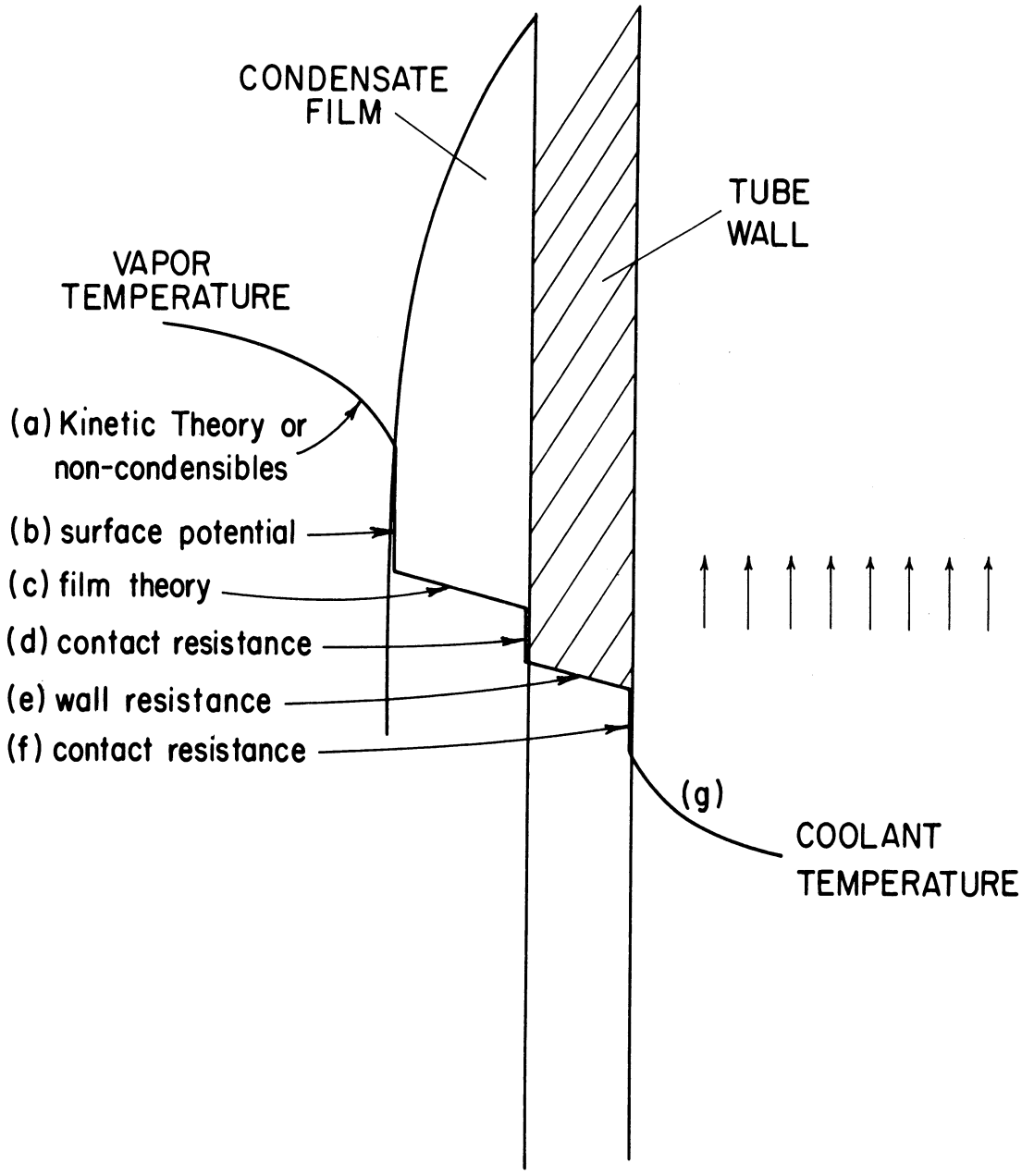

Figure 97 Resistances to Condensing Heat Transfer

No trends were noted in the calculated value of the overall heat transfer coefficient which could be ascribed to a cleaning of the tube wall surface during the experiment. Furthermore, the experimental results for heat transfer to alkali metals flowing in tubes correspond closely to the theoretical predictions based upon the assumption of no interfacial resistance (27, 95, 161, 168).

Based upon the manufacturer's reported values of the thermal conductivity of the .012-inch thick Haynes 25 tube wall, the temperature drop through the tube wall was calculated as ranging from 16°F at the lower fluxes to 44°F at the higher fluxes.

The temperature drop within the bulk of the coolant was calculated from the estimated potassium film heat transfer coefficient. The most reliable data for heat transfer in long tubes for alkali metals (27, 95, 161, 168) can be represented by:

$$Nu = 6.5 + 0.025\ Pe^{0.8} \qquad (51)$$

However, since the 2-inch long test section constitutes a thermal entrance region for the coolant, an analysis was performed to determine the correction factor to be applied to Equation 51 in order to account for this. It would be expected that because of the thin developing thermal boundary layer in the 2-inch test section, the potassium film heat transfer coefficient would be somewhat higher than that represented by Equation 51. As shown in Appendix K, the ratio of the eddy diffsuivity for heat to the eddy diffusivity for momentum plays an important role in theoretical analyses of heat transfer. However, it was found that within a Peclet number range of 130 to 190 (corresponding to the conditions of this experiment), this ratio could be varied from .005 to 1.0 with little change in the computed correction factor. The correction factor applied to Equation 51 to account for the existance of a thermal entrance region varied from 1.19 at a Peclet number of 130 to 1.25 at a Peclet number of 190. (The effect of axial conduction was also considered and found to be negligible (159).) The resultant potassium heat transfer coefficient ranged from 4600 to 5500 BTU/(hr)(sq ft)(°F). The temperature drop within the bulk of the coolant thus ranged from 48°F at a flux of 215,000 BTU/(hr)(sq ft) to 113°F at a flux of 583,000 BTU/(hr)(sq ft).

The sodium condensing heat transfer coefficient thus calculated had an average value of 10,800 BTU/(hr)(sq ft)(°F). At the 95 percent confidence level, this value exhibits a scatter of 2200 BTU/(hr)(sq ft)(°F). A scatter of this magnitude is predicted by the error analysis in Appendix M. Within this scatter, the condensing heat transfer coefficient was constant over a vapor temperature range of 1240°F to 1525°F and a heat flux range of 215,000 to 583,000 BTU/(hr)(sq ft). The resultant temperature drop between the sodium vapor and the tube wall thus ranged from 22$\pm$ 4°F at the lower fluxes to 67$\pm$13°F

at the higher fluxes. These latter values are the temperature drops that are attributed to the combination of resistances in the vapor phase, at the vapor-liquid interface and through the condensate film.

Because it is primarily the value predicted for the potassium film coefficient which sets the absolute value of the sodium condensing heat transfer coefficient, an analysis of error was conducted (shown in Appendix M) to determine the effects of different assumptions concerning the value of the potassium film coefficient. The error of bias thus involved in the sodium condensing heat transfer coefficient is believed to have a range of $\pm$ 10 percent. Thus, one can set limits on the absolute value of the sodium condensing heat transfer coefficient. The bias and scatter taken together indicate that the sodium condensing heat transfer coefficient has a value between 7500 and 14,000 BTU/(hr)(sq ft)(°F).

The bias introduced by the estimate of the potassium film coefficient adds another 3°F of uncertainty in the temperature drop between the sodium vapor and the tube wall at the lower flux levels and another 7°F at the higher flux levels. With this in mind, the data can be examined further to determine if it is possible to separate the resistances attributed to the vapor phase, the condensate film, and surface effect at the vapor-liquid interface.

The temperature drop through the condensate film (in the absence of surface effects) can probably be accounted for by Nusselt's film theory. There are no obvious mechanisms which would produce a thicker film than that predicted by this theory, and observations on mercury condensation (169) indicate no large discrepancies between the film thickness and the theory. Based upon Nusselt's theory, then, the calculated heat transfer coefficients range from 149,000 BTU/(hr)(sq ft)(°F) at the lower flux level to 108,000 BTU/(hr)(sq ft)(°F) at the higher flux level. The resultant temperature drop across the condensate film is thus 2°F at a flux of 215,000 BTU/(hr)(sq ft) and 6°F at a flux of 583,000 BTU/(hr)(sq ft). There remains then, a temperature drop of 20°F at the lower fluxes ranging up to 61°F at the higher fluxes which must be attributed to either a resistance in the vapor phase or a surface resistance at the vapor liquid interface.

A resistance to heat and mass transfer in the vapor phase could be attributed to the presence of non-condensible gases. A good deal of care was taken in removing non-condensible gases from the system prior to start-up. In addition, the sodium condensing chamber was periodically bled to an evacuated vessel during the condensing runs. The overall heat transfer coefficient between the sodium vapor and the potassium coolant, calculated before and after such bleeding of the condensing chamber, did not vary. The vapor pressure of sodium at the temperatures involved in this experiment ranged from 1.3 to 8.7 psia thus insuring a good driving force during the bleeding process. The location of the bleed line at the top of the condensing chamber would serve to sweep any non-condensibel gases from this location.

The experimental data of Noyes (139) for condensing sodium in the presence of inert gases confirmed his predictions based upon simple diffusion theory.

His equations predict a direction dependence of the heat flux on the partial pressure of the sodium. No trend of heat flux with vapor temperature was evident in Barry's study (14). Temperatures ranged from 1240°F to 1508°F and the flux level was 280,000 BTU/(hr)(sq ft). If it is assumed that the sodium vapor pressure corresponds to the saturation pressure at these temperatures, then a vapor pressure varying from 1.3 to 7.9 psia apparently had no affect on the heat flux. This fact suggests that non-condensible gases were absent in this experiment.

In view of the low vapor velocities involved in the present investigation (9 ft/sec maximum) and the constancy of the mass condensing flux over a wide range of vapor density, it is concluded that the resistance to condensing heat transfer observed for liquid metals does not lie within the vapor phase.

These arguments thus lead to a focusing of attention on the surface of the condensate film in order to explain the temperature differences involved in this experiment. A review of these temperature differences may be in order. The overall temperature difference between the sodium vapor and the potassium coolant ranged from 86°F at a flux of 215,000 BTU/(hr)(sq ft) to 224°F at a flux of 583,000 BTU/(hr)(sq ft). The temperature drop in the tube wall ranged from 16°F at the lower flux to 44°F at the higher flux. The temperature drop within the bulk of the coolant ranged from 48°F at the lower flux to 113°F at the higher flux. The temperature drop in the condensate film ranged from 2°F at the lower flux to 6°F at the higher flux. Arguments were presented indicating that the temperature drops at the solid-liquid interfaces were negligible, and it was further argued that the temperature drop within the vapor phase was also negligible. From these arguments one can conclude that the remaining temperature difference ranging from 20°F at the lower flux to 61°F at the higher flux is due to a resistance at the vapor-liquid interface.

The significance of such a resistance for metallic fluids was suggested by Sukhatme and Rohsenow (169) based on their mercury data taken at low pressures. For water, whose thermal conductivity is at least an order of magnitude lower than that of the liquid metals, the condensate film itself accounted for practically all the resistance to heat transfer in condensation. Thus, Nusselt's theory, which is based upon this assumption, correlates the data for water and organic fluids quite well. For liquid metals, however, where the resistance of the condensate film is substantially less, it appears that the other resistances, such as the vapor or the vapor-liquid interface, may control the rate of heat transfer in condensation.

The kinetic theory of condensation provides for such controlling conditions. For "clean" systems where non-condensibles are absent and hence the vapor resistance is small, the interface apparently controls the process. The accommodation coefficient is used in the kinetic theory treatment to account for the interfacial behavior. Prior to the work of Labuntsov and Smirnov (102), attempts had been made to correlate liquid metal data assuming that the so-called accommodation coefficient had a constant value. As indicated above, Sukhatme and Rohsenow (169) suggest that a value of 0.45 for the accommodation coefficient

would adequately describe their mercury data. However, Wilhelm (183) concluded that the actual value of their accommodation coefficient varied from 0.38 to 0.61. Similarly, Wilhelm showed that the accommodation coefficient determined from the data of Misra and Bonilla varied from 0.02 to 0.61. Although these findings have been cited by some investigators as evidence of the inadequacies in using kinetic theory to describe condensation, such a conclusion seems premature. Since the accommodation coefficient accounts for interfacial phenomena which might vary with changes in system parameters such as vapor density, temperature, etc., one could hardly expect to use a constant value for this coefficient.

Labuntsov and Smirnov (102) observed that the results of their investigation indicated that the accommodation coefficient for potassium and sodium varied from approximately 0.05 to 0.35. They plotted the logarithm of the accommodation coefficient versus the logarithm of the saturation pressure and obtained a linear relation between the two. Subsequent to this, Aladyev et al (4) condensed potassium inside a vertical tube and found that the value determined for their accommodation coefficient varied from approximately 0.045 to 0.38. Again, they found a linear variation in the logarithm of the accommodation coefficient with the logarithm of the saturation pressure which agreed with Labuntsov and Smirnov. The data from this investigation also indicated a variation in the accommodation coefficient ranging from approximately 0.042 to 0.170. The pressure dependence of σ_c also agreed with the earlier relationships proposed by Russian workers and cited above.

Based on the above, it would appear that the kinetic theory of condensation used in conjunction with the above-mentioned pressure dependency of the accommodation coefficient best describes the available alkali metal data. Thus, one might use the above as a basis for heat transfer calculations for liquid metal condensing systems in lieu of Nusselt's film theory where non-condensibles are absent. The presence of non-condensibles produces an additional resistance in the vapor phase which cuases further depression of the condensing coefficient.

CONCLUSIONS

1. For the range of variables considered in this investigation, it may be stated that the condensing heat transfer coefficient for sodium vapor has a value of 10,800 $\pm$ 3300 BTU/(hr)(sq ft)(°F). This value represents data taken over a temperature range of 1240°F to 1525°F and heat fluxes ranging from 215,000 to 583,000 BTU/(hr)(sq ft). Variations with either flux or vapor temperature were not discernible over these ranges.

2. The vapor-liquid interfacial resistance and the diffusion resistance in the vapor phase control the rate of condensation of metallic vapors. It appears that in the absence of non-condensibles the interfacial resistance itself dominates.

3. The data of this study is consistent with kinetic theory predictions if a pressure dependent accommodation coefficient is used. The pressure dependency observed in these studies is in good agreement with that observed by Russian investigators working with alkali metals and Rohsenow and Sukhatme with mercury.

4. Nusselt's theory overestimates condensing coefficients for liquid metals. Kinetic theory predictions utilizing a pressure dependent accommodation coefficient appears to produce more reliable results if non-condensibles are absent.

TWO PHASE FLOW INVESTIGATIONS

Michael R. Samuels
Robert L. Gahman
Lowell R. Smith

I. TWO PHASE PRESSURE DROP

INTRODUCTION

In recent years the area of two phase flow has been receiving much experimental and analytical investigation intended to develop a better understanding of the mechanisms and behavior of two phase flows. Much of this effort has been directed towards studying the fluids used, or proposed for use, in heat and power cycles. In particular, water and metallic fluids have come under extensive study. Activity in the area of liquid metals has been spurred on by continued interest in liquid metals as reactor coolants for nuclear power stations and space energy conversion cycles. The need for accurate design data for liquid metal systems is particularly critical for space applications where large design safety factors are undesirable because of the added weight they cause.

This report deals with the studies of two phase flows of potassium which have been performed in the Liquid Metals Laboratory at The University of Michigan. Specifically, pressure drop and void fraction have been investigated. To date two sets of pressure drop and void fraction data have been obtained. Void fractions were measured by use of a gamma-ray attenuation method. Comparison of the void fractions from the two sets of data suggests that vastly different flow regimes may have occurred in the two studies.

The studies presented herein have been performed in a liquid metal heat transfer test loop. The flows studied were horizontal and essentially adiabatic. Since the pressure decreases along the test section some of the liquid will evaporate. Thus as the flow proceeds through the test section a measureable drop in pressure and temperature with a corresponding increase in quality is experienced.

The experimental data which have been gathered will be presented and compared with the results of several other investigations in this area. Deviations from conventional correlations used for predicting pressure drop will be cited and a technique, consistent with the data obtained in this study, for estimating pressure drop will be discussed.

LITERATURE REVIEW

No attempt will be made at this point to present an exhaustive review of

the two phase flow literature. This literature is voluminous and has been reviewed by several previous investigators (17, 74, 84, 120, 177). Rather an attempt will be made to continue and extend the review presented by Smith (8) in the 1963 preliminary report on this project.

Until recently almost all two phase flow investigations were concerned either with two component systems such as air-water, or mercury-nitrogen, or with the one component steam-water system. However, recently information has become available on the two phase flow of single component liquid metals such as sodium and potassium.

Smith (164) has presented void fraction and pressure drops for the flow of an 8% Na 92% K mixture at The University of Michigan liquid metals test loop. Although the study intended to use pure potassium, a bellows leak introduced sodium and the mixture studied was of the composition cited. Very high liquid fractions were obtained for the range of qualities studied. However, comparison of Smith's liquid fractions with those independently obtained by Noyes (137) for liquid sodium and by Tang et al for liquid mercury (163) and mercury-potassium amalgams (170) indicated good agreement despite the scatter in Smith's results. As shown by Smith (164) these liquid fractions were considerably higher than those predicted by the Lockhart - Martinelli correlation. In addition to high liquid fractions, Smith also measured extremely high slip ratios. (The slip ratio is calculated from:

$$S = \frac{V_v}{V_l} = \frac{x}{1-x} \frac{1-\alpha}{\alpha} \frac{\rho_l}{\rho_v} \qquad (52)$$

These slip ratios were one to two orders of magnitude greater than values normally reported for two phase flows. High slip ratios were also encountered by Noyes (137) and Tang (163, 170). The occurrence of high slip ratios combined with the large liquid fractions led Smith (164) to postulate the existence of stratified flow in his work. More recently Lurie (112) presented an extension of Noyes' (137) work for vertical up flows of sodium. As with Noyes' original data, very high liquid fractions and slip ratios were obtained. Liquid fractions in both Noyes and Lurie's study were measured by use of an electromagnetic flow meter.

Tippets (172) et al have presented pressure drop data for flows of boiling potassium in the tube side of a double pipe potassium boiler. A tubular helical insert was placed within the potassium side of the boiler, and thermocouples placed within the insert to determine the temperature profile within the potassium. The boiling pressure losses were determined from slack-diaphragm absolute pressure transducers positioned at each end of the boiling tube. The frictional component of the pressure loss was calculated by subtraction of the momentum pressure loss. The integrated two phase frictional pressure drop multiplier was computed as the ratio of the two phase frictional pressure drop divided by the pressure drop for all liquid flowing at the same total flow rate. Two phase frictional pressure drop multipliers were plotted versus exit qualities for the potassium flows.

Unfortunately, due to the completely different test section characteristics no direct comparison of Tippets data with the current investigation is possible.

Wichner (182) et al also presented pressure drop data for forced convection boiling potassium in vertical up flow. The pressure distribution along the boiler tube was estimated using both homogeneous and Lockhart - Martinelli descriptions of the flow. The calculated pressure drops compared favorably with the measured values. Using the Lockhart - Martinelli correlation the pressure drop was over-estimated by 15%.

Correlation of two phase flow data to date has been accomplished almost exclusively by empirical procedures. Two techniques which have been subjected to numerous modifications have been most commonly used. The first of these approaches to the presentation of two phase flow properties was developed by Lockhart and Martinelli et al (110, 118, 119). This method was used to correlate frictional pressure drops and void fractions which occurred in horizontal, isothermal gas-liquid flows. An empirical correlation of the following form was developed:

$$\left.\frac{\Delta P}{L}\right|_{TP} = \left.\frac{\Delta P}{L}\right|_{l(v)} \varphi^2_{l(g)}\,(X) \qquad (53)$$

where

$\left.\frac{\Delta P}{L}\right|_{TP}$ = two phase frictional pressure drop

$\left.\frac{\Delta P}{L}\right|_{l(v)}$ = pressure drop computed if only the liquid (or gas) were flowing in the tube

X = ratio of single phase pressure drops:

$$\frac{\left(\frac{\Delta P}{L}\right)_l}{\left(\frac{\Delta P}{L}\right)_v} = X$$

φ = Lockhart - Martinelli parameter: correlated as function of X

Lockhart - Martinelli also found empirically that void fractions could also be correlated by means of the X parameter. Although the correlations leave a good deal of scatter in the experimental data, this method of correlation has probably been used more extensively than any other.

Several attempts have been made to improve the Lockhart - Martinelli type correlations by adding more parameters, or by using new ones altogether. The reader is referred to Smith (8) for a review of some of the less recent attempts at correction. Recently, Baroczy (12, 13) has developed correlations for both φ and void fractions using data for steam-water flows at various pressures, and the mercury-nitrogen data of Kiraly and Koestal (94). In his correlation for φ, Baroczy found that three independent flow properties were needed; these were: mass velocity, inlet quality, and a new parameter,

$$\left(\frac{\mu_g}{\mu_\ell}\right)^{-0.2} \cdot \left(\frac{\rho_g}{\rho}\right)$$

which he called "The Property Index". From these three quantities Baroczy's correlation allows one to rapidly predict φ_ℓ. Baroczy was able to correlate the data he used to a high degree of precision, and was then able to predict accurately the φ_ℓ's for several systems not used in deriving his correlation. In his correlation for liquid fraction Baroczy extends the Lockhart - Martinelli correlation by noting that a series of correlations occurred for fluids with different property indexes. Baroczy suggests the applicability of both of these correlations to two phase liquid metal systems.

Levy (104) has used an analytical approach to predict φ's from void fractions for two phase flows. In particular, single phase turbulent mixing length methods were used to predict two phase flows. Two phase density and velocity distributions, and pressure drops were derived by treating the two phase system as a continuous medium where turbulent changes of momentum and density are equal. Levy obtained good agreement between predicted and experimental values.

A second basic approach to the presentation of two phase pressure drop data is through the friction factor concept. In this concept the two phase system is treated as a single phase, where the friction factor may be presented as a function of Reynolds number as done by Govier and Coworkers (32, 33, 71, 72, 73), or as a function of quality, as done by Smith (164).

The friction factor concept has the distinct advantage of directly predicting the two phase pressure drops, whereas the Lockhart - Martinelli type correlations require the calculation of the single phase pressure drop.

DESCRIPTION OF EQUIPMENT

The two phase pressure drop data of this study were obtained in The University of Michigan boiling heat transfer test loop, Figure 98. Two phase

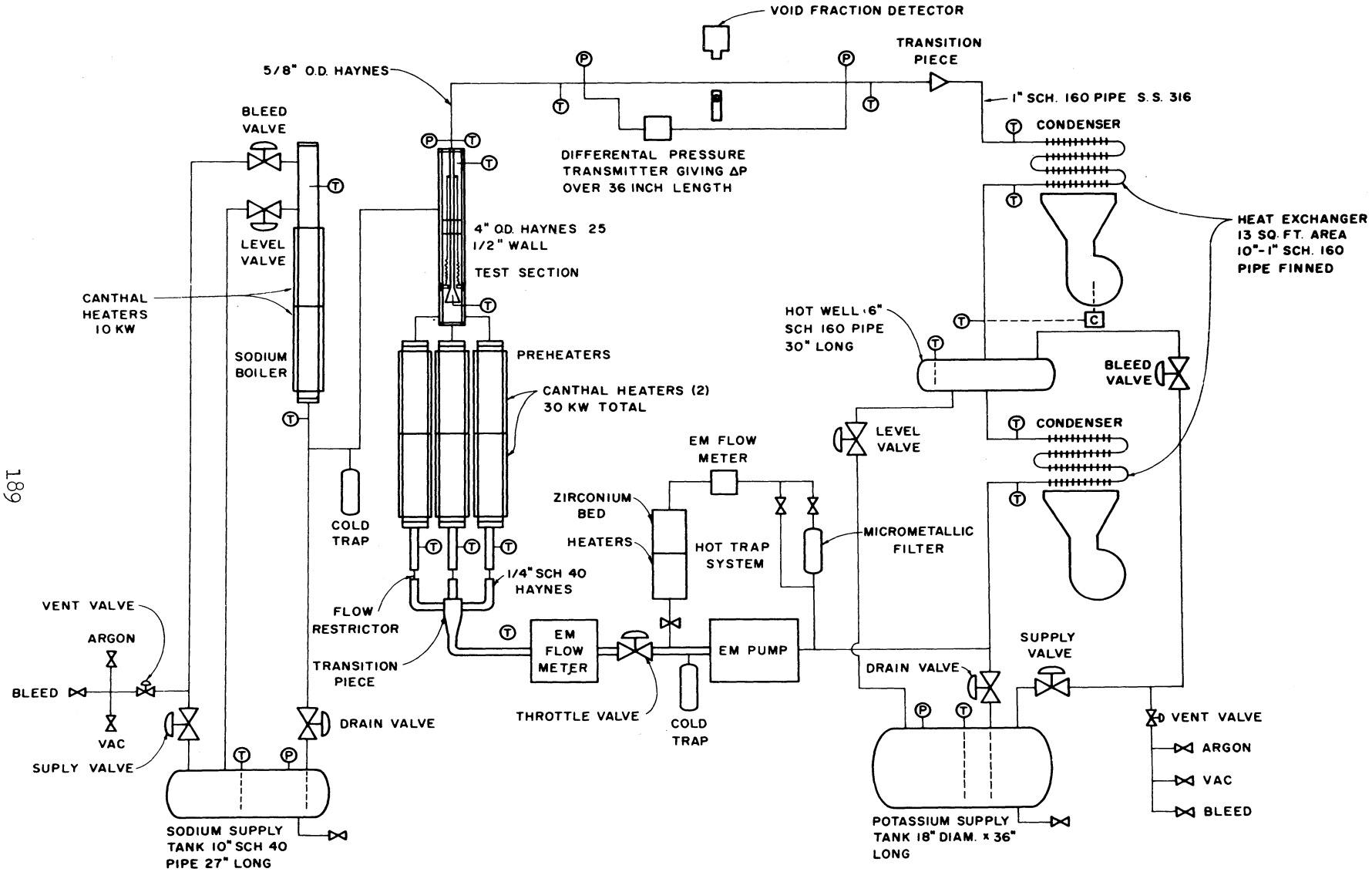

Figure 98

FLOW SCHEMATIC-BOILING LIQUID METAL SYSTEM

mixtures were generated in a preheater section, and the pressure drops were measured over a horizontal 3-foot length of 0.495-inch I.D. Haynes-25 alloy tube. The differential pressure taps were 1/4-inch schedule 40, four-inch long Haynes-25 alloy pipe nipples welded vertically onto the bottom of the tube. They were spaced 36-inches apart.

Two phase flows were generated in three parallel, vertical preheaters. The three streams merged and flowed upward through the heat transfer test section. Downstream of the heat transfer section the two phase mixture entered a ten-inch long (20 tube diameters) horizontal calming section from which it entered the pressure drop measurement section. The calming section was merely a portion of the pressure drop tube which extended upstream from the first pressure tap.

The pressure drops were measured with a Taylor Transaire Volumetric D-P transmitter. Pressure transmitting diaphragm assemblies of 316 stainless steel were transition-welded to the Haynes-25 pressure taps. These 5-ply diaphragms were 5 1/8-inches in diameter. Trace heaters were located along the pressure taps and the upper portion of the diaphragm housings to keep the potassium in contact with the diaphragms liquid at all times. The upper diaphragm housings and pressure taps were insulated with Johns-Manville Cerafelt and Banrock insulation materials.

Flexible steel capillary hoses were attached from the lower side of the diaphragm housings to opposite faces of a single diaphragm. The capillary hoses and lower portions of the diaphragm housings were filled with NaK eutectic which was liquid at room temperature.

The differential transmitter was horizontally mounted at floor level. Since a pressure drop occurred in the test section, the single diaphragm received unequal signals from the two static legs and was deflected in proportion to the pressure difference. This deflection in turn caused motion of a lever assembly which was translated by the differential pressure transmitter into a proportional air signal at the loop control panel. The pressure differential was recorded on a Taylor Transcope Recorder strip chart as per cent of either 100, 300 or 600 inches of water, depending on which notch was used on the force beam.

The pressure differentials measured by this system were accurate to within 1% of maximum range — i.e. to within 6-inches of water or about .2 psi. Further details of the instruments are given in Taylor Instrument Company bulletins.

Fluid temperatures at the inlet of the calming section and about 6-inches from the downstream pressure tap were measured with Pt-Pt, 10% Rh thermocouples. These thermocouples were calibrated against a National Bureau of Standards standard thermocouple. The thermocouples are well type, and electrically insulated from the loop. Thermocouple potentials were read on a Leeds and Northrup type K-2 potentiometer. Standardized thermocouple lead wire was used

to connect all thermocouples to the readout switch at the control point.

Mixture qualities into and out of the test section were determined by means of a heat balance around the loop. Details and an uncertainty analysis of the quality measurement is given in Appendix R. Total preheater power was read to within 0.2 Kw on a 0-30 Kw General Electric Ac Kw meter. A Superior Electric Company powerstat variable transformer was used to vary the electric power to the preheaters.

The liquid metal flow rates were measured by a Mine Safety Appliance Research, Style FM-2 magnetic flowmeter. Calibration curves for the meter as a function of meter temperatures were supplied with the meter. These calibrations were checked and found to be accurate. Accuracy of the flow meter is about $\pm$ 7 lb/hr which corresponds to less than 5.5% for all runs.

EXPERIMENTAL PROCEDURES

Pressure drop data were obtained for flow rates ranging from 110 to 740 lb. per hour, and for preheater powers ranging from 7.3 to 21 Kw. Data were taken after the loop was running at essentially steady state for any given pump and preheater setting. For most operating conditions several sets of data were obtained. These data included all Pt-Pt, 10% Rh thermocouple readings, flow rates, flow meter temperatures, and preheater power settings. The differential pressure transmitter was zeroed frequently to avoid errors caused by drifting of the zero point.

For most of the data reported, the pressure drop fluctuated regularly about a mean value which is the result reported. In addition to fluctuation in the pressure drop, oscillation in the flow rate occurred (also recorded on the Taylor chart for some of the experiments). From these oscillations it is noted that the potassium loop exhibited hydrodynamic instabilities — a phenomenon commonly found in two phase test loops.

Heat loss calibrations for the various sections of the loop were determined by measuring the enthalpy change which occurred during singel-phase flow at a given temperature level. Preheater losses were determined as a function of outlet temperature (TC 26), while the test section and pressure drop section heat losses were determined as a function of inlet temperatures to the respective sections. The preheater and heat transfer section heat losses were found to be independent of mass flow rate; the pressure drop section heat losses were, however, dependent on flow rate.

The heat loss calibrations were used in the heat balance by which the quality of the two phase flow was determined. The quality is defined as the weight fraction of the mixture which occurs as a vapor. Physical and thermodynamic properties for potassium were obtained from Weatherford (178) and the liquid metals handbook (89).

RESULTS

Two separate sets of data will be presented and discussed in this section. The first set of data was taken in the latter part of 1963 and were partially presented in an earlier report (8). The second set of data was taken in the early part of 1966 and are being presented for the first time. Comparison of the two sets of data will be made.

A typical section of the Taylor chart showing pressure drop and flow rate (millivolt) traces is given in Figure 99. The section shown is for a flowmeter output of about 4 millivolts and 18.5 Kw preheater power. The pressure drop here is being recorded in the 0-300 inches of water range. The zero for this range is 30 per cent. Thus, the mean pressure drop at 3:00 is 2.38 psi. The pressure and flowrate fluctuations were found to be greatest at high preheat powers and low pumping rates, while at low preheat values or high pumping rates, the fluctuations were not as severe.

The pressure drop data are presented in Tables A and B in Appendix N. These data were obtained while keeping the flowmeter output as nearly constant as possible. Inlet and outlet temperature and quality are presented in addition to average pressure drop test section qualities and preheater powers. The fact that the actual mass flow rates vary slightly even though the flowmeter output is constant is due to a shift in the flowmeter temperature with preheater power.

Following the procedure suggested by Smith (165) the two phase pressure drops have been converted to two phase friction factors which are plotted versus average test section qualities for the two sets of data in Figure 100. The two phase friction factor has been defined as:

$$f = \frac{\rho_v D(\Delta P/\Delta L)_{(\Delta P/\Delta L)_{TP}} g_c}{G^2} \qquad (54)$$

A least squares analysis was used to determine the "best" empirical fit of the data. In Figure 101 the best fits of the two sets of data are compared with the empirical correlations of Baroczy and Lockhart - Martinelli and the theoretical predictions of Levy.

The overall ranges of pertinent variables may be summarized as follows:

a)	Pressure drop	0.545	-	3.10 psia
b)	Mass flow rate	110	-	740 lbm/hr
c)	Inlet quality	0.0023	-	0.402
d)	Average quality	0.00433	-	0.400
e)	Inlet temperature	926	-	1432°F
f)	Inside pipe diameter	1495 inches		
g)	Test section length	3 feet		

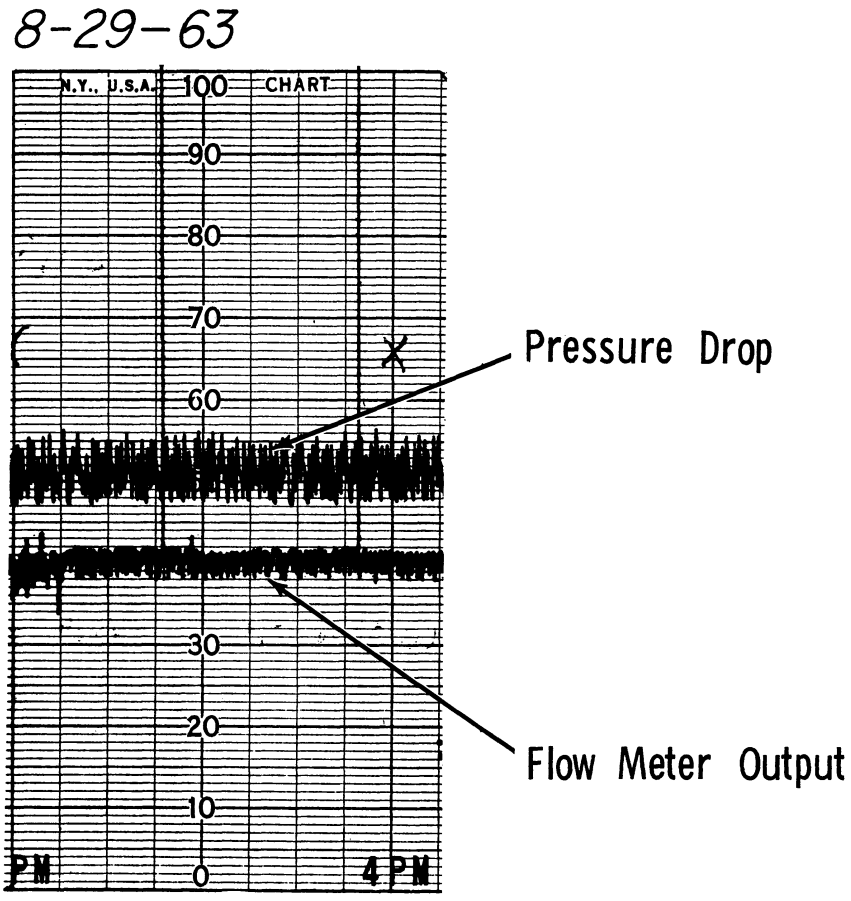

Figure 99 Typical Section of Taylor Transcope Recorder Chart, Showing Pressure Drop and Flow Meter Traces

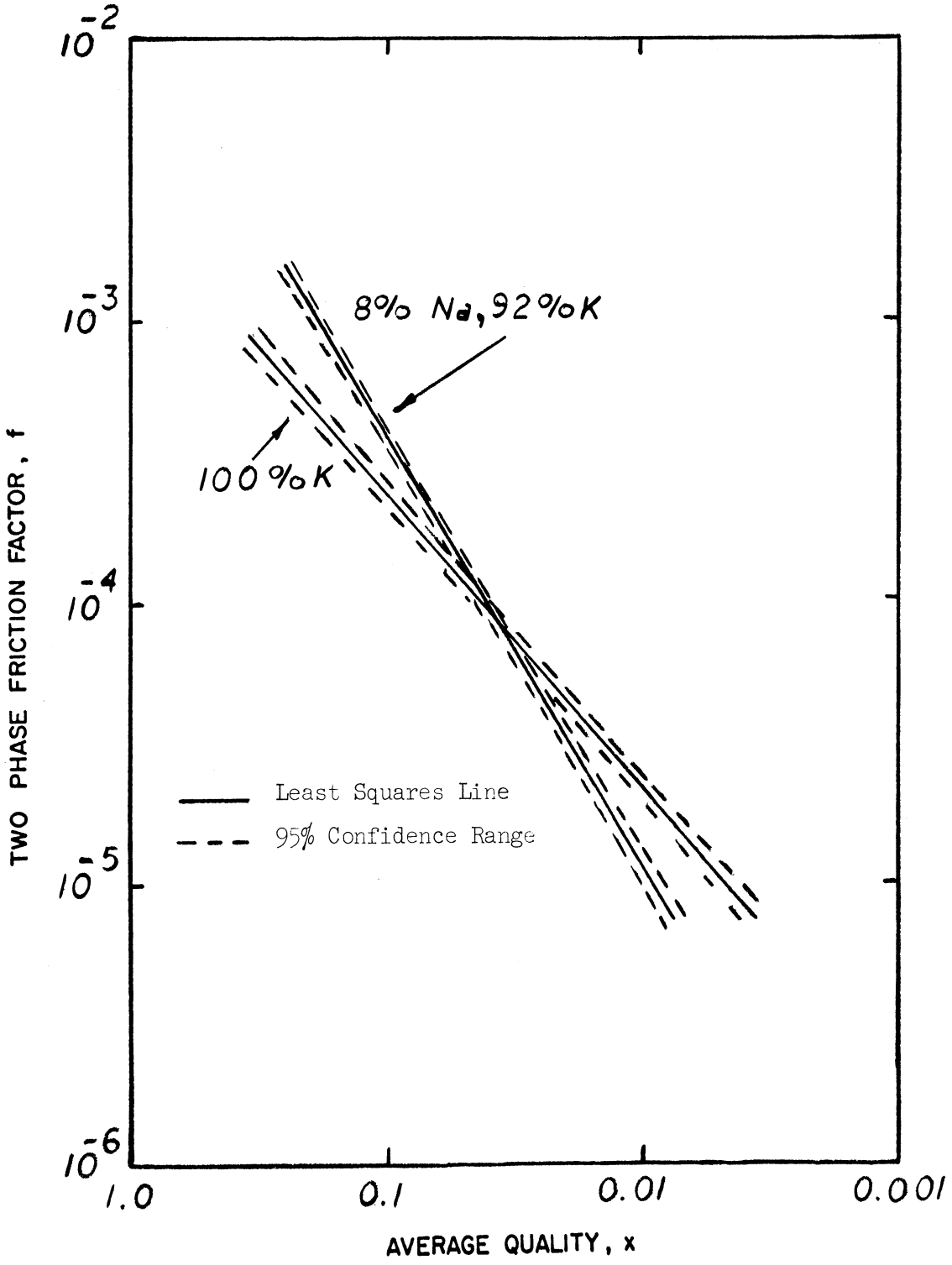

Figure 100 Comparison of Friction Factors from 1963 and 1966 Data

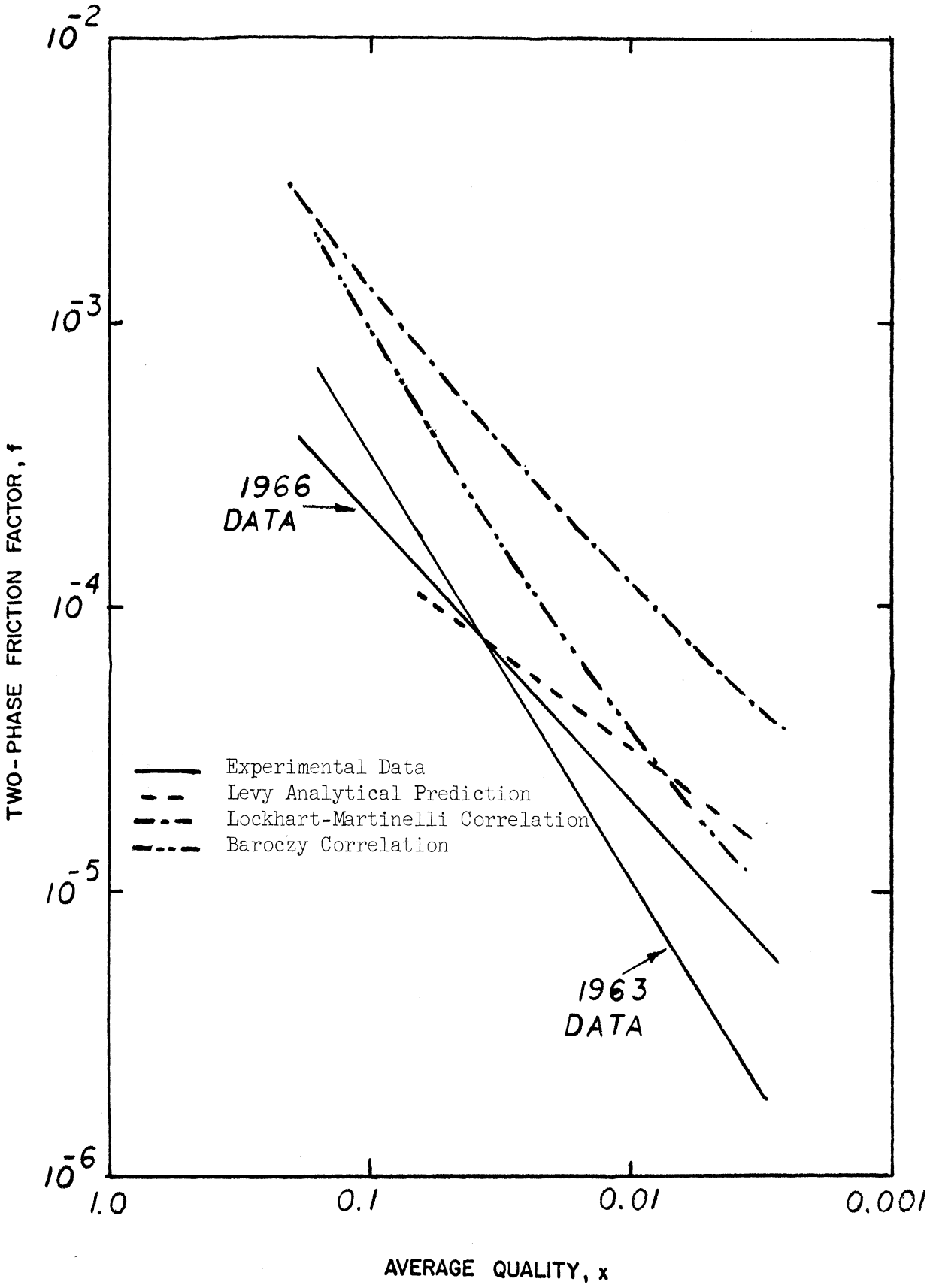

Figure 101 Comparison of Experimental Data with Other Correlations and Predictions

DISCUSSION OF RESULTS

Examination of data in Appendix N shows that in nearly all cases the pressure drop is accompanied by a temperature drop and an increase in quality. For the two sets of data the heat losses in the pressure drop test section ranged from 800 to 1500 BTU/hr. Since the heat supplied to the fluid in the preheaters ranged from about 20,000 to 50,000 BTU/hr (excluding losses) it is evident that the heat lost in the pressure drop section represents only a small portion of the fluid's total enthalpy (however, not necessarily a small fraction of the vapor enthalpy). Thus, the two phase flows in the pressure drop section are nearly adiabatic for the data included. Therefore, the flows under consideration are of the "nearly-adiabatic, evaporating" type. The evaporation or flashing occurs as the fluid cools itself while attempting to maintain thermodynamic equilibrium in a decreasing pressure field.

Prior to making the initial runs in 1963 a crack developed in the bellows and sodium leaked into the potassium system. After about 1/2 of the two phase flow experiments of the first set had been conducted a chemical analysis indicated that the Na content of the potassium was 8.2%. At the end of the runs the Na content was found to be 8.3%. Therefore, in reducing the data from the first set of runs the pertinent physical and thermodynamics properties of potassium were corrected for the 8% Na content. Properties were examined in the temperature range 900-1400°F, and the average deviations between the two systems are shown in Appendix O.

The data taken during the second set of runs is for pure potassium.

An analysis of the uncertainty in the quality calculation is presented in Appendix N, and is based upon the known precision of the experimental measurements. As seen in Figure 102 the uncertainty in the quality is about 5% for qualities above 5%. However, for qualities below 5% the uncertainty rises rapidly to above 50% at a quality of 1%.

The disagreement between the two sets of data is not surprising for several reasons: (1) it must be remembered that different fluids were studied; (2) from the void fraction observations to be discussed later it appears that two completely different flow regimes may have been involved. In particular, it appears that a stratified regime occurred during the first set of runs, while a dispersed or annular regime appears to have occurred during the second set of runs (this question will receive further consideration in the section discussing the void fractions studies).

One of the primary goals of this study was to compare the two phase potassium pressure drop data with the existing correlations in order to determine their effectiveness when applied to metallic systems.

In Figure 101 a comparison of the experimental friction factors, the friction factors predicted by the Baroczy and the Lockhart - Martinelli correlations,

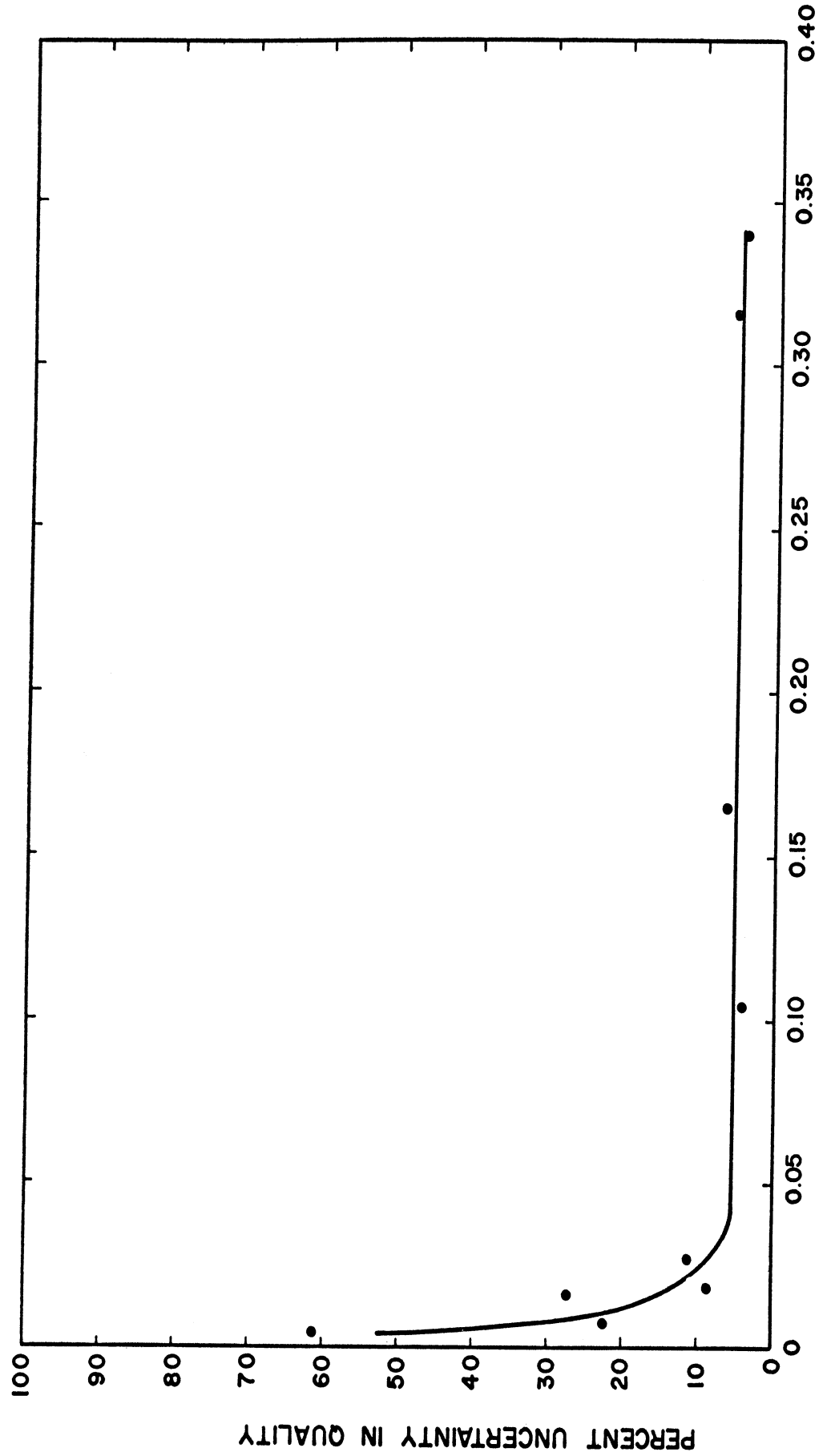

Figure 102 Uncertainty in Calculated Qualities, Based on Average Loop Operating Characteristics

and the friction factors predicted by Levy's method (using the void fractions from the second run) is presented. (Values predicted from the void fractions measured during the first set of runs would fall considerably lower than those presented here.) As can be seen from Figure 101, values predicted by the Lockhart - Martinelli, Baroczy and Levy correlations all have the proper trend when compared with the experimental values, and all are of the same order of magnitude as the measured friction factors. The Lockhart - Martinelli correlation yields friction factors which are too high over the entire range of values studied. The Baroczy correlation on the other hand yields very high values only for the higher qualities. For qualities less than 3% the Baroczy correlation yields values which are within a factor of 3 of the measured values. At lower qualities the Baroczy correlation gives even better agreement. Of the three proposed predictions, Levy's analytical prediction appears to yield the most accurate friction factors when applied to experimental conditions for which the model is valid, such as the second set of data. Since the flow regime encountered in the first set of runs does not agree with the model used by Levy, it is not expected that these results would agree with the theory.

In conclusion, it appears that neither the Lockhart - Martinelli nor Baroczy correlations correctly predict two phase liquid metal pressure drop behavior over a large range of qualities. Levy's analytical method, on the other hand, appears to show the greatest promise of yielding accurate results provided the flow regime is of the type used in his flow model and reliable void fraction data are available. For other flow regimes other models and predictions will be necessary. A serious drawback of Levy's method is the necessity of knowing void fractions, which are considerably more difficult to measure than pressure drops. However, the development of better void fraction predictions should increase the interest in extending and refining Levy's work. In addition, it is possible that by measuring pressure drops and friction factors, one may be able to work Levy's method in reverse, thereby using friction factors to determine void fractions.

As more and more two phase flow analytical models and flow characteristics are developed the importance of being able to predict accurately the flow regime will become of greater and greater importance. Flow regime characterization is an area of study in itself, which cannot be entirely separated from the other aspects of two phase flow. At the present time, flow regime studies have been carried out for some hydrocarbon and aqueous systems. Vohr (176) presents a survey of these two phase flow regime studies. However, to date no such investigation has been performed on liquid metal systems. A study of the two phase flow regimes of liquid metals under various configurations, mass velocities, and qualities would be of tremendous aid in comparing and reconciling much of the two phase liquid metal flow data, particularly in light of Levy's work.

II. VOID FRACTION STUDIES

INTRODUCTION

In recent years metallic fluids have received consideration as possible heat transfer media in space electrical power generation cycles which involve

boiling and condensing of the carrier fluid. The rigorous designs required in such applications necessitate the ability to make highly accurate predictions of two-phase flow phenomena. Although a voluminous literature exists on the subject of two-phase fluid flow, little has been reported on flow of metallic systems. The two-phase pressure drop along a tube in general is the summation of losses due to friction, acceleration effects, and hydrostatic head. Two-phase values usually are greater than those experienced in single-phase flows with comparable fluid throughputs. Frictional losses are always present and occur for any orientation of the flow channel and for adiabatic or heated conditions. Acceleration losses occur in forced-circulation boiling flows, where the continuous phase change causes the mixture density to vary along the tube. Such losses also occur in adiabatic flow at low pressure levels. Hydrostatic head terms are present only for vertical or inclined flow systems.

Knowledge of the mean two-phase mixture density is necessary in prediction of acceleration losses and hydrostatic head. In vapor-liquid flow, the mean velocities of the two phases, based on the cross sectional area of each, generally are not equal. Because of this "slip", the true fraction of the pipe cross section occupied by either phase differs from that calculated on the basis of the volumes of gas and liquid entering the tube. As a result, the mean mixture density cannot be calculated on the basis of quality (vapor mass fraction) alone, but requires a knowledge of the void fraction (fraction of the channel cross section occupied by vapor). Void fraction, then, is an important parameter in predicting the hydraulics of many two-phase flow systems, since without it the accelerative and hydrostatic contributions to the pressure drop cannot be evaluated.

Most experimental studies of void fractions have used one of three procedures to obtain data. Quick closing valves located at the inlet and outlet of a test section can be used for liquid-vapor flows where the amount of the two phases can be measured accurately after the valves are closed and the mixture is trapped. This method is better suited to two component flows in which the liquid and vapor are different components and no vaporization or condensation occurs between the instant the flow is stopped and a determination made in the liquid mass. For single component flows of potassium several obvious difficulties exist. The extremely corrosive nature of alkali metals and the temperature level of operation combine to make conventional quick closing valves unsuitable for these purposes. The further difficulty of determining the exact amount of potassium liquid in the test section at the instant of stoppage is also difficult. Thus, this technique has not been utilizied in studies with potassium mixtures.

The use of probes to distinguish between liquid and vapor has been used in both metallic and non-metallic flows. One can take advantage of the different electrical conductivities of liquid and vapor phases to design such probes. The probe must be moveable such that one can traverse the pipe cross section if overall void fractions are to be measured. This poses certain sealing problems which become severe when alkali metals are to be studied. The technique was used by Neal (133) to study void distributions in mercury-nitrogen flows. Although problems exist, the technique does have possibilities

for studying flows of the type investigated in this program.

The third approach, radiation attenuation by the flowing mixture, has the advantage that all instrumentation is external to the flowing system. Thus, it is equally appropriate for studying high temperature metallic flows or more conventional water-air or water-steam systems. It can be used to make either a single shot measurement to obtain the average void fraction or to make chordal measurements from which a radial phase distribution can be determined. In the study reported here the single shot technique was used.

Appendix P shows the void fraction results obtained by Smith (8) in his study with the Na-K system. Although the data scattered appreciably, it appeared to concur with the mercury and potassium-mercury data of Tang, Smith and Ross (170) and the sodium data of Noyes (137) in yielding much lower void fractions (higher liquid fractions) than nonmetallic fluids. Only Koestel's mercury-nitrogen data (94) deviated from this behavior for metallic flows.

The slip ratio, gas phase velocity to liquid velocity, corresponding to these void fractions was much higher than those ordinarily experienced with nonmetallic flows. No explanation other than the possible effect of wetting was offered at that time. For this reason further refinements to the apparatus were suggested by Smith which hopefully would reduce scatter. These suggestions and others have been analyzed and changes made in the equipment. These modifications and subsequent operating experience are discussed in this report.

Two phase flows were produced in a specially instrumented test section incorporated within the forced circulation heat transfer loop described earlier. In this study potassium two-phase pressure drop and void fraction data were obtained from the test loop. Two phase mixtures were generated in the preheater section, and the pressure drops were measured over a horizontal three-foot length of 0.495-inch ID tube. Mixture qualities within this test section were obtained by heat balance. Void fractions were measured at the middle of the pressure drop section using single-shot gamma-ray attenuation.

The theoretical basis of the gamma-ray attenuation technique for measuring void fractions has been reviewed elsewhere (165, 149). Although the mean two-phase fluid density in the region traversed by the radiation beam is sought, this value is not directly obtained in practice due to lack of appropriate absorption coefficients. The usual procedure is to obtain the void fraction by interpolation between detector signals read for single phase liquid and vapor flows. For the probable flow regimes encountered, it can be shown from Beer's law that:

$$\alpha = \frac{\ell n\ (N_{TP}/N_l)}{\ell n\ (N_v/N_l)} \qquad (55)$$

Correct application of Equation 55 requires that all the count rates be observed at the same flow temperature. However, single values of N_v and N_l at

one temperature may be adjusted for use at all two-phase flow temperatures encountered (165, 59).

DESCRIPTION OF RADIATION ATTENTUATION APPARATUS

Source: Thulium-170 which decays by beta particle emission to Yb-170, yields two soft rays — a 0.053 Mev K shell X-ray and a 0.084 Mev unconverted gamma ray. Equation (55) assumes the radiation is mono-energetic, but since the low energy photons were almost completely absorbed by the pipe wall, the detector saw primarily the 0.084 Mev radiation.

For the purposes of these studies it was necessary to obtain an isotope with a sufficiently long half-life to insure essentially constant source strength during any one experimental run. The 127-day half-life of Tm-170 meets this requirement, although it is short when considering experimental operations over several months. In long range use, however, corrections can be made for the decay. In addition to half-life considerations, the photon energy and approximation to mono-energeticity were examined. The density ratio of the potassium vapor-liquid system is in about the same range as for the air-water system. This fact suggested choosing a low energy gamma emitter which would be more sensitive to small changes in mixture density. However, if a photon too low in energy were chosen, the constant attenuation due to the channel wall would lower the mergent intensity below detection level and also damp out sensitivity. Calculations showed that for photon energies lower than about 60 Kev the tube wall attenuation would require using an unreasonably large source. On the other hand, for energies greater than 100 Kev the sensitivity in the potassium would suffer. These considerations led to the choice of Tm-170, which has a photon in the desirable energy range.

The source supplied by the Atomic Energy of Canada Limited was metallic thulium, encapsulated in stainless steel. When obtained, it has a strength of 9.8 curies. At the time of Smith's potassium-sodium void fraction runs (165), the course strength was about 4.7 curies. During the most recent studies the activity had decreased to about 0.03 curies.

Detection Equipment: The schematic diagram of Figure 103 indicates the counting equipment which was employed. Scintillation detection was chosen over Geiger-Muller, or proportional detection, because of negligible dead time correction and high intrinsic counting efficiency.

The detector unit is an Integral Line Assembly, Model 4Ss produced by the Harshaw Chemical Company. It consists of a 1-inch diameter by 1-inch thick, thallium activated, sodium iodide crystal coupled optcially to a 2-inch photo-multiplier tube. The assembly includes an external magnetic shield to minimize the effects of the various electric and magnetic fields present near the potassium test loop. The detector has a pulse height resolution of 8.3 percent at 661 Kev photon energy.

A Radiation Counter Laboratories Decade Sealer Model 10 D was used for the most recent study in combination with a Baird Atomic University Series

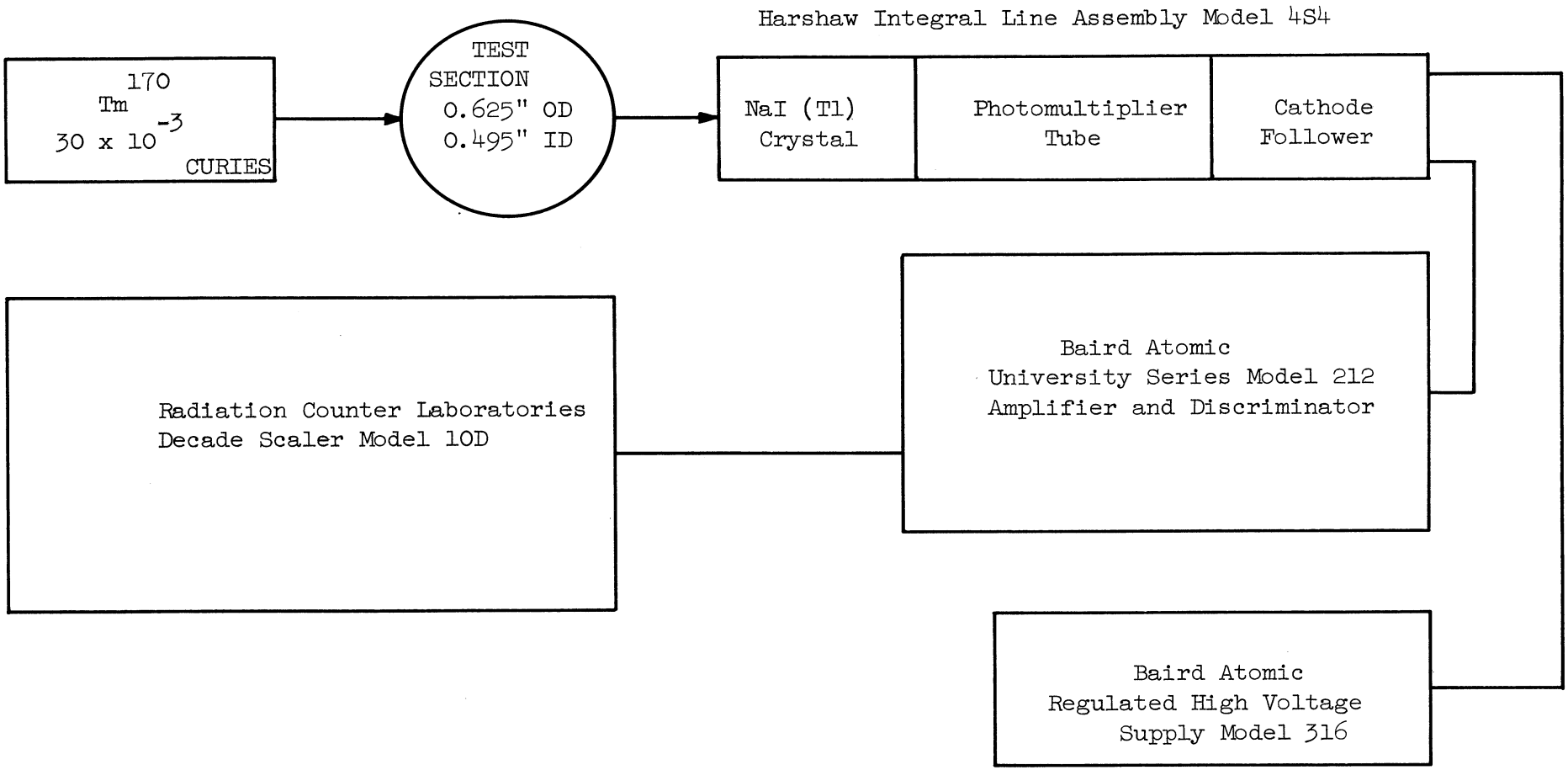

Figure 103 Schematic Diagram of Void Fraction Measuring System

Model 212 amplifier and discriminator. The discriminator is necessary to eliminate effects due to amplifier and phototube noise. In the early potassium experiments Tracerlab SC-18 Superscaler was used with a self-contained discriminator which was set at 0.25 volt. In recent studies the discriminator level was increased to just below the energy of the principal gamma, .084 Mev as shown in Figure 104. This discrimination reduced a good bit of the fluctuating background experienced in Smith's studies and permitted only the primary gamma produced by the source to reach the counting circuit.

In addition to the insertion of the pulse height selector, an attempt was also made to better control the temperature of the detection system. Air was blown over the detector so that its temperature was maintained below 80°F. As can be seen from Figure 105, the count rate is less sensitive to temperature in this temperature region than at the higher detector temperatures (approximately 135° to 160°F) at which Smith operated. These modifications, plus better voltage stabilization in the high voltage power supply, appeared to have a very significant effect on the results obtained.

Before concluding this discussion of the detection equipment, mention should be made of its efficiency. The resolving time of the photomultiplier tube is about 0.25 microsecond (77). Inorganic scintillation crystals such as NaI(Tl), due to their high density, have a high stopping power and consequently a greater counting efficiency for gamma rays than do gaseous detectors. The alkali halides — particularly NaI(Tl) — have the added advantage of high light output, transparency, and suitable refractive index. The high atomic number of inorganic scintillators aids in photon conversion.

The theoretical absorption coefficients of NaI(Tl) for gamma rays having energies ranging over three orders of magnitude are available (77). Using these coefficients, the theoretical efficiencies of crystals of various thicknesses can be obtained as a function of gamma energy. These theoretical, or "intrinsic", efficiencies depend on source-to-crystal distance. They do not account for absorption by the crystal contained or for the fact that only a fraction of the total interactions in the crystal are counted. (This latter factor depends on the scaler's discriminator setting.) Price (146) presents intrinsic efficiencies for 1 1/2-inch diameter by 1-inch thick NaI(Tl) crystals. For the source-to-detector distances used in these studies and for the low energy radiation employed, the theoretical detection efficiency approaches unity.

Shields and Collimator: Shielding and collimation modifications were made as shown in Figure 106. It will be noted that collimation was used on both source and detector sides of the pipe. Improved collimation, better shielding, of the source and reduced activity due to decay all combined to produce count rates which were low enough to eliminate the problem of scaler overloading. Background counts taken with the source in place, but shielded on the detector side of the pipe with a 2-inch lead brick, agreed within 10 percent of the background count taken with the source completely removed. The background count in these studies was reduced to less then a tenth of the count rate obtained in the actual tests. Unlike the background counts reported in Smith's work, the readings obtained in these more recent studies showed little variation with time.

Alignment at all temperatures was assured by fixing the position of source

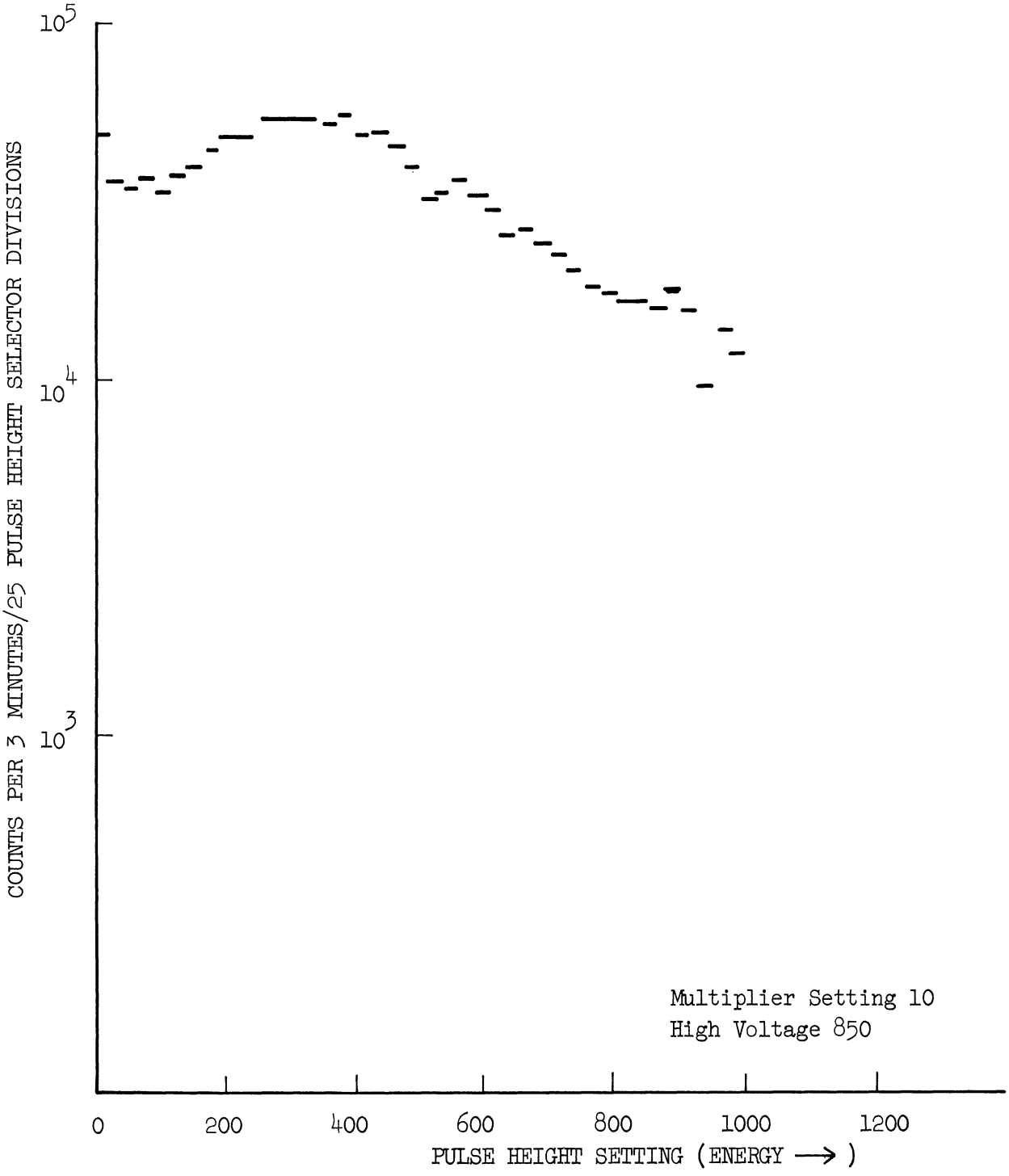

Figure 104 Differential Pulse Height Spectra

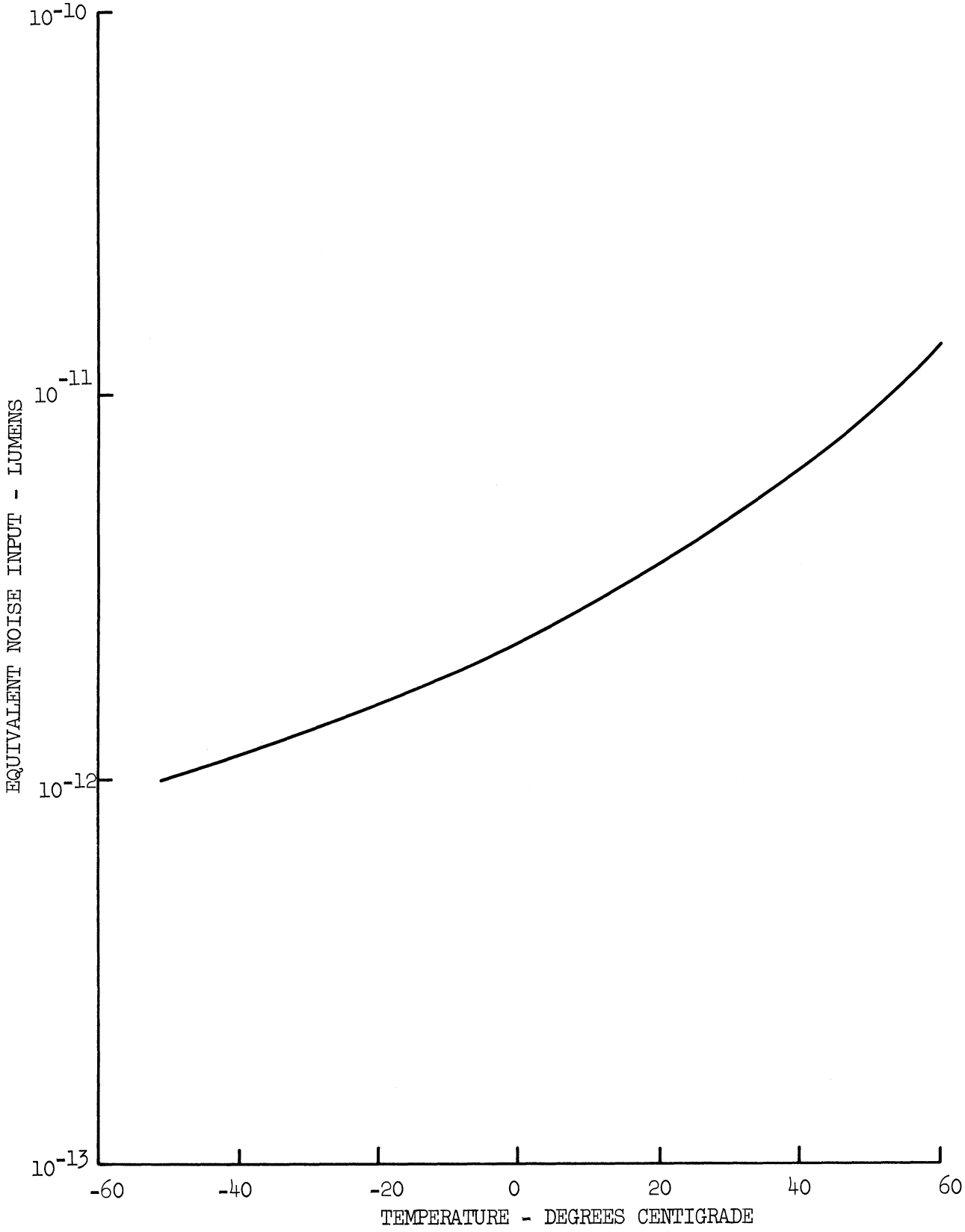

Figure 105 Temperature Dependence of Noise

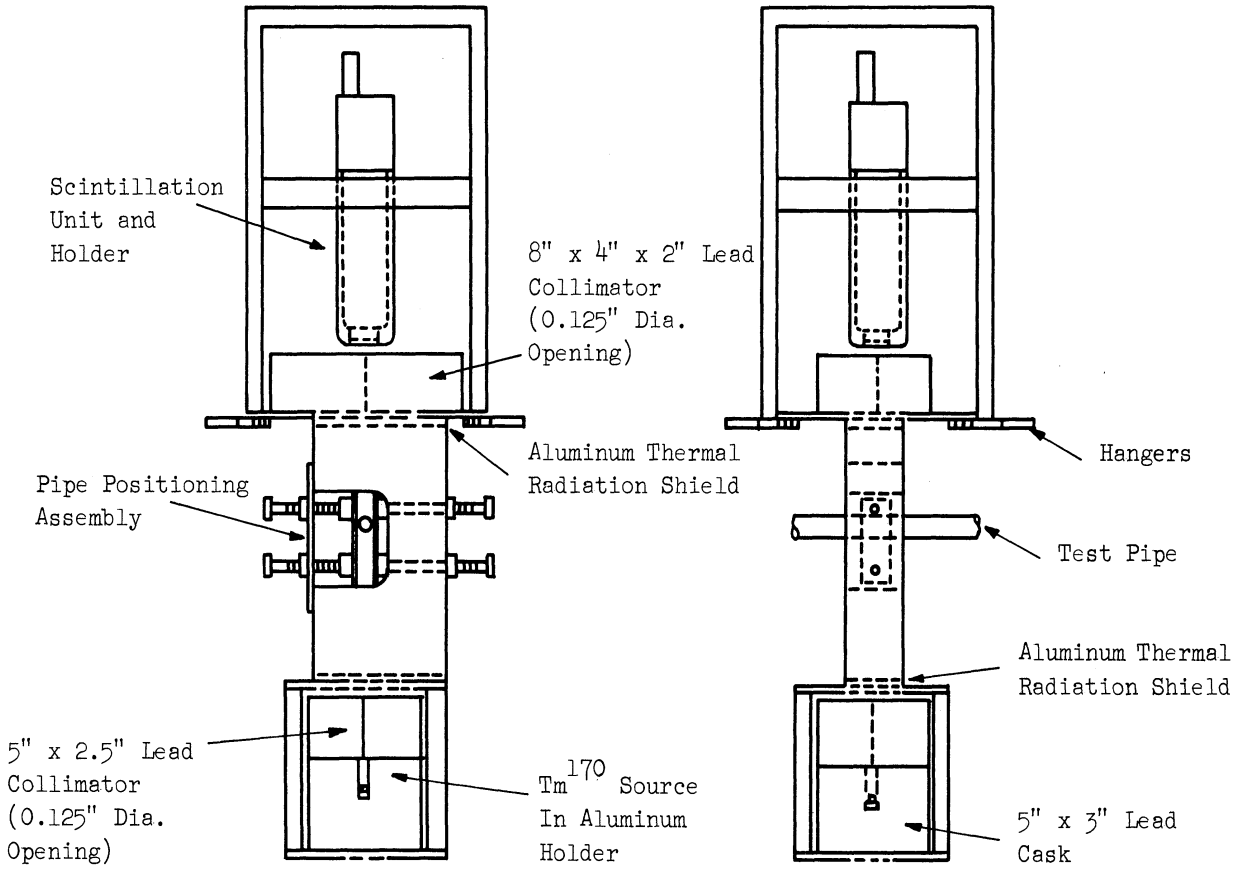

Figure 106 Gamma-Ray Source and Scintillation Crystal Holder

and detector, both with respect to one another, and with respect to the flowing system by means of a driving mechanism, as shown in Figure 106. The system was aligned initially without having the source in place. The source was then inserted and the driving mechanism was used to vary the position of source and detector with respect to the pipe while count rates were obtained. A plot of count rate versus position of the test pipe is shown in Figure 107. The system was finally fixed in that position which corresponded to the center of the pipe and locked in place. The source was then inserted and the driving mechanism was used to vary the position of source and detector with respect to the pipe while count rates were obtained. A plot of count rate versus position of the test pipe is shown in Figure 107. The system was finally fixed in that position which corresponded to the center of the pipe and locked in place. Any thermal expansion resulting from operation at test temperatures would not alter the relative position of the source, detector and pipe.

EXPERIMENTAL PROGRAM

Alignment was assured by the procedures discussed in the preceding section. These two procedures checked on another thus re-enforcing the claims that the beam was centered on the vertical diameter of the pipe.

The background count was then checked with the source in place but with the detector collimating plate replaced by a lead brick of the same overall dimensions. A count rate of 6074 counts/2 minutes was obtained and used in all studies discussed in this paper.

Determination of the void fraction by attenuation procedures requires the measurement of both full and empty pipe count rates. These readings should be taken at test temperatures when possible or corrections made for temperature dependence. In these studies full pipe readings were made at temperatures about 100°F above two phase test temperatures. However, values for liquid temperatures 100° to 200°F above two phase test temperatures showed no detectable difference. It was thus assumed for purposes of calculating void fractions that these readings which averaged 72,500 counts per two minutes represented full pipe count rates over the temperature range studied.

All vapor values at these temperatures could not be obtained since the pipe warmup heating elements alone could not maintain temperatures above 400°F. Since the preheaters were not capable of producing qualities of 100 percent at this temperature level it was necessary to utilize data for flows below 100 percent quality to estimate the all-vapor attenuation at test temperatures. Readings were taken at qualities up to 16 percent with no detectable change in count rate observed for qualities between 7 percent and 16 percent (23 determinations were made over this range) as shown in Figure 108. It was thus assumed that the plateau in Figure 108 represents essentially an all-vapor value at the operating temperature.

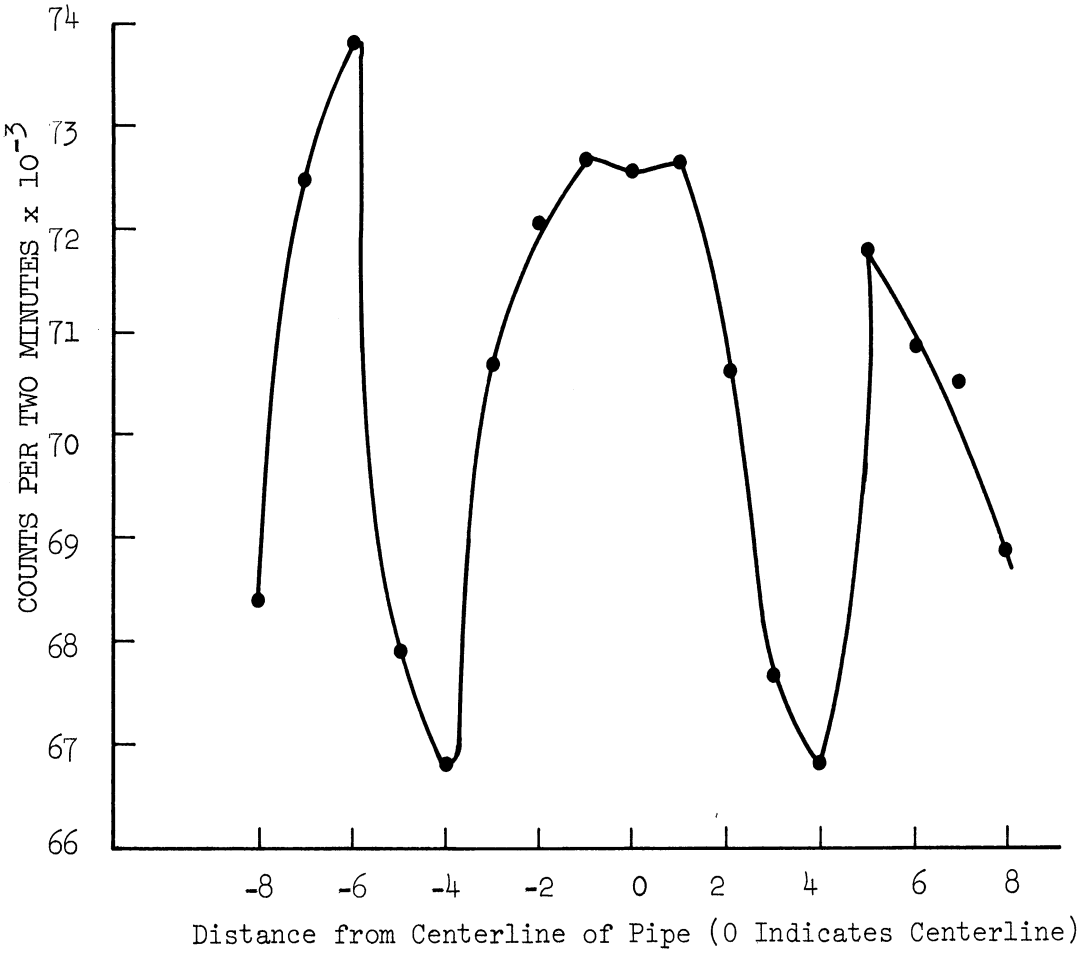

Figure 107 Alignment with Pipe

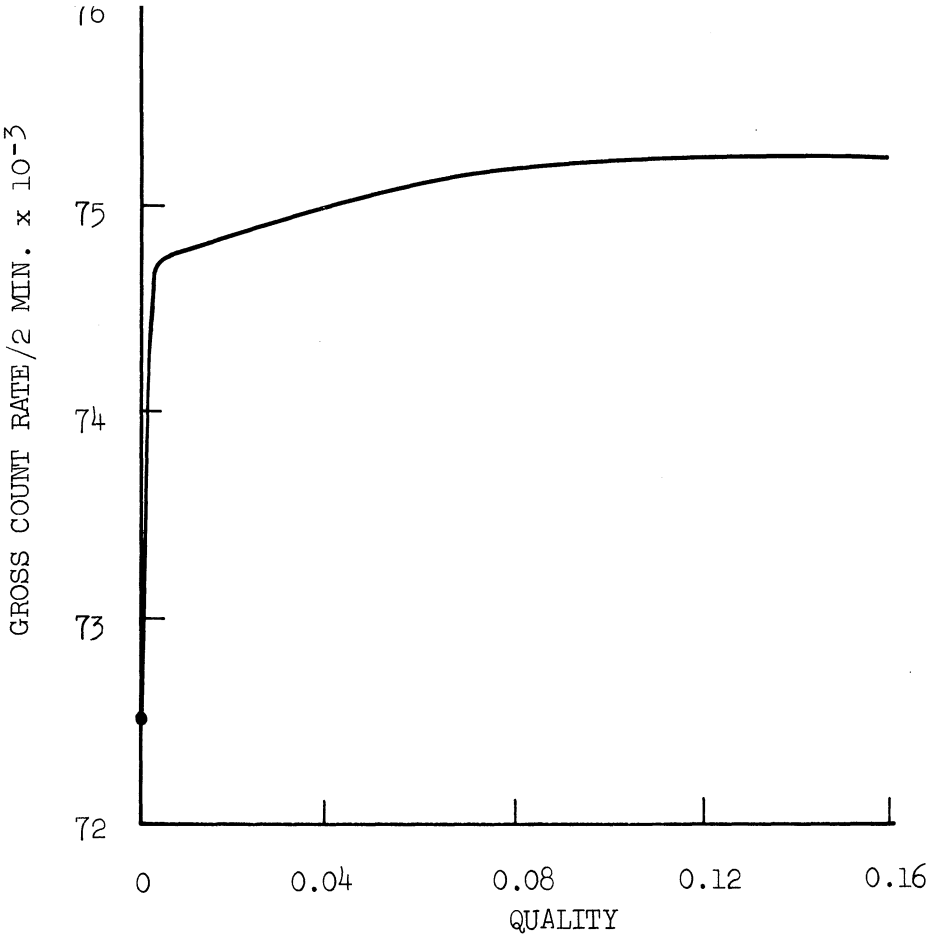

Figure 108 Effect of Quality on Gross Count Rate

As a result of the plateau two phase flow studies were limited to a quality range of 0.433 percent up to 4.08 percent at temperatures between 1236°F and 1325°F. Saturation pressures ocrresponding to the aforementioned temperature level is approximately 6 to 10 psia. Mass velocities were varied from 3.02 x 10^5 lb/hr. ft^2 to 4.57 x 10^5 lb/hr. ft^2. Each point represents the average of 4 or 5 readings made for two minute periods.

RESULTS

Void fraction results are presented in Appendix P; Table A presents the results of the 1963 (165) void fraction studies, while Table B presents the results obtained during the most recent studies. The same data are plotted in Figure 109 as liquid fraction vs the Martinelli parameter, X. Slips calculated from the 1966 data were all between 5 and 10, substantially lower than the values from the earlier measurements by Smith (165) on the 8% Na - 92% K mixture.

Table B in Appendix P shows the precision of the recent data to be substantially improved over that of the first set of data. All void fractions over this quality range fell between .830 and .875. The measured void fractions appeared to increase with quality, however the changes were small and within the uncertainty band of the data. As seen in Figure 109 these data fall below the earlier results of Smith and are more in line with non-metallic results, and the Baroczy prediction.

DISCUSSION OF RESULTS

As seen in Figure 109, the data from the first set of runs shows a significant amount of experimental scatter and uncertainty. This scatter is particularly important in view of the fact that the data from these runs do not agree with the previously (and even more recently) accepted correlations for two-phase void fractions (12, 110). However, when these data were compared with other two-phase liquid metal void fraction studies, as shown in Figure 109, they all appeared to be in the same general region, and thus tended to lend credence to each other. This argument is further strenghtened by the recent publication by Lurie (112) of a series of metallic sodium void fractions which agree with those of the first set of data. Lurie's data are shown in Figure 110. Thus, it appears that at least for liquid metal two-phase flows it is possible to have liquid fractions considerably higher than those predicted by either the Baroczy, or Lockhart - Martinelli correlations.

The extremely high void fractions measured by Smith (165), Lurie (112), and others, result in extremely high values of the slip ratio — at times as high as 750-900. These slip ratios tend to indicate that there has been an almost complete segregation of the liquid and vapor phases — as might occur in annular or stratified flow. It is hard to conceive of these slip ratios without a mechanism of this type. This kind of phase segregation would undoubtedly be more likely to occur at low mass velocities where interfacial

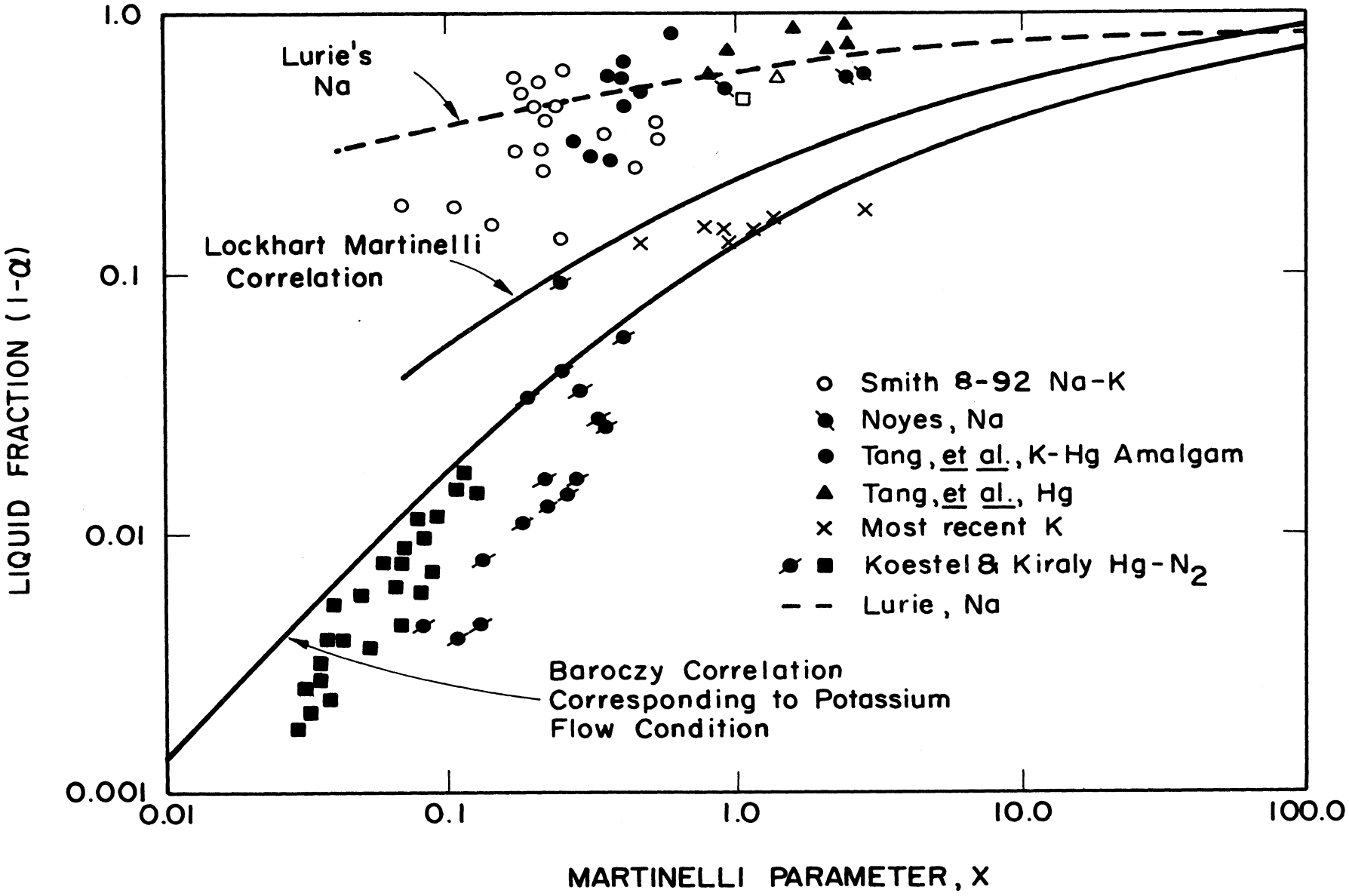

Figure 109 Metallic Liquid Fraction Data Compared with Other Data and Correlations

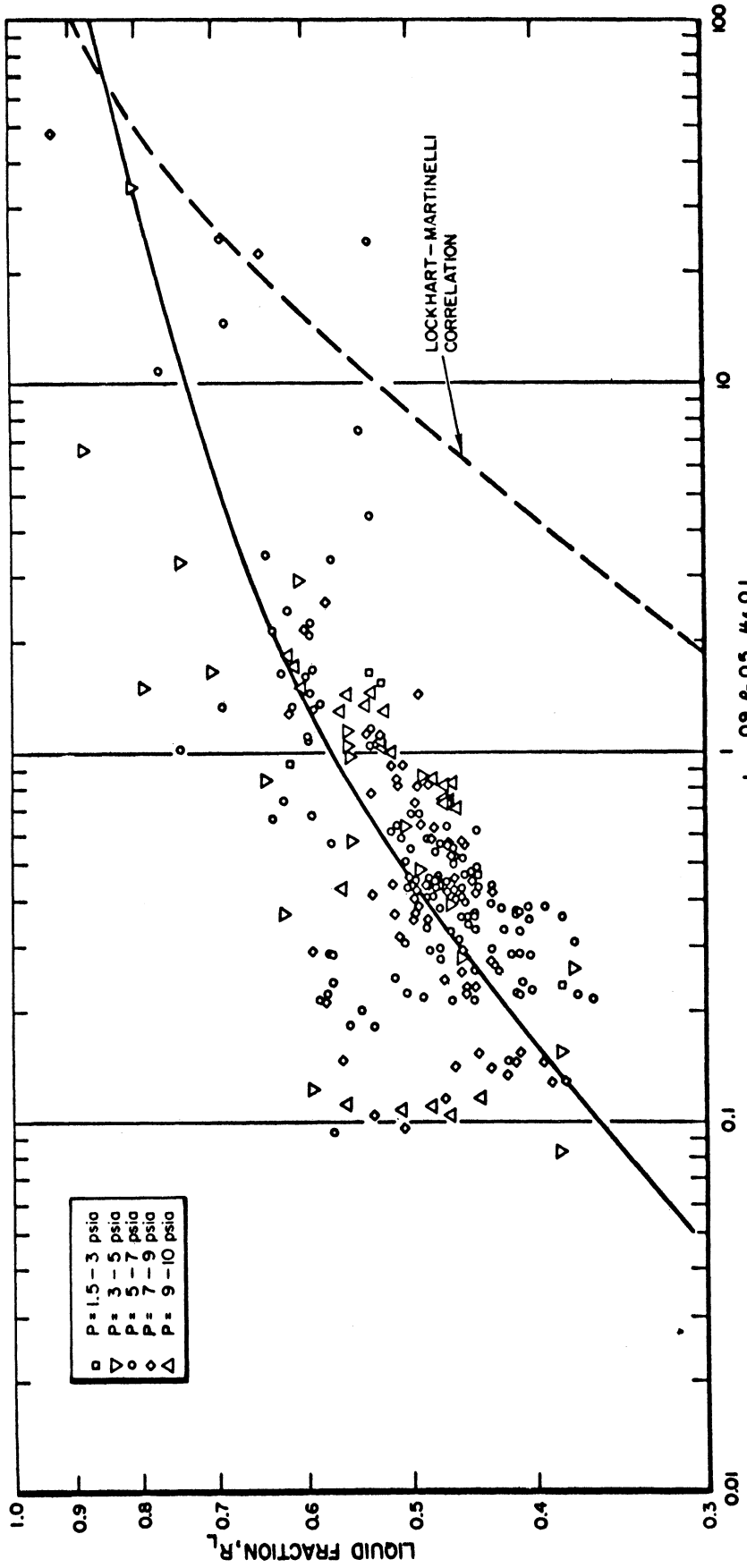

Figure 110 Lurries (112) Liquid Fraction for Vertical Upflow of Sodium

shearing would not be sufficient to "tear" the liquid phase away from the wall.

The second set of runs were performed at mass flow rates about double those of the first set. As illustrated in Figure 109 the data from the second set of runs exhibits considerably less scatter than that of the first run. It is felt that the improvements in the void fraction measuring instrumentation is mainly responsible for the decrease in experimental scatter.

It is noted that the liquid fractions measured in the second set of runs is considerably lower than that found in the first set of runs. Comparison of these data with the correlations of Baroczy and Lockhart - Martinelli indicated good agreement — especially with the Baroczy correlation. The slip ratios for the second set of data were of the order of 5-10 which tends to indicate more entrainment of liquid through the void fraction test section, rather than the segregated flow which was postulated for the first set of runs. This wide variation of slip ratio tends to substantiate the suggestion that highly different flow regimes may have existed in the two sets of runs.

CONCLUSIONS

Two sets of void fraction measurements have been made for two-phase flows of potassium. The void fraction results from the two sets of measurements differ appreciably, yet neither set seems unreasonable in the light of other experimental work. One explanation which can be offered for this paradox is the possibility of the presence of distinctly different flow regimes during the two sets of runs. Since no work has been done to delineate the various flow regimes which may exist in two-phase liquid metal flows it is impossible to confirm or deny this hypothesis.

Secondly the possibility of a bias in either set of data resulting from geometric or source considerations may very well exist. It is impossible to provide a numerical estimate of such uncertainties over and above the treatment in Smith's work (165) which estimated uncertainties in the void fraction of from 4-19% for all except one reading. The reduced scatter in the second set of data suggests that the refinements described herein did have an appreciable effect. However, in view of the compositional changes and the different flow conditions it is not felt that the initial results should be ignored. More experimental work with metallic flows is definitely needed before meaningful conclusions can be reached.

III. TWO PHASE HEAT TRANSFER

INTRODUCTION

Two-phase flow without heat transfer is a very complex situation to analyze rigorously as discussed in the preceding sections. Volumious literature exists

concerning two-phase flow characteristics which for the most part treat the problem expirically. Before treating heat transfer to these flowing mixtures, an understanding of the various flow regimes which can exist is essential.

Figure 111 is a pictorial representation of the flow regimes as the fluid quality increases along the flow channel. For adaibatic flows, the regime depends in a complex manner on parameters such as flow rate, quality, pressure (density) in addition to fluid properties, duct orientation and geometry. Figure 112 illustrates this dependence for water-steam mixtures. It was prepared for mass flows of 100 lb/sec ft^2. Curves (dashed lines) for pressures of 1, 10, 75 and 100 atmospheres and for different qualities were constructed and mapped using Ros' (154) parameters and flow regime maps.

When a heat flux is imposed at the wall of the duct further complications are introduced by the temperature gradients which result and the turbulence created if boiling should occur. In addition to these effects, momentum changes in the flow resulting from vaporization also must be considered.

Figure 111 represents changes that might occur at an intermediate heat flux level. Bubbles are shown as forming initially at active sites along the wall, much as they would under normal pool boiling conditions. Bergles and Rohsenow (20) and Chen (42) have treated heat transfer under such conditions with reasonable success by employing superposition techniques for computing heat transfer coefficients.

The presence of vapor bubles in the fluid provides other locations at which vaporization can occur if superheating of the liquid tends to exist away from the wall. Metallic liquids possessing high liquid thermal conductivities and requiring high wall superheats to nucleate bubbles could produce these conditions. Pressure drop along a flow channel which results in a decreasing saturation temperature also tends to create superheating in the fluid if not accompanied by fluid vaporization or a compensating heat loss.

The slug regime represents a transition between liquid continuous flows and the annular - mist configurations. It seems to be inherently unstable in that it leads to flow pusation.

The existence of a thin annular film would seem to preclude nucleate boiling for highly conducting liquid films because of the vaporization occurring at the liquid-vapor interface. It this interface remains at the saturation temperature, then it seems unlikely that sufficiently high superheats could be developed at the soild-liquid interface to produce nucleation.

At high heat fluxes the large vaporization rates could lead to film instability and thus further complicate the orderly progression of regimes pictured in Figure 111.

At sufficiently high flux levels (not necessarily the same for liquid continuous as for annualr regimes) a vapor film could form next to the wall long before the quality reaches the level of Section 7 as shown in Figure 111.

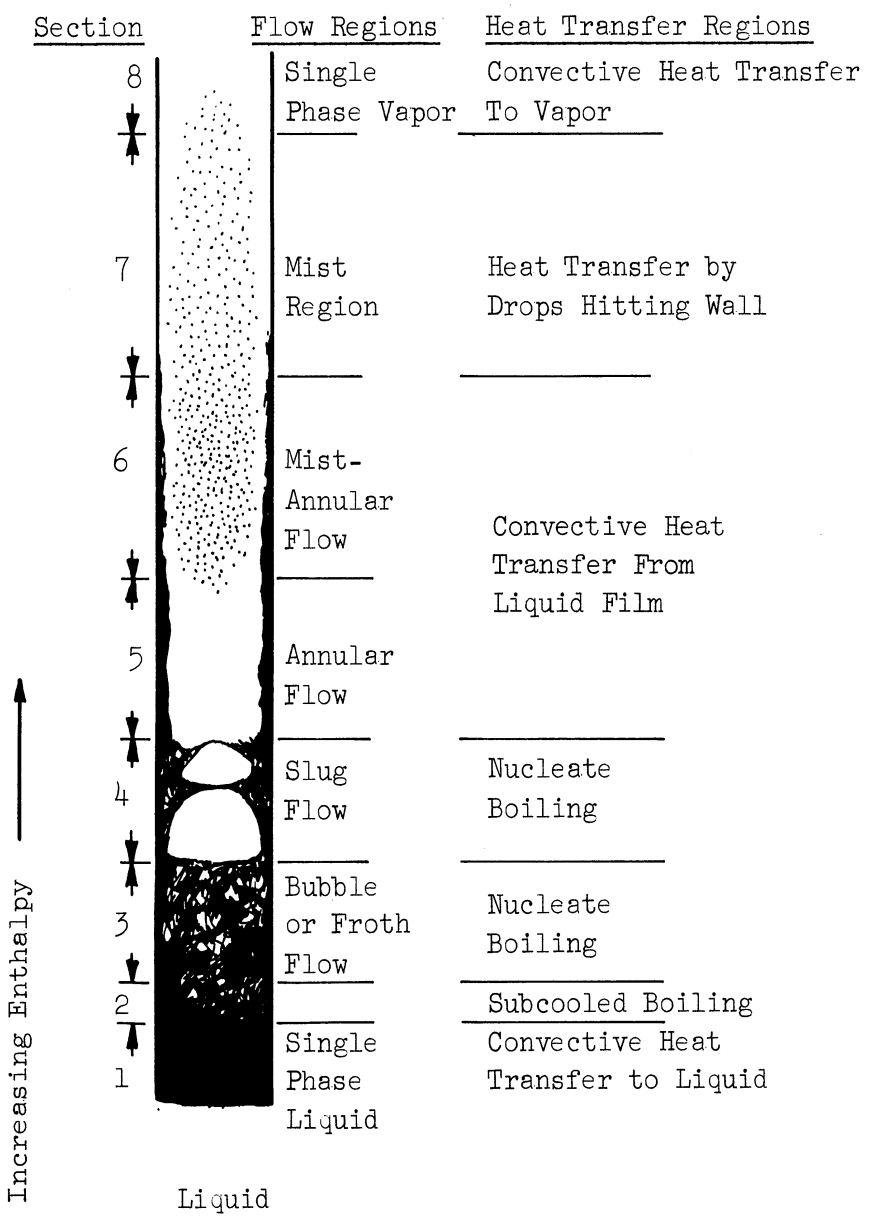

Figure 111 Flow Regimes

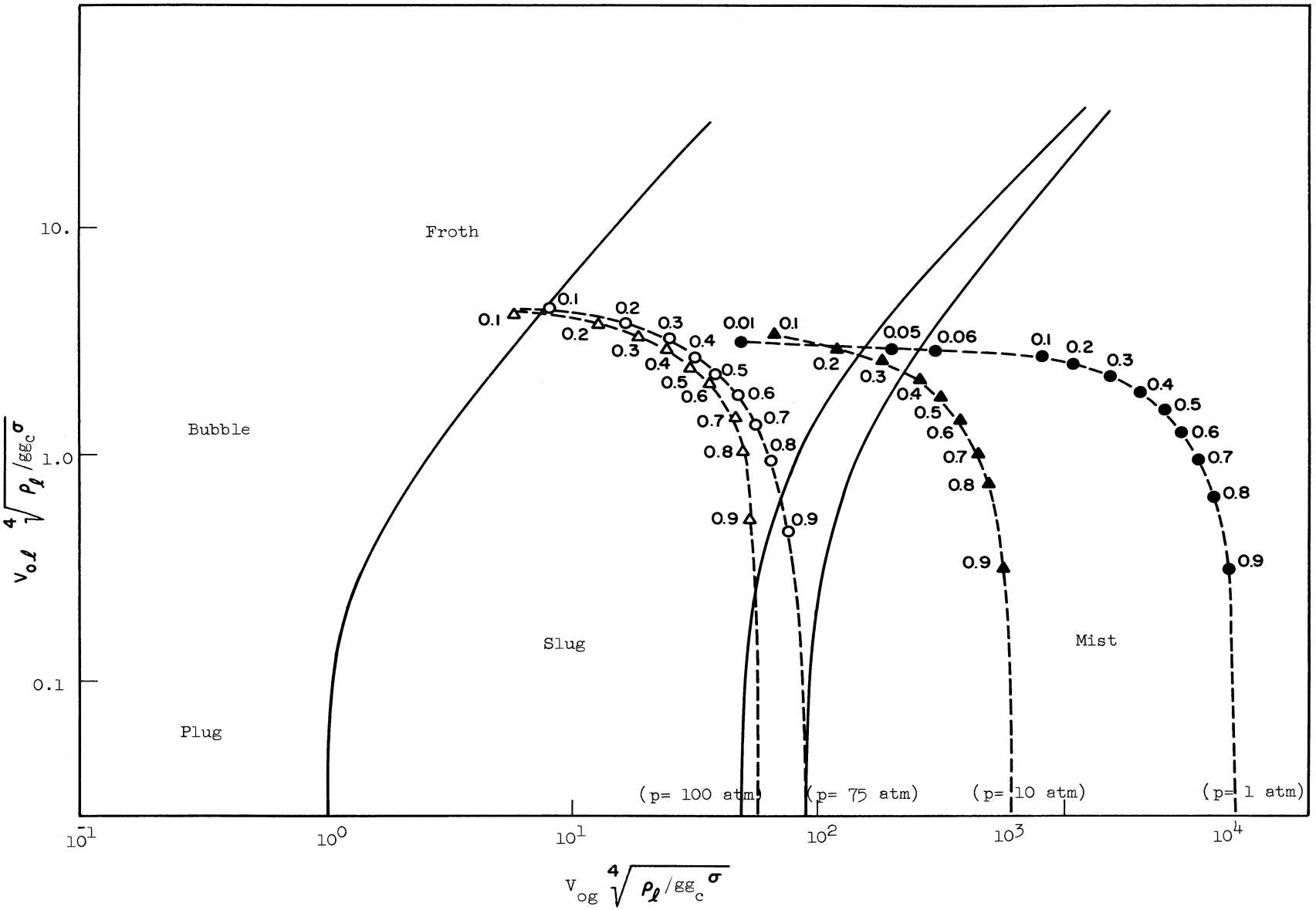

Figure 112 Correlation of Flow Regimes

Such a phenomenon would be similar to the film boiling regime discussed in an earlier section of this report and would also be accompanied by a sharp reduction in the heat transfer coefficient.

The so-called critical flux or burnout condition associated with pool boiling systems can result from another rather different phenomenon in forced convection flows. The "critical flux" condition is ordinarly associated with a sharp drop in the film coefficient due to blanketing of the surface with vapor. At higher qualities the amount of liquid in the flow eventually decreases to the point that the surface sees essentially a vapor (Section 8 of Figure 16). When an insufficient number of liquid droplets impinge on the wall, the wall temperature begins to rise. At some level it becomes sufficiently high to prevent further liquid-surface contact as droplets are repelled by virtue of a Leidenfrost type of phenomenon. Such a condition is frequently referred to in the literature as the "dry wall" condition.

The purpose of this study was to measure heat transfer coefficients to a two phase potassium mixture in forced convection. It was hoped that those conditions which lead to sharp reductions of the film coefficient could be defined more precisely for flows of this type. Operation at high qualities was prevented by failure of some preheater elements. Studies were thus restricted to qualities below 17%. Some evidence of the critical flux condition did occur in the data taken.

REVIEW OF POTASSIUM FORCED CONVECTION BOILING LITERATURE

The Oak Ridge National Laboratory (78) has conducted a program in the heat transfer characteristics of potassium in forced convection saturation boiling. Their work has been concerned with upward flow through a vertical circular tube and has included the determination of the magnitude of the critical heat flux.

Two boiler sections, a high flux boiler and a low flux boiler, were used. The high flux boiler was a 0.325 inch ID tube with a maximum design heat flux of 500,000 BTU/(hr)(sq ft). The low flux boiler was a 0.87 inch ID tube with a heat flux capability of 40,000 BTU/(hr)(sq ft).

Their data is presented in Appendix Q. Calculated heat transfer coefficients have been added to their data.

Critical heat fluxes were obtained by decreasing the flow rate through the boiler while keeping the heat flux constant hence increasing the outlet quality until the critical was reached. They were able to correlate their data with the dimensional equation of Lowdermilk, Lanzo and Siegel (111).

$$q_c = 270\ (1/d)^{0.2}\ (d/L)^{0.85}\ G^{0.85} \qquad (56)$$

This relation was developed for saturation boiling of water under low velocity high exit quality conditions. The data of ORNL indicate exist qualities at

the critical condition generally in excess of 50%.

General Electric has conducted a program in the investigation of forced convection heat transfer, condensation, and pressure drop in a potassium system. The 300 Kw facility was used to obtain boiling and condensing data. The system is temperature controlled in that the temperature of the heat rejection fluid and the acceptance fluid are controlled rather than the heat flux. The maximum temperature limit of the facility is 1850°F. The 100 Kw facility has a controlled heat input with operating capabilities at temperature up to 2200°F. Reference (5) gives detailed description of the systems.

Linear flow boiling potassium heat transfer data obtained by General Electric in the 100 Kw facility are shown in Figure (113) along with curves representing three superheated liquid film models developed by Geoscience Limited (145). All three models are for heat transfer in idealized, annular, liquid layers contiguous to the wall. The first model consists of a superheated liquid layer that is heated through the tube wall. Heat is dissipated from the liquid vapor interface by evaporative heat transfer. Conduction is the only method of heat transfer through the liquid layer. The second model differs from the first in that a uniform volume heat sink representing volume boiling is introduced in the liquid layer. The third model uses a volume heat sink that varies linearly from a maximum value at the wall to zero at the liquid vapor interface.

The thickness of the liquid layer for the above models was derived by Geoscience Limited for the case of both the vapor and the liquid in the viscous flow regime. Then they related thickness of the layer to the vapor quality. It should be noted that the Martinelli approach was used in the analysis. It is not apparent how the liquid could be in laminar flow when any type of volume heat sink was present. General Electric (5) questioned the assumption that the film thickness could be calculated independently of the heat flux.

General Electric has also developed a qualitative approach to the problem of a design procedure for calculating heat transfer coefficients at heat fluxes less than the critical. However, the procedure is not refined sufficiently to be used for quantitative purposes. However, they have been able to predict the following trends qualitatively for two phase heat transfer:

1. At constant heat flux, saturation pressure, and for a given maximum cavity size, nucleate boiling tends to be suppressed with increasing quality. The cavity size referred to is the dimension of those surface cavities in which bubbles are able to nucleate.

2. If all the other variables mentioned above are held constant, except for cavity size, nucleate boiling tends to be suppressed as the maximum cavity size decreases. In other words, the smoother the surface the more superheat is required for nucleation.

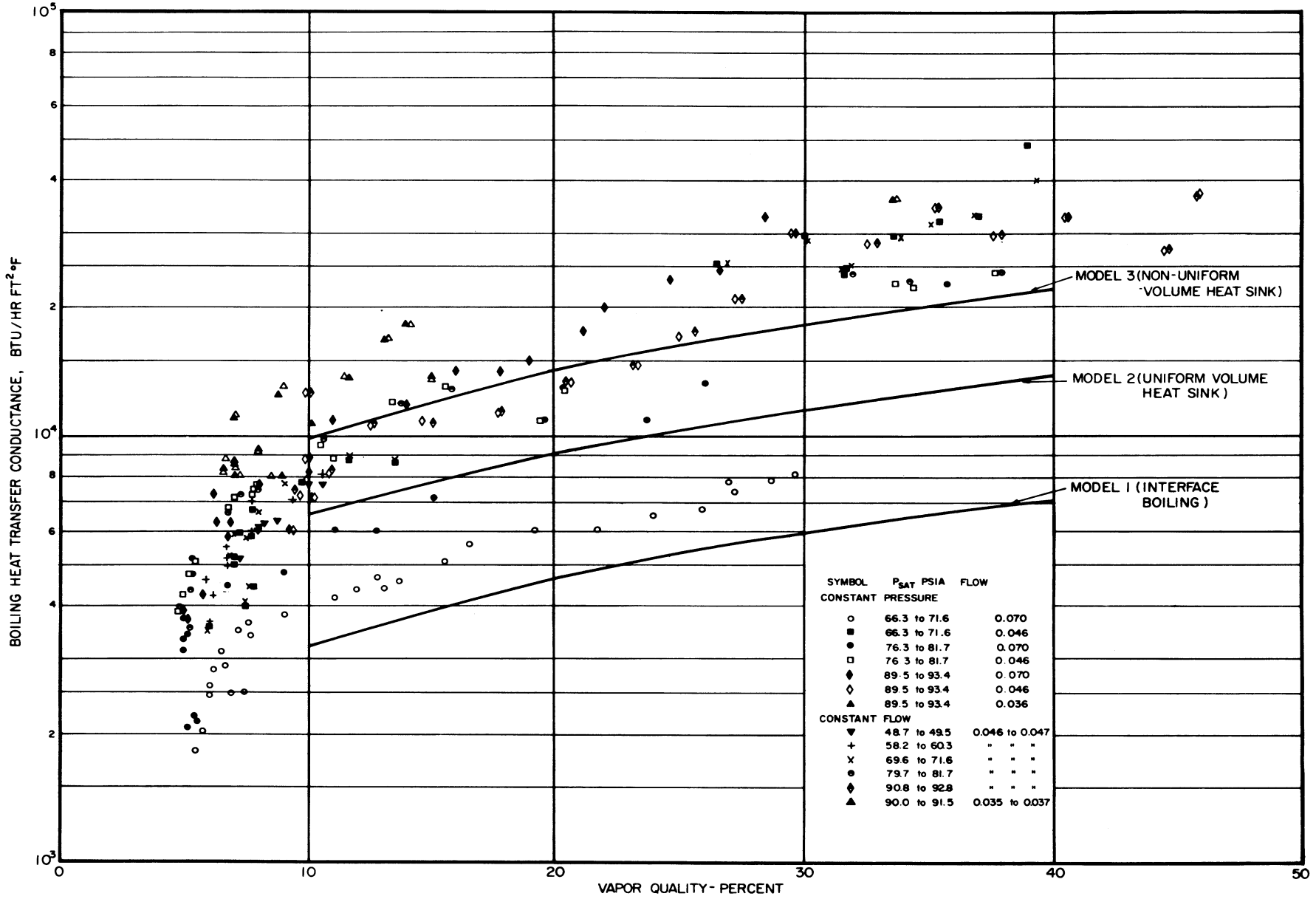

Figure 113 Comparison of superheated liquid film models with GE boiling potassium data

3. If all other variables are held constant, lowering the heat flux supresses nucleate boiling.

4. If all other variables are held constant lowering the pressure supresses nucleate boiling.

General Electric investigators have observed that for the conditions under which they have conducted their studies, heat transfer coefficients are all high. From a design point of view, it is their conclusion that a determination of the critical flux condition (or conditions) is more important.

General Electric's critical heat flux data with and without swirl devices is tabulated in (5 - Rept. 12). The data obtained in the 300 Kw facility ranges in temperature from 1550°F to slightly over 1700°F; whereas, the data obtained on the 100 Kw facility is all in the range of 2100°F with the exception of one point at 1838°F. The relatively small magnitude of the nucleate boiling resistance made it difficulty to measure coefficients accurately in this regime. Possible errors were of the same magnitude as the coefficient. For this reason, the 300 Kw facility investigations emphasized critical heat flux determinations and transition boiling coefficients.

For the range of conditions investigated, General Electric observed no effect of temperature or mass velocity on the critical heat flux. They did find, however, that the fourth root of acceleration permitted correlation of helical flow data with straight tube data. In addition a definite decrease in the critical heat flux as the quality increases was observed. They finally obtained the following equation for the critical heat flux on high quality flows:

$$\frac{(q/A)_c \dfrac{x_c}{1-x_c}}{\sqrt[4]{\dfrac{\alpha_{radial}}{g_c}}} = 3.5 \times 10^5 \frac{Btu}{hr\ ft^2} \qquad (57)$$

where $(q/A)_c$ is the critical heat flux, x_c is the critical quality and α_{radial} is the radial acceleration.

DESCRIPTION OF EQUIPMENT

A detailed description of the forced circulation apparatus is included under the sodium condensing studies section of this report. Figure 84, 85, 86, 87, 88 and 89 of that section provide both schematic and pictorial representation of the equipment.

Figure 98 and 114 of this section are duplicates of two of these figures which have been included in this section for purposes of direct reference. Figure 98 shows the points in the system where temperature measurements are made that have a direct bearing on the two phase heat transfer studies.

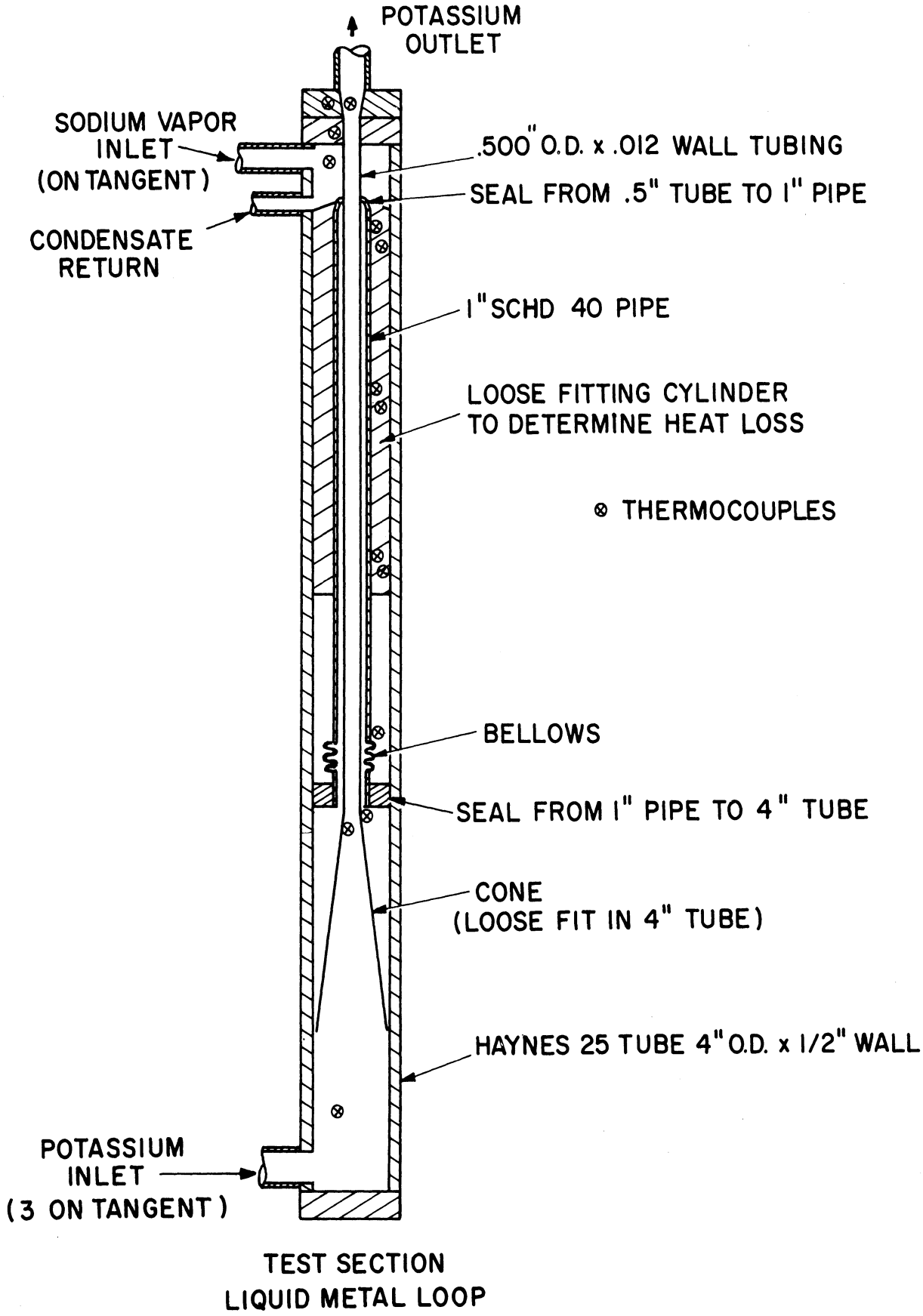

Figure 114 Heat Transfer Test Section

Quality determinations were made by conducting a heat balance around the preheaters tes section. Platinum/Platinum - 10% rhodium thermocouples are located at the inlet to the preheater (TC-25) and the inlet to the test section (TC-26). After leaving the preheaters the fluid mixture enters the heat transfer test section shown in detail in Figure 114. A funnel channels the flow up the 1/2-inch central tube. The tube is surrounded by an annular space in which potassium vapor or an inert gas is maintained to reduce heat transfer between the fluid and the surroundings.

Heat transfer data is actually obtained over the 2-inch length of tubing at the top of the test section. Sodium vapor is generated in the sodium boiler shown at the left in Figure 98. Condensation occurs on the outer surface of the tubing through which the potassium flows. The flux must be determined by a heat balance on the sodium boiler since no direct measurement of the potassium enthalpy is possible nor is it possible to measure the temperature gradient in the 0.012 inch thick wall. TC-27, a platinum/platinum - 10% rhodium thermocouple, measures the sodium temperature while the potassium temperature is measured by TC-29 at the outlet of the test section. These two thermocouples provide an overall temperature difference from which an overall heat transfer coefficient can be measured. The potassium film coefficient is then calculated by predetermining the condensing and tube wall resistances.

EXPERIMENTAL PROCEDURE

Before the heat transfer runs were initiated, an attempt was made to eliminate non-condensibles from the sodium vapor space in order to obtain a uniform condensing coefficient and a high flux. A vacuum of less than 10 microns was maintained on the sodium system prior to charging while the boiler and associated lines were kept in excess of 700°F.

The potassium system was evacuated through the vent and bleed valves to a pressure of less than 40 microns. During evacuation the potassium system was being heated to a level necessary for charging. The preheaters were heated to above 1200°F and the other components were heated with the trace heaters to around 600°F.

The system was circulated at 2 GPM with one third of the preheater power until the system was hot. When the temperatures around the loop were at the desired level the flow rate was systematically decreased and the preheater power was increased. Simultaneously the sodium boiler was bled through the bleed and vent lines into a vapor trap whose capacity was roughly equal to the sodium boiler. During each of the three bleeds, the sodium vapor temperature would drop and rise quickly to its former value after bleeding. These bleeds were necessary to remove any noncondensibles which were released during the heat up process. Three bleeds were carried out as Barry (14) has observed no further change in the condensing coefficient after such a series of steps.

The run was programmed as follows:

1. Obtain two phase heat transfer data at temperatures of 1400°F over as wide a quality range as possible and at fluxes of approximately 200,000, 300,000 and 400,000 BUT/hr ft^2.

2. Obtain void fraction data at low quality flows with gamma ray attenuation as discussed earlier.

3. Revert to single phase potassium flow by pressuring the potassium system to check the sodium condensing coefficient and heat losses in a particular run.

A given set of conditions during the two phase heat transfer runs was held long enough to determine that the loop had reached steady state. The criterion for this condition was the constancy of temperatures taken hourly. Thermocouples TC 25, 26, 27, 28, 29 were used for this determination although some 50 other thermocouples around the loop verified the steady state conditions.

DISCUSSION OF RESULTS

The experimental data and the results calculated from these data are tabulated in Appendix S. In the medium quality range the potassium two phase mixture temperature as denoted by TC 29 ranged from 1316°F to 1403°F. The heat flux was varied from 213,000 to 424,000 BTU/hr ft^2. The flow rate was varied from 222 to 380 lb/hr which corresponds to mass velocities of 1.89×10^5 to 3.08×10^5 lb/hr ft^2. The quality of the potassium flow was varied from 0.0507 to 0.173. Operating temperatures were limited by the need to avoid damaging the bellows shown in Figure 114. The upper quality was limited by failure of 50 percent of the preheater heating units during the run period. These units which are similar to the heaters in the sodium boiler had a considerably shorter life than the manufacturer had indicated.

In the low quality range the flow rate was varied from 404 lb/hr to 612 lb/hr corresponding to mass velocities of 3.28×10^5 lb/hr ft^2 to 4.97×10^5 lb/hr ft^2. The flux was essentially constant and ranged from 233,000 to 282,000 BTU/hr ft^2. The potassium temperature was varied from 1285°F to 1345°F. The quality ranged from 0.002 to 0.038.

The heat flux was calculated by the power input less the heat loss from the sodium boiler. The heat loss calibration curve is shown in Figure 115. It was determined during the condensing runs, which were conducted before and after the two phase runs, to serve as a check on the condensing coefficient and heat losses. The sodium vapor temperature TC 27 was used as the basis for predicting the sodium system losses. Similarly the preheat losses were determined and plotted against TC 26, the potassium temperature out of the preheaters. The preheat loss calibration is shown in Figure 116.

The quality was determined by a heat balance, including the losses, between TC 25 and TC 29. The two phase coefficient was calculated knowing the sodium condensing coefficient prevalent during the run, the thermal resistance of the wall, the temperature of the sodium vapor, TC 27, and the temperature of

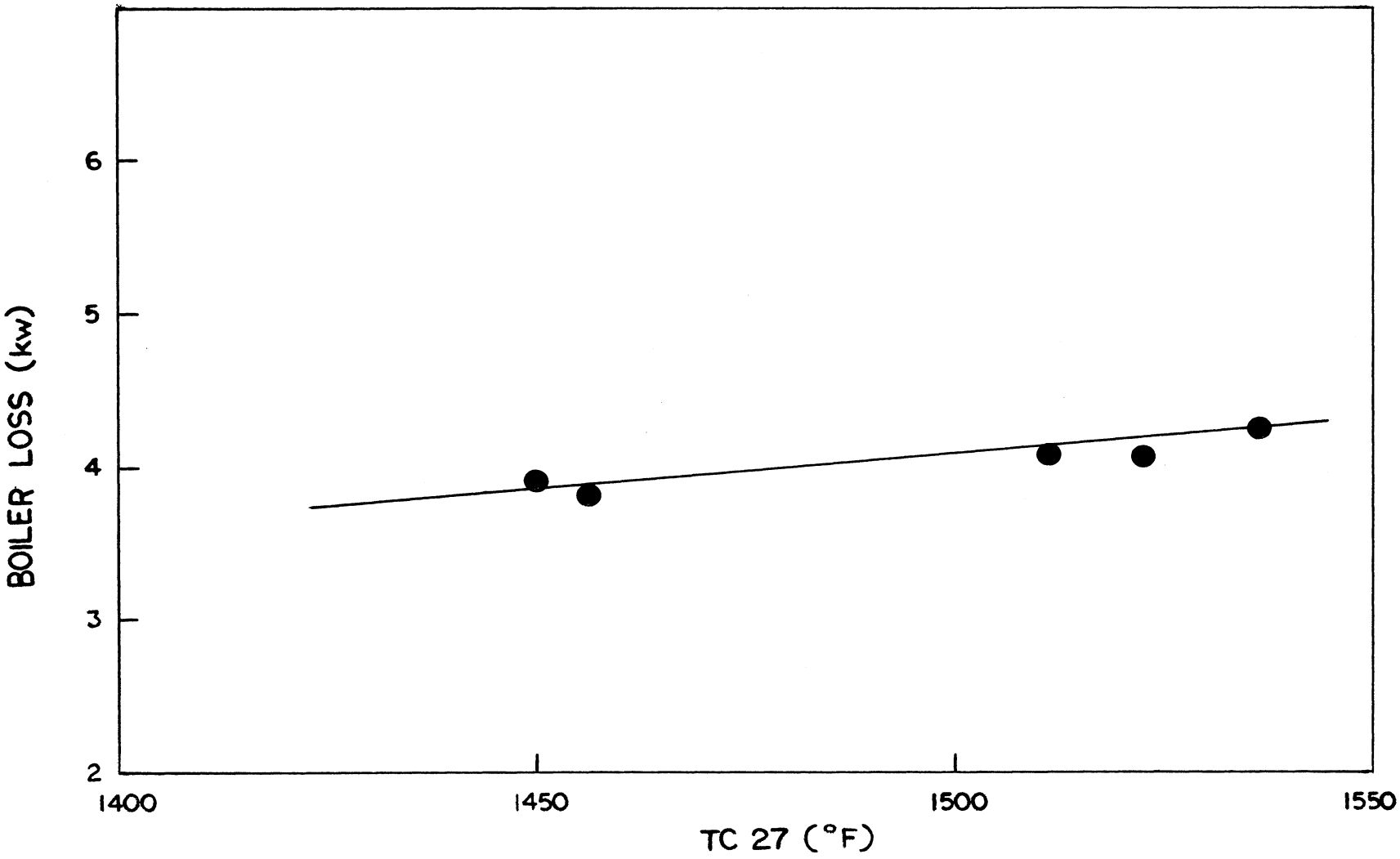

Figure 115 Boiler Loss Calibration

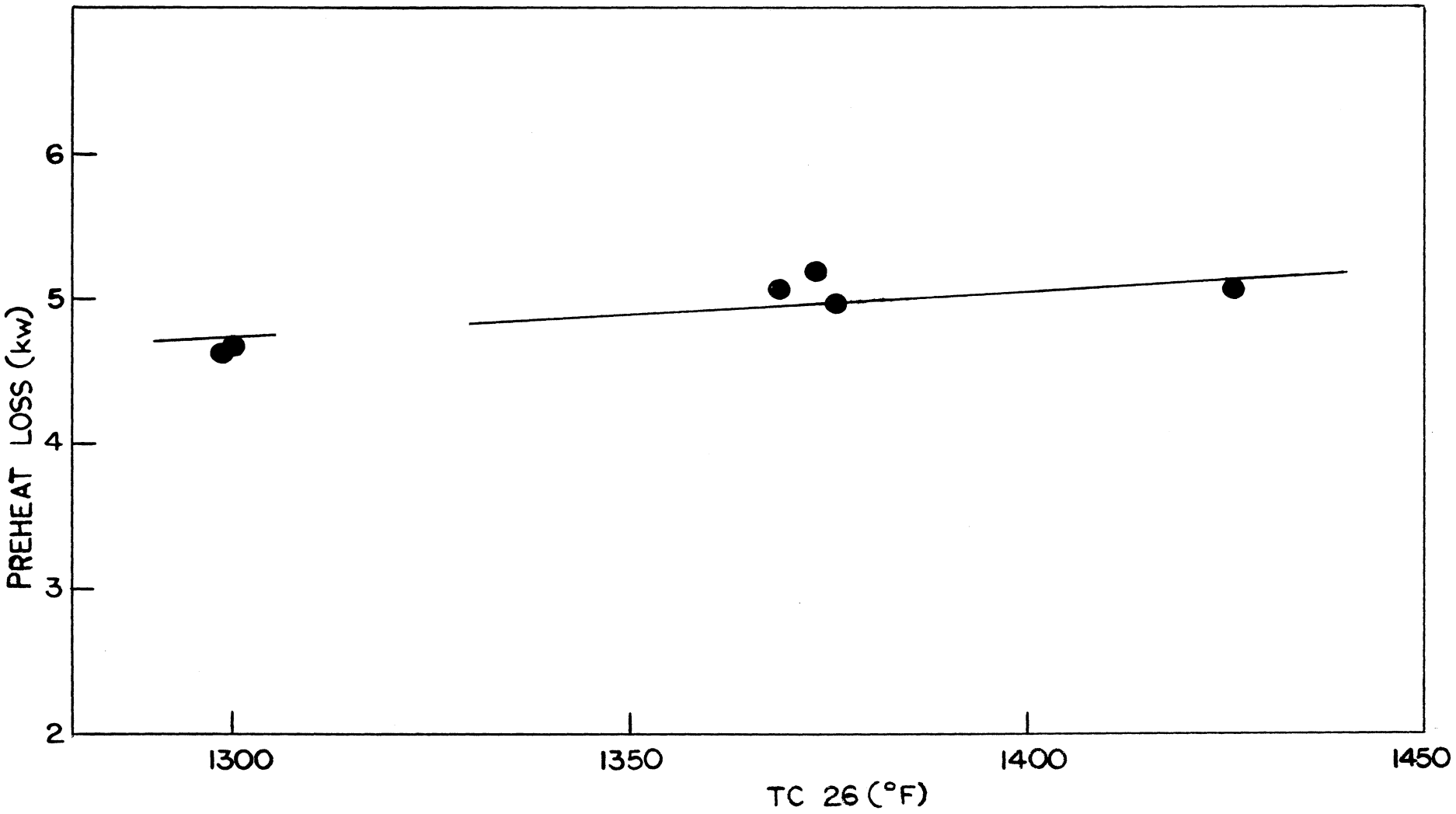

Figure 116 Preheat Loss Calibration

the potassium outlet, TC 29.

It would have been useful to have a measurement of the wall temperature and thus obtain a direct determination of the condensing heat transfer coefficient. However, the tube wall was too thin to permit placement of a thermocouple. The measurement of the electrical resistance of the tube wall was impractical because of the difficulty of insulating the electrical leads from the walls in the high temperature liquid and vapor metal environment. The thin wall was necessitated by the requirements of operating over a wide range of heat fluxes at a particular temperature level while still maintaining a reasonably low temperature difference between the condensate film and the potassium.

A 21-inch claming section before the heat transfer section allowed the flow to develop before entering the zone of heat transfer. It is developed in the sense that any flow pattern should have reasonably arrived at a "steady" pattern in an L/D of 42. "Steady" as used here includes the pulsating type flows illustrated by the flowmeter readings shown in Figure 99. The pulsing occurred in all of the two phase operations with the largest pulsation occurring at the higher qualities.

RESULTS

The two phase potassium heat transfer coefficient varied from 4020 to 8850 BTU/hr ft^2 °F in the medium quality range. The principal cause of the variation appears to be the heat flux as shown in Figure 117. Note that for the quality range studied the effect of quality and mass velocity can not be determined.

The low quality heat transfer coefficients were essentially constant and varied from 3040 to 3700 BTU/hr ft^2. Since the flux was held reasonably constant, this is in agreement with the conclusions drawn from the medium quality runs.

Figure 118 is a plot of the heat flux versus $(T_w - T_{sat})$. T_{sat} was assumed to be TC 29 for this investigation. A comparison of the ΔT's observed in this investigation with those of other investigators showed reasonable agreement.

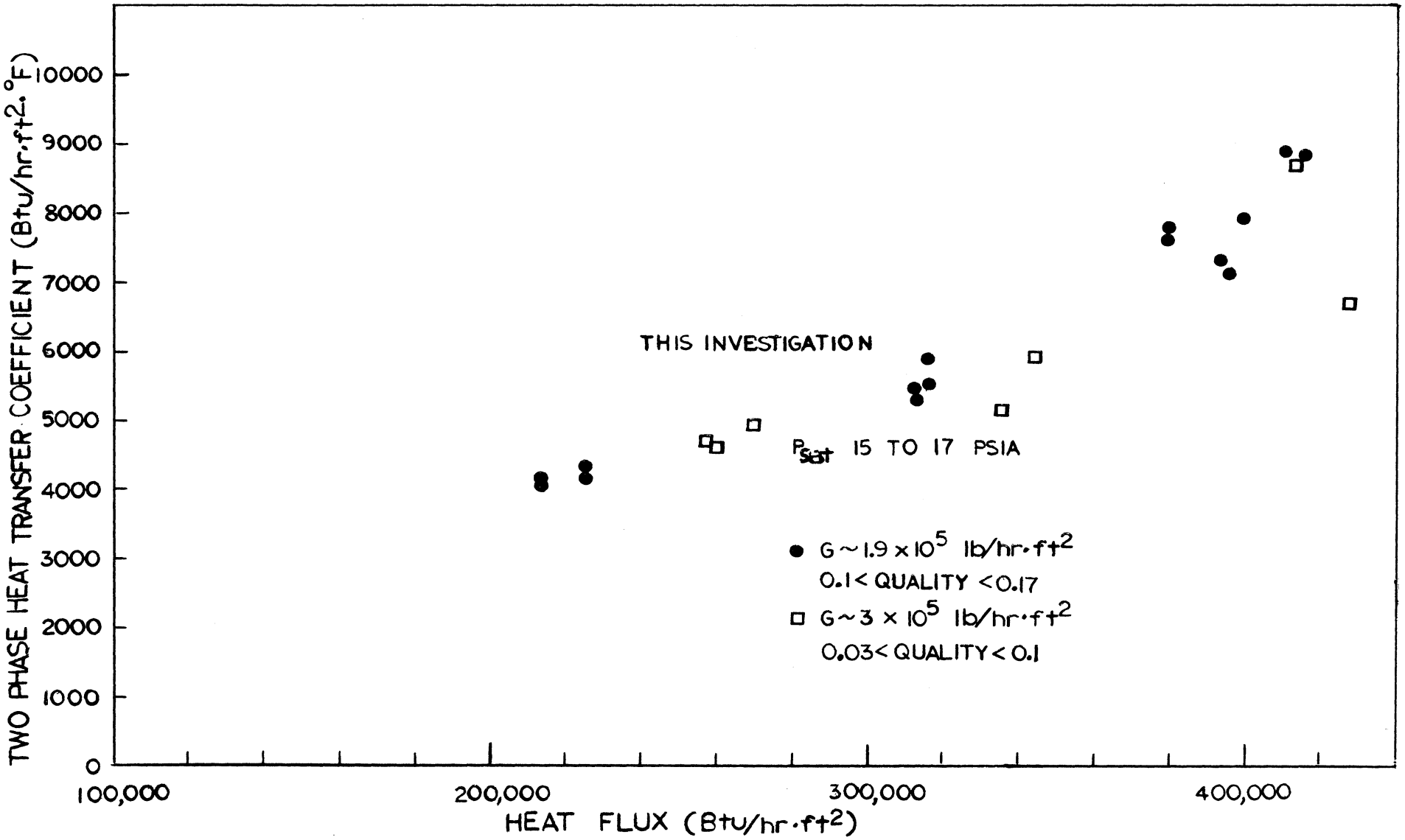

Figure 117 Two Phase Heat Transfer Characteristics

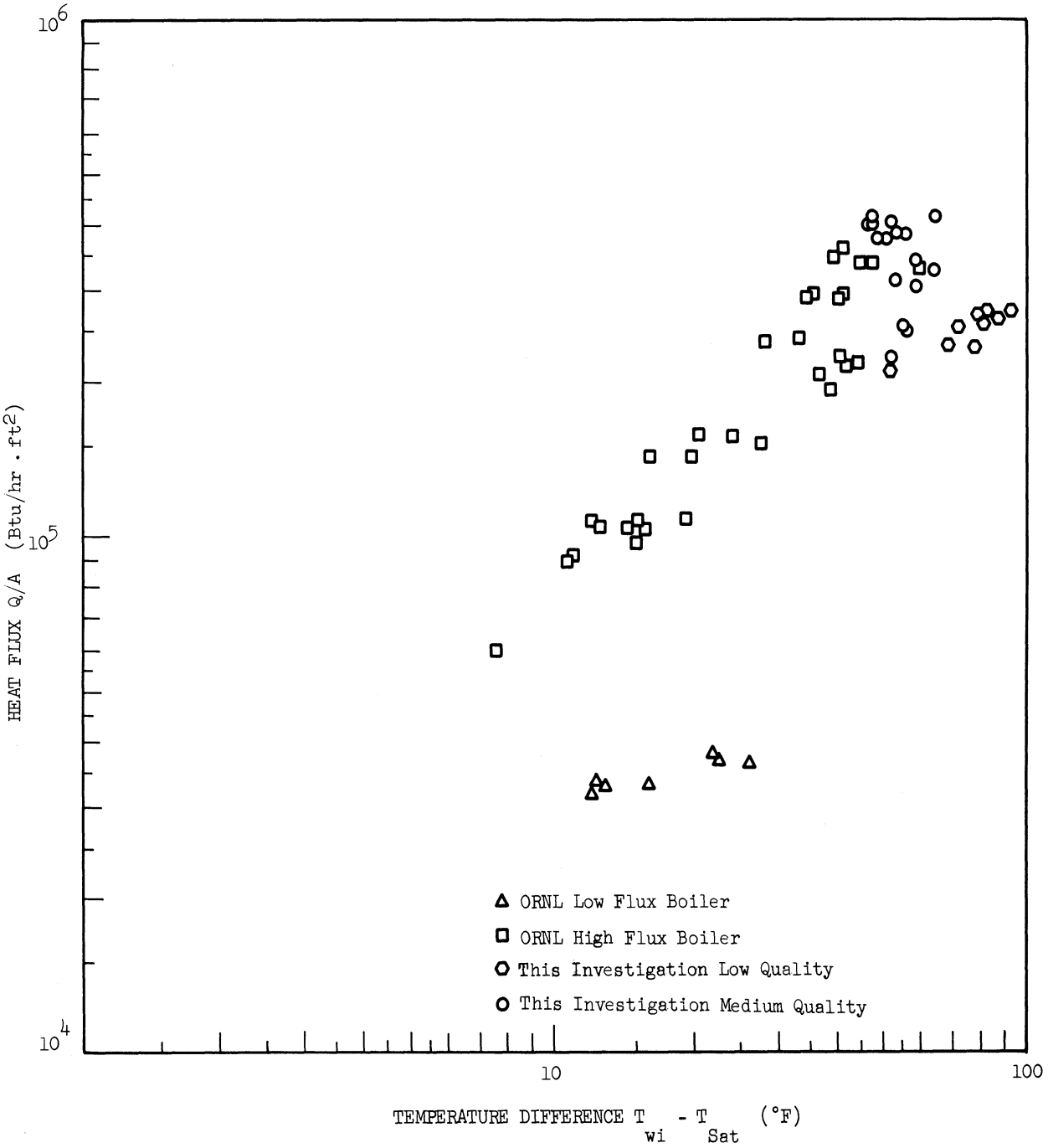

Figure 118 Heat Flux Versus Temperature Difference

LIST OF APPENDICES

		Page
A	Heat Loss Calibration for Film Boiling Apparatus	230
B	Film Boiling Data	231
C	Nucleate Boiling Data	234
D	Preliminary Film Boiling Data	236
E	Treatment of Data - Film Boiling	238
F	Physical Properties of Potassium	242
G	Calculation of Effective Thermal Conductivity of Potassium Vapor	244
H	Calibration of Thermocouples	248
I	Data for Boiling Mercury under High Gravity	251
J	Table A - Experimental Condensing Data - Barry	255
J	Table B - Experimental Condensing Data - Gahman, Sartor and Balzhiser	257
K	The Potassium Film Coefficient	258
L	Treatment of Data - Condensing	263
M	Error Analysis - Condensing	266
N	Pressure Drop Data for 92% Potassium and 8% Sodium and Pure Potassium Runs	273
O	Average Per Cent Deviation in Properties Between Pure Potassium and Mixture Containing 8% by Weight Sodium over the Temperature Range 900-1400°F	279
P	Results of the 1963 Void Fraction Studies for 92% K, 8% Na	280
Q	Summary of Results on Potassium Boiling - ORNL	282
R	Uncertainty in Quality Determination	284
S	Summary of Results on Two-Phase Potassium Heat Transfer	289

APPENDIX A

Heat Loss Calibration for Film Boiling Apparatus

Main Heater Power (Watts)	Guard Heater Power (Watts)	Bottom Plate Temperatures (°F)			Top Plate Temperatures (°F)			Outer Tube Wall Temperatures (°F)		
		TC1	TC3	TC5	TC2	TC4	TC6	TC8	TC9	TC10
24	12	462	464	452	467	457	449	451	460	455
53	184	750	751	733	754	748	730	739	752	743
70	92	997	997	972	997	992	972	979	995	980
80	184	1224	1225	1195	1222	1225	1195	1210	1227	1211
92	254	1366	1368	1335	1367	1364	1336	1349	1369	1351
95	288	1418	1419	1385	1418	1415	1386	1400	1420	1400
104	288	1424	1425	1389	1423	1421	1391	1403	1424	1403
110	348	1526	1529	1490	1526	1524	1493	1506	1526	1506
113	374	1576	1579	1538	1576		1541	1554	1575	1553
120	428	1632	1634	1592	1632		1596	1607	1628	1605

APPENDIX B

FILM BOILING DATA

Main Heater Power (Watts)	Guard Heater Power (Watts)	Pressure (mm Hg)	Liquid Temperature (°F)	Bottom Plate Temperature (°F)			Top Plate Temperature (°F)			Outer Tube Wall Temperature (°F)		
			TC7	TC1	TC3	TC5	TC2	TC4	TC6	TC8	TC9	TC10
221.	428	2	718	1494	1495	1436	1474		1439	1445	1470	1435
256	428	2	717	1545	1544	1481	1520		1486	1492	1518	1481
270	407	2	718	1576	1575	1509	1548		1514	1517	1542	1505
296	400	2	720	1634	1631	1559	1600		1565	1568	1597	1555
270	407	2	728	1622	1619	1549	1586		1560	1564	1588	1546
242	400	2	721	1530	1532	1469	1506	1506	1474	1482	1508	1470
228	414	2	722	1497	1498	1436	1475	1474	1441	1448	1474	1438
208	414	2	722	1455	1456	1400	1436	1434	1402	1408	1432	1400
192	407	2	719	1417	1420	1367	1401	1398	1367	1375	1399	1369
180	407	2	718	1391	1393	1343	1376	1373	1343	1351	1375	1346
165	414	2	718	1356	1359	1313	1344	1340	1312	1322	1343	1317
154	421	2	714	1334	1337	1292	1323	1320	1293	1305	1325	1300
157	449	2	725	1375	1377	1331	1364	1361	1333	1344	1366	1338
143	421	2	720	1299	1301	1260	1289	1286	1260	1271	1291	1268
108	414	2	728	1253	1255	1218	1245	1243	1220	1234	1251	1230
120	414	2	718	1260	1262	1225	1252	1249	1226	1239	1254	1236
108	393	2	723	1234	1237	1200	1227	1225	1202	1215	1231	1212
108	367	2	720	1208	1211	1175	1201	1198	1175	1190	1207	1187
106	335	2	721	1176	1179	1144	1170	1167	1143	1157	1172	1155
106	317	2	719	1164	1166	1131	1158	1155	1130	1141	1160	1140
106	288	2	718	1132	1135	1100	1127	1122	1096	1107	1124	1107
106	293	2	723	1133	1136	1099	1127	1122	1098	1111	1129	1110

APPENDIX B (Continued)

Main Heater Power (Watts)	Guard Heater Power (Watts)	Pressure (mm Hg)	Liquid Temperature (°F)	Bottom Plate Temperature (°F)			Top Plate Temperature (°F)			Outer Tube Wall Temperature (°F)		
			TC7	TC1	TC3	TC5	TC2	TC4	TC6	TC8	TC9	TC10
106	265	2	732	1113	1117	1083	1109	1104	1082	1090	1110	1090
106	243	2	733	1103	1105	1067	1097	1097	1064	1071	1093	1072
106	233	2	731	1053	1055	1021	1046	1040	1017	1024	1043	1024
106	228	2	728	1034	1036	1004	1027	1022	1001	1010	1028	1009
103	223	2	725	1020	1021	988	1013	1008	985	992	1008	990
103	218	2	724	1008	1009	976	1000	995	973	983	997	980
103	213	2	724	984	985	952	976	968	950	961	969	952
221	414	50	983	1522	1519	1456	1499	1497	1464	1470	1498	1456
259	400	50	983	1603	1598	1532	1579		1540	1544	1570	1529
259	442	50	983	1655	1651	1585	1630		1594	1598	1624	1584
263	471	50	986	1681	1676	1610	1656		1620	1624	1650	1610
234	471	50	986	1635	1632	1569	1612		1578	1583	1608	1568
221	471	50	986	1600	1598	1537	1580		1546	1552	1577	1537
208	471	50	986	1560	1557	1498	1539		1508	1515	1539	1500
208	442	50	985	1499	1496	1438	1479	1478	1448	1456	1481	1441
208	414	50	984	1484	1481	1422	1464	1461	1430	1437	1463	1422
208	387	50	983	1439	1436	1377	1419	1416	1382	1387	1416	1375
278	414	50	983	1688	1681	1614	1659		1622	1624	1653	1610
245	428	61	1011	1686	1680	1617	1662		1624	1627	1654	1615
263	414	62	1013	1701	1695	1629	1676		1636	1639	1667	1626
263	414	75	1035	1707	1701	1636	1682		1643	1646	1674	1634
263	414	88	1052	1713	1707	1642	1690		1649	1653	1680	1642
263	414	100	1070	1720	1714	1650	1697		1657	1661	1688	1650

APPENDIX B (Continued)

Main Heater Power (Watts)	Guard Heater Power (Watts)	Pressure (mm Hg)	Liquid Temperature (°F)	Bottom Plate Temperature (°F)			Top Plate Temperature (°F)			Outer Tube Wall Temperature (°F)		
			TC7	TC1	TC3	TC5	TC2	TC4	TC6	TC8	TC9	TC10
106	265	2	732	1113	1117	1083	1109	1104	1082	1090	1110	1090
106	243	2	733	1103	1105	1067	1097	1097	1064	1071	1093	1072
106	233	2	731	1053	1055	1021	1046	1040	1017	1024	1043	1024
106	228	2	728	1034	1036	1004	1027	1022	1001	1010	1028	1009
103	223	2	725	1020	1021	988	1013	1008	985	992	1008	990
103	218	2	724	1008	1009	976	1000	995	973	983	997	980
103	213	2	724	984	985	952	976	968	950	961	969	952
221	414	50	983	1522	1519	1456	1499	1497	1464	1470	1498	1456
259	400	50	983	1603	1598	1532	1579		1540	1544	1570	1529
259	442	50	983	1655	1651	1585	1630		1594	1598	1624	1584
263	471	50	986	1681	1676	1610	1656		1620	1624	1650	1610
234	471	50	986	1635	1632	1569	1612		1578	1583	1608	1568
221	471	50	986	1600	1598	1537	1580		1546	1552	1577	1537
208	471	50	986	1560	1557	1498	1539		1508	1515	1539	1500
208	442	50	985	1499	1496	1438	1479	1478	1448	1456	1481	1441
208	414	50	984	1484	1481	1422	1464	1461	1430	1437	1463	1422
208	387	50	983	1439	1436	1377	1419	1416	1382	1387	1416	1375
278	414	50	983	1688	1681	1614	1659		1622	1624	1653	1610
245	428	61	1011	1686	1680	1617	1662		1624	1627	1654	1615
263	414	62	1013	1701	1695	1629	1676		1636	1639	1667	1626
263	414	75	1035	1707	1701	1636	1682		1643	1646	1674	1634
263	414	88	1052	1713	1707	1642	1690		1649	1653	1680	1642
263	414	100	1070	1720	1714	1650	1697		1657	1661	1688	1650

APPENDIX C

NUCLEATE BOILING DATA

Main Heater Power (Watts)	Guard Heater Power (Watts)	Pressure (mm Hg)	Liquid Temperature (°F)	Bottom Plate Temperature (°F)			Top Plate Temperature (°F)			Outer Tube Wall Temperature (°F)		
			TC7	TC1	TC3	TC5	TC2	TC4	TC6	TC8	TC9	TC10
162	0	2	603	640	640	624	621	617	615	621	633	622
106	0	2	674	690	689	677	678	676	672	681	686	682
714	0	1	676	872	886	832	735		771	770	809	773
738	0	1	670	864	877	824	726		763	764	801	768
441	0	1	655	768	775	744	690		708	712	732	711
884	0	1	703	937	948	883	769		815	816	853	817
205	0	2	695	724	724	707	707	705	700	708	716	709
281	0	2	705	771	774	749	730		730	737	752	738
366	0	2	711	800	804	773	740		748	753	771	753
446	0	2	718	826	828	795	752		764	769	790	769
545	0	2	726	864	866	826	770		788	792	817	791
643	0	2	733	898	900	855	784		808	812	840	812
743	0	2	740	929	930	879	795		826	830	861	830
344	0	709	1381	1450	1451	1407	1409		1397	1406	1424	1404
432	0	659	1368	1455	1456	1408	1402		1393	1400	1422	1400
510	0	684	1376	1481	1483	1432	1415		1409	1416	1440	1416
604	0	704	1381	1508	1511	1452	1427		1425	1430	1458	1430
761	0	728	1387	1549	1552	1482	1445		1449	1452	1481	1451
626	0	707	1379	1513	1518	1453	1430		1427	1432	1460	1437
743	0	721	1384	1544	1550	1478	1442		1446	1446	1475	1444
856	0	736	1389	1573	1577	1498	1454		1463	1464	1492	1460

APPENDIX C (continued)

Main Heater Power (Watts)	Guard Heater Power (Watts)	Pressure (mm Hg)	Liquid Temperature (°F)	Bottom Plate Temperature (°F)			Top Plate Temperature (°F)			Outer Tube Wall Temperature (°F)		
			TC7	TC1	TC3	TC5	TC2	TC4	TC6	TC8	TC9	TC10
1008	0	751	1394	1606	1600	1525	1466		1482	1479	1506	1474
805	0	730	1384	1557	1561	1486	1449		1456	1460	1482	1454
696	0	717	1381	1530	1532	1466	1438		1440	1445	1467	1440
582	0	724	1384	1504	1508	1449	1430		1426	1434	1454	1429
485	0	723	1384	1479	1480	1430	1420		1413	1422	1440	1420
418	0	708	1378	1455	1453	1411	1407		1397	1453	1470	1452
285	0	640	1357	1409	1406	1370	1378		1365	1377	1392	1374
214	0	602	1269	1327	1323	1283	1304	1304	1284	1295	1313	1290
352	0	680	1373	1440	1440	1397	1400		1388	1397	1412	1394
127	0	707	1380	1464	1466	1417	1414		1404	1412	1428	1408
535	107	700	1377	1486	1490	1434	1422		1414	1422	1440	1418

APPENDIX D

PRELIMINARY FILM BOILING DATA

Main Heater Power (Watts)	Pressure (mm Hg)	Liquid Temperature (°F)	Bottom Plate Temperature (°F)			Top Plate Temperature (°F)			1/2" Radius Calculations		
			1/2" radius	1" radius	1 1/2" radius	1/2" radius	1" radius	1 1/2" radius	q/A (Btu/hr-ft^2)	ΔT (°F)	h (Btu/hr-ft^2-°F)
419	N.A.	685	1565	1562	1556	1551	1535	N.A.	6,300	860	7.3
419	"	684	1568	1564	1553	1552	1536	"	6,600	863	7.6
388	"	693	1487	1471	1457	1470	1453	"	8,000	775	10.3
375	"	691	1488	1480	1465	1474	1460	"	6,500	781	8.3
403	"	684	1593	1587	1581	1577	1566	"	7,100	890	8.0
479	N.A.	815	1560	1554	1554	1549	1534	N.A.	4,800	730	6.6
493	"	814	1564	1557	1555	1552	1534	"	4,700	734	6.4
451	"	814	1482	1469	1461	1468	1447	"	5,900	650	9.1
457	"	814	1470	1458	1455	1460	1439	"	4,500	643	7.0
470	"	814	1506	1493	1492	1491	1471	"	6,700	673	10.0
476	"	814	1602	1590	1588	1573	1566	"	13,300	759	17.5
476	"	815	1636	1625	1618	1614	1598	"	10,700	795	13.5
476	"	815	1614	1603	1599	1594	1576	"	9,300	775	12.0
476	"	814	1592	1573	1572	1569	1553	"	10,300	753	13.7
476	"	814	1596	1578	1576	1573	1558	"	10,600	757	14.0
476	"	814	1609	1594	1592	1587	1571	"	10,500	769	13.7
467	N.A.	749	1669	1658	1654	1645	1631	N.A.	11,400	891	12.8
411	"	744	1552	1536	1534	1530	1518	"	10,000	785	12.7
419	"	742	1558	1543	1539	1536	1523	"	10,200	792	12.9
473	"	742	1677	1665	1663	1655	1639	"	10,300	907	11.4
452	"	741	1685	1673	1670	1666	1648	"	9,100	919	9.9
435	"	740	1658	1644	1640	1641	1620	"	7,900	895	8.8
342	2	773	1581	1572	1571	1564	1552	N.A.	7,800	788	9.9
319	2	773	1499	1489	1490	1484	1473	"	6,800	708	9.6
298	2	773	1462	1451	1453	1446	1434	"	6,800	670	10.2
277	2	773	1434	1425	1428	1422	1411	"	5,700	646	8.8

APPENDIX D (continued)

Main Heater Power (Watts)	Pressure (mm Hg)	Liquid Temperature (°F)	Bottom Plate Temperature (°F) 1/2" radius	1" radius	1 1/2" radius	Top Plate Temperature (°F) 1/2" radius	1" radius	1 1/2" radius	1/2" Radius Calculations q/A (Btu/hr-ft^2)	ΔT (°F)	h (Btu/hr-ft^2-°F)
348	1	727	1519	1506	1506	1502	1490	N.A.	7,500	773	9.7
396	"	"	1685	1675	1675	1667	1653	"	8,600	935	9.2
354	"	"	1597	1588	1587	1581	1568	"	7,300	850	8.6
314	"	"	1516	1508	1506	1501	1489	"	6,500	770	8.4
314	"	"	1502	1495	1493	1489	1477	"	5,600	759	7.4
298	"	"	1483	1475	1476	1471	1460	"	5,500	741	7.4
302	"	"	1466	1459	1458	1454	1443	"	5,200	725	7.2
282	"	"	1472	1465	1463	1459	1448	"	5,600	728	7.7
267	"	"	1360	1353	1355	1352	1342	"	3,700	623	5.9
256	"	"	1348	1340	1342	1339	1329	"	3,800	610	6.2
256	"	"	1443	1434	1442	1431	1425	"	5,100	702	7.3
208	"	"	1430	1428	1431	1420	1416	"	4,500	691	6.5
145	"	"	1371	1373	1383	1365	1365	"	2,400	636	3.8
174	"	"	1152	1145	1145	1142	1138	"	4,400	417	10.5
236	"	"	1480	1477	1480	1468	1463	"	5,200	739	7.0
204	"	"	1403	1400	1402	1392	1387	"	4,800	661	7.3
204	"	"	1393	1390	1392	1381	1376	"	4,800	651	7.4
186	"	"	1264	1261	1264	1256	1252	"	3,400	528	6.4
251	"	"	1226	1216	1214	1217	1206	"	3,600	489	7.4
409	2	750	1543	1537	1539	1530	1514	"	6,200	775	8.0
267	N.A.	724	1534	1530	1540	1515	1514	"	11,400	789	14.5
364	1	717	1434	1420	1421	1414	1408	"	8,800	700	12.6
382	"	714	1570	1562	1565	1550	1544	"	9,300	834	9.0
371	"	714	1577	1569	1570	1557	1550	"	9,100	841	10.8
347	"	713	1536	1529	1528	1518	1510	"	8,300	804	10.3
314	"	710	1428	1419	1417	1410	1402	"	7,800	700	11.1
318	"	711	1390	1378	1376	1372	1365	"	7,700	663	11.6
318	"	710	1372	1357	1358	1354	1348	"	7,700	646	11.9
342	"	714	1404	1387	1390	1384	1380	"	8,300	671	12.4
342	"	711	1451	1440	1442	1433	1426	"	8,000	722	11.1
382	"	713	1588	1580	1582	1570	1562	"	8,400	855	9.8
382	"	714	1607	1599	1603	1588	1579	"	8,900	871	10.2
369	N.A.	655	1569	1562	1565	1550	1542	"	8,700	892	9.7

APPENDIX E

TREATMENT OF DATA

Given: Power to main heater P, watts
Temperature of bottom 1/2-inch radius thermocouple in boiling plate TC1
Temperature of top 1/2-inch radius thermocouple in boiling plate TC2
Temperature of liquid TC7

1. Heat flux, q/A BTU/hr-sq ft

$$q/A = k \frac{TC1 - TC2}{x_1 - x_2} \qquad \text{(E-1)}$$

where k = thermal conductivity of type 316 stainless steel evaluated at $\frac{TC1 + TC2}{2}$ and obtained from Figure E-1

x_1 = vertical distance between TC1 and boiling surface = .434 inch

x_2 = vertical distance between TC2 and boiling surface = .072 inch

2. Temperature difference, ΔT °F

$$\Delta T = TC2 - \frac{.072}{.362} (TC1 - TC2) - TC7 \qquad \text{(E-2)}$$

.072 = vertical distance between TC2 and boiling surface in inches

.0362 = vertical distance between TC1 and TC2 in inches

3. Heat transfer coefficient, h BTU/hr-sq ft-°F

$$h = \frac{q/A}{\Delta T} \qquad \text{(E-3)}$$

4. Average heat flux, $(q/A)_{avg}$ BTU/hr-sq ft-°F

$$(q/A)_{avg} = \frac{(P-P_L)\ 3.412}{A} \qquad (E-4)$$

P_L = heat loss evaluated at TC1 and obtained from Figure E-2, watts

3.412 = conversion factor, watts to BTU/hr

A = area of boiling surface = .0491 sq ft

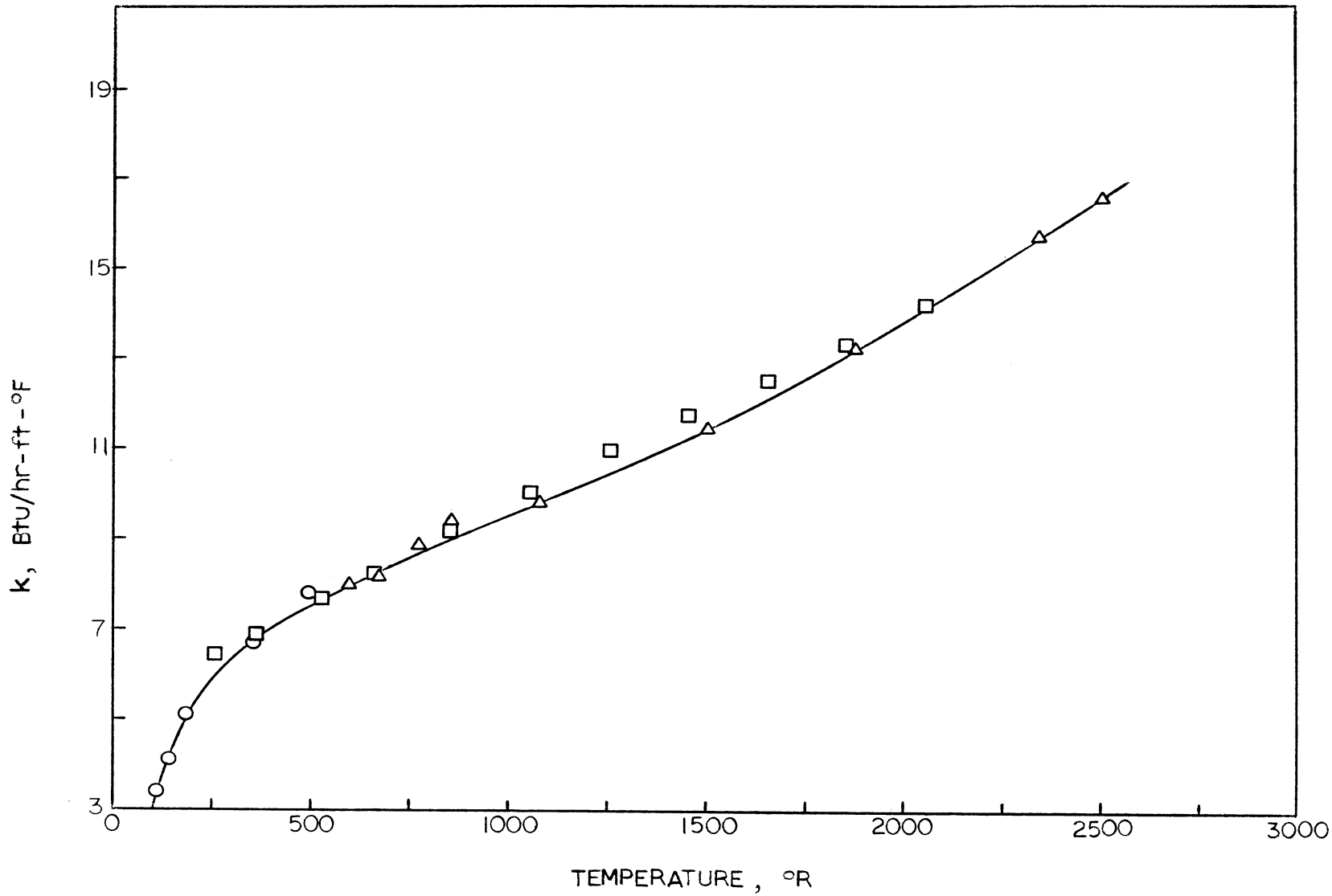

Figure E-1 Thermal Conductivity of Type 316 Stainless Steel (70)

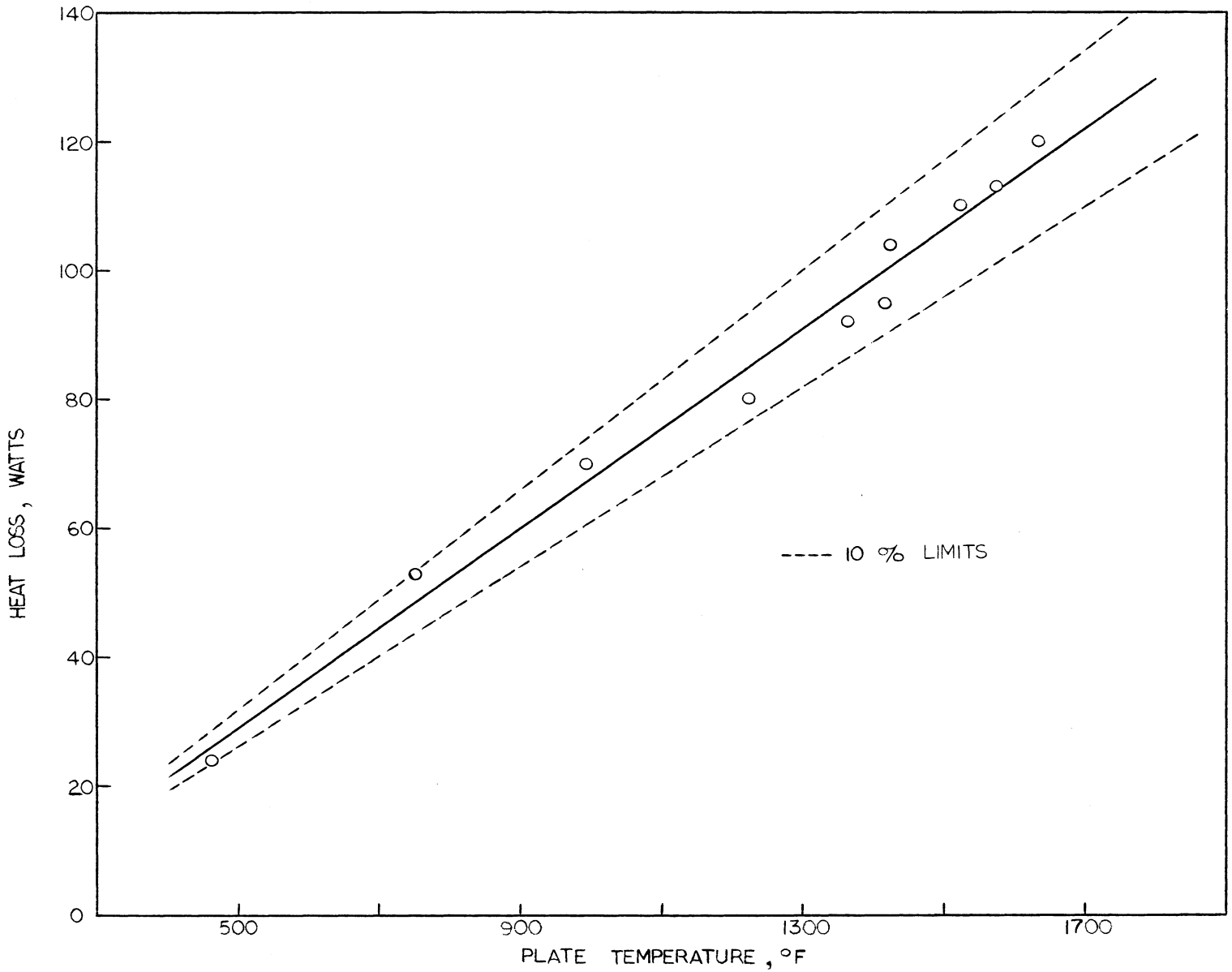

Figure E-2 Heat Loss Calibration

APPENDIX F

PHYSICAL PROPERTIES OF POTASSIUM

The vapor volumes of potassium as a function of temperature and pressure are tabulated in BATT-4673 (103) and the vapor density was obtained by taking the reciprocal of the vapor volume.* The surface tension was taken from Coe (45) and the vapor thermal conductivity and viscosity were obtained from Weatherford (178).

The thermal conductivity of superheated potassium vapor was calculated by taking the value for saturated conditions and employing Figure 7-3 in Reid and Sherwood (148). The viscosity of the vapor was assumed to be independent of pressure at low pressures and thus the temperature dependence was obtained by using the data for saturated conditions. The physical properties for potassium at 0.1 atm are summarized in Table F-1.

*Values for the liquid density, latent heat of vaporization, and vapor specific heat were also obtained from this report.

TABLE F-1

PHYSICAL PROPERTIES OF POTASSIUM AT 0.1 ATM

T °R	ρ_v lb/ft^3	k_v Btu/ft-hr-°F	C_{pv} Btu/lb-°F
1500	.00376	.00723	.1987
1600	.00348	.00772	.2060
1700	.00325	.00820	.2148
1800	.00306	.00869	.2172
1900	.00289	.00917	.2150
2000	.00275	.00965	.2103

Saturation temperature = 1500°R

ρ_l = 44.07 lb/ft^3 (1500°R)

L = 887.4 Btu/lb (1500°R)

σ = .0030 lb/ft

APPENDIX G

CALCULATION OF EFFECTIVE THERMAL CONDUCTIVITY OF POTASSIUM VAPOR

It has been found experimentally that the heat transfer rate to a gas undergoing a chemical reaction may be many times the rate predicted using accepted correlations and a weight average of the physical properties of the gas. This increase has been attributed to a diffusional mechanism associated with the chemical reaction. Thus, heat is transferred away from a wall by ordinary molecular collisions and by molecular diffusion associated with chemical reaction. The usual method of treating the effect on the heat transfer coefficient is to define an effective thermal conductivity:

$$k_{eff} = k_f + k_r \qquad \text{(G-1)}$$

where k_f is the thermal conductivity in the "frozen" system which has the equilibrium composition at a given temperature but is not undergoing a reaction and k_r is the contribution due to the reaction.

The only type of reaction which has been treated extensively in the literature has been the "equilibrium" reaction in which the reaction rate is so high that the gas mixture may be assumed to have its equilibrium composition instantaneously after a change in temperature. The thermal conductivity due to reaction for this case is given by:

$$k_r = D_{12}\,\rho\,\frac{\alpha(1-\alpha^2)}{2\,RM}\left(\frac{\Delta H_r}{T}\right)^2 \qquad \text{(G-2)}$$

For the reaction

$$2K = K_2 \qquad \text{(G-3)}$$

the degree of dissociation, α, can be expressed in terms of the mole fraction of K_2

$$y_{K_2} = \frac{1 - \alpha}{1 + \alpha} \qquad (G\text{-}4)$$

Equation (G-2) can then be written as

$$k_r = D_{12}\, \rho\, \frac{y_{K_2}(1 - y_{K_2})}{RM\,(1 + y_{K_2})^2} \left(\frac{\Delta H_r}{T}\right)^2 \qquad (G\text{-}5)$$

Assuming the ideal gas law, the gas density is given by

$$\rho = \frac{PM}{RT} \qquad (G\text{-}6)$$

substituting Equation (G-6) into Equation (G-5) gives

$$k_r = 0.692\, D_{12}\, \rho\, \frac{y_{K_2}(1 - y_{K_2})}{(1 + y_{K_2})^2} \frac{\Delta H_r^2}{T^3} \qquad (G\text{-}7)$$

Equation (G-7) can be used to calculate the thermal conductivity due to reaction provided that the composition of the gas, the binary diffusion coefficient, and the heat of reaction can be determined.

Since Weatherford has tabulated the equilibrium molecular weight of potassium vapor as a function of temperature for saturated conditions, it is possible to calculate the vapor composition from this data. Using fugacity charts, the equilibrium constant for the reaction described by Equation (G-3)

can be determined. Since the equilibrium constant is a function of temperature only, it can then be used to calculate y_K and y_{K_2} at various constant pressures.

Several methods are available for calculating binary diffusion coefficients: the Arnold equation, the Gilliland equation, the Slattery equation, and the Hirshfelder equation. These equations are presented and discussed by Reid and Sherwood (148) and the hirschfelder equation was arbitrarily chosen.

Values for the heat of formation of K and K_2 at 25°C are tabulated in Rossini (155). Using these values and the enthalpy differences for the ideal monatomic and diatomic species tabulated in Weatherford, the heat of reaction as a function of temperature can be calculated.

The method for calculating the frozen thermal conductivity was presented in Appendix F. The results are summarized in Figure G-1 for a pressure of 0.1 atm.

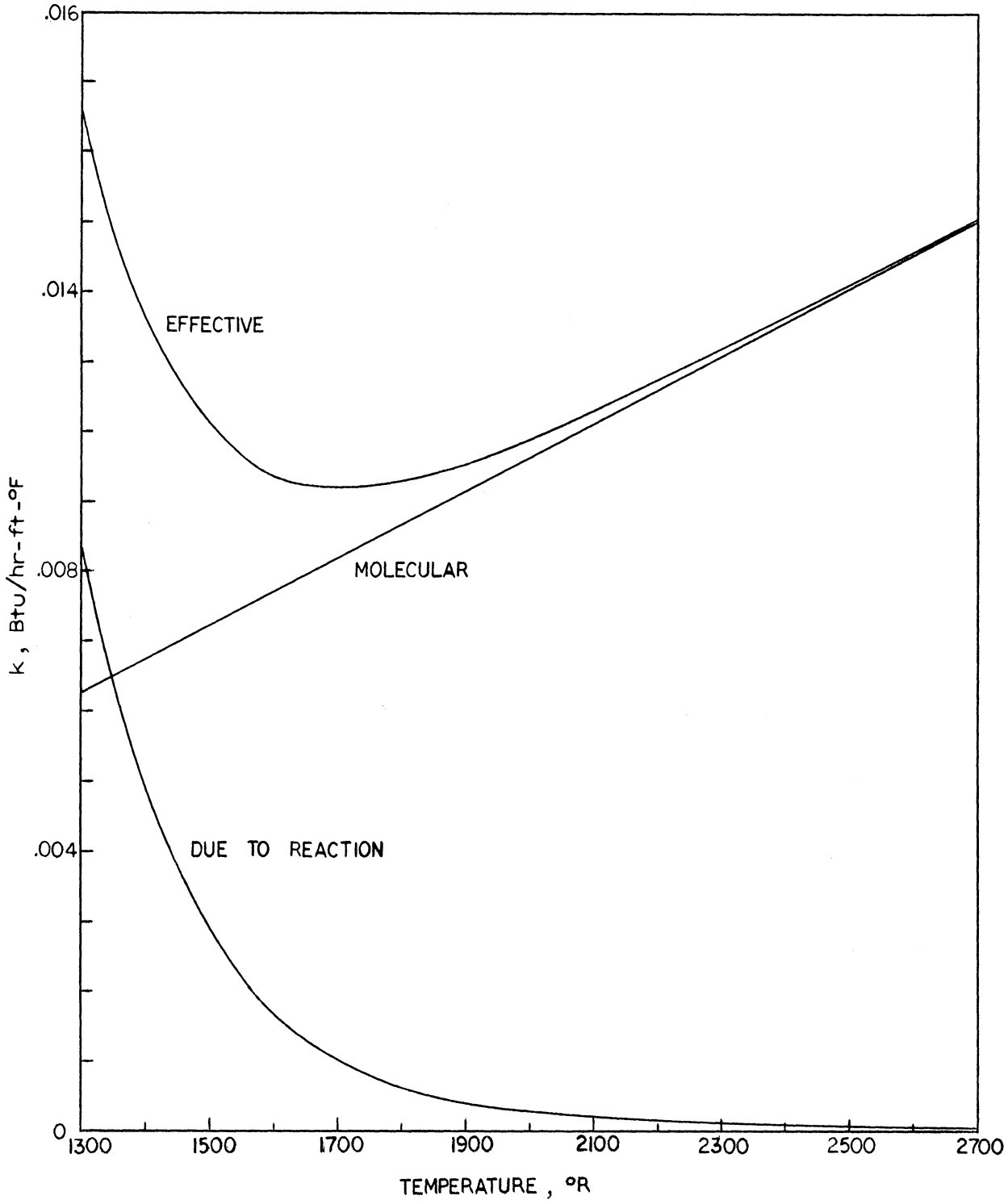

Figure G-1 Effective Thermal Conductivity of Potassium Vapor at 0.1 Atm.

APPENDIX H

CALIBRATION OF THERMOCOUPLES

The calibration of the 1/16-inch OD by 2-ft long thermocouples used in the boiling plate was carried out in a flanged stainless steel pipe 2-inches OD by 1 3/4-inches ID by 2-ft long. The brass head contained a Conax multi-hole gland for the swaged thermocouples, a Conax MPG gland for the standard thermocouple, and a 1/4-inch tube for evacuation. The standard was a Pt-Pt 10% Rh thermocouple made from 20-gauge wires which had been calibrated by the Bureau of Standards. A copper equilizing block 1 11/16-inches diameter by 2-inches long was used to insure isothermal conditions. The 1/16-inch OD thermocouples were inserted into .065-inch holes to a depth of 3/4-inch. When the thermocouples were calibrated inside of 1/8-inch OD wells, the wells were inserted into the copper block to a depth of 1-inch. The standard was contained in a 3/16-inch OD well which was inserted 1 1/4-inches into the copper equilizing block.

The stainless steel vessel was inserted into a Leeds and Northrup thermocouple checking furnace which has a maximum operating temperature of 1800°F. The vacuum pump was turned on and the power to the furnace adjusted with a rheostat. After steady state conditions were reached, the emf output of the standard and the swaged thermocouples were recorded using a Leeds and Northrup No. 8662 portable precision potentiometer, and the rheostat was reset. Data was obtained while both increasing and decreasing the temperature of the furnace.

A cubic equation was used to express the temperature-emf relationship for each thermocouple. The results of the calibration and a comparison with the theoretical values in the Leeds and Northrup Bulletin 077989, Issue 3,

are presented in Table H-1. The thermocouples T1 and T2 in Table H-1 were calibrated in 1/8-inch OD stainless steel wells whereas the rest of the thermocouples were calibrated without wells.

TABLE H-1

CALIBRATION OF BOILING PLATE THERMOCOUPLES

EMF (mv)	TC1 (°F)	TC2 (°F)	RANGE (°F)	TC3 (°F)	TC4 (°F)	TC5 (°F)	TC6 (°F)	TC7 (°F)	RANGE (°F)	L & N Bulletin 07789 Issue 3 (°F)
2.012	497.4	496.5	0.9							500
2.547	597.0	597.0	0							600
3.103	697.5	697.8	0.3							700
3.677	798.0	798.5	0.5							800
4.264	897.8	898.1	0.3	896.8	896.9	897.1	897.2	898.3	1.5	900
4.868	997.6	997.6	0	999.1	998.4	998.9	999.0	998.7	0.7	1000
5.488	1097.3	1097.0	0.3	1100.4	1099.3	1099.9	1100.0	1098.8	1.6	1100
6.125	1197.2	1196.7	0.5	1201.0	1199.7	1200.4	1200.4	1198.9	2.1	1200
6.773	1296.5	1296.0	0.5	1300.1	1299.0	1299.6	1299.6	1298.1	0.5	1300
7.436	1396.2	1396.1	0.1	1398.7	1398.0	1398.4	1398.5	1397.2	1.5	1400
8.116				1497.5	1497.2	1497.5	1497.5	1496.5	1.0	1500
8.809				1596.3	1596.4	1596.5	1596.6	1595.8	0.8	1600
9.516				1695.7	1696.2	1696.2	1696.2	1695.3	0.9	1700
Average			$\overline{0.3}$						$\overline{1.2}$	
Std. dev. (°F)	0.9	0.4		0.8	1.0	1.1	1.2	0.9		

Appendix I

Data For Boiling Mercury Under High Gravity

Run No.	P Nominal Psia	q/A Btu/HR-FT^2	a/g	$T_{H.S.}$ °F	T_{SAT} H.S. °F	ΔT_{SAT} °F	T_B (TC-3) °F	ΔT_B °F	T_{V1} (TC-4) °F	T_{V2} (TC-5) °F	T_{SAT} F.S. °F	Subc. at H.S. °F	Subc. at F.S. °F
6	80	23,000	1	878.8	872.2	6.6	868.1	10.7	853.4	279.3	871.8	4.1	3.7
7	80	46,900	1	895.8	872.2	23.6	868.8	27.0	857.8	768.8	871.8	3.4	3.0
17	80	18,000	1	1157.3	875.3	282.0	873.7	283.6	—	—	874.9	1.6	1.2
			5	978.2	877.2	101.0	874.8	103.4	—	—	874.9	2.4	0.1
19	80	18,500	1	Film Boiling- Transient									
			5	880.0	880.0	0	869.2	10.8	752.6	392.6	878.0	10.8	8.8
			1	874.1	878.4	-	870.1	4.0	789.6	416.3	878.0	8.3	7.9
20	80	18,000	1	879.2	878.7	0.5	874.1	5.1	805.3	413.9	878.4	4.6	4.3
			10	834.0	881.9	-	828.4	5.6	619.3	380.4	877.8	53.5	49.4
			15	736.3	884.2	-	731.4	4.9	508.7	359.9	877.0	152.8	145.6
21	80	19,500	1	953.7	878.6	75.1	875.7	78.0	855.4	421.2	878.1	2.9	2.4
			5	860.4	879.4	-	850.7	9.7	697.6	380.9	877.3	28.7	26.6
22	80	34,000	1	919.7	877.4	42.3	872.6	47.1	860.3	822.6	877.1	4.8	4.5
			5	903.2	879.3	23.9	875.9	27.3	870.8	687.6	877.1	3.4	1.2
			10	895.2	881.3	13.9	876.4	18.8	870.3	698.9	877.1	4.9	0.7
			15	891.0	882.7	8.3	875.5	15.5	869.0	694.4	876.4	7.2	0.9
			1	914.0	877.4	36.6	871.9	42.1	860.8	835.3	877.1	5.5	5.2
23	80	46,000	1	942.7	877.0	65.7	873.9	68.8	867.0	862.8	876.6	3.1	2.7
			5	909.1	877.6	31.5	874.8	34.3	870.1	863.9	875.5	2.8	0.7
			10	898.6	879.7	18.9	875.0	23.6	867.4	857.4	875.5	4.7	0.5
			15	895.9	881.8	14.1	875.7	20.2	867.4	858.3	875.5	6.1	-0.2
			1	936.0	877.0	59.0	874.0	62.0	871.0	870.8	876.6	3.0	2.6

APPENDIX I

Data For Boiling Mercury Under High Gravity

Run No.	P Nominal Psia	q/A Btu/Hr-Ft^2	a/g	$T_{H.S.}$ °F	T_{SAT} H.S. °F	ΔT_{SAT} °F	T_B (TC-3) °F	ΔT_B °F	T_{V1} (TC-4) °F	T_{V2} (TC-5) °F	T_{SAT} F.S. °F	Subc. at H.S. °F	Subc. at F.S. °F
24	80	61,000	1	919.8	876.1	43.7	874.8	45.0	874.4	875.0	875.8	1.3	1.0
			5	909.9	877.7	32.2	875.3	34.6	874.4	875.0	875.6	2.4	0.3
			10	904.4	879.6	24.8	875.7	28.7	873.9	874.6	875.4	3.9	-0.3
			15	902.4	881.8	20.6	876.4	26.0	873.7	873.9	875.4	5.4	-1.0
			1	919.6	875.8	43.8	873.9	45.7	874.1	874.4	875.4	1.9	1.5
25	80	78,000	1	915.3	874.5	40.8	872.6	42.7	872.1	872.6	874.0	1.9	1.4
			5	915.0	876.2	38.8	874.3	40.7	873.5	874.1	874.0	1.9	-0.3
			10	910.1	879.1	31.0	875.9	34.2	872.6	873.0	874.9	3.2	-1.0
			15	907.8	880.1	27.7	874.8	33.0	871.9	871.9	873.6	5.3	-1.2
26	80	98,300	1	906.2	875.7	30.5	873.5	32.7	873.0	873.7	875.3	2.2	1.8
			5	903.8	876.2	27.6	873.7	30.1	872.4	873.5	874.0	2.5	0.3
			10	903.0	878.4	24.6	874.6	28.4	872.6	873.7	874.0	3.8	-0.6
			15	902.6	880.5	22.1	876.1	26.5	872.6	873.2	874.0	4.4	-2.1
			1	908.9	875.4	33.5	873.5	35.4	873.2	873.5	875.0	1.9	1.5
27	80	32,000	1	1099.9	874.4	225.5	867.4	232.5	857.2	840.7	873.9	7.0	6.5
			1	917.2	874.2	43.0	871.0	46.2	859.0	825.0	873.8	3.2	2.8
			5	911.3	875.0	36.3	872.6	38.7	869.7	692.0	872.8	2.4	0.2
			1	912.3	873.8	38.5	870.1	42.2	857.2	857.2	873.4	3.7	3.3
28	80	32,000	1	899.0	875.0	24.0	872.8	26.2	855.0	782.0	874.6	2.2	1.8
			5	895.1	876.0	19.1	873.9	21.2	869.7	437.0	873.7	2.1	-0.2
			10	885.7	878.0	7.7	873.9	11.8	869.0	360.0	873.7	4.1	-0.2
			15	883.4	880.1	3.3	874.1	9.3	869.0	345.0	873.7	6.0	-0.4
			1	902.6	875.0	27.6	872.8	29.8	855.8	761.0	874.6	2.2	1.8

APPENDIX I

Data For Boiling Mercury Under High Gravity

Run No.	P Nominal Psia	q/A Btu/Hr-Ft^2	a/g	$T_{H.S.}$ °F	T_{SAT} H.S. °F	ΔT_{SAT} °F	T_B (TC-3) °F	ΔT_B °F	T_{V1} (TC-4) °F	T_{V2} (TC-5) °F	T_{SAT} F.S. °F	Subc. at H.S. °F	Subc. at F.S. °F
29	80	60,000	1	909.3	874.9	34.4	873.5	35.8	872.6	873.2	874.5	1.4	1.0
			5	903.6	875.9	27.7	873.7	29.9	872.4	873.2	873.7	2.2	0
			10	899.0	877.9	21.1	874.4	24.6	871.7	871.9	873.6	3.5	-0.8
			15	896.5	880.0	16.5	875.5	21.0	870.6	869.0	873.6	4.5	-1.9
			1	903.1	874.9	28.2	872.8	30.3	872.1	872.6	874.5	2.1	1.7
30	80	100,000	1	910.1	875.0	35.1	873.7	36.4	873.2	874.1	874.6	1.3	0.9
			5	908.9	876.6	32.3	874.1	34.8	873.0	873.9	874.5	2.5	0.4
			10	905.5	878.5	27.0	875.0	30.5	872.6	873.2	874.3	3.5	-0.7
			15	903.8	880.7	23.1	875.5	28.3	872.6	872.6	874.3	5.2	-1.2
			1	909.7	875.2	34.5	873.0	36.7	873.0	872.1	874.9	2.2	1.9
31	20	32,000	1	715.6	705.2	10.4	703.0	12.6	698.2	695.5	704.0	2.2	1.0
			5	714.5	710.0	4.5	705.9	8.6	701.4	698.9	703.5	4.1	-2.4
			10	717.7	715.8	1.9	705.3	12.4	700.1	698.2	703.5	10.5	-1.8
			15	719.7	721.7	-2.0	707.3	12.4	698.7	695.3	703.5	14.4	-3.8
			1	713.3	705.2	8.1	703.0	10.3	698.2	695.3	703.9	2.2	0.9
32	20	60,000	1	720.4	705.6	14.8	703.9	16.5	703.7	703.9	704.5	1.7	0.6
			5	716.5	710.8	5.7	706.6	9.9	704.1	704.1	704.5	4.2	-2.1
			10	721.6	716.6	5.0	708.9	12.7	704.3	704.6	704.3	7.7	-4.6
			15	725.7	722.4	3.3	708.4	17.3	704.3	704.6	704.3	14.0	-4.1
			1	717.3	705.9	11.4	704.6	12.7	704.3	704.3	704.6	1.3	0
35	20	100,000	1	726.7	706.7	20.0	705.9	20.8	705.0	705.3	705.5	0.8	-0.4
			5	723.6	711.7	11.9	707.0	16.6	705.0	705.5	705.2	4.7	-1.8
			10	728.1	717.5	10.6	706.8	21.3	704.6	704.8	705.1	10.7	-1.7
			15	733.7	723.1	10.6	709.8	23.9	704.3	703.9	705.0	13.3	-4.8
			1	720.2	706.6	13.6	705.9	14.3	704.6	704.8	705.4	0.7	-0.5

APPENDIX I

Data For Boiling Mercury Under High Gravity

Run No.	P Nominal Psia	q/A Btu/Hr-Ft^2	a/g	$T_{H.S.}$ °F	T_{SAT} H.S. °F	ΔT_{SAT} °F	T_B (TC-3) °F	ΔT_B °F	T_{V1} (TC-4) °F	T_{V2} (TC-5) °F	T_{SAT} F.S. °F	Subc. at H.S. °F	Subc. at F.S. °F
37	300	34,000	1	1097.5	1091.7	5.6	1086.0	11.5	1072.0	449	1091.5	5.7	5.5
			5	962.4	1090.9	-	952.0	10.4	638	446	1090.1	38.9	38.1
			10	891.5	1086.9	-	881.0	10.5	631	418	1085.4	205.9	204.4
			15	834.5	1081.1	-	823.9	10.6	603	401	1078.6	257.2	254.7
			1	1090.9	1090.3	0.6	1084.9	6.0	1066.5	456	1090.1	5.4	5.2
38	300	63,000	1	1097.4	1091.6	5.8	1089.9	7.5	1076.1	1035	1091.4	1.7	1.5
			5	1097.4	1092.2	5.2	1091.0	6.4	1088.7	772	1091.4	1.2	0.4
			10	1097.8	1093.0	4.8	1091.0	6.8	1088.1	428	1091.4	2.0	0.4
			15	1098.5	1093.8	4.7	1091.3	7.2	1087.5	380	1091.4	2.5	0.1
			1	1097.0	1091.6	5.4	1090.4	6.6	1073.9	1039	1091.4	1.2	1.0
39	300	100,000	1	1099.0	1091.6	7.4	1090.3	8.7	1090.3	1091.0	1091.4	1.3	1.1
			5	1097.9	1092.3	5.6	1090.8	7.1	1089.9	1087.5	1091.6	1.5	0.8
			10	1097.9	1093.1	4.8	1091.0	6.9	1088.8	1078.5	1091.6	2.1	0.6
			15	1098.1	1093.8	4.3	1091.2	6.9	1087.6	1076.5	1091.6	2.6	0.4
			1	1097.4	1091.4	5.7	1090.5	6.9	1090.3	1091.0	1091.6	1.2	1.1
40	300	205,000	1	1099.7	1091.5	8.2	1090.4	9.3	1089.9	1090.8	1091.3	1.1	0.9
			5	1099.9	1092.1	7.8	1090.8	9.1	1090.4	1091.3	1091.3	1.3	0.5
			10	1099.7	1092.9	6.8	1090.8	8.9	1090.1	1091.3	1091.3	2.1	0.5
			15	1100.5	1093.7	6.8	1091.5	9.0	1090.4	1091.5	1091.3	2.2	-0.2
			1	1097.7	1091.5	6.2	1090.1	7.6	1090.1	1090.8	1091.3	1.4	1.2
41	300	405,000	1	1101.1	1091.6	9.5	1090.9	10.2	1090.7	1091.5	1091.4	0.7	0.5
			5	1102.8	1092.2	10.6	1090.7	12.1	1090.5	1091.6	1091.4	1.5	0.7
			10	1102.8	1093.0	9.8	1090.9	11.9	1090.3	1091.2	1091.4	2.1	0.5
			15	1102.4	1093.8	8.6	1091.2	11.2	1090.0	1091.4	1091.4	2.6	0.2
			1	1100.3	1091.6	8.7	1090.9	9.4	1090.9	1092.0	1091.4	0.7	0.5

APPENDIX J

TABLE A

Experimental Data Barry

March 1965

T_v	T_{ki}	T_{ko}	m	P_e	h_k	q x 10^{-3}	U	t/k x 10^{4}	h_c	W/A	ΔT	T_f
1317	1078	1170	638	187	5490	493	2605	.78	8850	12.34	56	1263
1322	1080	1177	625	186	5450	507	2675	.78	9610	12.70	53	1273
1326	1077	1179	615	183	5400	522	2710	.78	10200	13.12	51	1280
1330	1090	1187	618	186	5310	500	2675	.78	10100	12.56	50	1284
1383	1097	1212	615	186	5400	583	2605	.76	8770	15.00	67	1321
1381	1095	1210	611	185	5400	579	2585	.77	8620	14.66	67	1319
1408	1130	1240	610	186	5310	563	2580	.75	8700	14.28	65	1348
1442	1161	1271	610	188	5250	563	2535	.74	8340	14.36	68	1379
1434	1158	1270	595	184	5180	559	2595	.74	9250	14.24	60	1379
1474	1203	1313	608	190	5170	565	2665	.72	10000	14.54	57	1422
1495	1218	1332	596	188	5150	575	2680	.72	10300	14.76	56	1444
1501	1225	1342	584	184	5040	577	2720	.72	11370	14.88	51	1455
1525	1271	1384	583	187	4960	519	2700	.71	11250	13.40	46	1484
1503	1266	1374	571	184	4950	483	2715	.71	11770	12.44	41	1466
1492	1313	1389	544	177	4830	352	2550	.71	9700	9.06	36	1459
1499	1316	1396	545	175	4770	371	2670	.71	12050	9.54	31	1471
1503	1275	1370	560	178	4880	452	2570	.71	9700	11.66	47	1460
1505	1320	1401	532	173	4740	366	2610	.71	11000	9.42	33	1475
1508	1357	1424	519	168	4630	297	2570	.71	10880	7.64	27	1483
1417	1300	1352	487	155	4630	215	2440	.73	8770	5.46	25	1393
1396	1251	1316	488	154	4670	269	2465	.74	9350	6.82	29	1369
1376	1238	1303	484	153	4740	271	2650	.75	12050	6.84	23	1355
1370	1232	1297	476	149	4630	261	2550	.75	11100	6.62	24	1348
1347	1206	1273	479	148	4750	271	2705	.76	11500	6.82	24	1325
1341	1203	1268	465	144	4730	255	2515	.76	10000	6.40	26	1317

APPENDIX J

TABLE A (Continued)

T_v	T_{ki}	T_{ko}	m	P_e	h_k	q x 10^{-3}	U	t/k x 10^4	h_c	W/A	ΔT	T_f
1328	1182	1252	465	143	4740	274	2550	.77	10750	6.88	25	1305
1314	1172	1240	459	141	4740	262	2510	.77	10000	6.60	26	1290
1309	1167	1237	459	141	4740	270	2620	.77	12050	6.76	22	1289
1299	1146	1219	459	141	4780	281	2500	.78	9800	7.04	29	1272
1288	1137	1210	462	141	4800	283	2560	.78	10750	7.06	26	1264
1280	1131	1203	449	137	4800	271	2480	.78	9530	6.76	28	1254
1268	1110	1186	443	134	4780	282	2430	.79	8850	7.02	32	1238
1263	1106	1183	442	134	4780	286	2505	.79	9900	7.10	29	1236
1258	1102	1179	444	133	4800	286	2530	.79	10300	7.12	28	1232
1240	1080	1159	438	130	4810	290	2500	.80	10000	7.20	29	1213
1272	1060	1167	441	131	4820	395	2590	.79	11230	9.86	35	1240
1263	1060	1164	444	132	4910	388	2675	.78	12350	9.62	31	1235
1310	1152	1231	446	137	4730	296	2595	.77	11610	7.42	25	1287
1347	1184	1265	441	136	4650	301	2560	.76	11220	7.58	27	1322
1398	1206	1302	443	138	4600	358	2585	.75	11900	9.10	30	1371
1417	1198	1306	465	146	4720	425	2670	.74	12810	10.82	33	1388
1416	1201	1307	465	146	4720	417	2670	.74	12810	10.60	33	1386
1416	1179	1298	445	138	4610	447	2610	.73	12200	11.36	37	1383
1396	1160	1279	445	138	4650	447	2630	.73	12350	11.34	36	1364
1401	1146	1274	453	139	4690	487	2650	.73	12500	10.80	39	1366
1396	1128	1267	440	135	4700	513	2700	.73	13700	13.04	37	1364
1378	1100	1241	453	138	4760	534	2680	.73	12500	13.50	43	1340
1353	1085	1222	453	137	4800	520	2720	.75	13700	13.12	38	1320
1333	1087	1213	457	138	4810	483	2740	.75	14100	12.12	34	1304

APPENDIX J

TABLE B

Experimental Data Gahman, Sartor and Balzhiser

T_v	T_{ki}	T_{ko}	m	P_e	h_k	q x 10^{-3}	U	t/k x 10^4	h_c	W/A	ΔT	T_f
1469	1307	1367	611	196	4800	312	2440	.72	8045	7.98	39	1421
1468	1320	1378	586	188	4710	289	2490	.71	8420	7.45	34	1431
1463	1320	1377	589	189	4700	286	2550	.71	9160	7.29	31	1429
1478	1320	1381	586	188	4700	305	2440	.70	7860	7.81	39	1436
1463	1308	1368	612	196	4810	312	2540	.72	8780	7.96	36	1424
1454	1310	1365	612	196	4810	286	2510	.72	8470	7.26	34	1417
1468	1310	1368	635	204	4880	314	2470	.72	7810	8.05	40	1425
1483	1346	1418	562	182	4570	245	2520	.71	9290	6.30	26	1455
1462	1318	1371	646	209	4870	291	2480	.71	7880	7.41	37	1422
1496	1340	1406	556	180	4585	314	2620	.71	11050	8.05	27	1466
1535	1313	1408	539	174	4550	436	2540	.70	9580	11.20	46	1484
1534	1308	1405	540	175	4570	445	2620	.70	10730	11.40	40	1489
1510	1312	1399	540	175	4570	395	2750	.71	13480	10.10	29	1476
1493	1289	1381	540	174	4588	423	2760	.71	14706	10.80	29	1459
1489	1302	1383	551	178	4639	380	2665	.71	12005	9.70	32	1453
1493	1311	1391	551	180	4806	376	2715	.71	11891	9.60	32	1457
1493	1316	1390	539	175	4565	340	2485	.71	9363	8.67	36	1454
1475	1335	1397	527	173	4533	280	2640	.71	10060	7.16	26	1446

APPENDIX K

THE POTASSIUM FILM COEFFICIENT

The heat transfer length of 2 inches in the liquid metal loop gives a length to diameter ratio of 4 and since this is within the usually accepted range for entrance region effects, a theoretical analysis has been conducted to determine what correction factor should be applied to the available data for heat transfer in long tubes.

The salient features of the theoretical analysis are given here and since the results are based on premises which have proven very successful in predicting fully developed heat transfer coefficients, it is felt that they may be applied with confidence to the prediction of entrance region data.

In the theoretical determination of temperature profiles and, hence, the heat transfer coefficient, the following equations are commonly used:

$$\frac{\tau}{\rho} = \left(\frac{\mu}{\rho} + \epsilon_m\right) \frac{du}{dy} \tag{1}$$

$$\frac{q}{\rho C_p} = \left(\frac{k}{\rho C_p} + \epsilon_h\right) \frac{dT}{dy} \tag{2}$$

In Equation (1) μ/ρ represents the contribution of molecular processes and ϵ_m represents the contribution of turbulent eddies to the total local shear stress. In Equation (2) k represents the contribution

of molecular thermal conductivity and ϵ_h represents the contribution of turbulent eddies to the heat transfer.

Dividing Equation (2) by (1) gives for T

$$dT = - \frac{q}{\rho C_p} \cdot \frac{\rho}{\tau} \cdot \frac{\mu/\rho + \epsilon_m}{k/\rho C_p + \epsilon_h} du \qquad (3)$$

This equation may be integrated if q, τ, ϵ_m and ϵ_h are known and thus a bulk temperature obtained from

$$T_b = \frac{\int_o^R u \; T \, dr}{\int_o^R u \, dr}$$

Then the heat transfer coefficient may be obtained by

$$h = \frac{q_w}{T_w - T_b}$$

and the Nusselt number by

$$Nu = \frac{h D}{k}$$

In Equation (3) q is obtained from a heat balance over an element of fluid. τ can be obtained from the friction factor by

$$\tau_w = \frac{f}{2} \rho u_b^2$$

and

$$\tau = \frac{r}{R} \tau_w$$

and ϵ_m can be obtained from Equation (1) along with a generalized velocity distribution for flow in tubes (56).

Alternatively, ϵ_m can be obtained (using a generalized velocity distribution) from

$$\epsilon_m = n^2 u y$$

for flow close to the wall, and the von Karman relation:

$$\epsilon_m = K^2 \frac{(du/dy)^3}{(d^2u/dy^2)}$$

for flow at a distance from the wall, where n and K are experimentally determined constants. The alternate method has been experimentally verified for air in reference (56) and (57).

The crucial problem in theoretical analyses of liquid metal heat transfer has been the determination of ϵ_h. Reasonably successful results have been obtained by assuming there is a close relationship between the contribution of turbulent eddies to heat and momentum transfer which can be described by:

$$\psi = \epsilon_h/\epsilon_m$$

A knowledge of ψ thus permits the integration of Equation (3). Martinelli (118) chose $\psi = 1.0$ in his analysis which led to the Martinelli-Lyon equation:

$$Nu = 7.0 + 0.025\ Pe^{0.8}$$

This approach has, in general, given theoretical results slightly higher than the experimental data and Deissler (54) and other workers

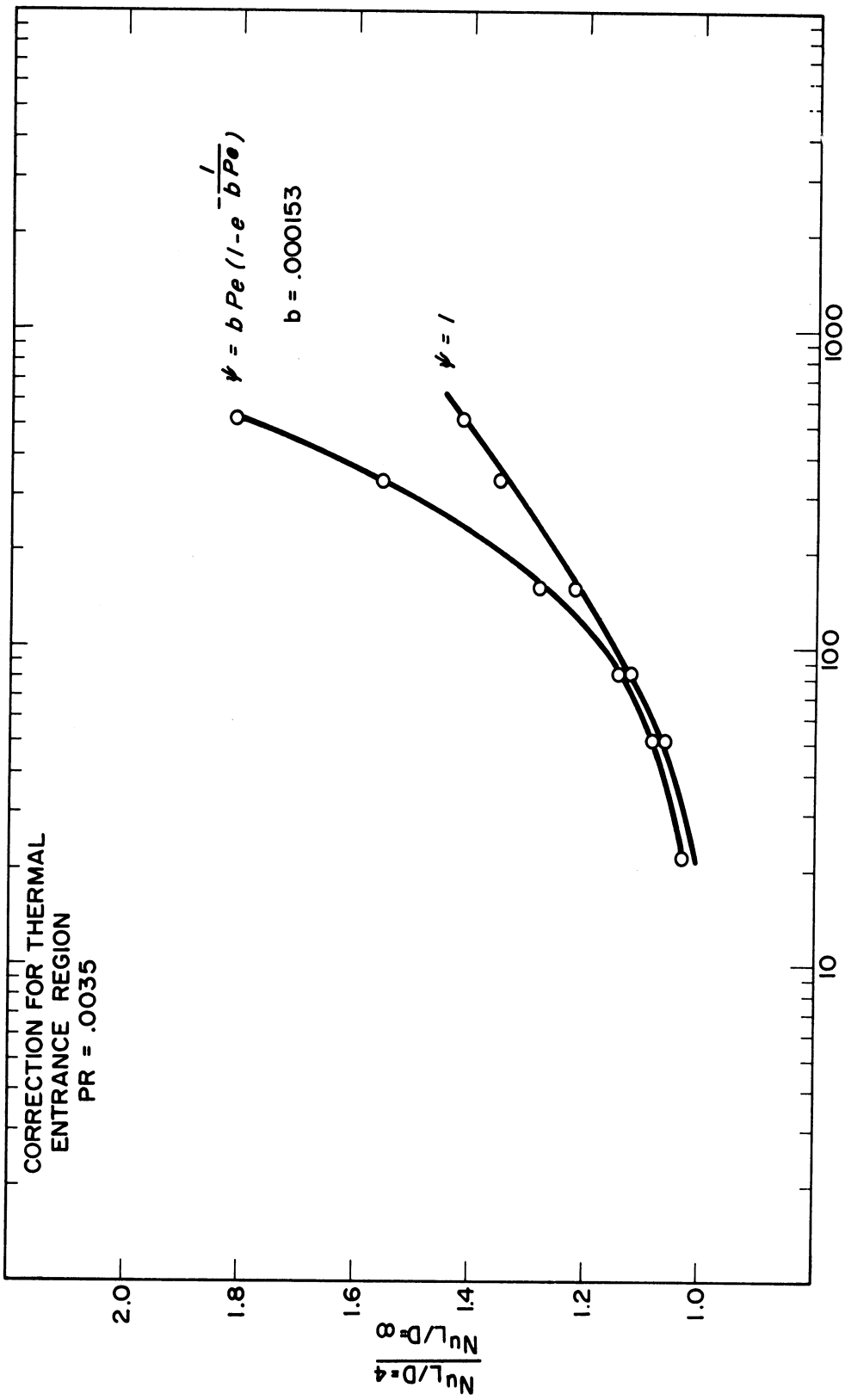

Figure K-1. Correction Factor for Thermal Entrance Region

this condensing experiment, it is a reasonable assumption that the conditions on the potassium side correspond to a constant heat flux.) The results of four investigators are summarized below in terms of an equation which fits their data best in the Peclet number range of 100 to 200.

$$Nu = 6.9 + .025\ Pe^{0.8}$$
for Sodium-Potassium alloy (95)

$$Nu = 6.1 + .025\ Pe^{0.8}$$
for Sodium-Potassium alloy (27)

$$Nu = 7.0 + .025\ Pe^{0.8}$$
for Sodium (161)

$$Nu = 6.0 + .025\ Pe^{0.8}$$
for Sodium-Potassium alloy (168)

The above data are considered to be the most reliable of the alkali metal investigations and therefore the equation chosen to evaluate the fully developed heat transfer coefficient for the potassium in this experiment is:

$$Nu = 6.5 + .025\ Pe^{0.8}$$

The appropriate correction for entrance section effects is then applied to this equation.

APPENDIX L

TREATMENT OF DATA

Given: Sodium vapor temperature T_v

Potassium inlet temperature T_{ki}

Potassium outlet temperature T_{ko}

Potassium flow rate signal in millivolts V

1. Log-mean temperature difference $\Delta T_{\ell m}$

$$\Delta T_{\ell m} = \frac{(T_v - T_{ki}) - (T_v - T_{ko})}{\ln \frac{T_v - T_{ki}}{T_v - T_{ko}}}$$

2. Potassium flow rate, m lb/hr

$$m = F \rho V (8.02)$$

where F = meter calibration factor qpm/millivolt

ρ = liquid density at temperature of flowmeter

V = millivolt signal

8.02 = conversion factor 60 min/hr/7.48 gal/ft^3

3. Heat flux, q BTU/(hr)(sq ft)

$$q = mC_p (T_{ko} - T_{ki})/A$$

where C_p = heat capacity at temperature equal to

$$\frac{T_{ko} + T_{ki}}{2}$$

A = outside area of 1/2-inch tube = .0218 ft^2

4. Peclet Number, Pe

$$Pe = \frac{m/A_c\ D}{\mu}\ Pr$$

where A_c = cross sectional area of tube = .001238 ft^2

D = inside diameter of tube = .0397 ft

μ = viscosity evaluated at $(T_{ko} + T_{ki})/2$

Pr = Prandtl No. evaluated at $(T_{ko} + T_{ki})/2$

5. Nusselt Number, Nu

$$Nu = E(6.5 + 0.025\ Pe^{0.8})$$

where E = correction factor for thermal entrance region taken from Figure K-1 using $\psi = bPe\left(1-e^{-\frac{1}{bPe}}\right)$

6. Potassium Film Coefficient, h_k

$$h_k = \frac{Nu\ k}{D}$$

where k = thermal conductivity evaluated at $(T_{ki} + T_{ko})/2$

D = inside diameter of tube

7. Overall Coefficient U

$$U = \frac{q}{\Delta T_{\ell m}}$$

8. Sodium Condensing Film Coefficient, h_c

$$\frac{1}{h_c} = \frac{1}{U} - \frac{1}{\alpha h_k} - \frac{t}{k_w}$$

where t = tube wall thickness = .012 inch

k_w = tube wall thermal conductivity taken from manufacturer's literature and evaluated at average temperature of tube wall

α = ratio of cooling to condensing wall area

9. Temperature Differences

$$T_v - T_w = q/h_c = \Delta T$$

$$T_{wi} - T_k = q/h_k$$

where T_w = sodium side wall temperature

$T_k = (T_{ki} + T_{ko})/2$

T_{wi} = potassium side wall temperature

10. Estimated Film Surface Temperature, T_f

$$T_f = T_w + \Delta T_{th}$$

where ΔT_{th} = theoretical ΔT across film based on Nusselt's theory

11. Sodium Condensing Mass Flux, W/A moles/hr-ft^2

$$W/A = q/M\lambda$$

where M = sodium molecular weight

λ = latent heat of vaporization evaluated at T_v, BTU/lb

APPENDIX M

ERROR ANALYSIS

There are two types of errors that can affect an experiment; errors of bias wherein some factor operates to continually bias the results, and random errors due to a number of factors which produce experimental scatter. These types of errors are discussed in the following paragraphs with reference to this experiment.

1. Errors of Bias

Non-condensibles: The presence of a large amount of non-condensible gas in the vapor space would result in an observed coefficient much below the values expected from Nusselt's theory. The methods used to eliminate non-condensibles from the system were discussed in the section on Experimental Procedure and are believed adequate to insure the absence of non-condensibles insofar as they would operate to lower the coefficient. The absence of a pressure dependence of the coefficient tends to substantiate this belief. Furthermore, the data of Misra and Bonilla compare closely with the data of the present investigation and it would be unreasonable to expect that the same concentration of non-condensible gases was present in both experiments.

The Potassium Film Coefficient: The estimation of the potassium film coefficient will bias all the results for the sodium condensing heat transfer coefficient. The effect of different assumptions concerning the film coefficient will now be examined.

The estimate for the potassium film coefficient was based on

$$Nu = E\,(6.5 + .025\ Pe^{0.8})$$

where E was chosen from Figure K-1 for the curve representing $\psi = bPe\left(1 - e^{-\frac{1}{bPe}}\right)$

One can consider 6 cases:

1. $Nu = E(6.5 + .025\ Pe^{0.8})$
2. $Nu = E'(6.5 + .025\ Pe^{0.8})$

   where E' is chosen from Figure K-1 for the curve representing

   $\psi = 1$
3. $Nu = E(7.0 + .025\ Pe^{0.8})$
4. $Nu = E'(7.0 + .025\ Pe^{0.8})$
5. $Nu = E(6.0 + .025\ Pe^{0.8})$
6. $Nu = E'(6.0 + .025\ Pe^{0.8})$

and examining a representative data point where Pe = 143 and U = 2550

Case	Nu	h_k	h_c
1.	9.75	4740	10750
2.	9.40	4570	11780
3.	10.39	5050	9450
4.	10.01	4860	10100
5.	9.14	4430	13310
6.	8.82	4280	15400

So it can be seen that the choice of correction factor makes a relatively small difference in the result for the condensing coefficient, whereas the effect of the choice of correlation for fully developed flow of potassium is somewhat more substantial, becoming moreso as the estimated potassium film coefficient is lessened. However, since the potassium was at a high temperature, there should be no effects due to wall contamination (the oxide melts at 940°F) and the coefficient should be at the high end of existing correlations.

End Effects: End effects can contribute to errors in two ways: To lower the flux in the test section, and to allow condensing of the vapor on the top plate of the test section which might allow excess liquid to run onto the 1/2-inch tube and thus thicken the condensate layer. The boundary value problem shown in Figure M-1 was solved and the results are also shown in Figure M-1. Integration of the area under the curve shows that the effective length of the 2-inch long tube is increased by about .046-inch. That is, about 2.3% of the heat at a particular flux level would flow outside the confines of the measured 2-inch length. Since the model chosen to represent this condition also represents the worst case, this effect was not taken into account in the calculations.

A thermocouple located in the plate on top of the test section allowed a check on these end effects. Under the worst conditions about 0.3 lb/hr could condense on the top plate. Even if all this condensate ran down on the 2-inch tube, it would have a negligible effect since the minimum condensing rate on the tube was 3 lb/hr.

Vapor Velocity: The maximum vapor velocity in the test section was about 9 ft/sec. This velocity is low and should have a negligible effect upon the film thickness.

Conduction along the Thermocouple: A simple analysis of the errors due to conduction along the thermocouple results in the following equation (23)

$$\frac{T - T_a}{T_w - T_a} = \frac{1}{\cosh\sqrt{\frac{2h\,L^2}{k\,R}}}$$

Considering a 1-inch immersion of a 1/4-inch thermocouple in an alkali metal, a 1000°F difference between the wall and the fluid ($T_w - T_a$) results in an error ($T - T_a$) of 0.4°F in the measured temperature. This error is negligible.

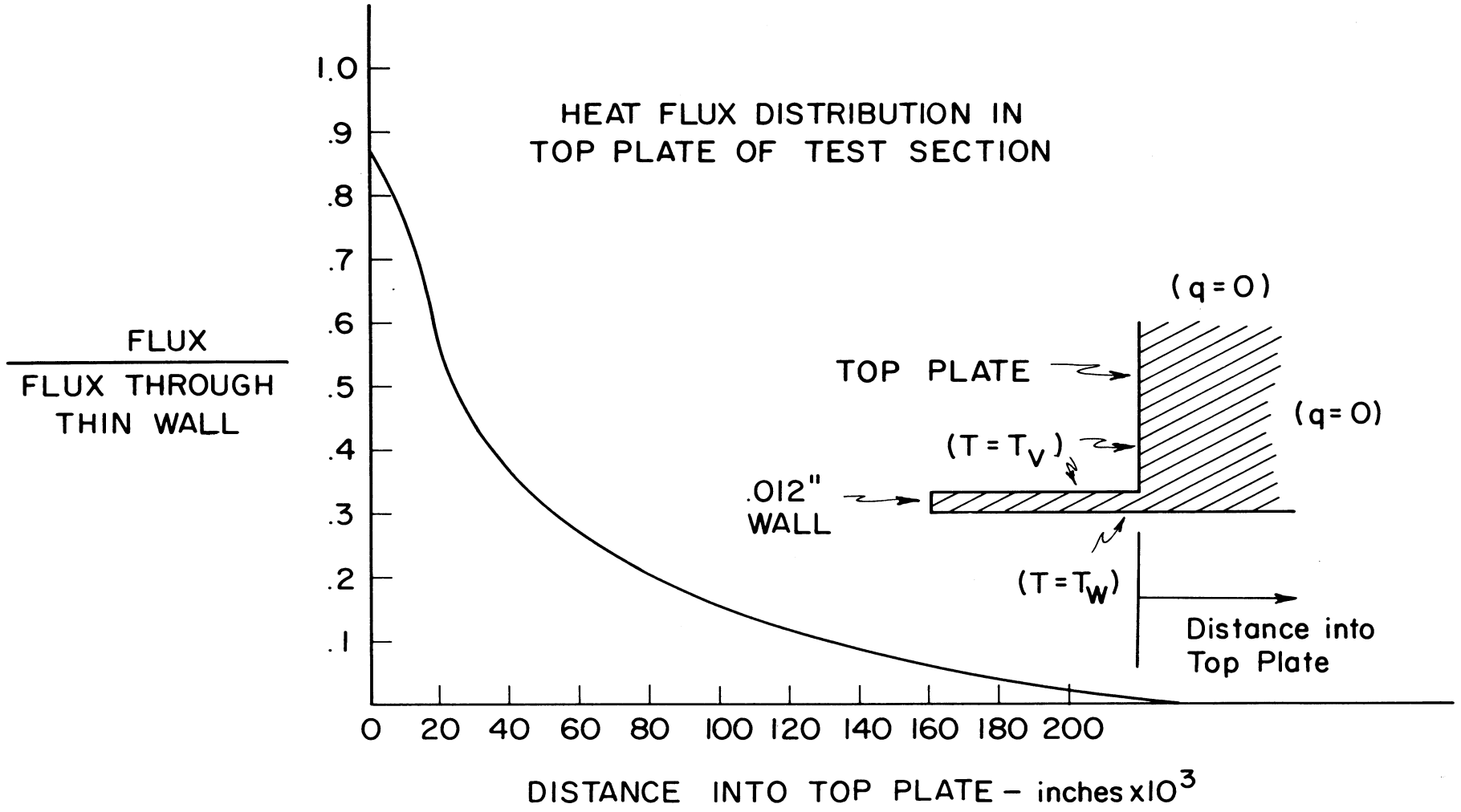

Figure M-1. End Effects on Thin-Wall Tube

Wall Thermal Conductivity: This is probably accurate to within 5% which would result in an 4% error in the value of the sodium condensing heat transfer coefficient.

It can be seen therefore, that the errors of bias come almost entirely from the choice of the potassium film coefficient. The average value of the condensing heat transfer coefficient could be as high as 15,400 or as low as 9450 BTU/hr-sq ft-°F. In other words, an estimate of the potassium film coefficient that was 10% high would result in a sodium condensing coefficient that was 30% low. An estimate of the potassium film coefficient that was 6% low would result in a sodium condensing coefficient that was 13% high.

2. Random Errors

These errors can be analyzed by using the notion of a differential of a function of several variables, as suggested by Mickley, Sherwood and Reed (129). The calculation for the condensing heat transfer coefficient as shown in Appendix L can be reduced to the following equation:

$$\frac{1}{h_c} = \frac{.00272}{F\rho VC_p \ln\left(\frac{T_v - T_{ki}}{T_v - T_{ko}}\right)} - \frac{.012}{k_w} - \frac{1}{k\left[210 + 66.5\left(\frac{F\rho VC_p}{k}\right)^{0.8}\right]}$$

$$= \frac{1}{U} - \frac{t}{k_w} - \frac{1}{h_k}$$

The potassium density ρ, is evaluated at the temperature of the flowmeter, whereas the heat capacity C_p and thermal conductivity k, are evaluated at the average of the potassium inlet and outlet temperatures, T_{ki} and T_{ko}. The tube wall thermal conductivity k_w, is evaluated at the calculated average temperature of the wall. Consider the error in each of the terms contributing to the determination of the condensing heat transfer coefficient.

$$\Delta U = \frac{\partial U}{\partial F}\Delta F + \frac{\partial U}{\partial \rho}\Delta\rho + \frac{\partial U}{\partial V}\Delta V + \frac{\partial U}{\partial C_p}\Delta C_p$$

$$+ \frac{\partial U}{\partial T_v}\Delta T_v + \frac{\partial U}{\partial T_{ki}}\Delta T_{ki} + \frac{\partial U}{\partial T_{ko}}\Delta T_{ko}$$

F, the meter calibration factor could be read to within .0005 giving $\Delta F = .0005$

ρ, the density, changed 0.8 lb/cu ft for 100° variation in temperature. This temperature was accurate to within 2°F, thus

$$\Delta\rho = .016$$

V, the flowmeter signal could be read to within .05 mv

C_p varies by .000013 BTU/lb °F/°F, thus for a 4° cumulative error in T_{ki} and T_{ko}

$\Delta C_p = .00005$

T_v was read to the nearest degree as was T_{ki} and T_{ko}, thus

$$\Delta T_v = \Delta T_{ki} = \Delta T_{ko} = 0.5$$

Then $\Delta U = 7530\ (.0005) + 57.3\ (.016) + 675\ (.05) + 14{,}000\ (.00005)$

$+ 25\ (.5) + 55.4\ (.5) + 55.4\ (.5)$

$= 107.1$

The error in k_w is due to errors in temperature measurement and flow rate being carried along in the calculation of the average wall temperature.

$$\Delta k_w = 2 \text{ BTU/hr-ft}^2\text{-°F/in}$$

$$\Delta h_k = \frac{\partial h_k}{\partial k}\Delta k + \frac{\partial h_k}{\partial F}\Delta F + \frac{\partial h_k}{\partial \rho}\Delta\rho + \frac{\partial h_k}{\partial V}\Delta V + \frac{\partial h_k}{\partial C_p}\Delta C_p$$

The error in the potassium thermal conductivity, k, is derived from errors in T_{ki} and T_{ko}. With a .5°F error in each, then one could have a 1° error in evaluating k, or $\Delta k = .009$

$$\Delta h_k = 210\,(.009) + 1.33\,(.009) + 66\,(.0005) + 25\,(.016)$$
$$+ 40.7\,(.05) + 74.6\,(.00005)$$
$$= 7.6$$

$$\Delta\left(\frac{1}{U}\right) = \frac{\Delta U}{U^2} = .18 \times 10^{-4}$$

$$\Delta \frac{t}{k} = .01 \times 10^{-4}$$

$$\Delta\left(\frac{1}{h_k}\right) = \frac{\Delta h_k}{h_k^2} \quad .003 \times 10^{-4}$$

$$\Delta\left(\frac{1}{h_c}\right) = .19 \times 10^{-4}$$

$$\Delta h_c = h_c^2 \Delta\left(\frac{1}{h_c}\right) = 2200$$

Thus, it can be seen that random errors, if acting in the same direction could produce a scatter of ± 2200 BTU/hr-sq ft-°F in the value for the condensing heat transfer coefficient. The scatter actually observed was ± 2400 BTU/hr-sq ft-°F.

APPENDIX N

Pressure Drop Data for
92% Potassium and 8% Sodium
and Pure Potassium Runs

TABLE A*

PRESSURE DROP DATA OBTAINED AT 2 MILLIVOLT AVERAGE FLOWMETER OUTPUT

MASS FLOW RATE: Average 256 lb/hr Range 210-289 lb/hr

DATA POINT DESIG-NATION	MASS FLOW RATE lb/hr	PREHEATER POWER INPUT KW	INLET TEMPERATURE (TC 30) °F	OUTLET TEMPERATURE (TC 31) °F	INLET QUALITY X_1	OUTLET QUALITY X_2	AVERAGE QUALITY	PRESSURE DROP PSI
56-7	271	19.2	1305	1237	0.1090	0.1200	0.1145	1.95
56-8	271	19.1	1322	1238	0.1070	0.1230	0.1150	1.95
56-9	246	19.1	1297	1225	0.1330	0.1420	0.1375	1.95
56-12	289	17.0	1244	1156	0.0870	0.1016	0.0943	1.73
56-121	289	16.8	1261	1159	0.0810	0.0995	0.0902	1.84
57-5	254	15.9	1221	1134	0.0827	0.1038	0.0932	2.44
57-6	232	15.9	1246	1127	0.1020	0.1220	0.1120	2.44
58-10	229	15.0	1238	1096	0.1015	0.1227	0.1121	2.13
58-11	278	14.9	1225	1102	0.0668	0.0856	0.0762	2.10
58-113	246	15.1	1205	1089	0.0931	0.1118	0.1025	2.16
58-115	266	15.1	1239	1094	0.0841	0.0968	0.0905	2.10
58-12	259	15.1	1184	1085	0.0839	0.1040	0.0939	2.02
58-122	250	15.0	1188	1099	0.0804	0.1057	0.0930	2.16
58-123	247	14.8	1208	1086	0.0863	0.1076	0.0969	2.06
59-4	285	13.7	1183	1058	0.0499	0.0715	0.0607	1.70
59-45	238	14.2	1160	1056	0.0765	0.0921	0.0843	1.70
59-5	210	14.1	1152	1038	0.1090	0.1230	0.1160	1.66
59-51	252	14.3	1171	1050	0.0698	0.0881	0.0789	1.95
59-53	286	14.2	1189	1063	0.0452	0.0645	0.0549	1.73
60-9	252	12.0	1121	994	0.0445	0.0676	0.0560	1.08
60-10	260	12.1	1088	1005	0.0500	0.0624	0.0562	1.12
60-102	256	12.0	1151	982	0.0411	0.0690	0.0550	1.15
60-104	256	12.0	1092	984	0.0511	0.0679	0.0595	1.12
60-11	254	12.0	1106	985	0.0479	0.0686	0.0582	1.08
61-1	256	11.3	1118	990	0.0420	0.0589	0.0505	0.975
61-2	256	11.3	1080	969	0.0398	0.0621	0.0510	0.975
61-3	251	11.2	1075	1036	0.0443	0.0488	0.0465	0.940
61-4	246	11.3	1037	974	0.0502	0.0675	0.0589	0.940
61-5	251	11.3	1080	979	0.0382	0.0639	0.0510	0.940
61-6	256	11.2	1175	983	0.0453	0.0594	0.0524	0.940
61-7	256	11.2	1091	991	0.0437	0.0584	0.0510	0.940
61-8	256	11.0	1075	971	0.0419	0.0582	0.0500	0.795
62-84	256	11.0	1081	966	0.0397	0.0570	0.0483	0.940
62-9	247	11.0	1070	990	0.0453	0.0576	0.0515	0.865
62-10	256	11.3	1109	992	0.0488	0.0590	0.0539	0.865
63-2	264	7.4	926	855	0.0143	0.0257	0.0200	0.0545
64-10	258	9.0	971	887	0.0187	0.0333	0.0260	0.271
64-103	251	9.0	974	889	0.0252	0.0394	0.0323	0.289
64-11	251	9.1	981	896	0.0258	0.0414	0.0336	0.307
64-12	255	9.0	983	896	0.0222	0.0378	0.0300	0.307
64-2	255	9.0	984	898	0.0222	0.0378	0.0300	0.324

*For 92% K, 8% Na

TABLE A (Continued)

PRESSURE DROP DATA OBTAINED AT 2 MILLIVOLT AVERAGE FLOWMETER OUTPUT

MASS FLOW RATE: Average 256 lb/hr Range 210-289 lb/hr

DATA POINT DESIG-NATION	MASS FLOW RATE lb/hr	PREHEATER POWER INPUT KW	INLET TEMPERATURE (TC 30) °F	OUTLET TEMPERATURE (TC 31) °F	INLET QUALITY X_1	OUTLET QUALITY X_2	AVERAGE QUALITY	PRESSURE DROP PSI
65-7	257	10.0	1046	940	0.0227	0.0463	0.0345	0.595
65-8	257	10.0	1042	940	0.0227	0.0463	0.0345	0.612
65-9	253	9.8	1040	939	0.0216	0.0446	0.0331	0.595
65-10	257	10.0	1046	940	0.0227	0.0463	0.0345	0.612
66-4	256	11.0	1095	986	0.0403	0.0580	0.0492	1.01
66-5	260	11.1	1096	988	0.0397	0.0576	0.0487	1.05
66-6	259	11.0	1090	984	0.0409	0.0576	0.0493	1.08
66-62	260	11.1	1102	983	0.0386	0.0589	0.0487	1.08
66-7	256	11.1	1100	997	0.0398	0.0600	0.0499	1.08
82-12(1)	250	11.1	1106	985	0.0404	0.0617	0.0510	1.01
82-1	264	7.3	949	872	0.0091	0.0228	0.0159	0.091
82-3	254	10.0	1023	925	0.0249	0.0458	0.0353	0.47
82-4	254	10.0	1030	930	0.0249	0.0458	0.0353	0.54
82-12(2)	228	11.0	1081	974	0.0454	0.0628	0.0541	0.95

TABLE A (Continued)

PRESSURE DROP DATA OBTAINED AT 3 MILLIVOLT AVERAGE FLOWMETER OUTPUT

MASS FLOW RATE: Average 376 lb/hr Range 352-400 lb/hr

DATA POINT DESIG-NATION	MASS FLOW RATE lb/hr	PREHEATER POWER INPUT KW	INLET TEMPERATURE (TC 30) °F	OUTLET TEMPERATURE (TC 31) °F	INLET QUALITY X_1	OUTLET QUALITY X_2	AVERAGE QUALITY	PRESSURE DROP PSI
50-2	382	12.0	1091	982	0.0097	0.0300	0.0199	0.74
50-3	356	12.0	1103	994	0.0157	0.0370	0.0264	0.58
50-4	363	13.0	1137	1016	0.0158	0.0371	0.0265	0.82
50-5	383	12.9	1150	1029	0.0110	0.0350	0.0230	0.96
50-6	387	13.1	1127	1014	0.0163	0.0390	0.0277	0.80
51-10	354	13.8	1170	1056	0.0354	0.0500	0.0427	1.63
51-11	390	14.0	1174	1047	0.0458	0.0466	0.0462	1.63
51-12	382	13.8	1152	1056	0.0300	0.0466	0.0383	1.70
52-4	376	15.0	1203	1000	0.0405	0.0544	0.0475	2.24
52-5	366	15.0	1213	1090	0.0390	0.0624	0.0507	2.24
52-6	365	15.0	1214	1089	0.0413	0.0545	0.0484	2.24
52-9	377	16.2	1244	1127	0.0501	0.0646	0.0574	2.60
52-10	400	16.0	1213	1109	0.0355	0.0585	0.0470	2.56
53-102	400	16.0	1227	1118	0.0380	0.0575	0.0478	2.55
53-2	395	16.9	1263	1148	0.0405	0.0625	0.0515	3.00
53-3	385	16.8	1264	1149	0.0434	0.0640	0.0537	3.00
54-85	370	18.0	1277	1171	0.0580	0.0765	0.0672	2.37
54-10	400	18.0	1292	1178	0.0475	0.0665	0.0570	2.37
55-3	374	19.0	1314	1205	0.0651	0.0793	0.0722	2.44
55-34	380	18.8	1311	1207	0.0582	0.0758	0.0670	2.38
55-4	386	19.2	1304	1208	0.0623	0.0794	0.0709	2.44
67-12	372	11.0	1070	972	0.0138	0.0308	0.0223	0.65
67-123	365	11.0	1070	971	0.0134	0.0302	0.0218	0.65
67-1	374	11.0	1065	966	0.0134	0.0314	0.0224	0.65
67-2	365	11.0	1057	960	0.0190	0.0358	0.0274	0.65
68-7	378	16.5	1333	1258	0.0769	0.0925	0.0847	2.75
68-8	378	16.3	1307	1264	0.0885	0.0940	0.0913	2.78
68-9	352	16.3	1341	1282	0.0955	0.1060	0.1007	2.82
75-7	366	19.0	1344	1293	0.0934	0.0985	0.0959	2.16
75-8	376	19.3	1335	1290	0.0908	0.0988	0.0948	2.06
75-9	360	18.9	1361	1295	0.0915	0.1018	0.0967	2.06
81-3	351	15.0	1187	1092	0.0507	0.0635	0.0571	2.24
81-7	358	16.1	1226	1100	0.0515	0.0692	0.0603	2.46
83-3	356	10.0	1044	953	0.0123	0.0284	0.0203	0.58

TABLE A (Continued)

PRESSURE DROP DATA OBTAINED AT 4, 5, 6, AND 1 MILLIVOLT AVERAGE FLOWMETER OUTPUTS

AVERAGE FLOWMETER OUTPUT Millivolts	DATA POINT DESIG-NATION	MASS FLOW RATE lb/hr	PREHEATER POWER INPUT KW	INLET TEM-PERATURE (TC 30) °F	OUTLET TEM-PERATURE (TC 31) °F	INLET QUALITY X_1	OUTLET QUALITY X_2	AVERAGE QUALITY	PRESSURE DROP PSI	MASS FLOW RATE (lb/hr) Average Range
	69-11	486	16.1	1350	1258	0.0562	0.0659	0.0610	2.96	
	69-12	484	16.1	1321	1256	0.0555	0.0653	0.0604	3.03	
	69-1	498	16.2	1338	1270	0.0530	0.0594	0.0562	3.06	
	69-14	498	16.2	1320	1252	0.0484	0.0615	0.0549	3.10	
	69-2	498	16.2	1310	1242	0.0484	0.0626	0.0555	3.06	
	74-3	481	18.7	1350	1271	0.0573	0.0712	0.0642	2.38	
4	74-4	500	18.7	1340	1256	0.0525	0.0645	0.0585	2.38	479
	74-5	485	18.6	1341	1257	0.0568	0.0698	0.0633	2.38	440-500
	83-9(1)	461	15.8	1328	1238	0.0507	0.0671	0.0589	2.92	
	83-10(1)	459	16.6	1310	1242	0.0553	0.0680	0.0616	3.07	
	83-8(2)	485	16.9	1323	1236	0.0458	0.0634	0.0546	2.06	
	83-9(2)	440	16.9	1327	1242	0.0560	0.0720	0.0640	2.06	
	84-12(1)	450	18.5	1339	1266	0.0681	0.0830	0.0755	2.38	
	70-12	613	16.7	1312	1236	0.0384	0.0507	0.0445	3.07	
	70-1	590	16.5	1308	1234	0.0356	0.0512	0.0434	3.03	
	73-8	615	18.3	1345	1274	0.0349	0.0485	0.0417	2.44	
	73-9	590	18.4	1349	1265	0.0425	0.0536	0.0480	2.44	
5	73-10	611	18.0	1348	1259	0.0356	0.0482	0.0419	2.44	607
	73-11	613	18.0	1344	1261	0.0335	0.0458	0.0397	2.44	590-637
	83-10	637	16.7	1327	1242	0.0167	0.0341	0.0254	2.06	
	84-6	597	19.0	1356	1253	0.0340	0.0578	0.0454	2.44	
	84-7	597	19.0	1349	1277	0.0375	0.0533	0.0474	2.49	
	71-11	730	17.0	1317	1250	0.0213	0.0330	0.0271	1.95	
	72-2	701	18.5	1353	1264	0.0280	0.0440	0.0360	2.58	
	72-3	727	18.2	1357	1257	0.0248	0.0444	0.0346	2.58	
6	72-4	740	18.5	1353	1268	0.0260	0.0411	0.0335	2.33	725
	72-5	732	18.5	1358	1272	0.0243	0.0409	0.0326	2.58	701-740
	84-1	710	18.8	1350	1262	0.0419	0.0607	0.0513	2.38	
	83-4	732	16.5	1307	1230	0.0224	0.0366	0.0295	2.86	
	76-1	115	18.8	1395	1375	0.402	0.399	0.400	1.08	
	76-2	125	18.9	1385	1388	0.374	0.363	0.368	1.08	
	76-3	124	19.0	1432	1399	0.378	0.368	0.373	1.08	
	77-7	128	15.0	1290	1265	0.286	0.280	0.283	1.08	
	77-8	125	15.0	1285	1254	0.294	0.291	0.292	1.08	
	77-9	110	14.9	1267	1252	0.342	0.335	0.338	1.08	
1	78-12	125	11.2	1184	1143	0.211	0.210	0.210	0.76	125
	78-1	129	11.1	1183	1128	0.197	0.201	0.199	0.86	110-134
	84-11	126	18.8	1364	1337	0.360	0.356	0.358	1.18	
	84-12(2)	122	18.9	1388	1378	0.379	0.383	0.381	1.18	
	85-4	125	15.0	1331	1314	0.294	0.290	0.292	1.08	
	85-5	134	15.0	1318	1296	0.267	0.264	0.265	1.08	
	85-6	131	15.0	1320	1281	0.271	0.271	0.271	1.18	
	85-11	125	11.1	1202	1164	0.210	0.204	0.207	0.76	

NOTE: The number preceding the dash in DATA POINT DESIGNATION refers to the page number in University of Michigan Research Institute Data Book No.3496 on which the raw data are recorded. The number following the dash refers to the time readings were taken.

TABLE B

PRESSURE DROP DATA FROM THE 1966 RUN

FOR 100% POTASSIUM

MASS FLOW RATE lb/hr	PREHEATER POWER INPUT KW	INLET TEMPERATURE (TC 30) °F	OUTLET TEMPERATURE (TC 31) °F	INLET QUALITY X_1	OUTLET QUALITY X_2	AVERAGE QUALITY	PRESSURE DROP Inches of Water
738	20.8	1356	1311	.01752	.02507	.0213	16
705	20.8	1366	1316	.0234	.0319	.0276	17
663	20.8	1379	1326	.0273	.0362	.0317	17
583	20.8	1385	1331	.0334	.0422	.0378	19
536	20.8	1385	1327	.0418	.0513	.0476	19
549	20.8	1386	1328	.0366	.0461	.0413	19
461	20.8	1388	1334	.0552	.0632	.0592	19
464	20.5	1388	1332	.0543	.0624	.0583	19
416	19.6	1378	1316	.0594	.0689	.0641	17
368	19.4	1370	1310	.0750	.0836	.0793	17
380	19.4	1365	1302	.0687	.0776	.0731	17
392	19.6	1361	1298	.0802	.0899	.0850	19
379	19.6	1374	1310	.0883	.0979	.0931	20
368	19.6	1370	1301	.0945	.1151	.1023	21
246	16.8	1378	1339	.1334	.1347	.1340	12
234	16.8	1373	1334	.1414	.1426	.1420	13
247	16.8	1367	1328	.1272	.1289	.1280	12
246	19.7	1395	1353	.1661	.1679	.1670	15
245	19.7	1395	1360	.1619	.1622	.1621	14
404	15.5	1350	1299	.0378	.0439	.0403	15
608	15.5	1343	1279	.0125	.0237	.0181	17
548	13.0	1283	1227	.0127	.0221	.0174	13
537	14.3	1299	1227	.00975	.0228	.0163	16
536	14.4	1300	1233	.0124	.0243	.0183	16
514	13.1	1269	1221	.00751	.0152	.0114	12
515	13.1	1258	1214	.00613	.0130	.00956	11
612	13.1	1252	1222	.00231	.00635	.00433	8
612	11.8	1239	1214	.00832	------	------	12
380	17.34	1338	1266	.0646	.0763	.0704	18
369	17.34	1328	1266	.0631	.0726	.0679	18
364	16.55	1321	1260	.0574	.0669	.0621	16
382	16.82	1315	1257	.0507	.0595	.0551	16
309	16.82	1313	1265	.0757	.0819	.0788	14
320	16.82	1332	1291	.0760	.0801	.0781	12
344	16.82	1340	1297	.0633	.0681	.0657	12
258	16.82	1355	1321	.109	.110	.110	10
234	16.82	1373	1347	.125	.123	.124	10
234	16.80	1381	1354	.135	.134	.133	11
245	16.80	1392	1364	.123	.123	.123	10

APPENDIX O

AVERAGE PER CENT DEVIATION IN PROPERTIES BETWEEN PURE POTASSIUM AND MIXTURE CONTAINING 8 PER CENT BY WEIGHT SODIUM OVER THE TEMPERATURE RANGE 900-1400°F

Property	Average deviation of mixture from pure potassium
Liquid Density	1.6 per cent higher
Liquid Viscosity	1.0 per cent higher
Liquid Heat Capacity	5.1 per cent higher
Liquid Enthalpy*	5.1 per cent higher
Vapor Pressure**	11.3 per cent lower
Heat of Vaporization***	3.6 per cent higher

* Saturated Liquid, referred to 0°F

** Raoult's Law assumed

*** Based on equilibrium vapor composition — i.e., for partial vaporization

APPENDIX P

TABLE A

RESULTS OF THE 1963 VOID FRACTION STUDIES
FOR 92% K, 8% Na

M(lb/hr.)	T(°F)	QUALITY	VOID FRACTION
388	1114	.0313	.7456
397	1123	.0404	.8603
390	1266	.0633	.5700
274	1285	.1100	.8442
249	1255	.1368	.8151
291	1130	.0581	.4170
259	1057	.0468	.6996
259	1060	.0386	.4447
267	879	.0195	.4712
255	936	.0214	.5995
255	945	.0234	.6820
261	1002	.0259	.3951
371	1028	.0172	.4416
358	1315	.0870	.5561
507	1292	.0467	.6470
749	1320	.0273	.1528
131	1159	.1647	.8108

APPENDIX P (Continued)

TABLE B

RESULTS OF THE 1966 VOID FRACTION STUDIES
FOR PURE POTASSIUM

M(lb/hr.)	T(°F)	QUALITY	VOID FRACTION
404	1325	.0408	.875
608	1311	.0181	.868
537	1263	.0163	.860
536	.267	.0188	.857
514	1245	.0114	.852
515	1236	.00956	.844
612	1237	.00433	.830

APPENDIX Q

SUMMARY OF RESULTS ON POTASSIUM BOILING - ORNL

Run No. Series A‡	10^{-5} x Inlet Mass Flow (lb/hr-ft^2)	Inlet Fluid Temperature (°F)	Exit Fluid Temperature (°F)	Exit Quality (wt % vapor)	Boiler ΔP (psi)	Heat Flux Q/A (fluid) (Btu/hr-ft^2)	h_{2p}	ΔT_{sat} ($T_{w,i} - T_{sat}$)
1	1.58	1422.0	1392.8	10.9	2.7	60,200	8020	7.5
2	1.49	1428.8	1389.7	17.9	3.4	94,000	8540	11.0
3	1.21	1423.6	1388.0	21.4	2.8	92,300	8310	11.1
4	1.51	1448.7	1402.1	21.1	4.4	112,000	5900	19.0
5	1.33	1427.7	1394.2	23.1	3.3	107,600	6580	16.3
6	1.09	1425.3	1395.6	27.9	2.8	99,900	6530	15.3
7	1.23	1434.7	1404.6	27.1	3.4	109,400	7250	15.1
8	0.99	1439.4	1409.2	33.4	2.8	108,600	8900	12.2
9	1.41	1443.9	1373.9	34.3	6.8	155,600	5650	27.6
10	1.13	1438.5	1373.3	43.2	6.1	158,000	6550	24.1
11	0.99	1436.3	1374.7	48.4	5.3	157,200	7820	20.1
12	1.40	1508.2	1428.4	50.4	7.1	245,800	8600	28.6
13	1.21	1494.6	1413.7	58.3	6.4	247,500	7500	33.0
14	1.08		1410*	67.1	6.4	253,000		
15	1.35		1385*	60.7	9.8	266,800		
16	1.44	1469.7	1370.5	47.8	8.9	220,300	4930	44.6
17	1.25	1463.0	1470.8	54.0	7.9	218,200	5200	42.0
18	1.17	1458.2	1366.6	58.2	7.7	221,100	5500	40.1
19	1.04	1451.9	1366.6	64.8	6.9	220,400	5630	39.2
20	0.90	1453.2	1360.6	75.6	6.3	222,700	5550	40.2
21	0.87		1362*	77.7	6.1	220,500*		
22	0.77		1360*	86.2	5.7	220,500*		
23	1.421	1424.4	1394.5	19.4	3.9	106,920	7450	14.34
24	1.126	1418.9	1392.8	24.3	3.6	107,740	8620	12.50
25	1.143	1448.6	1403.0	31.7	5.4	145,690	7430	19.57
26	1.226	1442.6	1401.6	37.2	4.8	146,200	8950	16.35
27	1.782	1461.1	1382.3	35.4	8.6	197,220	5000	39.68
28	1.578	1460.7	1386.5	40.5	7.8	201,600	5630	35.75
29	1.844	1466.4	1386.7	36.8	8.9	292,590	7150	40.72
30	2.115	1479.0	1397.3	32.2	9.6	290,020	7060	41.12

APPENDIX Q (Continued)

SUMMARY OF RESULTS ON POTASSIUM BOILING - ORNL

Run No. Series A‡	10^{-5} x Inlet Mass Flow (lb/hr-ft^2)	Inlet Fluid Temperature (°F)	Exit Fluid Temperature (°F)	Exit Quality (wt % vapor)	Boiler ΔP (psi)	Heat Flux Q/A (fluid) (Btu/hr-ft^2)	h_{2p}	ΔT_{sat} ($T_{x,i}$ - T_{sat})
31	1.467	1472.1	1402.0	46.5	7.7	297,350	8150	36.43
32	1.147	1465.9	1402.6	58.7	6.7	296,430	8540	34.77
33	0.9367	1460.0*	1402.0*	73.4	6.5	304,960		
34	2.06	1447.4	1415.7	17.1	3.7	174,000		
35	2.05	1481.9	1401.9	34.2	8.3	343,200	7490	45.2
36	1.54	1463.7	1393.5	45.5	6.9	349,500	8770	39.8
37	1.27	1450.6	1388.0	53.8	6.1	345,100	7160	47.1
38	1.20	1462.4	1395.8	57.5	4.9	347,100	6250	55.5
39	2.08	1484.1	1405.3	34.2	8.7	346,900	8000	43.4
40	1.81	1472.8	1394.4	39.9	7.7	357,000	8690	41.1
Series B**								
6.2	0.37	1401.5	1404.7	32.5	1.9	31,890	2680	11.9
6.3	0.37	1404.3	1390.9	34.3	2.0	32,970	2480	13.3
6.4	0.21	1378.1	1354.6	60.8	1.8	33,060	2100	15.7
6.5	0.15	1361.2	1363.6	81.3	1.6	32,370	2340	13.8
7.1	0.29	1373.0	1369.5	48.9	2.2	37,630	1660	22.7
7.2	0.29	1365.5	1348.7	49.5	2.5	37,630	1440	26.0
7.3	0.28	1395.1	1365.3	51.2	2.3	37,970	1720	22.1

‡High-flux boiler (0.325-in.-ID).

*Estimated.

**Low-flux boiler (0.87-in.-ID).

APPENDIX R

UNCERTAINTY IN QUALITY DETERMINATION

An enthalpy balance is used to calculate inlet and outlet qualities for the pressure drop section. The inlet quality is given by

$$x_1 = \left[\frac{Q_1 - Q_2 - Q_3}{\dot{m}} - (h_{\ell 3} - h_{\ell 1})\right] \frac{1}{\lambda_3} \qquad \text{(R-1)}$$

where x_1 = quality at inlet of pressure drop section

Q_1 = heat supplied to preheaters (electrical), Btu/hr

Q_2 = heat loss from preheaters, Btu/hr

Q_3 = heat loss from heat transfer section, Btu/hr

$\dot{m}$ = total mass flow rate, lb/hr

$h_{\ell 1}$ = enthalpy of liquid entering preheaters, based on reading of TC-25, Btu/lb

$h_{\ell 3}$ = enthalpy of saturated liquid entering pressure drop section, based on reading of TC-30, Btu/lb

λ_3 = latent heat of vaporization, based on inlet temperature, TC-30, Btu/lb

The exit quality is given by

$$x_2 = \left[\frac{Q_1 - Q_2 - Q_3 - Q_4}{\dot{m}} - (h_{\ell 4} - h_{\ell 1})\right] \frac{1}{\lambda_4} \qquad \text{(R-2)}$$

where x_2 = quality at outlet of pressure drop section

Q_4 = heat loss from pressure drop section, Btu/hr

$h_{\ell 4}$ = enthalpy of saturated liquid leaving pressure drop section, based on reading of TC-31, Btu/lb

λ_4 = latent heat of vaporization, based on exit temperature, TC-31, Btu/lb

The average quality in the pressure drop section, which has been used in presenting results, is the arithmetic average of inlet and outlet qualities. From Equations (R-1) and (R-2), the average quality is

$$\bar{x} = \frac{Q_1 - Q_2 - Q_3 - Q_4/2}{\lambda \dot{m}} + \frac{2h_{\ell 1} - h_{\ell 3} - h_{\ell 4}}{2\lambda} \qquad \text{(R-3)}$$

where $\bar{x}$ = average quality in pressure drop section. In nearly every case $\lambda_3 \approx \lambda_4$, and this has been given in Equation (R-3) as λ.

For the purpose of assessing the uncertainty in average quality, all quantities on the right side of Equation (R-3) are taken as variables. The error or uncertainty in $\bar{x}$ may be written, using the notion of a differential of a function of several variables, as

$$\Delta\bar{x} = \frac{\partial\bar{x}}{\partial Q_1}\Delta Q_1 + \frac{\partial\bar{x}}{\partial Q_2}\Delta Q_2 + \frac{\partial\bar{x}}{\partial Q_3}\Delta Q_3 + \frac{\partial\bar{x}}{\partial Q_4}\Delta Q_4 + \frac{\partial\bar{x}}{\partial\dot{m}}\Delta\dot{m} \qquad \text{(R-4)}$$

$$+ \frac{\partial\bar{x}}{\partial\lambda}\Delta\lambda + \frac{\partial\bar{x}}{\partial h_{\ell 1}}\Delta h_{\ell 1} + \frac{\partial\bar{x}}{\partial h_{\ell 3}}\Delta h_{\ell 3} + \frac{\partial\bar{x}}{\partial h_{\ell 4}}\Delta h_{\ell 4}$$

where finite, rather than infinitesimal differences are taken, as indicated by the Δ's.

The first five terms on the right side of Equation (R-4) contribute a component to $\Delta\bar{x}$ which may be considered the error due to uncertainties in measurements taken from the loop. The last four terms in Equation (R-4) contribute a component to $\Delta\bar{x}$ which is due to uncertainty in fluid properties. The temperatures in all cases were measured very accurately, and fluid properties such as density, enthalpy, and heat of vaporization are known as functions of temperature. Although there is some uncertainty in the values of fluid properties, particularly those of the vapor phase, it is assumed that these properties are known sufficiently accurately to allow one to consider the property component of $\Delta\bar{x}$ as negligible for the pure potassium. But these terms will be used here to determine the error arising from the use of pure-potassium properties for the 8 percent sodium mixture.

It is convenient to break the $\Delta\bar{x}$ into its two components, as suggested above.

$$\Delta\bar{x}_{meas} = \frac{\partial x}{\partial Q_1}\Delta Q_1 + \frac{\partial\bar{x}}{\partial Q_2}\Delta Q_2 + \frac{\partial\bar{x}}{\partial Q_3}\Delta Q_3 + \frac{\partial\bar{x}}{\partial Q_4}\Delta Q_4 + \frac{\partial\bar{x}}{\partial\dot{m}}\Delta\dot{m} \qquad \text{(R-5)}$$

and

$$\Delta\bar{x}_{prop} = \frac{\partial\bar{x}}{\partial\lambda}\Delta\lambda + \frac{\partial\bar{x}}{\partial h_{\ell 1}}\Delta h_{\ell 1} + \frac{\partial\bar{x}}{\partial h_{\ell 3}}\Delta h_{\ell 3} + \frac{\partial\bar{x}}{\partial h_{\ell 4}}\Delta h_{\ell 4} \qquad \text{(R-6)}$$

where $\Delta\bar{x}_{meas}$ = component of $\Delta\bar{x}$ due to uncertainty in loop measurements

$\Delta\bar{x}_{prop}$ = component of $\Delta\bar{x}$ due to neglecting presence of 8 per cent sodium

From Equation (R-3), the following partial derivatives may be written

$$\frac{\partial \bar{x}}{\partial Q_1} = \frac{1}{\lambda \dot{m}}$$

$$\frac{\partial \bar{x}}{\partial Q_2} = \frac{\partial \bar{x}}{\partial Q_3} = -\frac{1}{\lambda \dot{m}}$$

$$\frac{\partial \bar{x}}{\partial Q_4} = -\frac{1}{2 \lambda \dot{m}}$$

$$\frac{\partial \bar{x}}{\partial \dot{m}} = -\frac{(Q_1 - Q_2 - Q_3 - Q_4/2)}{\lambda \dot{m}^2}$$

$$\frac{\partial \bar{x}}{\partial \lambda} = -\left[\frac{Q_1 - Q_2 - Q_3 - Q_4/2}{\dot{m} \lambda^2} + \frac{2h_{\ell 1} - h_{\ell 3} - h_{\ell 4}}{2 \lambda^2}\right] = -\frac{\bar{x}}{\lambda}$$

$$\frac{\partial \bar{x}}{\partial h_{\ell 1}} = \frac{1}{\lambda}$$

$$\frac{\partial \bar{x}}{\partial h_{\ell 3}} = \frac{\partial \bar{x}}{\partial h_{\ell 4}} = -\frac{1}{2 \lambda}$$

Inserting these derivatives in Equations (R-5) and (R-6),

$$\Delta \bar{x}_{meas} = \frac{1}{\lambda \dot{m}} \left[\Delta Q_1 - \Delta Q_2 - \Delta Q_3 - \frac{1}{2} \Delta Q_4 - \frac{(Q_1 - Q_2 - Q_3 - Q_4/2)\Delta \dot{m}}{\dot{m}}\right] \qquad (R\text{-}7)$$

$$\Delta \bar{x}_{prop} = \frac{1}{\lambda} \left[-\bar{x} \Delta \lambda + \Delta h_{\ell 1} - \frac{1}{2} \Delta h_{\ell 3} - \frac{1}{2} \Delta h_{\ell 4}\right] \qquad (R\text{-}8)$$

Equations (R-7) and (R-8) show that the error terms are worse when $\dot{m}$ is low, λ is low (implying high temperature), and Q_1 is high.

The scatter in the heat loss correlation data shows the following uncertainties in heat losses.

Preheaters	ΔQ_2	$= \pm$ 1000 Btu/hr
Heat Transfer Section	ΔQ_3	$= \pm$ 500 Btu/hr
Pressure Drop Section	ΔQ_4	$= -$ 300 Btu/hr

The power input to the preheaters is known to within 0.2 KW, so that

$$\Delta Q_1 = \pm 682 \text{ Btu/hr}$$

An error analysis, similar to this one, showed that the mass flow rate is known to within 7 lb/hr, that is

$$\Delta \dot{m} = \pm 7 \text{ lb/hr}$$

For pure potassium the Δ's in fluid properties are negligible, but the results of Appendix O may be used to evaluate the Δ's arising from neglect of sodium in the fluid.

A "worse case" chosen from the data will now be examined.

DATA POINT DESIGNATION 84-12(2)

$$Q_1 = 64{,}500 \text{ Btu/hr}$$

$$Q_2 = 9{,}800$$

$$Q_3 = 4{,}100$$

$$Q_4 = 1{,}500$$

$$\dot{m} = 122 \text{ lb/hr}$$

$$\bar{x} = 0.380$$

with pure potassium properties

$$\lambda = 850 \text{ Btu/lb}$$

$$h_{\ell 1} = 261 \text{ Btu/lb}$$

$$h_{\ell 3} = 349$$

$$h_{\ell 4} = 345$$

The data are at high temperature (1400°F), high preheat power and low flow rate. From Appendix O

$$\Delta\lambda = + (0.036)(850) = 30.6$$

$$\Delta h_{\ell 1} = + (0.051)(261) = 13.3$$

$$\Delta h_{\ell 3} = + (0.051)(349) = 17.8$$

$$\Delta h_{\ell 4} = + (0.051)(345) = 17.6$$

Using the average value between pure potassium and the mixture for λ, Equation ($_R$-8) gives the property error.

$$\Delta\bar{x}_{prop} = \frac{1}{865}\left[(-0.38)(30) + 13.3 - \frac{17.8}{2} - \frac{17.6}{2}\right]$$

$$= \frac{-14.9}{865} = -0.0183$$

This error amounts to 4.8 per cent of the previously calculated $\bar{x} = 0.38$.

Again using an average value for λ, Equation (R-7) gives the error from measurement uncertainty. Here each Δ increment is given a sign which will make the error contribution in each case positive, yielding a worst value.

$$\Delta\bar{x}_{meas} = \frac{1}{(865)(122)}\left[682 + 1000 + 500 + \frac{300}{2} + \frac{(64{,}500-9800-4100-750)(7)}{122}\right]$$

$$= \frac{2332 + 2910}{(865)(122)} = \frac{5242}{(865)(122)} = 0.0495$$

This worst possible error amounts to 13 per cent of the calculated value $\bar{x} = 0.38$.

It must be remembered this is a "worst case." The $\Delta\bar{x}$ meas for other data points is not as severe, especially at higher flow rates. It should also be recalled that adjusting the physical properties will eliminate the $\Delta\bar{x}$ prop term.

APPENDIX S

TABLE VII SUMMARY OF RESULTS ON TWO-PHASE POTASSIUM HEAT TRANSFER - MEDIUM QUALITY

TC25	TC26	TC27	TC28	TC29	Flux Btu/hr ft^2	$\dot{m}$ lb/hr	Outlet Quality	h2p	(Twall - T29)	Inlet Quality
935	1390	1532	1438	1367	418,000	380	.0890	8850	47.4	.0609
942	1396	1544	1451	1377	410,000	379	.0883	7940	51.8	.0596
938	1397	1536	1449	1372	415,000	368	.0945	8695	47.8	.0657
897	1363	1523	1421	1340	424,000	380	.0648	6620	64.0	.0363
889	1394	1486	1397	1349	334,000	369	.0556	5210	64.2	.0327
892	1344	1479	1396	1324	344,000	369	.0574	5950	58.0	.0337
886	1337	1448	1376	1318	260,000	382	.0523	4630	56.3	.0350
877	1338	1450	1375	1319	269,000	382	.0527	4900	54.8	.0348
887	1338	1446	1375	1316	260,000	382	.0507	4630	56.3	.335
909	1397	1497	1431	1381	225,000	234	.136	4273	52.5	.111
910	1399	1499	1439	1384	224,000	234	.135	4310	52.0	.109
925	1413	1541	1470	1396	315,000	245	.123	5560	56.8	.090
910	1399	1542	1465	1380	411,000	246	.133	8850	46.0	.090
892	1388	1541	1462	1376	394,000	234	.141	7299	54.0	.098
880	1386	1538	1451	1370	396,000	247	.127	7042	56.2	.086
912	1422	1557	1468	1400	380,000	246	.172	7580	50.2	.132
920	1421	1558	1474	1403	380,000	246	.173	7810	48.8	.133
901	1413	1536	1461	1394	316,000	231	.166	5880	53.6	.133
914	1427	1543	1460	1401	313,000	232	.168	5320	58.8	.135
931	1420	1516	1454	1403	213,000	222	.159	4020	53.2	.137
927	1419	1510	1447	1396	216,000	223	.162	4050	53.2	.139

APPENDIX S

TABLE VII SUMMARY OF RESULTS ON TWO-PHASE POTASSIUM HEAT TRANSFER - LOW QUALITY

TC25	TC26	TC27	TC28	TC29	Flux Btu/hr ft^2	$\dot{m}$ lb/hr	Outlet Quality	h2p	(Twall - T29)	Inlet Quality
972	1373	1486	1412	1352	233,000	404	.038	3420	68	.024
1034	1365	1478	1408	1345	236,000	608	.0125	3080	77	.026
965	1271	1446	1361	1285	282,000	548	.0127	3480	81	.000
957	1318	1445	1366	1300	262,000	537	.0098	3700	71	-.003
967	1332	1458	1369	1303	274,000	536	.0124	3550	78	-.005
937	1270	1430	1349	1272	272,000	514	.0075	3380	81	-.006
916	1255	1424	1339	1260	276,000	515	.0061	3240	86	-.006
950	1227	1417	1334	1256	282,000	612	.002	3040	93	-.010

REFERENCES

1. Adams, J. M., "An Analysis of the Critical Heat Flux in Nucleate Boiling." Paper No. 1313, Presented at the 50th National AIChE Meeting, Buffalo, New York, May 5-8, 1963.

2. Adams, J. M., "An Investigation of Heat Transfer to Pool Boiling Magnesium." ASME Paper 65-HT-49, Presented at 8th National Heat Transfer Conference, Los Angeles, California, August 10, 1965.

3. Addoms, J. N., Sc.D. Thesis in Chemical Engineering, Massachusetts Institute of Technology, 1948. Also McAdams, W. H., Heat Transmission, Third Edition, pp. 382, 385, McGraw-Hill, New York, 1954.

4. Aladyev, et. al., "Thermal Resistance of Phase Transition with Condensation of Potassium Vapor," Paper presented at International Heat Transfer Conference, Chicago, August 7-11, 1966.

5. Alkali Metals Boiling and Condensing Investigations, Quarterly Reports 2-12, Contract NAS 3-2528, General Electric Company.

6. Averin, E. K., Izvest, Akad, Nauk, SSSR, No. 3, pp. 116-122, 1954. AERE Lib. Transl., p. 562, 1955.

7. Balzhiser, R. E., "Fundamental Consideration in Liquid Metal Heat Transfer," Proceedings of the Symposium on Chemical Engineering Under Extreme Conditions, AIChE - I Chemical Engineering Symposium Series No. 2, London, 1965.

8. Balzhiser, R. E., et. al. "Investigation of Liquid Metal Boiling Heat Transfer," United States Air Force Systems Command, Wright-Patterson Air Force Base, Ohio, Report RTD-TDR-63-4130, November, 1963.

9. Balzhiser, R. E., et. al. "Investigation of Liquid Metal Boiling Heat Transfer," The University of Michigan, Ann Arbor, Michigan. Report 05750-19-P, February, 1965.

10. Balzhiser, R. E., et. al., "Literature Survey on Liquid Metal Boiling," ASD-TR-61-594, The University of Michigan, Ann Arbor, Michigan (Dec. 1961).

11. Bardeen, J., "Theory of the Work Function: The Surface Double Layer," Phys. Rev. 49, 653 (1936).

12. Baroczy, C. J., "Correlation of Liquid Fraction in Two-Phase Flow with Application to Liquid Metals." Atomics International, Div. of North American Aviation, Inc., Canoga Park, California. Report NAA-SR-8171, April 1963.

13. Baroczy, C. J., "A Systematic Correlation for Two-Phase Pressure Drop," Presented at the Eighth National Heat Transfer Conference. Los Angeles, California, August 8-11, 1965.

14. Barry, R. E., "Condensation of Sodium at High Heat Fluxes," PhD Thesis, University of Michigan, 1965.

15. Barry, R. E. and Balzhiser, R. E., "Condensation of Sodium at High Heat Fluxes," Proceedings of Third International Heat Transfer Conference, Chicago, August, 1966.

16. Baumeister, K. J., Hamill, T. D. and Schoessow, G. J., "A Generalized Correlation of Vaporization Times of Dorps in Film Boiling on a Flat Plate," NASA TM X-52177 (1966).

17. Bennett, J. A. R., "Two-Phase Flow in Gas-Liquid Systems: A Literature Survey," AERE CERI-2497, March, 1958.

18. Berenson, P. J., "Film Boiling Heat Transfer from a Horizontal Surface," J. of Heat Transfer, 83, No. 3 (1961).

19. Berenson, P. J., "Transition Boiling Heat Transfer from a Horizontal Surface," NP-8415, MIT Heat Transfer Laboratory March, 1960.

20. Bergles, A. E. and Rohsenow, W. M., "Forced Convection Surface-Boiling Heat Transfer and Burnout in Tubes of Small Diameter," ASME Paper No. 63-HT-22, 6th National Heat Transfer Conference, Boston, Massachusetts, August, 1963.

21. Bernath, L. A., Chemical Engineering Progress Symposium Series No. 30, 56, p. 95, 1960.

22. Bikerman, J. J., Surface Chemistry: Theory and Applications, 2nd ed., pp. 441 et seq., Academic Press, New York (1958).

23. Bird, R. B., Stewart, W. E., and Lightfoot, E. N., Transport Phenomena, p. 291, John Wiley and Sons, New York, 1960.

24. Bokris, J., Modern Aspects of Electrochemistry, p. 119, Butterworths Scientific Publications, London (1954).

25. Bonilla, C. F., "Alkali Metals Boiling and Condensing Investigations. Vol. 1 - Experimental Prgoram," NASA CR-54050, June, 1964.

26. Bonilla, C. F., "Pool Boiling Heat Transfer with Mercury," Reactor Heat Transfer Conference of 1956, TID-7529, Pt. 1, 324-341.

27. Borishanskii, V. M., Zablotskaya, T. V., Ivashenko, N. I., "Heat Transfer to Molten Metals During Flow in Pipes," Soviet Journ. Atomic Energy, 14, 318-20, (1964).

28. Braunlich, R. H., "Heat Transfer to Boiling Liquids Under Vacuum," Sc.D. Thesis, Massachusetts Institute of Technology, 1941.

29. Breen, B. P. and Burnet, G., "Peak Heat Flux in Necleate Boiling Heat Transfer," Iowa State University, Research and Development Report IS-810, January, 1964.

30. Bromley, L. A., "Heat Transfer in Condensation - Effect of Heat Capacity of the Condensate," Ind. Eng. Chem., 44, No. 12, 2966-9 1952.

31. Bromley, C. A., "Heat Transfer in Stable Film Boiling," Chem. Eng. Prog., 46, No. 5, 221, 1950.

32. Brown, R. A. S. and Govier, G. W., "High Speed Photography in the Study of Two-Phase Flow," Canadian Journal of Chemical Engineering Vol. 39, 1961, p. 159.

33. Brown, R. A. S., Sullivan, G. A., and Govier, G. W., "The Upward Vertical Flow of Air-Water Mixtures--III. Effect of Gas Phase Density on Flow Pattern, Holdup and Pressure Drop," Canadian Journal of Chemical Engineering, Vol. 38, 1960, p. 62.

34. Buhl, A., "The Electrical Double Layer on a Mercury Surface," ASTIA Report No. AD 268520, 1961.

35. Carbon, M. W., AEC and University of Wisconsin Report, May 30, 1964.

36. Carne, M., "Some Effects of Test Section Geometry in Saturated Pool Boiling, on the Critical Heat Flux for Some Organic Liquids and Liquid Mixtures," AIChE Paper No. 6, Presented at the 7th National Heat Transfer Conference, Cleveland, Ohio, August 9-12, 1964.

37. Carne, M. and Charlesworth, D. H., "Thermal Conduction Effects on the Critical Heat Flux in Pool Boiling," AIChE Paper No. 11, Presented at the 8th National Heat Transfer Conference, Los Angeles, California, August 9, 1965.

38. Castles, J. T., S. M. Thesis in Chemical Engineering, Massachusetts Institute of Technology, 1947. Also McAdams, W. H., Heat Transmission, Third Edition, p. 387.

39. Caswell, B. F. and Balzhiser, R. E., "The Critical Heat Flux for Boiling Liquid Metal Systems," Presented at 8th National Heat Transfer Conference, Los Angeles, California, August 10, 1965.

40. Chang, Y. P., "Wave Theory of Heat Transfer in Film Boiling," J. of Heat Transfer, 81, February, 1959.

41. Chang, Y. P. and Snyder, N. W., "Heat Transfer in Saturated Boiling," Chemical Engineering Progress Symposium Series No. 30, 56, 1960.

42. Chen, J. C., "A Proposed Mechanism and Method of Correlation for Convective Boiling Heat Transfer with Liquid Metals," Proceedings of 1963 High-Temperature Liquid Metal Heat Transfer Meeting, ORNL-3605, 1963.

43. Cichelli, M. T. and Bonilla, C. F., Transactions AIChE, 41, pp. 755-787, 1945.

44. Clark, J. A. and Merte, H., "Nucleate, Transition, and Film Boiling Heat Transfer at Zero Gravity," 14, Advances in the Astronautical Sciences, Western Periodicals Co., N. Hollywood, California, 1963.

45. Coe, H. H., "Summary of Thermophysical Properties of Potassium." NASA TN D-3120, December, 1965.

46. Cohn, P. D., "Heat Transfer and Thermodynamic Properties of Mercury," NAA-SR-Memo 4666, Atomics International (Nov. 1959).

47. Colburn, A. P., "Calculation of Condensation with a Portion of the Condensate Layer in Turbulent Motion," Ind. Eng. Chem., 26, No. 4, 432-4, 1934.

48. Colver, C. P., "Measurements of the Temperature Profiles Adjacent to the Surface During the Nucleate Boiling of Water and Methanol," M.S. Thesis in Chemical Engineering, University of Kansas, July, 1960.

49. Colver, C. P., "A Study of Saturated Pool Boiling Potassium up to Burnout Heat Fluxes," Ph.D. Thesis in Chemical Engineering, University of Michigan, September, 1963.

50. Colver, C. P. and Balzhiser, R. E., "A Study of Saturated Pool Boiling Potassium up to Burnout Heat Fluxes," Presented at 7th National Heat Transfer Conference, Cleveland, Ohio, August 9-12, 1964.

51. Costello, C. P. and Adams, J. M., "Burnout Heat Fluxes in Pool Boiling at High Accelerations," International Developments in Heat Transfer II, pp. 255-261, August, 1961.

52. Costello, C. P. and Frea, W. J., "The Role of Surface Deposits in the Attainment of High Pool Boiling Burnout Heat Fluxes," AIChE Journal, 10, No. 3, pp. 393-398, May, 1964.

53. Costello, C. P. and Heath, C. A., "The Interrelation of Surface Effects and Acceleration in the Burnout Heat Flux Problem," AIChE Journal, 10, No. 2, p. 278, March, 1964.

54. Deissler, R. G., "Analysis of Fully Developed Heat Transfer at Low Peclet Numbers in Smooth Tubes with Application to Liquid Metals," NACA RM E52F05 (1952).

55. Deissler, R. G., "Analysis of Turbulent Heat Transfer and Flow in Entrance Region of Smooth Passages," NACA TN 3016, 1953.

56. Deissler, R. G., "Analytical and Experimental Investigation of Adiabatic Turbulent Flow in Smooth Tubes," NACA TN 2138, 1950.

57. Deissler, R. G., Eian, C. S., "Analytical and Experimental Investigation of Fully Developed Turbulent Flow of Air in a Smooth Tube with Heat Transfer with Variable Fluid Properties," NACA TN 2629, 1952.

58. Drew, T., et al., "Boiling," Trans. AIChE, 23, 1937.

59. Egen, R. A., Dingee, D. A. and Chastain, J. W., "Vapor Formation and Behavior in Boiling Heat Transfer," Battelle Memorial Institute, Report BMI-1163, February 4, 1957.

60. Ellion, M. E., "A Study of the Mechanism of Boiling Heat Transfer," JPL Memorandum No. 20-88, March, 1954.

61. Ewing, C. T., et al., "High-Temperature Properties of Potassium," NRL Report 6233, September, 1965.

62. Farber, E. A. and Scorah, R. L., "Heat Transfer to Water Boiling Under Pressure," Transactions ASME, 70, p. 369, 1948.

63. Farmer, Liquid Metals Handbook, R. N. Lyon, Editor, AEC and Bureau of Ships, Department of Navy, Washington, D. C., 1950.

64. Frea, W. J., et al., "Some Experimental and Analytical Investigations on the Critical Heat Flux in Pool Boiling," AIChE Paper No. 10, Presented at the 8th National Heat Transfer Conference, Los Angeles, California, August 9, 1965.

65. Frederking, T. H. K., and Clark, J. A., "Natural Convection Film Boiling on a Sphere," Paper presented at 1962 Cryogenic Engineering Conference. Advances in Cryogenic Engineering, Vol. 8, K. D. Timmerhaus, Editor.

66. Gambill, W. R., "An Experimental Investigation of the Inherent Uncertainty in Pool Boiling Critical Heat Fluxes to Saturated Water," AIChE Journal, 10, No. 4, pp. 502-508, July, 1964.

67. Gambill, W. R., "A Survey of Boiling Burnout," Brit. Chem. Eng., 8, No. 2, pp. 93-98, February, 1963.

68. Gambill, W. R. and Bundy, R. D., "High Flux Heat Transfer Characteristics of Pure Ethylene Glycol," AIChE Journal, 9, No. 1, pp. 55-59, January, 1963.

69. General Electric Company, "Alkali Metals Boiling and Condensing Investigations," Quarterly Report No. 8, Space Power Operations, Flight Propulsion Lab. Dept., NASA-CR-54138, October, 1964.

70. Goldsmith, A., Waterman, T. E., and Hirschborn, H. J., Handbook of Thermophysical Properties of Solid Materials, Vol. 11 Alloys, The Macmillan Company, New York, 1961.

71. Govier, G. W. and Omer, M. M., "The Horizontal Pipeline Flow of Air-Water Mixtures," Canadian Journal of Chemical Engineering, Vol. 40, 1962, p. 93.

72. Govier, G. W., Radford, B. A. and Dunn, J. S. C., "The Upward Vertical Flow of Air-Water Mixtures," Canadian Journal of Chemical Engineering, Vol. 35, 1957, p. 59.

73. Govier, G. W. and Short, W. L., "The Upward Vertical Flow of Air-Water Mixtures--III. Effect of Tubing Diameter on Flow Pattern, Holdup and Pressure Drop," Canadian Journal of Chemical Engineering, Vol. 36, 1958, p. 195.

74. Gresham, W. A., Foster, P. A. and Kyle, R. J., "Review of the Literature on Two-Phase (Gas-Liquid) Fluid Flow in Pipes," WADC-55-433, PartI, June, 1955.

75. Gunther, F. C. and Kreith, F., "Photographic Study of Bubble Formation in Heat Transfer to Subcooled Water," Progress Report No. 4-120, JPL, 1950.

76. Hamill, T. D., and Baumeister, K. J., "Film Boiling Heat Transfer From a Horizontal Surface as an Optimal Boundary Value Process," NASA TM X-52183, 1966.

77. "Harshaw Scintillation Phosphors," Harshaw Chemical Company, Cleveland, Ohio, pp. 43, 1962.

78. Hoffman, H. W. and Krakoviak, A. I., "Convective Boiling with Liquid Potassium," Proceedings of the 1964 Heat Transfer and Fluid Mechanics Institute, Stanford University Press, 1964.

79. Hosler, E. R., and Westwater, J. W., "Film Boiling on a Horizontal Plate," ARS Journal, 32, 553-558, 1962.

80. Howell, J. R. and Bell, K. J., Chemical Engineering Progress Symposium Series No. 41, 59, pp. 88-95, 1963.

81. Hsu, Y. Y., and Westwater, J. W., "Approximate Theory for Film Boiling on Vertical Surfaces," Chem. Eng. Prog. Sym. Ser., 56, No. 30, 15-24, 1960.

82. Huang, K., Wyllie, G., "On the Surface Free Energy of Certain Metals," Proc. Phys. Soc., 62A, 180, 1949.

83. Huber, D. A. and Hoehne, J. C., "Pool Boiling Investigation of Benzene, Diphenyl, and Benzene-Diphenyl Mixtures Under Pressure," NAA-SR-6681, December, 1961.

84. Isbin, H. S., Moen, R. H., and Mosher, D. R., "Two-Phase Pressure Drops," AECU-2994, November, 1954.

85. Ishigai, S., et al., "Boiling Heat Transfer from a Flat Surface Facing Downward," International Developments in Heat Transfer II, pp. 224-229, August, 1961.

86. Ivey, H. J., "Acceleration and the Critical Heat Flux in Pool Boiling Heat Transfer," Institute of Mechanical Engineering, London, England, November, 1962.

87. Ivey, H. J., "Preliminary Results on the Effect of Acceleration on Critical Heat Flux in Pool Boiling," AEEW-R99, September, 1961.

88. Ivey, H. J. and Morris, D. J., "The Effect of Test Section Parameters on Saturation Pool Boiling Burnout at Atmospheric Pressure," AEEW-R-176, 1962.

89. Jackson, C. B., Editor, Liquid Metals Handbook, Na-NaK Supplement, Atomic Energy Commission and Bureau of Ships, Third Edition, 1955, pp. 32-45.

90. Jakob, M., Heat Transfer, Vol. I, John Wiley and Sons, New York, 1949.

91. Jordon, D. P. and Leppert, G., "Nucleate Boiling Characteristics of Organic Reactor Coolants," Nucl. Sci, and Eng., 5, pp. 349-359.

92. Kazakova, E. A., "The Influence of Pressure on the First Crisis in Boiling Water From a Flat Surface," C.E.I., Moscow, 1953.

93. Kepple, R. R., and Tung, T. V., "Two-Phase (Gas-Liquid) System: Heat Transfer and Hydraulics, An Annotated Bibliography," ANL-6734.

94. Kiraly, R. and Koestel, A., TRW Report No. ER-4104. June, 1960.

95. Kirillov, P. L., Subbotin, V. I., Suvarov, N. Ya., Troyanov, M. F., "Heat Transfer in Pipes to a Sodium-Potassium Alloy and to Mercury," Soviet Journ. Atomic Energy, 6, 253-60 (1960).

96. Koh, J. C. Y., "An Integral Treatment of Two-Phase Boundary Layer in Film Condensation," Trans. ASME, Series C, J. Heat Transfer, 83, No. 3, 359-61, 1961.

97. Kutateladze, S. S., "Boiling Heat Transfer," Minsk, USSR Heat Transfer Conference; AD 270076, June, 1961.

98. Kutateladze, S. S., "A Hydrodynamic Theory of Changes in the Boiling Process Under Free Convection Conditions," AEC-TR-1441, 1951.

99. Kutateladze, S. S., "Heat Transfer on Condensation and Boiling," AEC TR 3770, 1952.

100. Kutateladze, S. S., et al., "Heat Transfer in Liquid Metals," J. Nucl. Energy II, 9, pp. 214-219, 1959.

101. Kutateladze, S. S. and Schneiderman, L. L., "An Experimental Study of the Influence of the Temperature of a Liquid on a Change in the Rate of Boiling," AEC TRANSL° 3405, 1953.

102. Labuntsov, D. A., Smirnov, S. I., "Heat Transfer in Condensation of Liquid Metal Vapors," Paper presented at International Heat Transfer Conference, Chicago, August 1966.

103. Lemmon, A. W., Deem, H. W., Eldridge, E. A., Hall, E. H., Matolich, J., Walling, J. F., "Engineering Properties of Potassium," Battelle Memorial Institute Report BATT-4673, December, 1963.

104. Levy, S., "Prediction of Two-Phase Pressure Drop and Density Distribution from Mixing Length Theory," J. Heat Trans., Vol. 85, 137, 1963.

105. Levy, S. and Mausteller, J. W., "Heat Transfer-Natural Circulation," Liquid Metals Handbook, Sodium-NaK Supplement, p. 54, 1955.

106. Lewis, E. W., Merte, H., Jr., and Clark, J. A., "Heat Transfer at 'Zero Gravity'" Paper presented at 55th National Meeting of AIChE at Houston, Texas, February 7-11, 1965.

107. Lienhard, J. H. and Schrock, V. E., ASME Paper No. 62-HT-3, Presented at the 5th National Heat Transfer Conference, Houston, Texas, August, 1962.

108. Lienhard, J. H. and Watanabe, K., "On Correlating the Peak and Minimum Boiling Heat Fluxes with Pressure and Heater Configuration," ASME Paper No. 65-HT-5, Presented at the 8th National Heat Transfer Conference, Los Angeles, California, August 9, 1965.

109. Lin, C., et al., "Boiling Heat Transfer of Liquid Metals," JPRS-3512, 1959.

110. Lockhart, R. W. and Martinelli, R. C., "Proposed Correlation of Data for Isothermal Two-Phase, Two-Component Flow in Pipes," Chemical Engineering Progress, Vol. 45, 1949, p. 39.

111. Lowdermilk, W. H., Lanzo, C. D. and Siegel, B. L., "Investigation of Boiling Burnout and Flow Stability for Water Flowing in Tubes," National Advisory Committee for Aeronautics Technical Note 4382, September, 1958.

112. Lurie, Henry, "Sodium Boiling Heat Transfer and Hydrodynamics," Presented at the Conference on Application of High Temperature Instrumentation to Liquid-Metal Experiments, ANL, September 28-29, 1965, p. 549.

113. Lyon, R. E., et al., Advances in Cryogenic Engr., 9, 1964.

114. Lyon, R. E., et al., "Boiling Heat Transfer with Liquid Metals," Chem. Eng. Prog. Sym. Ser., 51, No. 17, 41-47, 1955.

115. Lyon, R. E., Foust, A. S., and Katz, D. L., "Boiling Heat Transfer with Liquid Metals," Ph.D. Thesis, The University of Michigan, 1953.

116. Madsen, H., and Bonilla, C. F., "Heat Transfer to Sodium Potassium Alloy in Pool Boiling," Chem. Eng. Prog. Sym. Ser., 56, 1960.

117. Martinelli, R. C., "Heat Transfer to Molten Metals," Trans. ASME, 69, No. 8, 947-59, 1947.

118. Martinelli, R. C., et al., "Isothermal Pressure Drop for Two-Phase Two-Component Flow in Horizontal Pipe," Transactions ASME, Vol. 66, 1944, p. 139.

119. Martinelli, R. C., Putnam, J. A. and Lockhart, R. W., "Two-Phase, Two-Component Flow in the Viscous Region," Transactions AIChE, Vol. 42, 1946, p. 681.

120. Masnovi, R., "Literature Survey of Two-Phase Fluid Flow," WAPD-TH-360, 1958.

121. McAdams, W., Heat Transmission, Third Edition, Ch. 13, McGraw-Hill, New York, 1954.

122. McAdams, W., et al., Chem. Eng. Prog., 44, p. 639, 1948.

123. McFadden, P. W., et al., "An Analysis of Laminar Film Boiling with Variable Properties," Int. J. of Heat and Mass Transfer, 1, No. 4 January, 1961.

124. McFadden, P. W., et al., "High Flux Heat Transfer Studied. An Analytical Investigation of Laminar Film Boiling," ANL-6060, October, 1959.

125. Merte, H., Jr., "Investigation of Liquid Metal Boiling Heat Transfer," Contract No. AF 33(657)-11548, The University of Michigan, February, 1965.

126. Merte, H., Jr. and Clark, J. A., "Boiling Heat Transfer with Cryogenic Fluids at Standard, Fractional, and Near-Zero Gravity," Trans. ASME, 86, pp. 351-359, 1964.

127. Merte, H., Jr. and Clark, J. A., "Boiling Heat Transfer Data for Liquid Nitrogen at Standard and Near- Zero Gravity," Advances in Cryogenic Engr., K. D. Timmerhaus, Editor, 7, 1962.

128. Merte, H., Jr. and Clark, J. A., "Pool Boiling in an Accelerating System," Journal of Heat Transfer, Trans. ASME, Series C, Vol. 83, August, 1961, pp. 223-242.

129. Mickley, H. S., Sherwood, T. K., Reed, C. E., Applied Mathematics in Chemical Engineering, Second Edition, pp. 53-59, McGraw-Hill, New York 1957.

130. Misra, B., Bonilla, C., "Heat Transfer in the Condensation of Metal Vapors: Mercury and Sodium up to Atmospheric Pressure," Chem. Eng. Prog. Symposium Series, 52, No. 18, 7-21, 1956.

131. Moore, F. D. and Mesler, R. B., "The Measurement of Rapid Surface Temperature Fluctuations During Nucleate Boiling of Water," AIChE Journal, pp. 620-624, December, 1961.

132. Morozov, V. G., Intern'l. J. Heat and Mass Transfer, 5, pp. 661-666, July, 1962.

133. Neal, L. G. and Bankoff, S. G., "Local Parameters in Cocurrent Mercury-Nitrogen Flow," Argonne National Laboratory, Report ANL-6625 January, 1963.

134. Nishikawa, K., "Photographic Study of Stable Film Saturated Boiling," Trans. ASME, 26, p. 726, 1960.

135. Noyes, R. C., "Boiling Studies for Sodium Reactor Safety, Part I," August 30, 1963, NAA-SR-7909.

136. Noyes, R. C., "An Experimental Study of Sodium Pool Boiling Heat Transfer," Journal of Heat Transfer, Trans. ASME, Series C, Vol. 85, May, 1963, pp. 125.

137. Noyes, R. C., "Summary of Recent Results of Sodium Boiling Studies," Presented at Third Annual High-Temperature Liquid Metal Heat Transfer Technology Conference, Oak Ridge National Laboratory, September 4-6, 1963.

138. Noyes, R. C., Trans. ASME, No. 2, p. 125, 1963.

139. Noyes, R. C., Reed, G. L., "Sodium Condensing Heat Transfer: An Experimental Study of One Aspect of Sodium Cooled Reactor Safety," NAA-SR-7325, Atomics International, 1962.

140. Nukiyama, S., "Experiments on the Determination of the Maximum and Minimum Values of the Heat Transferred Between a Metal Surface and Boiling Water," AERE-TRANS-854, 1934.

141. Nusselt, W., "Die Oberflachenkondensation des Wasserdampfes," Zeitschrift des Vereines Deutscher Ingenieure, 60, 541, 561, 1916.

142. Park, E. L., et al., Cryogenic Eng. Conf., 1965.

143. Poppendiek, H. F., et al., "Quarterly Technical Report on High Acceleration Field Heat Transfer for Auxiliary Space Nuclear Power Systems," GLR-32, Geoscience Limited (November, 1964).

144. Poppendiek, H. F., et al., "Quarterly Technical Report on High Acceleration Field Heat Transfer for Auxiliary Space Nuclear Power Systems," GLR-36, Geoscience Limited (May, 1965).

145. Poppendiek, H. F., et al., "Summary Report on High Acceleration Field Heat Transfer for Auxiliary Space Nuclear Power Systems," Geoscience Limited, Solana Beach, California, January 1966.

146. Price, W. J., Nuclear Radiation Detection, McGraw-Hill, New York, 2nd. Ed., 1964.

147. Rallis, C. J. and Jawurek, H. H., "Latent Heat Transport in Saturated Nucleate Boiling," Intern'l. J. Heat and Mass Transfer, 7, pp. 1051-1068, March, 1964.

148. Reid, R. C., and Sherwood, T. K., The Properties of Gases and Liquids, McGraw-Hill Book Co., New York, 1958.

149. Richardson, B. L., "Some Problems in Horizontal Two-Phase, Two-Component Flow", Argonne National Laboratories, Report ANL-5949, December, 1958.

150. Richardson, J. L., Boynton, F. P., Eng., K. Y., and Mason, D. M., "Heat Transfer in Reacting Systems," Chem. Eng. Sci., 13, 130, 1961.

151. Roehlich, F., "The Electrical Resistivity and Thermal Conductivity of Liquid Alkali Metals to 2000°F," MSA Research Corp., MSAR 64-111, Callery, Pa., 1964.

152. Rohsenow, W. M., "Heat Transfer and Temperature Distribution in Laminar Film Condensation," Trans. ASME, 78, 1645-8, 1956.

153. Rohsenow, W. M. and Griffith, P., "Correlation of Maximum Heat Flux Data for Boiling of Saturated Liquids," Heat, Mass, and Momentum Transfer, Chapter 9, Prentice-Hall, New York, 1961.

154. Ros, N. C. J., "Simultaneous Flow of Gas and Liquid as Encountered in Well Tubing," Trans. Soc. Pet. Eng. of AIME, Vol. 222, 1037, 1961.

155. Rossini, F. D., et al., Selected Values of Chemical Thermodynamic Properties, Tables 84-96, Bureau of Standards Circular 500, February, 1952.

156. Roth, J. A., "Condensation of Sodium and Rubidium at Low Heat Fluxes," Report No. ASD-TR-63-738, October, 1962.

157. Roubeau, R., Progress in Refrig, Science and Tech., 1, p. 49, Pergamon Press, New York, 1960.

158. Sawle, D. R., "Sulfur-Cooled Power Reactor Study," Final Report, AGN-8015, December, 1960.

159. Schneider, P. J., "Effect of Axial Fluid Conduction on Heat Transfer in the Entrance Regions of Parallel Plates and Tubes," Trans. ASME, 79, 765, 1957.

160. Schrage, R. W., A Theoretical Study of Interphase Mass Transfer, Columbia University Press, New York, 1953.

161. Schroch, S. L., "Eddy Diffusivity Ratios in Liquid Metals," Ph.D. Dissertation, Purdue University, 1964.

162. Seban, R. A., "Remarks on Film Condensation with Turbulent Flow," Trans. ASME, 76, 299-303, 1954.

163. Smith C. R., Tang, Y. S. and Walker, C. L., "Slip Velocity in Two-Phase Metallic Fluids," Allison Division, General Motors Corp., Indianapolis, Indiana, Eng. Dept. Report No. 2809, May 25, 1962.

164. Smith, Lowell R., "Pressure Drops and Void Fractions in Horizontal Two-Phase Flow of Potassium," AIChE Journal, Vol. 12, p. 50, January, 1966.

165. Smith, Lowell R., "A Study of Pressure Drops and Void Fractions in Horizontal Two-Phase Flows of Potassium," Ph.D. Thesis, The University of Michigan, 1964.

166. Sparrow, E. M., Gregg, J. L., "A Boundary Layer Treatment of Laminar Film Condensation," Trans. ASME, Series C, J. Heat Transfer, 81, No. 1, 13-18, 1959.

167. Subbotin, V. I., et al., "Heat Removal From the Reactor Fuel Elements Cooled by Liquid Metals," Third United Nations Intern'l. Conf. on the Peaceful Uses of Atomic Energy, Paper No. A/CONF. 28/P/328/USSR, May, 1964.

168. Subbotin, V. I., Ibragimov, M. Kh., Ivanovskii, M. N., Arnol'bov, M. N., Nomofilov, E. V., "Heat Transfer During the Turbulent Flow of Liquid Metals in Tubes," Soviet Journ, Atomic Energy, 11, 769-74, 1962.

169. Sukhatme, S. P., Rohsenow, W. M., "Heat Transfer During Film Condensation of a Liquid Metal Vapor," Dept. of Mech. Eng., MIT, Technical Report No. 9167-27, 1964.

170. Tang, Y. S., Smith, C. R. and Ross, P. T., "Potassium-Mercury Amalgam Boiling Heat Transfer, Two-Phase Flow, and Properties Investigation," Allison Division, General Motors Corp., Indianapolis, Indiana, Eng. Dept., Report No. 3549, September 16, 1963.

171. Thompson-Ramo-Woolridge, Inc., TAPCO Division, "Space Radiator Study" Tech. Report No. ASD-TR-61-697, October, 1963.

172. Tippets, F. E., "Heat Transfer and Pressure Drop Measurements for High Temperature Boiling Potassium in Forced Convection," Presented at the Conference on Application of High Temperature Instrumentation to Liquid-Metal Experiments, ANL, September 28-29, 1965. p. 53.

173. Treshchov, G. G., Teploenergetika 3, 4, No. 5, pp. 44-48, 1957.

174. Van Wijk, W. R., et al., Chem. Eng. Sci., 5, pp. 68-80, 1956.

175. Velkoff, H. R., Miller, J. H., "The Effect of an Electrostatic Field on the Condensation of Vapor," Air Force Systems Command, Technical Documentary Report No. RTD-TDR-63-4008, February, 1964.

176. Vohr, J. H., "Flow Patterns of Two-Phase Flow--A Survey of Literature," TID-11514, December 15, 1960.

177. Ward, H. C., et al., "Analytical Investigation of Two-Phase Vapor-Liquid Ratio Measuring Systems and Two-Phase Flow Literature Survey Supplement," WADC Report No. 59-230. August, 1959.

178. Weatherford, W. D., et al., "Properties of Inorganic Energy-Conversion and Heat Transfer Fluids for Space Applications," WADD Technical Report 61-96. November, 1961.

179. Weatherford, W. D., Tyler, J. C., and Ku, P. M., "Properties of Inorganic Energy-Conversion and Heat Transfer Fluids for Space Applications," USAF, WADD-Tech. Report No. 61-96, November, 1961.

180. Westwater, J. W., "Boiling of Liquids," Advances in Chemical Engineering, Vol. 1, T. B. Drew, Editor, Academic Press Inc., New York 1956.

181. Westwater, J. W. and Santangelo, J. G., "Photographic Study of Boiling," Ind. Eng. Chem., p. 1605, August, 1955.

182. Wichner, R. P., "Pressure Drop with Forced-Convection Boiling of Potassium," Presented at the Conference on Application of High Temperature Instrumentation to Liquid-Metal Experiments, ANL, September 28-29, 1965. p. 535.

183. Wilhelm, D. J., "Condensation of Metal Vapors: Mercury and the Kinetic Theory of Condensation," Argonne National Lab. Report No. ANL-6948, October, 1964.

184. Zuber, N., "On the Stability of Boiling Heat Transfer," Trans. ASME, 80, pp. 711-720, April, 1958.

185. Zuber, N., "The Hydrodynamic Crisis in Pool Boiling of Saturated and Subcooled Liquids," Intern'l. Dev. in Heat Trans., Part II, pp. 230-236, August, 1961.

186. Zuber, N., "Hydrodynamic Aspects of Boiling Heat Transfer," Ph.D. Thesis, University of California, Los Angeles, June, 1959. (also AECU-4439)

187. Zuber, N., and Tribus, M., "Further Remarks on the Stability of Boiling Heat Transfer," AECU-3631, January, 1958.

Unclassified

Security Classification

14 **DOCUMENT CONTROL DATA - R&D**

(Security classification of title, body of abstract and indexing annotation must be entered when the overall report is classified)

ORIGINATING ACTIVITY (Corporate author)	2a. REPORT SECURITY CLASSIFICATION
The University of Michigan Department of Chemical and Metallurgical Engineering Ann Arbor, Michigan	Unclassified
	2b. GROUP

REPORT TITLE

INVESTIGATION OF LIQUID METAL BOILING HEAT TRANSFER

DESCRIPTIVE NOTES *(Type of report and inclusive dates)*

Final Report

5. AUTHOR(S) *(Last name, first name, initial)*

Balzhiser, Richard E., et al.

6. REPORT DATE	7a. TOTAL NO. OF PAGES	7b. NO. OF REFS
January 1967	304	187

8a. CONTRACT OR GRANT NO.	9a. ORIGINATOR'S REPORT NUMBER(S)
AF 33(657)-11548	05750-24-F
b. PROJECT NO.	
c.	9b. OTHER REPORT NO(S) *(Any other numbers that may be assigned this report)*
d.	AFAPL-TR-66-85

10. AVAILABILITY/LIMITATION NOTICES

Qualified requesters may obtain copies of this report from DDC.

11. SUPPLEMENTARY NOTES	12. SPONSORING MILITARY ACTIVITY
	Air Force Aero Propulsion Laboratory Research and Technology Division, AFSC Wright-Patterson Air Force Base, Ohio

13. ABSTRACT

Nucleate boiling for sodium, rubidium, cesium, and water was studied. The critical heat fluxes were lower than hydrodynamic theory had predicted.

Film boiling of potassium from a horizontal plate was studied. The flux level and the temperature difference between the surface and the fluid at the incipience of stable film boiling differed from earlier predictions.

Agravic studies with pool boiling mercury were studied at accelerations up to 20 g's. Increases in pressure and acceleration usually improved the heat transfer.

Sodium condensing studies resulted in coefficients of approximately 18,000 Btu/hr ft^2 for fluxes up to 500,000 Btu/hr ft^2. These are much lower than predictions from Nusselt's theory.

Two phase flow potassium pressure drop, void fraction and heat transfer studies were conducted. Pressure drop studies yielded lower results than predicted by Lockhart - Martinelli procedures. The void fraction studies agreed with Baroczy's predictions. The heat transfer studies were conducted at qualities up to 17%.

DD FORM 1 JAN 64 1473

Unclassified

Security Classification

Unclassified

Security Classification

14. KEY WORDS	LINK A		LINK B		LINK C	
	ROLE	WT	ROLE	WT	ROLE	WT
Heat Transfer						
Liquid Metal Boiling						
Sodium Condensation						
Two-phase Flow						
Film Boiling						
Pool Boiling						

INSTRUCTIONS

1. ORIGINATING ACTIVITY: Enter the name and address of the contractor, subcontractor, grantee, Department of Defense activity or other organization *(corporate author)* issuing the report.

2a. REPORT SECURITY CLASSIFICATION: Enter the overall security classification of the report. Indicate whether "Restricted Data" is included. Marking is to be in accordance with appropriate security regulations.

2b. GROUP: Automatic downgrading is specified in DoD Directive 5200.10 and Armed Forces Industrial Manual. Enter the group number. Also, when applicable, show that optional markings have been used for Group 3 and Group 4 as authorized.

3. REPORT TITLE: Enter the complete report title in all capital letters. Titles in all cases should be unclassified. If a meaningful title cannot be selected without classification, show title classification in all capitals in parenthesis immediately following the title.

4. DESCRIPTIVE NOTES: If appropriate, enter the type of report, e.g., interim, progress, summary, annual, or final. Give the inclusive dates when a specific reporting period is covered.

5. AUTHOR(S): Enter the name(s) of author(s) as shown on or in the report. Enter last name, first name, middle initial. If military, show rank and branch of service. The name of the principal author is an absolute minimum requirement.

6. REPORT DATE: Enter the date of the report as day, month, year; or month, year. If more than one date appears on the report, use date of publication.

7a. TOTAL NUMBER OF PAGES: The total page count should follow normal pagination procedures, i.e., enter the number of pages containing information.

7b. NUMBER OF REFERENCES: Enter the total number of references cited in the report.

8a. CONTRACT OR GRANT NUMBER: If appropriate, enter the applicable number of the contract or grant under which the report was written.

8b, 8c, & 8d. PROJECT NUMBER: Enter the appropriate military department identification, such as project number, subproject number, system numbers, task number, etc.

9a. ORIGINATOR'S REPORT NUMBER(S): Enter the official report number by which the document will be identified and controlled by the originating activity. This number must be unique to this report.

9b. OTHER REPORT NUMBER(S): If the report has been assigned any other report numbers *(either by the originator or by the sponsor)*, also enter this number(s).

10. AVAILABILITY/LIMITATION NOTICES: Enter any limitations on further dissemination of the report, other than those imposed by security classification, using standard statements such as:

(1) "Qualified requesters may obtain copies of this report from DDC."

(2) "Foreign announcement and dissemination of this report by DDC is not authorized."

(3) "U. S. Government agencies may obtain copies of this report directly from DDC. Other qualified DDC users shall request through _____."

(4) "U. S. military agencies may obtain copies of this report directly from DDC. Other qualified users shall request through _____."

(5) "All distribution of this report is controlled. Qualified DDC users shall request through _____."

If the report has been furnished to the Office of Technical Services, Department of Commerce, for sale to the public, indicate this fact and enter the price, if known.

11. SUPPLEMENTARY NOTES: Use for additional explanatory notes.

12. SPONSORING MILITARY ACTIVITY: Enter the name of the departmental project office or laboratory sponsoring *(paying for)* the research and development. Include address.

13. ABSTRACT: Enter an abstract giving a brief and factual summary of the document indicative of the report, even though it may also appear elsewhere in the body of the technical report. If additional space is required, a continuation sheet shall be attached.

It is highly desirable that the abstract of classified reports be unclassified. Each paragraph of the abstract shall end with an indication of the military security classification of the information in the paragraph, represented as *(TS), (S), (C), or (U)*

There is no limitation on the length of the abstract. However, the suggested length is from 150 to 225 words.

14. KEY WORDS: Key words are technically meaningful terms or short phrases that characterize a report and may be used as index entries for cataloging the report. Key words must be selected so that no security classification is required. Identifiers, such as equipment model designation, trade name, military project code name, geographic location, may be used as key words but will be followed by an indication of technical context. The assignment of links, rules, and weights is optional.

Unclassified

Security Classification